BLOCKING IMMUNOSUPPRESSIVE FACTORS AND TAKING ADVANTAGE OF THE NUTRIENT SUPPLY WITHIN THE TUMOR MICROENVIRONMENT: PATHWAYS TO ACHIEVE IMPROVED CANCER IMMUNOTHERAPEUTIC EFFICACY FOR PATIENTS WITH METASTATIC MELANOMA

Ying Zhang

A DISSERTATION

in

Cell and Molecular Biology

Presented to the Faculties of the University of Pennsylvania

in

Partial Fulfillment of the Requirements for the

Degree of Doctor of Philosophy

2016

Supervisor of Dissertation

_____

Hildegund C.J. Ertl, M.D.
Caspar Wistar Professor in Vaccine Research

Graduate Group Chairperson

_____

Daniel S. Kessler, Ph.D.
Associate Professor of Cell and Developmental Biology

Dissertation Committee

José R. Conejo-Garcia, M.D., Ph.D., Professor and Program Leader, The Wistar Institute
Meenhard Herlyn, D.V.M., D.Sc., Caspar Wistar Professor, Director, The Wistar Institute
Yvonne Paterson, Ph.D., Professor of Microbiology, University of Pennsylvania
Robert H. Vonderheide, M.D., D.Phil., Hanna Wise Professor in Cancer Research, University of Pennsylvania

BLOCKING IMMUNOSUPPRESSIVE FACTORS AND TAKING ADVANTAGE OF THE NUTRIENT SUPPLY WITHIN THE TUMOR MICROENVIRONMENT: PATHWAYS TO ACHIEVE IMPROVED CANCER IMMUNOTHERAPEUTIC EFFICACY FOR PATIENTS WITH METASTATIC MELANOMA

For the many teachers and mentors I have throughout all these years,

Thank you for your love and understanding, encouragement and support, patience and guidance, which help me reach this milestone.

In loving memory of my grandparents,

who inspired my endless curiosity towards nature.

ACKNOWLEDGMENT

It has been a wonderful six years of adventure filled with learning and questioning, explorations and discoveries, surprises and excitements, tears and joys. I enjoy the great serenity deep in heart science brings to me and cherish everyday of it.

I am eternally grateful to the many amazing people surround me, who inspired, witnessed and supported my scientific and personal growth. First and foremost, I am deeply appreciative of my mentor, Dr. Gundi Ertl. Thank you for all your inspirational and timely advice and constant support. I have learned so much from your unique perspective on research and your insights on almost any issue. Thank you for giving me the freedom to pursue various projects and ask numerous questions without objection. Thank you for generously devoting so much of your precious time to discuss research questions and data with me, to listen to my presentations and provide me with insightful suggestions, to edit my graphs and research papers, to help me with so many experiments, and to share with me life experiences working and living as a woman scientist. Your diligence, perseverance and passion are contagious, and you will always be my best role model for a scientist and mentor.

I am very fortunate to have had world-class experts in melanoma and cancer immunotherapy research field, Dr. José Conejo-Garcia, Dr. Meenhard Herlyn, Dr. Yvonne Paterson and Dr. Robert Vonderheide serve on my thesis committee. Thank you for all the long hours you spent in my committee meetings, initiating many enlightening discussions, challenging me to think critically and giving me your invaluable scientific and career advices. I would also like to thank my collaborators at Princeton University, Dr. Joshua Rabinowitz and Ling Liu, who introduced me to the fascinating world of metabolomics, helped me tremendously with sample processing and data analysis, and provided me with invaluable feedback on our manuscript-in-progress. My immunometabolism project cannot go so smoothly without your diligent work.

I am indebt to many other faculties, staff members and colleagues at the Wistar Institute and Penn. Thank you for sharing with me important scientific knowledge, teaching me the useful techniques, discussing technical details and troubleshooting with me and helping me with my experiments in one way or another. My special thanks goes to Dr. William Wunner, who is genuinely interested in my career success and offers me priceless teaching opportunities. To past and present members of the Ertl lab, thank you for creating such an agreeable and collaborative working environment. Your encouragement, technical and emotional supports are crucial for me to reach this point. Abeer and Flavia, thank you for all your help at the bench and working with me late at night. Thank you for your great company and I will easily miss hanging out with you two the most.

Finally, I would like to express my profoundest gratitude to my friends and family. To my friends in grad school, thank you for going through this path with me, sharing your experiences and offering me the friendship and support that I needed. To all my best friends who are scattered around the world now, although we are physically separated, you are still a major source of my emotional support and I feel extremely lucky to have you in my life. To all the friends I have made in the PCDC dancing group, thank you for offering me such a wonderful harbor to savor life outside of work. It is always joyous to practice and perform with you girls and you will become one of my sweetest memories at Penn. To my wonderful mom and dad, you have been the best parents I could ever imagine. Thank you for your unwavering love, always having faith in my abilities and encouraging me towards excellence. And last, but certainly not least, I am much obliged to my boyfriend Mr. Pengfei Han, whose knowledge, patience and humor have helped me stay calm, confident and strong during this stressful period of time. Thank you for sharing so much delightful time with me, and being a constant source of encouragement, support and love in my life.

ABSTRACT

BLOCKING IMMUNOSUPPRESSIVE FACTORS AND TAKING ADVANTAGE OF THE NUTRIENT SUPPLY WITHIN THE TUMOR MICROENVIRONMENT: PATHWAYS TO ACHIEVE IMPROVED CANCER IMMUNOTHERAPEUTIC EFFICACY FOR PATIENTS WITH METASTATIC MELANOMA

Ying Zhang

Hildegund C.J. Ertl

The incidence of melanoma is increasing. Immunotherapy commonly fails due to the immunosuppressive tumor microenvironment (TME). The aim of my dissertation is to develop strategies that dampen the TME's immunosuppressive capacity and improve the antitumor performance of vaccine-induced melanoma-associated antigen (MAA)-specific $CD8^+$T cells. I pursued this goal using three approaches. First, interactions between co-inhibitors on $CD8^+$ tumor-infiltrating lymphocytes (TILs) with immunoinhibitory ligands within the TME impair T cells' effector functions. I assessed whether blocking immunoinhibitory signaling during T cell priming augments their antitumor activity. I designed a melanoma vaccine expressing MAAs within herpes simplex virus (HSV) glycoprotein D (gD), which blocks the inhibitory BTLA/CD160-HVEM pathway. Compared to a non-gD vaccine, the gD-adjuvanted vaccine enhances $CD8^+$T cells to low avidity epitopes and prolongs survival of tumor-bearing mice. gD renders MAA-specific $CD8^+$TILs more resistant to functional impairment within TME, which increases their ability to limit tumor progression. Second, the stroma of solid tumors is crucial for tumorigenesis and suppresses the $CD8^+$TILs' effector functions. To determine whether destroying tumor stroma

could improve the MAA-specific $CD8^+$T cells' tumoricidal capacity, I designed a vaccine targeting the fibroblast activation protein (FAP), which is expressed at high levels on tumor-stromal fibroblasts. Combining the vaccines to FAP and MAAs significantly improves the survival of tumor-bearing mice. This is caused by destruction of FAP^+ cells, which reduces frequencies and inhibitory functions of immunosuppressive cells. It also decreases the MAA-specific $CD8^+$TILs' metabolic stress and delays their progression towards functional exhaustion. Finally, the TME commonly lacks nutrients and oxygen needed for the $CD8^+$TILs' energy production. My data demonstrate that these metabolic challenges profoundly contribute to the $CD8^+$TILs' functional impairment. Using ^{13}C-stable isotope tracing *in vivo*, I show that metabolically stressed $CD8^+$TILs in late stage tumors increasingly depend on fatty acids (FAs) catabolism for energy production. Promoting FA catabolism by $CD8^+$TILs improves their effector functions and capacity to delay tumor growth. Overall, my studies show that blocking inhibitory factors while taking advantage of the available nutrients within the TME could improve the performance of vaccine- or adoptive transfer-induced $CD8^+$TILs. These strategies provide new avenues for cancer immunotherapy that may benefit cancer patients.

TABLE OF CONTENTS

LIST OF FIGURES

CHAPTER 1:

CHAPTER 2:

CHAPTER 3:

CHAPTER 4:

CHAPTER 5:

Chapter 1

INTRODUCTION

1.1 Melanoma: discovery, development and epidemiology

Melanoma, the most aggressive and lethal form of skin cancer, is an impending health problem with a long history. Hippocrates was the first to record the disease as *melas* (dark), and *oma* (tumor) in the 5th century BC. Samuel Cooper in 1844 formally acknowledged the untreatable nature of melanoma and stated that " the only chance for benefit depends on early removal of the disease" (1). This statement still holds true today even with advances in our scientific knowledge. The study of melanoma development and treatment in the 19th and early 20th century progressed slowly and were mainly descriptive in nature. In 1956, Henry Lancaster for the first time pointed out the direct link between ultraviolet (UV) radiation exposure and melanoma incidences. Further work by Lancaster and Nelson identified the association between pale skin/hair color and melanoma development. This was confirmed by recent work, which identified the UV-mediated activation of a highly polymorphic protein called melanocortin receptor 1 (MC1R)(2). MC1R variants associated with pale skin phenotype are linked to deficiency of

melanin production in the skin upon UV exposure and compromised photoprotection. Other early genetic studies based on “melanoma families” identified mutations associated with CDKN2A gene, which regulates cell cycle entry at G1 checkpoint and p53 stabilization, conveys enhanced risk of melanoma formation(3). These works identify melanoma as a genetic disease and provide some mechanistic insights into the pathogenesis of this highly malignant lesion.

Today we know that metastatic melanoma arises from transformed melanocytes in 75% of the cases and from nevus in 25% of the situations (4-6). Melanoma pathogenesis is a complicated process that requires the interplay of environmental and host factors. It is a genetically and phenotypically heterogeneous disease; each tumor bears its unique combinations of epigenetic and genetic mutations and occurs at different body locations. Cancer genome deep sequencing has revealed that, with a median number of >10 mutations per megabase of DNA, melanomas carry the highest mutational load of all human tumors and harbor an overwhelming number of UV-signature mutations (7). Besides the commonly mutated genes BRAF, NRAS, PTEN, TP53, and p16, new candidate genes such as PPP6C, RAC1, STK19, PREX2 have been identified through large-scale melanoma exome sequencing (7-9). In most cases melanoma development is a multistep process regulated by a key set of genes. Cells must acquire sequential genetic alterations, including constitutive oncogenic pathway activation and loss of functions for tumor suppressor genes in order to form tumors and metastases (**Figure 1-1**). Since melanomas from a certain location and with different UV exposure histories often bear unique genetic mutation signatures, it was proposed that melanoma could be molecularly classified based on these factors (10). For example, the well-known $BRAF^{V600E}$ mutation occurs in up to 80% of nevus-derived cancers and is more common in melanomas arising on intermittent sun-exposed areas, while sun exposure-induced or mucosal and acral melanomas usually have no BRAF mutation but have higher rates of KIT alterations (11).

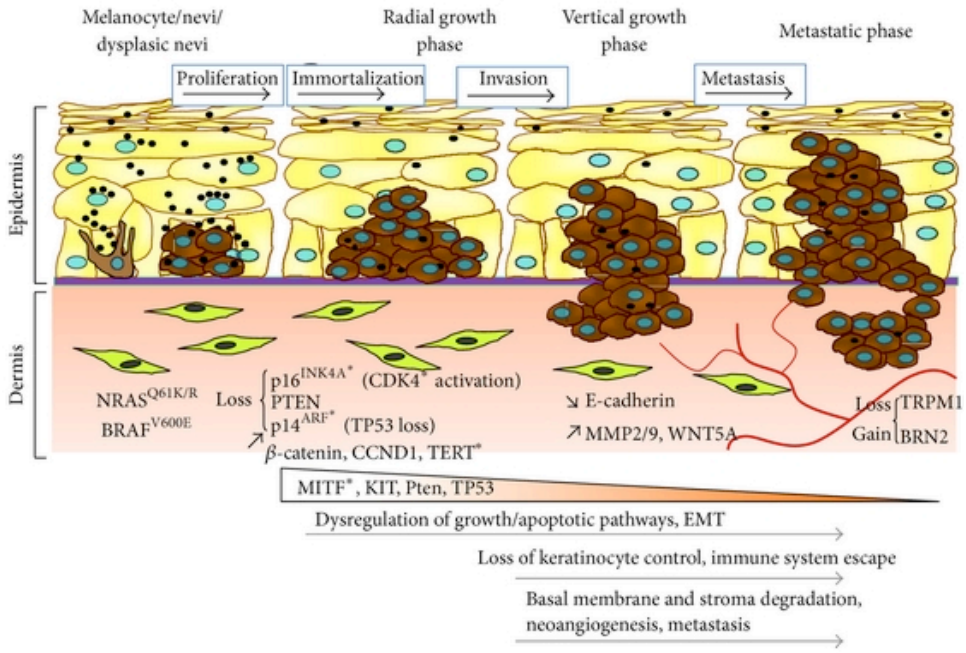

Figure 1-1: Hypothetical model of melanoma development from a pre-existing nevus following a cascade of genetic mutations that leads to tumor formation and metastasis. Figure is adapted from Bertolotto, 2013(6).

Although melanoma represents less than 5% of all skin cancers, it is responsible for over 75% of skin cancer-related deaths. Despite intensive research, public campaigns and screenings programs, the incidence of melanoma has been increasing at a steady rate over the last 8 decades, and its death rate continues to rise (5). In the early stages melanoma can be cured by surgical resection. However, the deeper melanoma invades into the skin, the worse the prognosis becomes due to increased chance that cancer cells metastasize to lymph nodes and visceral organs. Once it has progressed to the metastatic stage, melanoma is extremely hard to treat and largely refractory to current therapies (12). The median survival of patients with stage IV melanoma is less than 1 year (13).

1.2 Current treatment strategies

For patients with primary cutaneous melanoma with negative (localized) or positive (locoregional) regional lymph node invasion, surgery is the gold standard treatment. However, for the majority of patients with distant metastatic disease, the benefit from surgery is quite limited

and can only be curative in rare cases (9). Instead, systemic treatment strategies such as chemotherapy and immunotherapy play a major role in treating these advanced stage melanomas.

Prior to 2011 when I proposed my doctoral thesis, systemic therapy was limited to chemotherapy with agents such as dacarbazine, temozolomide and fotemustine; high-dose interleukin (IL)-2 or interferon alpha-2b administration and combination biochemotherapy. Adoptive cell transfer and cancer vaccines studies were in preclinical or Phase I-III clinical trials. Although promising clinical responses have been seen in some patients, none of these methods demonstrated an improvement in median progression-free survival (PFS) or overall survival (OS) based on randomized phase III clinical trial (14,15). However, since 2011 with the improved understanding of the BRAF-MEK-ERK mitogen-activated protein kinase (MAPK) pathway and breakthrough findings in the cancer immunotherapy field, the landscape of systemic therapeutic approaches has dramatically advanced. Four new agents, after demonstrating significant advantages in response and survival compared to traditional chemotherapy, have been approved by FDA. These include the MEK inhibitor trametinib (Mekinist^{TM}, 2013), the RAF inhibitors vemurafenib (Zelboraf^{TM}, 2012) and dabrafenib (Tafinlar^{TM}, 2013), the anti-programmed cell death protein (PD)-1 monoclonal antibody nivolumab (Opdivo^{TM}, 2014) and pembrolizumab (2014) and the anti-cytotoxic T-lymphocyte antigen-4 (anti-CTLA-4) monoclonal antibody ipilimumab (Yervoy^{TM}, 2011).

1.2.1 Oncogene-targeted small molecule drugs

Stratton and colleagues reported the seminal discovery of oncogenic BRAF mutations in 2002(16). The most common BRAF valine-to-glutamic acid alteration at codon 600 has been characterized in more than 50% of human melanomas (17,18) and to a lesser extent in some other cancers(19). BRAF^{V600E} mutation occurs early during melanomagenesis, which produces a senescence-like state in melanocytes that is insufficient to transform these cells by itself(20). However as BRAF is upstream of the MAPK pathway, studies have shown that the presence of mutated BRAF confers a stringent tumor dependency on MAPK signaling. RAF enzymes could

form “side-to-side” dimers between two RAF enzymes or heterodimers with RAF-related pseudo-kinase KSR (kinase suppressor of Ras), which can catalytically trigger the constitutive phosphorylation and activation of MEK (21). Knocking down mutated BRAF or its inhibition by selective small inhibitors can significantly suppress the growth of melanoma cells (22,23). The FDA-approved RAF inhibitors have modest preference for the mutated form of B-RAF compared to wild-type B-RAF. In addition, the inhibitors have differential ability to inhibit the activity of over 200 kinases and could potently suppress ERK phosphorylation and tumor cell proliferation in $BRAF^{V600E}$ cell lines (24).

Although both RAF and MEK inhibitors achieve potent antitumor activity in melanoma patients with $BRAF^{V600E}$ mutation, resistance develops at a median time of 6-7 months (25,26). Several models have been proposed that could explain the mutant cell drug resistance, including overexpression of the mutated BRAF, acquisition of NRAS or MEK1 mutations and post-transcriptional splice variant of the mutated BRAF with enhanced dimerization capacity (11). The bottom line is that BRAF or MEK inhibitors create high selection pressure for melanoma cells survival, and cells with any new mechanism to reactivate or bypass the MAPK signaling will likely lead to resistance. Combining the BRAF and MEK signaling pathway inhibitors is a strategy that can suppress the MAPK pathway more effectively. In three phase III clinical trial, patients with $Braf^{V600E}$-metastatic melanoma showed significantly improved response rate with this combination therapy compared to those receiving monotherapy and had a longer median PFS (27-29). The FDA has granted approval to the combined therapeutic strategy of dabrafenib and trametinib in 2014. Although BRAF and MEK inhibitors have achieved groundbreaking success in prolonging melanoma patient survival, there is the caveat that this strategy only works in ~50% of the patients with $BRAF^{V600E}$ mutation. In addition, one clinically untenable situation is the occurrence of multiple distinct resistances within different metastatic sites in one patient. Therefore, other, more universal and efficient therapeutic strategies are still urgently needed.

1.2.2 Immunotherapy

Immunotherapies rely on taking advantage of the host immune system to induce an anti-tumor immune response. Melanoma is highly immunogenic, with naturally occurred immune responses that could control melanoma growth or even lead to spontaneous tumor regression(30). Cellular inflammation, mainly tumor-infiltrating CD4+ and CD8+ T lymphocytes have been detected in regressing melanomas(31). In addition, tumor-associated antigens (TAAs) that could induce tumor-specific B and T cell responses were identified in melanoma earlier than in other cancer types(32,33). These advantages make melanoma an ideal cancer type for immunotherapy study.

1.2.2.1 Immune checkpoint inhibitors:

Immune checkpoints are a plethora of immunoinhibitory molecules expressed on T lymphocytes, which could bind to their receptor ligands on antigen-presenting cells (APCs) or tumor cells. Under physiological conditions, immunoinhibitory molecules are upregulated upon T cell activation, which put 'breaks' on T cells to prevent their overactivation. These are crucial molecules for maintaining self-tolerance and adjusting the duration and amplitude of physiological immune responses in peripheral tissue to minimize damage (34). Tumor cells or stromal cells within the tumor microenvironment (TME) usually overexpress inhibitory ligands, which dampen antitumor T cell responses. Antibodies that block the T cell-tumor cell inhibitory interaction can dramatically enhance the antitumor T cell responses and have achieved remarkable successes in the clinic.

Ipillimumab: CTLA-4 is the first immunoinhibitory molecule that was used clinically. It regulates the amplitude of immune response early after T cell activation and is exclusively expressed on T cells (34). CTLA-4 outcompetes T cell costimulatory receptor CD28 in binding CD80/CD86 ligands on APCs or tumor cells; therefore it dampens the activation of T cells (35). Several studies suggest that CTLA-4-CD80/CD86 ligation activates the protein phosphatases SHP2 and PP2A, which counteracts the kinase signals induced by T cell receptor (TCR) ligation and CD28 co-stimulation (36). Other studies show that CTLA-4 could sequester or remove CD80/CD86 ligands on APCs, therefore blocking their interaction with CD28 (37). CTLA-4 is also

expressed on helper T cells and regulatory T cells (Tregs). Blockade of CTLA-4 leads to markedly higher immune responses that are dependent on helper T cells and reduces the immunosuppressive activity of Tregs (38,39). Humanized anti-CTLA-4 antibody ipilimumab, which boosts the endogenous antitumor immune response if given alone, was the first immunotherapy that showed improved survival for patients with metastatic melanoma. In phase III clinical trial, nearly double the rates of patients treated with ipilimumab combined with dacarbazine showed durable responses and 3-year overall survival compared to patients treated with dacarbazine alone (40).

Anti-PD-1/PD-L1 antibodies: PD-1 is another potent immunoinhibitory molecule upregulated on activated T cells. Unlike CTLA-4 ligation that inhibits T cell activation, PD-1 mainly inhibits T cell effector responses at the site of inflammation or within tumor through binding to PD1 ligand 1 (PD-L1) or PD-L2 (41). The activation of PD-1 signaling dampens TCR ligation induced kinase activity through phosphatase SHP2 (42). PD-1 is one of the signature co-inhibitors that is upregulated early on 'exhausted' T cells during chronic infection and cancer (43). Blockade of PD-1 signaling on these cells may partially reverse the functional exhaustion of effector T cells and therefore improve their antitumor efficacy (44). Moreover, unlike CTLA-4, PD-1 expression is also detected on B-lymphocytes and nature killer (NK) cells, where it restricts their lytic functions (45,46). Anti-PD-1 antibody therefore can also improve tumor-killing efficacy through enhanced NK cell activities. In phase III clinical trial, PD-1 blocker nivolumab was associated with significantly enhanced PFS and OS compared with dacarbazine for patients with metastatic melanoma without BRAF mutation (47). Furthermore, another phase III trial showed that pembrolizumab could prolong PFS and OS and exhibit endless toxicity compared to ipilimumab in patients with advanced melanoma (48). Besides PD-1 inhibition, PD-L1 inhibitors received similar attention due to their high expression on tumor cells and tumor stroma cells in many types of cancers, including metastatic melanoma (49). In addition, PD-L1 is expressed on myeloid cells in the TME (50). There are two major pathways that promoted enhanced PD-L1 expression on tumor cells, either through oncogenic signaling (innate immune resistance) (51,52)

or the production of IFN-γ via T cells interacting with tumors by PD-1-PD-L1 ligation (adaptive immune resistance) (53). Anti-PD-L1 antibodies are under development and have shown promising results.

In 2015 FDA approved the combined usage of nivolumab with ipilimumab for patients with metastatic melanoma, as the combined treatment showed markedly improved PFS than single agent treatment(54). The study dictates future applications of combined therapies targeting multiple factors within TME to achieve enhanced antitumor efficacy.

1.2.2.3 Cancer vaccines

Cancer vaccines aim to harness the patients' own immune system to recognize tumor cells as 'foreign. Their goal is to generate or boost effective immune responses to destroy tumor cells. This is a difficult task due to the high mutation rates of melanoma antigens, unique combinations of mutations and diversified haplotypes in each melanoma patients and the complex and immunoinhibitory nature of the TME.

Melanoma antigens

One major factor that determines the efficacy of cancer vaccines is the set of antigens they express. The identification of large number of melanoma-associated antigens (MAAs) has facilitated vaccine design. MAAs can be characterized into several categories:

(**i**) Neo-antigens are tumor-specific antigens (TSAs) that are the results of numerous nucleotide point mutations, alternative transcripts or products from cryptic start sites, alternative reading-frames, pseudo-genes or antisense strands of DNA(33,55,56) generated during melanoma development. Novel T cell epitopes can be processed and presented depending on the HLA species in individual patients, and are recognized by $CD8^+$ and $CD4^+$ T cells. In addition, many proteins during melanoma transformation become phosphorylated, i.e. phosphorylated β-catenin, IRS2, generating unique phosphorylated epitopes(57).

(**ii**) Cancer testis antigens are a family of antigens that are only expressed in spermatozoa, some ovarian tissues and trophoblasts; they are normally silenced in somatic cells. These antigens can

re-emerge on tumor cells, often due to hypomethylation or histone acetylation of the genes(58). Proteins such as MAGE-1 and NY-ESO-1 belong to this category.

(**iii**) Melanoma-differentiation antigens are tissue-specific antigens expressed on normal melanocytes, which are usually overexpressed on melanoma cells. Carbohydrate antigens, particularly gangliosides and melanosome membrane glycoproteins, i.e., tyrosinase-related protein (Trp)-1, Trp-2, gp100, tyrosinase and MART-1, belong to this subset(59). Although high-avidity T cells against self-antigens are deleted during thymic selection, low-avidity T cells remain which could mount immune responses with enhanced antigen load and tumor-associated inflammation(60). This is confirmed as spontaneous T cell responses to melanoma-differentiation antigens can be detected in cancer patients(61).

Current approaches

Thus far melanoma vaccines have taken a variety of shapes and forms, ranging from whole-cell tumor preparations to recombinant viral vectors and exhibited different antitumor efficacies in preclinical models and patients with advanced melanoma.

(**i**) Peptide vaccines: Early vaccine trials using MAA-derived peptides showed low response rates and no indication of efficacy(15,62). This could be due to low avidity of the available T cell repertoire in patients. Further studies using modified peptides with enhanced HLA binding capacity enhanced the MAA-specific $CD8^+$T cell responses elicited in patients, although they still showed only limited clinical benefit(63). These paradoxical outcomes may result from the suboptimal induction of T cell responses by dysfunctional tumor-influenced APCs, downregulation of antigen-presenting molecules on tumor cells, mutations of tumor antigens under selection pressure and the immunoinhibitory factors within TME(64). To circumvent the outgrowth of antigen-loss variants, multipeptide immunization studies have been carried out. Some patients upon receiving this vaccine regimen showed prolonged PFS, which encourages more studies to understand factors that contribute to the success of these vaccine with the hope that their clinical potential can be maximized to benefit patients with advanced stage melanoma(65).

(**ii**) DNA/viral vector based vaccines: Naked DNA vaccines with electroporation are capable of inducing T cell responses in advanced melanoma patients, although similar as peptide vaccines they have thus far shown little to no antitumor efficacy(66,67). Other vectors as tumor-antigen delivery vehicles, such as attenuated bacteria S. typhimurium, alphavirus, coronavirus, vaccinia virus or adenovirus-based vaccines were shown to trigger inflammation and anti-viral danger signals that could enhance immune response to transgene(68,69). In some of the trials viral vector mediated gene delivery induced high avidity effector $CD8^+$T cell responses, and achieved regression of melanoma metastases and stable disease in a small proportions of melanoma patients(70,71). The differences in clinical outcomes highlight the importance to conduct more detailed studies to optimize the vectors, transgenes, vaccine regimens and other factors to improve the antitumor immune responses of the vaccines.

Adenovirus as vaccine carrier: For my thesis project the chimpanzee-derived adenoviral (Ad) vector of serotype 68 (AdC68) was selected as the vaccine backbone. Adenovirus contains 26-45kb pairs long linear, double stranded DNA genome that is surrounded by a non-enveloped icosahedral capsid. Ad can be modified into early (E)1 gene deleted replication-defective vectors(72) This deletion furthermore increases the space within the viral genome for insertion of transgenes(73). Importantly, Ad vectors are powerful vaccine delivery vehicles as they can induce innate immune responses in mammalian hosts and therefore exert adjuvant effects needed to elicit strong and sustained transgene product-specific immune responses upon a single dose injection(74,75). Moreover, Ad vectors have a broad tropism; they can transduce a series of different cell types(76). Ad vectors persist. After clearance of Ad-transduced cells at the site of vaccination, Ad vectors remain transcriptionally active at very low levels within muscles at injection site, livers and T cells including those directed to Ad vector encoded antigens(77). The continued presence of low amount of tumor antigens expressed by Ad vectors helps to maintain a fairly high population of effector and effector memory T cells against melanoma cells, which can be highly advantageous in suppressing cancer progression. One potential caveat of using Ad vectors as vaccine delivery vehicles is the high prevalence of neutralizing antibodies to human Ad

vectors, which may dampen T cell responses to Ad-delivered transgenes. To circumvent this problem, both serologically rare human Ads, such HAdV-26 and HAdV-35, and Ads that naturally infect non-human primates, such as chimpanzee-derived serotypes AdC6, AdC7 and AdC68 can be used as vaccine carriers(78). Vaccines based on these Ad vectors have achieved promising results in preventing or treating infectious disease and cancer in both preclinical and clinical studies.

(**iii**) Dendritic cell (DCs) based vaccines: One reason for the poorly activated $CD8^+$T cell responses by cancer vaccines in melanoma patients may be explained by the insufficient antigen-presentation by DCs. This could be due to tumor-derived factors, including inhibitory cytokines and Tregs, which dampen the functions of DCs. To overcome this problem, exogenous DCs can be pulsed with different forms of tumor-antigens (TAs), in the form of whole proteins, peptides, messenger RNAs or transgenes of viral vectors and be utilized as vaccines. These DCs have been matured and activated *in vitro*, thereby bypassing the processing and presenting of TA-derived epitopes by endogenous functionally compromised DCs in cancer patients. Various strategies have been studied to optimize exogenous DC-based vaccination protocols(79-81). A recent study has shown that a peptide-loaded DC vaccine targeting both helper $CD4^+$ and $CD8^+$T cells could enhance antitumor $CD8^+$T cell responses and lead to improved clinical outcome in melanoma patients(82). In a study reviewing 32 clinical trials on DC-based vaccines, clinical responses were significantly correlated with the selection of antigens, the use of helper antigen or adjuvant and the induction of TA-specific T cells(83). Despite the success in many melanoma patients, the $CD8^+$T cell responses induced are usually transient and there are still significant portions of patients who show little responses to this vaccine approach. Modulating other factors within DCs or effector T cells, i.e. different maturation stimuli, subsets of DCs used and route of vaccination, the mechanism of antigen delivery or blocking immunoinhibitory signals on $CD8^+$T cells or Tregs may enhance the clinical success of this immunotherapy(84-88).

1.2.2.3 Adoptive Cell Therapy

Adoptive cell therapy (ACT) has achieved very promising clinical results in a good proportion of patients with advanced metastatic melanoma. ACT works by transferring T cells with direct antitumor capacities into cancer patients. This approach bypasses the necessity of eliciting TA-specific T cell responses by cancer vaccines in the immunoinhibitory environment of cancer patients. Instead it could introduce large numbers of antitumor T cells with selected tumor reactivity, avidity, proliferation potential and effector functions(89). Moreover, the TME of cancer patients can be modified to create a better niche for the performance of TA-specific T cells prior to cell transfer.

Autologous tumor-infiltrating lymphocytes (TILs) with lymphodepletion

The first clinical trial with ACT was conducted in metastatic melanoma patients using autologous TILs expanded in IL-2 *in vitro*(90). Although 34% of the patients showed objective regression of cancer, the responses did not last long and the transferred T cells disappeared fast in circulation after the cell transfer. To overcome these limitations, in a later study the isolated autologous TILs were screened for their antitumor activity and TILs populations with high reactive potentials were expanded. In addition, ACT was conducted immediately after a nonmyeloablative lymphodepleting chemotherapy, which led to markedly improved clinical responses and complete tumor regression was achieved in some patients(91). Lymphodepletion contributes significantly to the positive outcome of ACT, which may result from the depletion of Tregs and myeloid-derived suppressor cells (MDSCs) that inhibit effector T cell functions(92). Other studies show that lymphodepletion increases the T cell growth factor IL-15 in blood in patients, which facilitates the expansion of transferred cells(93).

TILs targeting mutated melanoma-specific antigens

Besides the use of autologous TILs for ACT, recent studies show that transfer of T cells that recognize a specific mutated melanoma-specific antigen may achieve better antitumor efficacies. Melanoma is characterized by high mutation rates. One exomic mutation rates study show that melanomas and non-small cell lung cancers have 100 mutations/Mb, which are much

higher than those of other cancer types(94). Studies using other immunotherapeutic regimens suggest that T cells recognizing some mutated TAs naturally exist in the TME of melanoma patients. Dr. Linettes's group and Dr. Rosenberg's group have developed new methods to produce T cells targeting mutated melanoma antigens that could mediate complete cancer regression(89,95).

In order to determine which mutated antigens are immunogenic, polypeptides containing the mutated amino acid (AA) flanked by 10-12 unmutated AAs were linked and predicted with high binding capacity to the patient's HLAs. Those with the most promising binding potential (scores) were pulsed onto autologous APCs and cocultured with TILs. T cells with high reactivity and effector functions, which showed enhanced activation markers, could be expanded and infused back into cancer patients(96). As the prediction of peptide binding with some HLA molecules is not accurate, a minigene approach can be used(97). Minigenes containing the mutated genes flanked by normal sequences on each side were linked and transduced into patient's autologous APCs, in order to be processed and presented for recognition by TILs. These study show that each mutation recognized by TILs was from a distinct protein, and each melanoma sample possesses its unique immunogenic mutated proteins. TILs with antitumor capacity in these patients were reactive to random somatic mutations of melanoma cells. Clinical trials using expanded TILs or engineered chimeric antigen receptor (CAR) T cells targeting immunogenic mutated melanoma antigens led to dramatic regression of metastatic melanoma and significantly improved clinical outcomes, suggesting future studies with cancer vaccines or CAR T cells designed to target cancer-specific mutated antigens instead of overexpressed self antigens may achieve better therapeutic efficacy.

CAR T cells

To apply ACT to non-immunogenic cancers with limited T lymphocytes infiltration, CAR T cells were developed in which T cells isolated from the circulation are transduced with retroviral vectors. The vectors express variable regions of antibody heavy and light chains recognizing a

surface molecule on tumor cells, which are further linked to the intracellular signaling domains of T cell receptors (TCRs), including CD3-zeta chain together with costimulatory domains. CAR T cells recognize antigens expressed on target tumor cells without MHC restriction, and send T cell activation signals that could trigger their antitumor effector functions. Since 2010, CAR T cells have achieved great successes in treating CD19+ lymphoma and leukemia (ALL and CLL) (98,99). One major limitation of CAR T cells, however, is that they may recognize antigens not only expressed on tumor cells but also within normal tissues.

Further development of ACT for immunotherapy of melanoma and other non-immunogenic solid tumors depends on selecting the ideal T cell population with higher proliferation potential and survival advantage in the TME, as well as searching for suitable targets for transferred TCRs or CAR T cells. Preclinical studies have implied that less differentiated central memory T cells would be more potent at mediating tumor regression compared to effector memory T cells or effector T cells(100,101). Moreover, many studies have suggested that CD4+T cells also play an important role in the antitumor immune responses(102), therefore the transfer of TCRs or CAR CD4+T cells alone or in combination with CD8+T cell populations may provide survival advantage for patients with metastatic cancer. Finally, ACT usually targets a single ‘self’ or ‘mutated’ antigen, which may enhance the selection pressure against that antigen and lead to antigen-loss or further mutations. It would be worthwhile to combine several TCRs or CAR T cells subsets with different antigen specificities for ACT and investigate its impact on suppressing tumor growth.

1.3 Challenges within the TME and their impacts on T cells

Although novel melanoma treatment strategies, especially immunotherapy have achieved significant progresses in suppressing tumor growth and have markedly benefited a portion of patients with metastatic melanoma, the overall response rate is still low and more studies have to be conducted to further improve the efficiency of melanoma immunotherapy.

1.3.1 T cell exhaustion

1.3.1.1 Characteristics of exhausted T cells

One major barrier that blocks the efficiency of antitumor T cells is their 'functional exhaustion' they experience over time within the TME. T cell exhaustion was first described during chronic LCMV infection in mice, and was subsequently identified in human with HIV, HBV or HCV infection and cancer. T cell exhaustion is a hyporesponsive status of T cells characterized by sequential upregulation of co-inhibitory molecules on T cells and loss of effector T cell functions in a hierarchical manner. Exhausted T cells usually express enhanced levels of PD-1, lymphocyte activation gene 3 protein (LAG-3), CD244 (2B4), CD160, CTLA-4, T-cell immunoglobulin domain and mucin domain protein 3 (TIM-3) and so on(103). Functions such as IL-2 production and cytotoxic capacity are lost first, while production of tumor necrosis factor (TNF)-α and proliferation potentials are lost in the middle stage; IFN-γ production is lost at the advanced phase of exhaustion(43).

Both functionally exhausted $CD8^+$ and $CD4^+$ T cells possess unique transcriptional signatures that distinguish them from effector or memory T cells. Genes involved in co-stimulatory and co-inhibitory molecules expression, T cell signaling pathways, cytokines productions and various metabolism pathways are all significantly affected(104,105). Transcriptional factors T-bet and Eomes are well studied in exhausted T cells; they define the lineage of these cells and have crucial functions in maintaining the pool of exhausted T cells with certain antigen specificity. They mediate exhaustion-specific functions that are different from their functions in effector T cells. During acute infection, T-bet plays an important role in the formation of terminally differentiated cells while Eomes is involved in maintaining the homeostatic proliferation of central memory T cells(106,107). However in the case of chronic infection, T-bet suppresses the expression of PD-1 and maintains the proliferative potential of a fraction of exhausted T cells while Eomes is associated with the terminal differentiation of exhausted T cells(108). The $T\text{-}bet^{hi}PD\text{-}1^{int}$ cell population maintains a pool of exhausted antigen-specific T cells with weak effector functions, while a larger $Eomes^{hi}PD\text{-}1^{hi}$ cell subset is more terminally differentiated but has better cytotoxic

function. Both factors are crucial for the long-term maintenance of the exhausted T cells, depleting either factor will result in the disruption of immune system-pathogen/cancer balance and lead to accelerated disease progression. These findings have been observed in human HCV and HIV infection(108,109). In addition, many other transcription factors, such as Blimp1, NFAT, FoxO1 have special functions in regulating exhausted $CD8^+$T cells. More recently, it was found that co-inhibitors expression during T cell exhaustion is also regulated at the epigenetic level, suggesting another important layer of gene regulation in exhausted T cells that may imprint the exhaustion in the epigenome(110).

1.3.1.2 Mechanisms that contribute to T cell exhaustion within TME

Continuous antigen stimulation is traditionally viewed as the cardinal cause of T cell exhaustion. The level of antigen persistence during mouse LCMV infection or human HIV infection positively correlates with the severity of exhaustion (111,112). TME possess abundant tumor antigens, which combine with the inflammation in the microenvironment may contribute to the formation of exhausted antigen-specific TILs. In addition, TME contains various immunoinhibitory factors, such as inhibitory ligands, tumor stromal cells, immunosuppressive cells, inhibitory cytokines and deprivation of key nutrients, which form a dense network that may directly or indirectly promote T cell exhaustion.

Inhibitory ligands: Tumor cells, tumor stromal cells and other cells within TME usually show enhanced expression of different inhibitory molecule binding ligands, which through binding with co-inhibitory molecules overexpressed on TILs could send non-redundant signals that adjust the magnitude of T cell exhaustion. One of the most prevalent pathways in melanoma TME is the PD-L1-PD-1 interaction. Melanoma cells with enhance PD-L1 expression are mainly found in proximity to IFN-γ producing TILs, suggesting that immune response within melanoma TME contributes to PD-L1 expression, a phenomena termed “adaptive immune resistance”(113). The mechanism through which this pathway leads to T cell dysfunction is not well understood. Some studies suggest that PD-1 may modulate the activity of signaling networks downstream of the TCR by recruiting phosphatases SHP-1 and SHP-2 to its immunoreceptor tyrosine-based

inhibitory motif (ITIM) and immunoreceptor tyrosine-based switch motif (ITSM), which dephosphorylates the TCR signaling intermediaries and suppress downstream pathways including PI3K/ AKT/mTOR and RAS signaling(114).

Immunosuppressive cells: The presence of Tregs, MDSCs, tumor-associated macrophages (TAMs), tumor stromal cells and dysfunctional dendritic cells may contribute to T cell exhaustion through different pathways. Tregs express ectoenzymes CD39 and CD73, which may generate pericellular adenosine that dampen the function of effector T cells(115). In addition, Tregs have high expression of CD25, which could deplete IL-2 within the local microenvironment and impair T cell function(116). The production of inhibitory cytokines by Tregs, such as transforming growth factor β (TGF-β) and IL-10, could also suppress the functions of effector T cells and contribute to their exhaustion(117,118). MDSCs and TAMs may induce T cell exhaustion through PD-L1 and PD-1 interactions(119). Their abnormal activities of arginase 1 and nitric oxide synthase deplete local L-arginine, which inhibits T cell proliferation and functions. Tumor tissues also contain plasmacytoid dendritic cells, which express decreased co-stimulatory molecules such as CD86 and CD40 but increased levels of PD-L1 and indoleamine 2,3-dioxygenase (IDO)(120). IDO depletes the essential amino acid L-tryptophan, which will inhibit T cell functions.

Soluble mediators: These molecules include immunoinhibitory cytokines such as IL-10 and TGF-β, as well as inflammatory factors including IL-4, IL-6, IL-13 and type I interferons (IFNs). All factors may accelerate T cell exhaustion within the TME either directly or through regulating the functions of other cell types. Blocking the activities of these cytokines have the capacity to partially restore T cell functions and slow tumor progression(121). A summary of different pathways that contribute to T cell exhaustion is shown below (**Figure 1-2**). Finally, it is important to note that exhausted T cells still possess suboptimal but crucial functions that keep tumor progression in check. T cell exhaustion is also reversible; therefore immunotherapeutic strategies that recover the functions of exhausted T cells, such as the application of anti-PD-1/PD-L1 checkpoint inhibitors, could substantially prolong the survival of patients with metastatic melanoma.

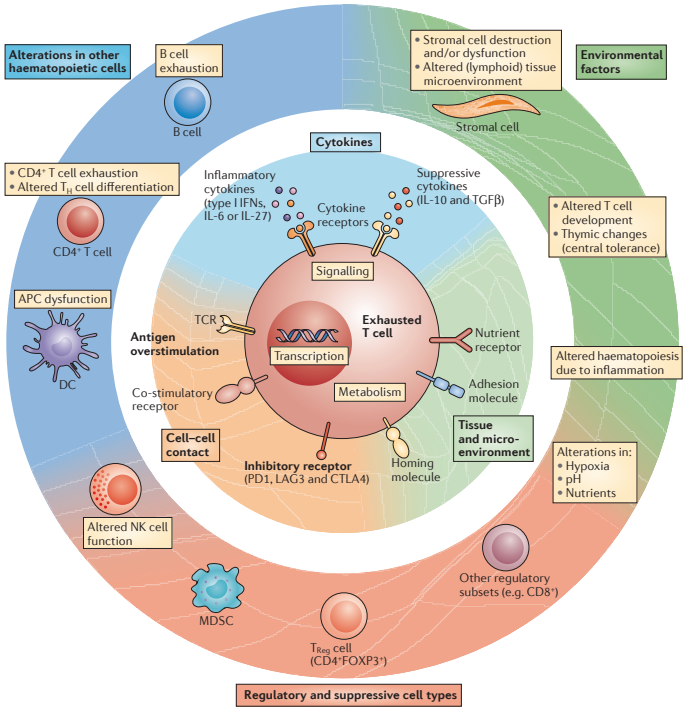

Figure 1-2: Overview of the mechanisms that contribute to T cell exhaustion. Inner circle: Three major factors may play important roles in driving T cell exhaustion: cell-cell contact including antigen overstimulation through TCR ligation, and the interaction of inhibitory receptors; the presence of suppressive cytokines; tissue and microenvironment factors such as local nutrients and oxygen depletion, altered pH, and dysregulation of lymphoid organizations. The outer circle shows different types of cells that may contributes to the changes in TME that affect T cell functions. Figure is adapted from Wherry and Kurachi, 2015(121).

1.3.2 Tumor stroma and cancer-associated fibroblasts (CAFs)

Tumor cells themselves are not fully responsible for the immunosuppressive microenvironment. Most epithelial-derived cancers require the support of mesenchymal-derived stromal cells, which play a pivotal role in the complicated communication network with cancer cells and immune cells to provide the appropriate TME for neoplastic cell expansion and metastasis. Tumor stroma promotes tumorigenesis by suppressing the immune control of tumor growth, providing nutritional support required for tumor mass maintenance, stimulating angiogenesis, cancer cell proliferation and invasion(122-124). Tumor cells and the tumor stroma exist in a dynamic network of interactions through the secretion of a plethora of growth factors and cytokines, including TGF-β, VEGF, IL-4 etc (123). The reactive tumor stroma constantly

modifies the ECM and induces neoangiogenesis, therefore creates a TME that is conductive to growth and metastasis of the tumors(125). The induction of reactive tumor stroma blocks immune cell infiltration and impairs T cell responses in the TME, and is linked to poor prognosis in various cancers.

The supporting stroma of melanoma contains an abundance of connective tissue, blood vessels, inflammatory cells such as lymphocytes and myeloid cells, extracellular matrix (ECM) components and cancer-associated fibroblasts (CAFs). CAFs are present in aberrantly high frequencies in the tumor. They are phenotypically and functionally distinct from normal fibroblasts in normal tissues by increased proliferation rate and differential expression of ECM components and growth factors(123,126). CAFs are activated by growth factors and cytokines in the TME and contribute to tumorigenesis in all stages of tumor progression. In addition, CAFs promotes angiogenesis through VEGF production, and enhance the metastatic potential of cancer cells through production of proinflammatory factors. Moreover, CAFs represent a major source of inhibitory cytokines such as IL-10 and TGF-β; they therefore contribute to the local immunosuppressive environment(123,127) and dampen antitumor T cell responses induced by immunotherapy. The functions of CAFs during tumorigenesis are shown below (**Figure 1-3**).

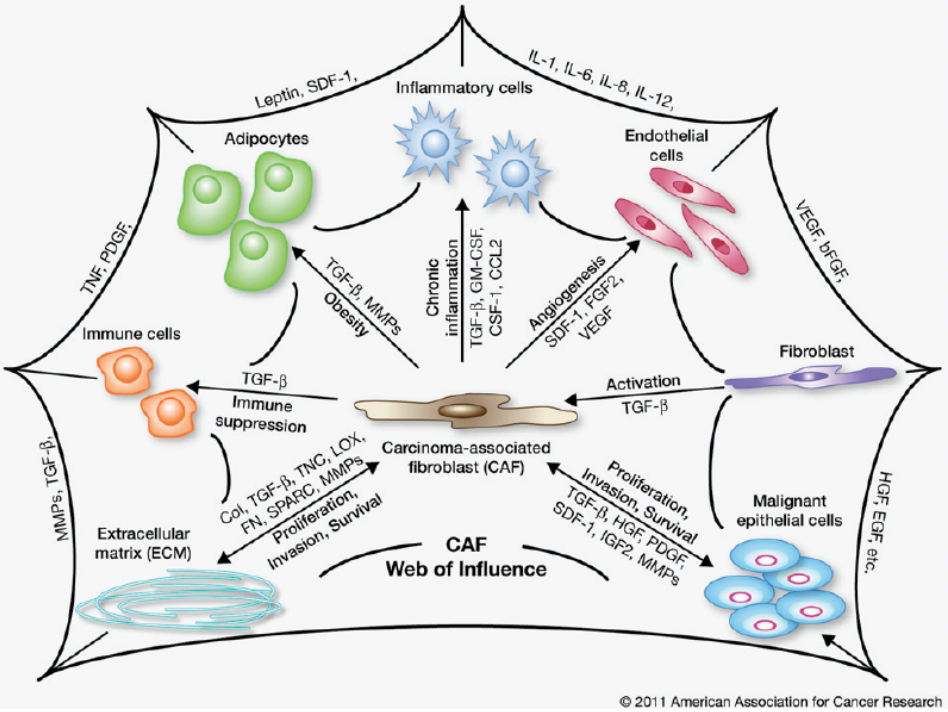

Figure 1-3: Illustration of the mechanisms utilized by CAFs to promote tumor development. CAFs are originated from endothelial cells, malignant epithelial cells through epithelial-to-mesenchymal transition (EMT) or are transformed from normal fibroblasts. CAFs enhance cancer cell proliferation, invasion, modify ECM composition, promote angiogenesis while inhibit immune cell functions. These effects are mediated through the secretion of numerous growth factors, cytokines and proteases as illustrated. CAFs also affect functions of adipocytes and inflammatory cells within TME, which indirectly promote tumor growth. Ac, acetyl; AFC, 7-amino-4-(trifluoromethyl) coumarin;bFGF, basic fibroblast growth factor; CCL2, chemokine (C-C motif) ligand 2;Col, collagen; DPP-II (IV, 6, 7, 8, 9, 10), dipeptidyl peptidase-II (IV, 6, 7, 8, 9, 10); FN, fibronectin; GM-CSF, granulocyte macrophage colony-stimulating factor; HGF, hepatocyte growth factor; IGF2, insulin-like growth factor 2; LOX, lysyl oxidase; SDF-1, stromal cell-derived factor 1; SFRP-1, secreted frizzled-related protein 1; SPARC, secreted protein, acidic and rich in cysteine; TNC, tenascin-c.
Figure is adapted from Brennen et al., 2012(127).

One key feature of transformed CAFs is that they express the highly selective fibroblast activation protein (FAP). FAP is a type II membrane-bound glycoprotein and a member of the serine protease family that has dipeptidyl peptidase and collagenase activities. FAP is not present at high levels on tumor cell, normal fibroblasts or in normal adult tissues(126). FAP+ stromal fibroblasts are required for maintenance of the tumor microenvironment(126). They suppress the immune response to tumors by producing stromal cell-derived factor-1 (SDF-1/CXCL12), which can attract regulatory T cells, MDSCs and TAMs into the tumor(128,129). They also induce random movement of effector T cells, which interferes with T cell-tumor cell interactions and hinders tumor destruction(130). Genetic FAP depletion can lead to profound

tumor growth inhibition, through a mechanism that was shown to be dependent on host immunity, in particular on IFN-γ and TNF-α production(124). Vaccines targeting FAP or T cells with a FAP-specific chimeric antigen receptor (CAR) inhibit tumor growth in part by enhancing tumor-specific immune responses and they increase tumor mice survival(131-133). A key advantage of FAP^+ CAFs over tumor cells is that they are genetically stable, they thus represent an ideal therapeutic target with reduced risk of development of resistance. Strategies that depleting the immunosuppressive CAFs or re-educating them to become normal fibroblasts have the potential to significantly improve the overall efficacy of melanoma immunotherapy in patients.

1.3.3 Immunosuppressive cells

As mentioned above, there are various immunosuppressive cell populations within the TME, all of them can promote tumorigenesis and suppress functions of TILs through different mechanisms.

Tumor-associated macrophages (TAMs): Macrophages are usually viewed as effector cells that enhance immune defense against cancer at the onset of tumor initiation. However during tumor development, macrophages are educated to become immunosuppressive and promote tumorigenesis(134). This transition is partially mediated by the change of the cytokine and growth factor milieu within TME, from a Th1 type inflammatory environment consisting of IFN-γ, GM-CSF etc. to a Th2-type anti-inflammatory setting containing TGF-β, IL-4, Il-10, IL-13 and M-CSF, with the former setting promoting 'classic activated' M1-macrophages formation while the latter facilitating the polarization of 'alternatively activated' M2-macrophages(135-137). In addition, it is suggested that other conditions such as lack of oxygen supply within the TME could induce this functional switch of macrophages(138). Within established melanoma, most of the TAMs bear a M2 phenotype, with enhanced secretion of IL-10 and TGF-β{Quatromoni:2012wp}. One major function of TAMs is to drive the tumor cell invasion through the colony-stimulating factor 1 (CSF-1)-epidermal growth factor (EGF) interaction loop. Tumor cells secrete CSF-1, which works as chemoattractant to recruit TAMs. TAMs produce EGF

and works in a paracrine manner to promote the invasive phenotype of cancer cells(139,140). In addition, TAMs secrete CCL22 and proteases such as cathepsin, which recruit Tregs to TME and promote tumor growth, angiogenesis and invasion(141,142). All of these conditions will suppress functions of TILs.

Myeloid-derived suppressor cells (MDSCs) and regulatory T cells (Tregs): MDSCs are a heterogeneous population of cells of myeloid origin, which consist of myeloid progenitor cells and immature myeloid cells (IMCs) that are originated from the bone marrow. In conditions such as infectious diseases and tumor development, IMCs can not fully differentiate into mature macrophages, dendritic cells or granulocytes and this immature cell subset with immunosuppressive activities will expand in different tissues(143). In mice, MDSCs are characterized by their expression of surface antigens Gr-1 and CD11b. They contain two subsets with distinct functions to suppress T cell activities, i.e., monocytic (MO) MDSCs, which are phenotypically Gr-$1^{int}CD11b^{+}$, and granulocytic (polymorphonuclear, PMN) MDSCs, which are Gr-$1^{hi}CD11b^{+}$(144).

The expansion and activation of MDSCs is induced by factors secreted by tumor cells, tumor stromal cells and activated T cells, i.e. VEGF, GM-CSF, G-CSF, IFN-γ, TGF-β, IL-4, IL-6, IL-10, IL-13, CCL2, CXCL5, CXCL12 etc., all of which stimulate myelopoiesis and inhibit the differentiation of IMCs(145-153). Most of these factors induce MDSCs expansion and inhibitory functions through activation of Janus kinase (JAK) family members and signal transducer and activator of transcription (STAT) pathway(143,154). MDSCs suppress T cell functions through the secretion of soluble factors including arginase 1(Arg1), inducible nitric oxide synthase (iNOS), reactive oxygen species (ROS) and peroxynitrite, which require direct cell-cell contact and suppress T cell activities through different mechanisms. For example, both Arg1 and iNOS catabolize L-arginine, an important amino acid that is required for T cell proliferation. Depleting its availability within TME limits T cell proliferation. In addition, the catabolism of L-arginine by iNOS produces nitric oxide (NO), which suppresses T cell function by inhibiting the JAK3-STAT5 pathway in T cells and inducing cell apoptosis(155,156). Peroxynitrite induces the nitration and

nitrosylation of amino acids such as cysteine, tryptophan and tyrosine(157,158). Studies have shown that during direct MDSC-T cell interaction, the production of peroxynitrite by MDSCs can lead to nitration of the TCR and CD8 molecules, which decrease the binding capacity of MHC-peptide complex to the TCR and reduce T cell effector functions in an antigen-specific manner(159,160). Moreover, it has been shown that MDSCs could promote the *de novo* generation of Treg cells through the production of cytokines such as IL-10(146,161). Tregs promote tumorigenesis and inhibit T cell functions through different mechanisms, such as by suppressing antigen presentation within the TME and inhibiting the cytolytic granule releases by effector $CD8^+$T cells(162).

Successful cancer immunotherapy depends on the inhibition or removal of immunoinhibitory factors and cell populations. Therefore, strategies that could promote MDSCs differentiation, or could inhibit their proliferation and functions will effectively improve the efficacy of cancer vaccines or adoptive T cell transfer in melanoma patients.

1.3.4 Metabolic defects

(This section is adapted from my review article: **Zhang Y**, Ertl HC. Starved and asphyxiated: how can CD8+ T cells within a tumor microenvironment prevent tumor progression. **Frontiers in Immunology** 2016; 7(32).)

The etiology of T cell exhaustion within the TME warrants further discussion. High levels of antigen as found during chronic viral infections may not be solely responsible. The amount of antigens within a tumor would not be expected to be overwhelming, especially as tumor cells commonly down-regulate MHC class I expression (163), which makes their antigens virtually invisible to $CD8^+$T cells. Instead I hypothesize that $CD8^+$T cell exhaustion may be triggered by metabolic stress within the TME.

Following antigenic stimulation, differentiation of naïve $CD8^+$T cells into effector cells is accompanied by metabolic reprogramming to accommodate their increased demand for energy and biomass formation. Resting $CD8^+$T cells primarily gain energy through oxidative phosphorylation (OXPHOS), the mitochondrial pathway of energy production (164). The tricarboxylic acid (TCA) cycle, which is linked to OXPHOS, oxidizes acetyl-CoA. This metabolite

can be derived from carbohydrates, amino acids or FAs. Upon $CD8^+$T cell activation, T cell receptor (TCR) and co-stimulator CD28 ligation activates the phosphatidylinositol 3-kinase (PI3K) / protein kinase B (Akt) / mammalian target of rapamycin (mTOR) pathways, which in turn increase the activity of hypoxia-inducible factor (HIF)-1α and Myc (165). HIF-1α augments surface expression of Glut1 and thereby allows for increased uptake of glucose, while Akt and Myc increase the activity of several glycolytic enzymes (166-168). All of these signals drive activated $CD8^+$T cells to rely increasingly on glycolysis after activation. The activity of the mitochondrial OXPHOS pathway is also enhanced (169). Cancer cells also ferociously consume glucose to fuel energy production through glycolysis, which can lead to hypoglycemia within tumors. In addition, angiogenesis often lags behind expansion of solid tumors, leading to hypoxia in some areas of the TME. T cells that infiltrate solid tumors thus face dual metabolic jeopardy; lack of glucose prohibits energy production through glycolysis while lack of O_2 prevents energy production through OXPHOS. How tumor-specific $CD8^+$TILs cope with these challenges and how metabolic reprograming of $CD8^+$TILs will affect their antitumor performance require further investigations, in order to improve the efficacy of cancer immunotherapy.

1.3.4.1 Effects of hypoxia on $CD8^+$TIL metabolism and functions

Solid tumors commonly have areas of hypoxia. This can be caused by lack of perfusion due to structural and functional abnormalities of the tumor microvasculature, general anemia of the patient or insufficient diffusion due to lack of angiogenesis. The latter affects cells once they are more than 70 μM away from a blood vessel. Studies have shown that up to 50-60% of solid tumors of a variety of different types possess unevenly distributed areas of hypoxia (170).

Tumor-infiltrating $CD8^+$T cells are initially activated under physiological O_2 tension in peripheral lymphatic tissues. Upon tumor entry, $CD8^+$T cells will be subjected to increasingly severe hypoxia once they leave areas close to blood vessels; this will activate HIF-1α. HIF-1α signaling adjusts the cells' metabolism to allow for energy production when O_2 is limiting. HIF-1α enhances glycolysis by $CD8^+$T cells mainly by promoting the activity of lactate dehydrogenase A (LDHa), while inhibits OXHPOS by increasing expression of pyruvate dehydrogenase kinase

1(PDK1), which prevents the oxidation of pyruvate to acetyl-CoA (171,172). $CD8^+$TILs under hypoxia therefore must increase glucose consumption to fuel glycolysis.

A series of *in vitro* and *in vivo* studies in the past two decades show that hypoxia dampens lymphocyte activation, diminishes their proliferation, and reduces the ability of activated T cells to produce cytokines or lytic enzymes (173-179). T cell activation causes release of Ca^{2+} from intracellular stores followed by sustained Ca^{2+} influx, which is inhibited by increased HIF-1α activity (180). Whole body hypoxia dampens inflammation and T cell functions in mice and humans (181,182). These data show that hypoxia is immunosuppressive and metabolic reprograming due to increased activity of HIF-1α may contribute to reductions of immune responses. This could be caused by reduced ATP production due to impaired OXPHOS under hypoxia. Additionally, hypoxia is known to increase accumulation of reactive oxygen species (ROS), which may induce apoptosis of activated T cells (183,184). *Vice versa,* activated $CD8^+$T cells with a partial deficiency in HIF-1α show enhanced production of cytokines (185,186). One study has shown that under hypoxia or with increased HIF-1a activity T cells increase expression of co-inhibitors including CTLA-4, CD244 and LAG-3 and decrease levels of T-bet (187), a key transcription factor that controls many of the T cells' functions, again indicating that hypoxia is immunosuppressive.

Conversely, two recent reports show that hypoxia and increases in HIF-1α activity promote effector T cell functions, especially production of the lytic enzymes granzyme B and perforin (187,188). There is a caveat with these studies; both used a protocol in which after an initial 48 hours of activation, $CD8^+$T cells were rested for several days in IL-2-supplemented medium before being subjected to hypoxia. Unlike highly activated $CD8^+$T cells, resting $CD8^+$T cells rely more on FAO and OXPHOS for energy production. This metabolic reprogramming and their decreased energy demand may allow $CD8^+$T cells to improve some functions upon hypoxia. In real life $CD8^+$T cells induced by a cancer vaccine or tumor antigens that leaked into lymphatic tissues are unlikely to rest before they infiltrate a tumor, where they may receive additional activation signals. Results obtained with resting cells are thus not pertinent to TILs exposed to

hypoxia. The same papers showed that genetic depletion of HIF-1α reduces $CD8^+$ T cell functions while its constitutive overexpression through functional depletion of the Von Hippel-Lindau (VHL) factor improves functions. During the initial phase of T cell activation, HIF-1α is essential to allow T cells to use glycolysis. The effects of its complete absence or increased expression during this critical phase of differentiation may differ from changes in HIF-1α activity during later phases of activation. These studies thus give limited insights into the effect of hypoxia or HIF-1α on $CD8^+$TILs, which encounter limited O_2 after activation in the periphery once they penetrate into the tumor.

Hypoxia and increased HIF-1α activity in tumor tissues in general correlate with poor prognosis of cancer patients (34, 35). Hypoxia not only affects protective immune responses but also promotes tumorigenesis by enhancing proliferation of cancer cells and increasing their PD-L1 surface expression (189). The latter in turn may further dampen functions and survival of PD-1^+TILs. Hypoxia may also increase the suppressive activity of tumor-infiltrating myeloid suppressor cells and tumor-associated macrophages, which will lead to further impairments of $CD8^+$TIL functions (190,191). Overall, all of these studies strongly suggest that lack of O_2 negatively affects metabolism and functions of $CD8^+$TILs.

1.3.4.2 Effects of hypoglycemia on metabolism and functions of TILs

Glucose is crucial during the initial stages of $CD8^+$ T cell activation. Naïve $CD8^+$T cells can differentiate into effectors in absence of glucose but then become functionally impaired (192). Lack of glucose also dampens effector functions of fully activated $CD8^+$T cells both *in vitro* and *in vivo* (192-197).

Attracted by chemokines, activated $CD8^+$T cells regardless of their antigen-specificity infiltrate solid tumors. Here they encounter an environment where key nutrients such as glucose may be limiting due to its consumption by tumor cells (198). Although activated $CD8^+$T cells express increased levels of the glucose transporter Glut1, *in vitro* studies show that their effort to take up glucose is thwarted by tumor cells, which are simply more effective at consuming this key nutrient (192). $CD8^+$T cell glycolysis within TME may further be reduced by accumulating

concentrations of tumor cell-derived lactate, which prevents the monocarboxylate transporter-1-mediated, gradient-dependent export of lactate from $CD8^+$T cells. Increasing concentration of lactate within $CD8^+$T cells in turn causes a fall in pH, which inhibits the activity of phosphofructokinase, a key enzyme of glycolysis (199). In addition, glucose deprivation increases co-inhibitor PD-1 expression on activated $CD8^+$T cells (200), which can further reduce glycolysis but enhance FA metabolism. Blockade of PD-1 has been shown to lessen the $CD8^+$TILs' metabolic stress by augmenting their glycolytic capacity through increased mTOR signaling (192).

It has been reported that FAO can maintain the survival of cancer cells when glucose is not available (201). T cells may also be able to cope with lack of glucose by enhancing other metabolic pathways. Sudden deprivation of glucose can lead to drops in ATP with enhanced AMP in activated $CD8^+$T cells. The increased AMP: ATP ratio activates the energy sensor AMP-activated protein kinase (AMPK). AMPK is a key regulator that reduces the T cells' energy expenditure by blocking production of cytokines (202). Furthermore, AMPK maintains T cell viability by decreasing glycolysis and anabolic processes through inhibition of the mTOR pathway, while enhancing OXPHOS fueled by FAs and glutamine (203,204). In agreement the studies showed that knockout of AMPK increases apoptosis of T cells activated with limited access to glucose (202).

To what degree $CD8^+$TILs' functions are impaired by lack of glucose within the TME may depend on the T cells' differentiation status, or, in other words on their metabolic programming prior to entering the tumors. Recently activated $CD8^+$ effector T cells conditioned to use glycolysis are likely most susceptible to sudden loss of exogenous glucose (205,206), as compensatory endogenous production of glucose through gluconeogenesis or glycogen degradation are not sustainable (207). In contrast, $CD8^+$T cells programmed to use other nutrients may cope better with restricted glucose access (208). This in turn invites the testing of metabolic drugs that reprogram T cell metabolism as adjuvant treatments for active cancer immunotherapy or adoptively transferred TA-specific T cells.

1.3.4.3 Effect of hypoxia combined with hypoglycemia on $CD8^+$TIL functions and metabolism

Hypoxia inhibits OXPHOS but allows cells to gain energy through glycolysis. Hypoglycemia on the other hand reduces glycolysis but cells can switch to OXPHOS by burning other nutrients. The problem is that many tumors have low levels of glucose combined with areas of hypoxia, which foils both pathways of energy production.

Malignant cancer cells increase lipogenesis, lipolysis, FA secretion and recruit adipose progenitors to the TME (209-211). In addition, dying tumor cells may release FAs. FAs provide ample energy through peroxisomal or mitochondrial FAO, which may be used by $CD8^+$TILs. FAO is preferred by some effector T cells such as those participating in graft versus host disease (212) and it is suggested that FAO may be preferred by T cells that encounter large quantities of antigens (213). Energy production through FAs requires more O_2 than energy production through glucose to generate equivalent amounts of ATP. OXPHOS fueled by glucose yields 36 molecules of ATP and consumes 6 molecules of O_2. In contrast, OXPHOS fueled by palmitate, a 16-carbon FA, results in a net yield of 129 ATP and requires 31 molecules of O_2. FAs thus require 1.44 times more O_2 than glucose to provide the same amount of energy, which makes it an inefficient fuel within an O_2-deprived TME.

Ketone bodies, i.e., acetoacetate, acetone and b-hydroxybutyrate, are produced during FA catabolism when the amount of acetyl-CoA produced by FAO overwhelms the processing capacity of the TCA cycle. When acetyl-CoA declines, ketone bodies can be converted back to acetyl-CoA providing a ready source of energy that requires less O_2 than catabolism of FAs (214). Previous studies showed that under conditions of hypoxia and hypoglycemia, cells of the nervous system maintain their energy balance through the use of ketone bodies (215). We propose that $CD8^+$TILs may do the same. T cells may take up ketone bodies from the surrounding or they could synthesis them directly (214,216,217).

$CD8^+$TILs are not stationary; they migrate throughout the TME (218) and we assume that their environment changes accordingly. When T cells are close to vessels and O_2 is readily available, FAs may fuel the TCA cycle and excess FA-derived acetyl-CoA can be converted into ketone bodies. When T cells penetrate deeply into the tumor and O_2 becomes

scarce, T cells may burn ketone bodies to sustain their energy requirement. As has been shown during heart ischemia, lack of O_2 results in increases in AMPK, which decreases the activity of acetyl-CoA carboxylase (ACC) that converts acetyl-CoA to malonyl-CoA. Once cells have access to O_2, such upon reperfusion of an ischemic heart or migration of TILs to areas close to vasculature, lack of malonyl-CoA will cause a surge in FAO (219). Lipid metabolism has been shown to correlated with long-term survival in many different cell types (220,221). It has been suggested that PD-1 ligation, which prevents terminal differentiation of effector $CD8^+$T cells (222), promotes survival by enhancing the cells' FA metabolism (223). Ketone body metabolism also promotes metabolic fitness and longevity of cells by regulating histone deacetylase (HDAC) activities (214). Catabolism of these carbon sources may allow T cells to survive under hypoglycemia and intermittent hypoxia. The potential metabolic pathways utilized by naive or activated T cells under normal or different metabolically stressed conditions are illustrated (**Figure 1-4**).

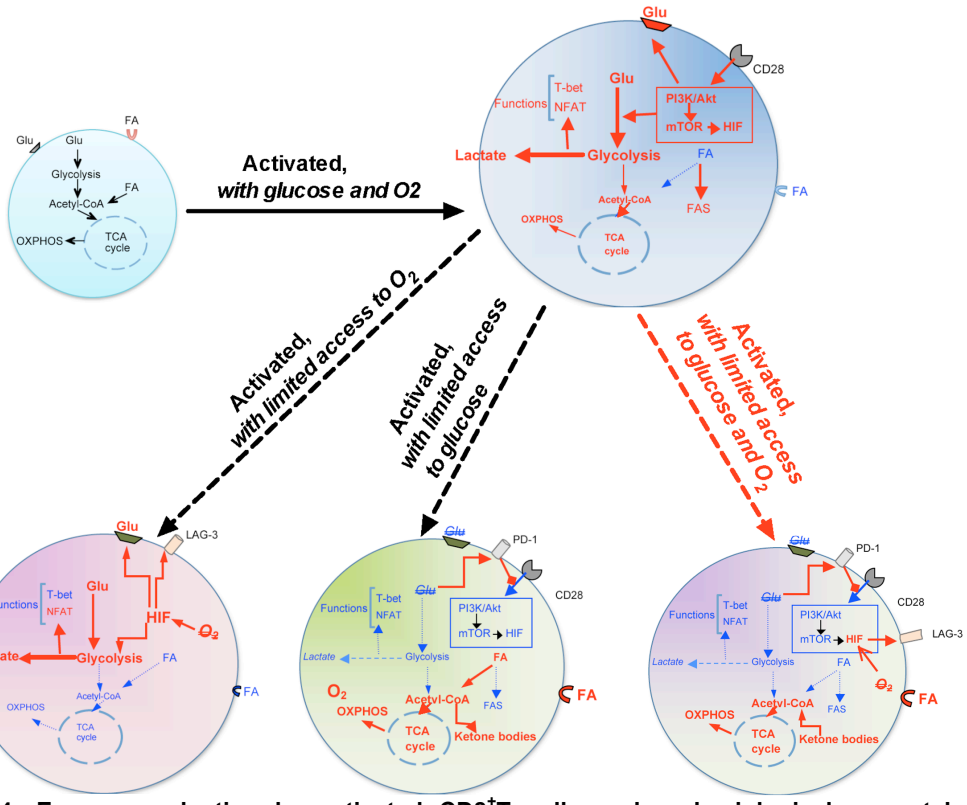

Figure 1-4: Energy production by activated CD8$^+$T cells under physiological or metabolically challenging conditions. The potential signaling pathways after T cell activation under different conditions and how they affect the metabolic pathways of activated CD8$^+$T cells are illustrated. Blue: activity goes down; Red: activity goes up; Bold: increased activity; Dashed: decreased activity; Italic with double strikes: limited access. Glu: Glucose; FA: Fatty acid; PI3K: Phosphoinositide 3-kinase; Akt: Protein kinase B; mTOR: Mechanistic target of rapamycin; HIF: Hypoxia-inducible factors; O_2: Oxygen; OXPHOS; Oxidative phosphorylation: NFAT: Nuclear factor of activated T cells; T-bet: T-box transcription factor TBX21; PD-1: Program Cell Death-1; LAG-3: Lymphocyte-activation gene 3.

1.3.4.4 Exploring metabolic manipulations to improve T cell-mediated immunotherapy of cancer

Adoptive transfer of e*x vivo* expanded TILs has achieved some successes in treatment of melanomas (224). Alternatively, T cells from peripheral blood can be modified to express chimeric antigen receptors (CARs) that recognize cell surface expressed tumor antigens independent of major histocompatibility antigens (225). Transfer of such CAR-T cells has been remarkably successful in treatment of acute lymphatic leukemia or B cell lymphoma but in general yielded disappointing results in patients with solid tumors (226-230). This has been blamed on the immunosuppressive nature of the TME (231,232). Treatments that reduce numbers or functions of regulatory T cells, myeloid suppressor cells, tumor-associated macrophages or that block

immune checkpoints have improved the efficacy of adoptive cell transfer for cancer therapy (233,234).

As already mentioned, the metabolic profile of $CD8^+$T cells prior to their tumor infiltration has significant impacts on their longevity and performance within TME. In addition, the metabolic profiles of the tumor cells will influence what nutrients are available to T cells. Some studies show that drugs, which inhibit glycolysis by tumor cells such as Glut1 inhibitors cause tumor regression and increase glucose supply within the TME (235,236). Its use prior to cell transfer could increase the efficacy of cell immunotherapy. Others have shown that reducing glucose consumption by tumor cells through blockade of PD-L1 signaling allows for increased glycolytic energy production by $CD8^+$TILs, which is accompanied by improvements of their functions (192). A recent study shows that glucose limitation leads to reduction of the glycolysis metabolite phosphoenoylpruvate (PEP), which is essential for Ca^{2+}-NFAT signaling in $CD8^+$TILs. Overexpressing phosphoenolpyruvate carboxykinase (PCK) 1, which converts the TCA cycle intermediate oxaloacetate to PEP, was shown to improve NFAT signaling and function of TILs (197).

However, glycolysis may accelerate terminal differentiation of $CD8^+$T cells and thereby shorten T cell survival (237); thereby, limiting glycolysis by $CD8^+$TILs may yield better therapeutic effects. One study showed that inhibition of glycolysis by 2-deoxyglucose during *in vitro* expansion of TA-specific $CD8^+$T cells increases their efficacy in a mouse melanoma model (205). A similar effect was seen when TILs were treated prior to adoptive transfer with an Akt inhibitor, which reduces their use of glycolysis and increases OXPHOS (208). Along the same line, when $CD8^+$T cells were cultured *in vitro* with IL-7 or IL-15, which drives their differentiation towards memory, their antitumor efficacies *in vivo* significantly improved (238-240). Further studies showed that adoptive transfer of central memory $CD8^+$ T cells confers better eradication of solid tumor masses than transfer of equal numbers of effector $CD8^+$ T cells (241,242), which led the authors to conclude that the T cell differentiation status, which dictates potential for proliferation, is crucial to ensure optimal efficacy of adoptive T cell transfer. I think that the

metabolic reprogramming towards preferential use of FAO and OXPHOS as naturally occurs during differentiation from effector to memory cells, may allow for the superior performance of the transferred T cells within TME.

Immunotherapy of cancer is still in its infancy. T cells are able to stop an infection by rapidly killing millions of infected cells but they clearly need additional help to eliminate tumors. In recent years exciting new studies have started to illuminate the metabolism of T cells under different conditions and its impact on T differentiation and functions. A better understanding of the metabolic programs utilized by $CD8^+$TILs and how they affect the TILs' antitumor performance is crucial to find new therapeutic targets for cancer immunotherapy. Metabolic manipulations that could prepare TA-specific T cells, which are either induced by cancer vaccines or expanded *ex vivo* in form of TILs or CAR-T cells, to optimally cope with the metabolic constrains within the TME may significantly improve the overall antitumor efficacy. Undoubtedly the type of cancer and peculiarities of its TME will dictate the most suited metabolic treatment.

1.4 Objectives Of The Study

Metastatic melanoma is largely refractory to existing therapies and has a very poor prognosis. Despite the significant progresses made in the cancer immunotherapy field in recent years, only a small proportion of melanoma patients show positive clinical responses. There are several major barriers to improve the efficacy of immunotherapy for solid tumors. First, the specific $CD8^+$ T cell responses against tumor antigens can be severely dampened by the prevalence of immunosuppressive ligands expressed within TME. Second, the immune control of tumor growth can be directly suppressed by tumor stromal fibroblasts, which suppress immune responses through different mechanisms. Third, tumor cells are capable of evading the immune pressure exerted by vaccine- or T cell transfer-induced immune responses due to the advantageous growth of non-targeted subpopulations, further impairing the efficacy of immunotherapy. In addition, T cells become functionally exhausted within the TME during tumor

progression, which is traditionally viewed as a result of chronic exposure to cancer antigens. Our preliminary data suggest that the metabolic stresses, including glucose and oxygen limitation in late stage tumors, may lead to the metabolic alteration and functional impairment of TILs.

The overall goal of my thesis project is to develop novel immunotherapeutic strategies against melanoma that can overcome the immunosuppressiveness of the TME, reduce the exhaustion of TILs and thus achieve sustained tumor regression. The vaccines I designed against melanoma are based on chimpanzee-derived adenoviral vector AdC68, which is known to induce potent $CD8^+$ T cell responses. I hypothesize that the melanoma cell targeting vaccine not only has to express multiple melanoma antigens in an immunogenic form but also has to overcome the low responsiveness of TA-specific $CD8^+$T cells. Furthermore, the novel cancer treatment strategies have to contain components that directly reduce the TME's ability to suppress tumor-specific immune responses. In my thesis I addressed this hypothesis through the following aims:

Specific Aim 1: To determine whether blocking prevalent immunoinhibitory pathway during T cell priming could reduce the exhaustion of melanoma-associated antigens (MAAs)-specific $CD8^+$T cells in the TME and improve the antitumor efficacy of cancer vaccine.

Co-expression of several different immunogenic antigens in one vaccine can minimize the frequent immune escape of tumor cells. In addition, studies by our lab have shown that vaccines expressing antigens as fusion proteins within herpes simplex virus glycoprotein D (gD) can induce markedly enhanced antigen-specific T cell responses through disruption of the immunosuppressive B-and T-lymphocyte attenuator (BTLA)-herpesvirus entry mediator (HVEM) signaling pathway in the TME(243,244). *I hypothesized that the Ad vaccine expressing multiple immunogenic MAA epitopes fused within gD can induce high frequencies of $CD8^+$T cells targeting melanoma cells for destruction. Blocking the immunosuppressive signaling in activated T cells may also reduce their exhaustion in tumors.* To address this hypothesis, I compared the functions

and exhaustion status of MAA-specific T cells induced by melanoma vaccine expressing multiple MAA epitopes fused within gD to those of T cells elicited by a vaccine expressing MAA epitopes without gD in melanoma-bearing mice.

Specific Aim 2: To determine whether depleting tumor stromal fibroblasts through vaccination could enhance the antitumor efficacy of melanoma cell targeting vaccine.

Tumor stromal fibroblasts express selectively the fibroblast activation protein (FAP), which is not expressed by normal fibroblasts or normal adult tissues. FAP+ stromal fibroblasts suppress the immune response to tumors by attracting regulatory T cells into the tumor and interfering with T cell-tumor cell interaction. *I hypothesized that combining an Ad-based vaccine directly targeting tumor stromal fibroblasts for destruction will enhance the efficacy of the melanoma antigen-expressing vaccine by reducing immunosuppression within TME. The frequencies and functions of immunosuppressive cells may change upon FAP+ stromal cell depletion, which may also reduce the exhaustion of MAA-specific TILs.* To study the effect of FAP+ stromal cell depletion, I designed an AdC68-based vaccine targeting murine full-length FAP protein. The effects of the vaccine given either alone or in combination with the MAA targeting vaccine were tested in both a B16 transplantable tumor model and a clinically relevant inducible transgenic melanoma mouse model.

Specific Aim 3: To determine whether metabolic challenges within TME contribute to T cell functional exhaustion and to explore novel strategies to alter the metabolism of TILs in order to improve their functions.

The TME poses significant metabolic challenges to TILs due to disorganized vascularization, presence of toxic products derived from tumor and stromal cells and lack of nutrients and oxygen (O_2)(245). TILs require energy to eliminate tumor cells. Upon activation T cells enhance energy production through glycolysis(246), which is less efficient than OXPHOS

but provides building blocks for biomass formation and cell proliferation. Tumor cells also use glycolysis(247), which may lead to Glu depletion within the TME(192,197). T cells with limited access to Glu have to rely on OXPHOS to produce energy. Although many substances including FAs can fuel OXPHOS, it requires O_2, which can become limiting within tumors due to insufficient blood supply(248). TILs therefore face dual metabolic jeopardy, *which I hypothesize drives their functional exhaustion and thereby impairs the efficacy of cancer immunotherapy.* I studied the effects of metabolic stress within the TME on differentiation and effector functions of CD8+TILs in a B16 melanoma mouse model. Melanoma-bearing mice were immunized with a mixture of vaccines that induce CD8+T cells specific for MAAs and an unrelated tumor antigen (TA), i.e. E7 of human papilloma virus (HPV)-16. I analyzed the metabolism, differentiation and functions of both MAA- and E7-specific TILs in spleens, small tumors or late stage tumors using a series of transcriptional profile, flow and metabolomics analysis. The impact of metabolic challenges on the tumoricidal functions of effector T cells was studied both *in vitro* and *in vivo*. Moreover, I explored strategies to manipulate the metabolism of TILs in order to improve their tumor-killing capacity in the TME.

Chapter 2

The effect of adjuvanting cancer vaccines with herpes simplex virus glycoprotein D on melanoma-driven $CD8^+$T cell exhaustion

ABSTRACT

Immunoinhibitory ligands within the tumor microenvironment (TME) represent a major barrier for vaccine-induced tumor antigen-specific $CD8^+$T cells to exert effector functions. To determine if blocking immunoinhibitory pathways could enhance the efficacy of cancer vaccine, I compared two chimpanzee-derived replication-defective AdC68 vectors expressing $CD4^+$ and $CD8^+$ T cell epitopes of melanoma-associated antigens (MAAs) in a mouse model of melanoma. In one vaccine, termed AdC68-gDMelapoly, the epitopes were expressed as a fusion protein within HSV-1 gD, which blocks immunoinhibitory signaling through the HVEM pathway. The other vaccine, termed AdC68-Melapoly only expressed the MAA epitopes. AdC68-gDMelapoly induced more potent MAA-specific $CD8^+$T cell responses especially to the subdominant MAA epitopes. Upon prophylactic vaccination, mice that developed $CD8^+$ T cell responses to the two vaccines that were comparable in magnitude showed equal protection against tumor challenge. When mice

were first challenged with tumor cells and then vaccinated results differed. In animals with comparable $CD8^+$T cell responses, the AdC68-gDMelapoly vaccine was more efficacious compared to the AdC68-Melapoly vaccine in delaying tumor growth. This effect was linked to reduced expression of 2B4, LAG-3 and PD-1 on tumor-infiltrating MAA-specific $CD8^+$ T cells elicited by the gD-adjuvanted vaccine, suggesting that $CD8^+$ T cells induced in presence of gD are less susceptible to tumor-driven exhaustion.

Portions of this chapter were adapted from:

Zhang Y, Ertl HC. The effect of adjuvanting cancer vaccines with herpes simplex virus glycoprotein D on Melanoma-Driven $CD8^+$ T cell exhaustion. **Journal of immunology** 2014; 193(4): 1836-1846.

INTRODUCTION

Even cancer vaccines that are highly immunogenic in animal models commonly fail to provide benefits to patients with advanced cancers(249,250). This has partially been linked to the highly immunosuppressive tumor microenvironment, which expresses immunoinhibitory ligands (251), recruits suppressive cell subsets such as regulatory T cells (252) and myeloid suppressor cells (253) and provides a metabolically stressed milieu (254). Biologicals that block immunoinhibitory pathways such as antibodies to PD-1 (34,255) or CTLA-4 (256) or both (257,258) are being tested alone or in combination with active immunotherapy in cancer patients and have yielded promising results.

My focus has been on the herpes virus entry mediator (HVEM) pathway. HVEM, which was first identified as a receptor for HSV-1 glycoprotein D (gD)(259), is a bimodal switch expressed on many cells including antigen presenting cells that can interact with the immunoregulatory molecules on lymphocytes (260). Binding of HVEM to LIGHT or lymphotoxin provides stimulatory signals; binding to the B and T lymphocyte attenuator (BTLA) or CD160 activates inhibitory pathways (261). Co-activators and co-inhibitors bind to different domains of HVEM and can form a trimolar complex, in which signaling through co-inhibitors dominates (261). The N-terminus of HSV-1 gD binds to a site on HVEM that is close to the BTLA/CD160 binding site and thereby blocks immunoinhibitory but not co-stimulatory HVEM signaling (262).

As I have shown previously, vaccines that express antigens fused into the C-terminus of gD elicit enhanced T cell responses, which is linked to blockade of the immunoinhibitory HVEM pathway (243). Adjuvanting vaccine antigens with gD is especially effective to augment $CD8^+$ T cell responses in aging mice (263) and in mice with advanced cancers (244). My previous cancer studies were based on human papilloma virus type 16 (HPV-16)-associated tumors, which express viral antigens that are foreign to the immune system. The current study was conducted to assess if expressing 'self'' antigens from non-viral tumors within gD would enhance the immunogenicity and efficacy of a cancer vaccine. Experiments were conducted in a

transplantable melanoma model, based on B16F10 cells that were stably transfected to express $Braf_{V600E}$ (B16$Braf_{V600E}$). The vaccine antigen, termed Melapoly, was designed to express $CD4^+$ and $CD8^+$ T cell epitopes of melanoma-associated antigens (MAAs) including tyrosinase-related protein (Trp)-1, Trp-2, gp100 and mutated $Braf_{V600E}$ linked to the universal T helper cell epitope PADRE and an endoplasmic reticulum targeting signal sequence. To test for the gD adjuvant effect, the Melapoly encoding sequence was fused into the C terminal domain of HSV-1 gD (gDMelapoly). The Melapoly and the gDMelapoly fusion proteins were expressed by a simian E1-deleted adenovirus vector of serotype 68 (AdC68).

As expected, the AdC68-gDMelapoly vector induced more potent MAA-specific $CD8^+$ T cell responses, especially to subdominant epitopes, compared to the AdC68-Melapoly vector and provided superior protection if given before tumor challenge. In the same token, in a therapeutic vaccination model, the AdC68-gDMelapoly vector was superior in delaying tumor progression compared to the AdC68-Melapoly vector. To assess if the improved efficacy of the gD-adjuvanted vaccine solely reflected differences in the magnitude of MAA-specific T cell responses, I vaccinated mice with different doses of the AdC68 vectors and selected subgroups with comparable frequencies of MAA-specific $CD8^+$ T cells. In a pre-challenge vaccination model, vaccine efficacy was shown to depend on frequencies of MAA-specific $CD8^+$ T cells. In contrast in a post-challenge vaccination model, AdC68-gDMelapoly vaccinated mice that had MAA-specific T cell frequencies comparable to those of AdC68-Melapoly vaccinated mice survived significantly longer. This was not caused by differences in production of mediators by AdC68-gDMelapoly-induced T cells but rather by their increased resistance against differentiation towards exhaustion.

RESULTS

The gD adjuvant enhances $CD8^+$ T cell responses to dominant and subdominant epitopes

Levels of transgene expression can affect the immunogenicity of viral vectors. I therefore tested the levels of transgene product expression in transfected cells and showed by

real-time PCR that both vectors expressed comparable levels of transgene-derived mRNA (data not shown).

I compared the magnitude of MAA-specific $CD8^+$ T cell responses induced by the vaccines in young female C57BL/6 mice. Each group (n=5) of mice received either the AdC68-Melapoly or the AdC68-gDMelapoly vector given i.m. at doses of 10^{10} or 10^{11} vp. Two and four weeks after vaccination, I measured $CD8^+$ T cell responses to two MAA epitopes, i.e. Trp-1_{455} and Trp-2_{180}, by staining T cells with the corresponding MHC class I tetramers (**Figure 2-1**).

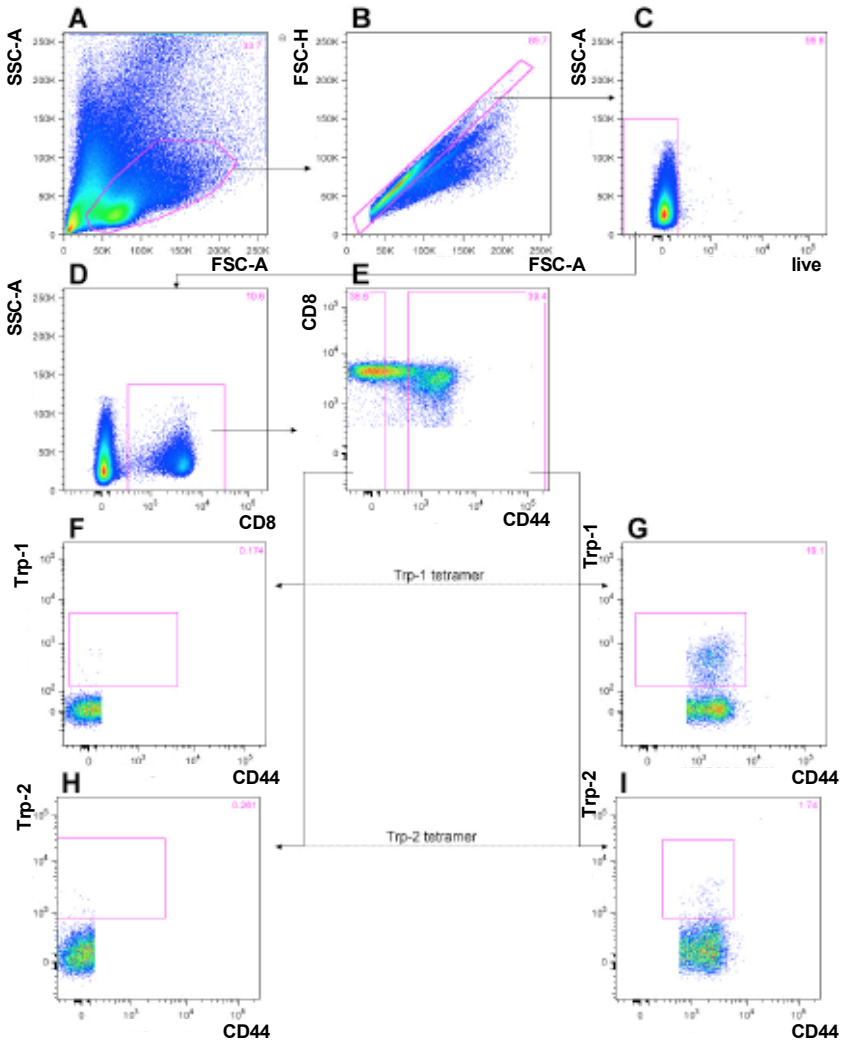

Figure 2-1: Gating scheme for tetramer$^+$CD8$^+$T cells. Samples were initially gated on lymphoid cells (**A**) and then singlets (**B**) using forwards and side scatters. Singlets were further gated on live cells (**C**). Live cells were gated on cells positive for CD8 (**D**). $CD8^+$ cells were blotted into $CD44^{low}$ and $CD44^{hi}$ cells (**E**) with the former serving as intrinsic controls. Using the CD44 gate $CD44^{low}$ (**F,H**) and $CD44^{hi}$ (**G,I**) cells were gated over the Trp-1 (**F,G**) and Trp-2 (**H,I**) tetramer. Counts for live $CD8^+$ cells as well as $CD44l^{ow}$tetramer$^+$ and $CD44^{hi}$tetramer$^+$ cells were recorded and used to calculate frequencies of tetramer$^+$ cells over all $CD8^+$ cells.

Both vaccines induced stronger $CD8^+$ T cell responses to Trp-1_{455} than Trp-2_{180} (mean frequencies of positive $CD44^+CD8^+$ cells for Trp-1_{455} vs. Trp-2_{180}: 10^{10} vp: week 2: Melapoly: 5.1% vs. 0.56%, gDMelapoly: 5.8% vs. 0.58%; week 4: Melapoly: 2.5% vs. 0.25%, gDMelapoly: 5.3% vs. 0.42%; 10^{11} vp: week 2: Melapoly: 8.7% vs. 0.86%, gDMelapoly: 14.7% vs. 0.51%; week 4: Melapoly: 7.8% vs. 0.18%, gDMelapoly: 8.5% vs. 0.56%; naive $CD44^-$ T cells: 0.043% vs. 0.056% and 0.043% vs. 0.078% for weeks 2 and 4, respectively, **Figure 2-2A-B**). All groups mounted significant responses to the Trp-1_{455} and Trp-2_{180} tetramer compared to the internal $CD44^-CD8^+$ T cell controls (adjusted p-values are listed in legend to Fig. 1) or to naïve mice (data not shown). At the 10^{11} vp dose at week 2 and the 10^{10} vp dose at week 4 Trp-1_{455}-specific $CD8^+$ T cell responses were significantly higher in AdC68-gDMelapoly vaccinated animals than in AdC68-Melapoly vaccinated mice. Responses to Trp-2_{180} were significantly higher in mice vaccinated with 10^{11} vp AdC68-gDMelapoly at both weeks 2 and 4. At the 10^{10} vp dose at week 4 Trp-2_{180} responses were significantly higher in Melapoly vaccinated mice.

Figure 2-2: Induction of MAA-specific $CD8^+$T cells by different vector doses

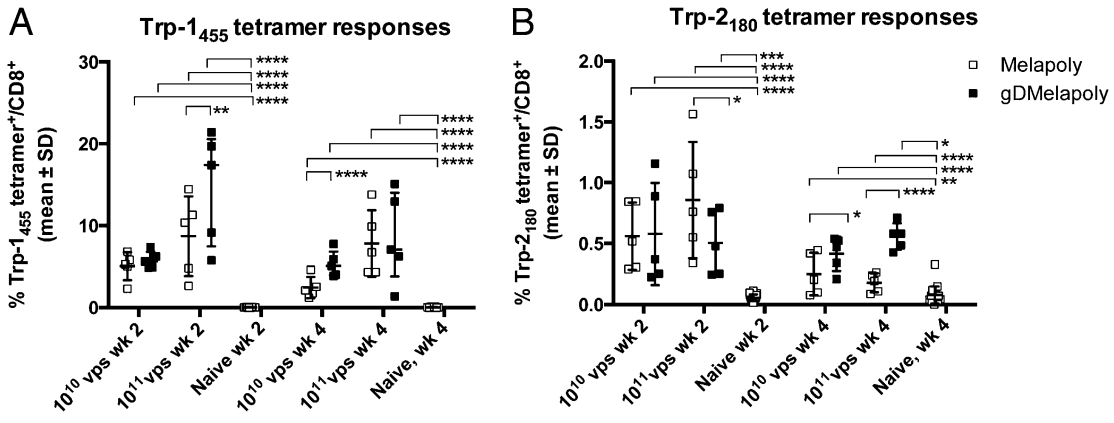

Figure 2-2: Induction of MAA-specific $CD8^+$ T cells by different vector doses: Groups (n=5/group) of C57BL/6 mice were vaccinated i.m. with 10^{10} vp or 10^{11} vp of either AdC68-Melapoly (open squares) or AdC68-gDMelapoly (closed squares) vector. PBMCs were collected 2 and 4 weeks later, (**A**) Trp-1_{455}- and (**B**) Trp-2_{180}-specific $CD8^+$ T cell responses were compared. The graphs show responses in individual animals, the lines indicate means ± standard errors. * indicates significant differences between groups connected by lines (* p = 0.01-0.05, ** p = 0.001-0.01, *** p = 0.0001-0.001, ****p<0.0001). The following differences had significant p-values: all groups Trp-1_{455} compared to $CD44^-CD8^+$ controls: p < 0.0001; Trp-1_{455}: Melapoly vs. gDMelapoly: 10^{11} vp, wk 2: p = 0.012, 10^{10} vp, wk 4: p <0.0001; Trp-2_{180} compared to

controls: Melapoly, 10^{10} vp: wk 2: $p < 0.0001$,wk 4: $p = 0.016$; 10^{11} vp: wk 2: $p < 0.0001$, wk 4: $p = 0.034$; gDMelapoly: both doses and both time points: $p < 0.0001$; Trp-2_{180}: Melapoly vs. gDMelapoly: 10^{11} vp: wk 2: $p = 0.027$, 10^{10} vp: wk 2: $p = 0.036$, wk 4: $p < 0.0001$.

To further assess differences, I immunized mice (n=7-8) with 10^{11} vp of the AdC68-Melapoly vector or 10^{10} vp of the AdC68-gDMelapoly vector. I collected blood at different time points after vaccination and measured the $CD8^+$ T cells to individual MAA epitopes by intracellular cytokine staining (ICS) for production of IFN-γ, TNF-α and IL-2 (**Figure 2-3, Figure 2-4**). For these experiments, blood had to be pooled to allow for testing the PBMC samples stimulated with the eight different peptides carrying $CD8^+$ T cell epitopes expressed by the vaccines. Both vectors induced significantly higher tumor-antigen specific $CD8^+$ T cell responses to both dominant and subdominant epitopes compared to naive controls ($CD44^-CD8^+$ T cells). In spite of the lower dose, there was a clear trend of the AdC68-gDMelapoly vaccine to induce higher responses mainly to the subdominant epitopes (Trp-1_{455} epitope: mean frequencies averaging all time points: 1.9 % and 2.9 % for Melapoly and gDMelapoly, respectively, **Figure 2-3A**; subdominant epitopes: mean frequencies of the sum of responses averaging all time points 1.3% and 3.0% for Melapoly and gDMelapoly, respectively, **Figure 2-3B**). The preferential increase of responses to subdominant epitopes by gD was confirmed by comparing responses to the dominant Trp-1_{455} epitope to those against the subdominant Trp-2_{180} epitope by tetramer staining at 4 and 26 weeks after vaccination with 10^{11} vp of AdC68-Melapoly or 10^{10} vp of AdC68-gDMelapoly (**Figure 2-3C-D**). At both early and late time points the responses to Trp-1_{455} epitope were comparable, while the responses to Trp-2_{180} epitope were significantly higher in mice immunized with AdC68-gDMelapoly (wk 4, mean tetramer frequencies for Trp-1_{455}: Melapoly vs gDMelapoly: 7.8% vs 5.3%; Trp-2_{180}: 0.18% vs 0.42%, $p = 0.0053$; wk26, Trp-1_{455}: Melapoly vs gDMelapoly: 4% vs 5.9%, Trp-2_{180}: 0.35% vs 0.66%, $p = 0.033$).

I selected three time points (weeks 6, 12 and 24) to compare the overall response pattern (**Figure 2-3E-J**). Responses to the subdominant epitopes developed with a delay as compared to Trp-1_{455}-specific responses. At all three time points the gD-adjuvanted vector

induced a more prominent $CD8^+$ T cell response to the subdominant epitopes compared to the AdC68-Melapoly vector (sum of frequencies to Melapoly and gD-Melapoly, respectively: wk 6: 3.8%, 4.4%, wk 12: 2%, 6.7%, wk 24: 4.5 %, 6.6%).

Figure 2-3: MAA-specific $CD8^+$ T cell responses to individual epitopes

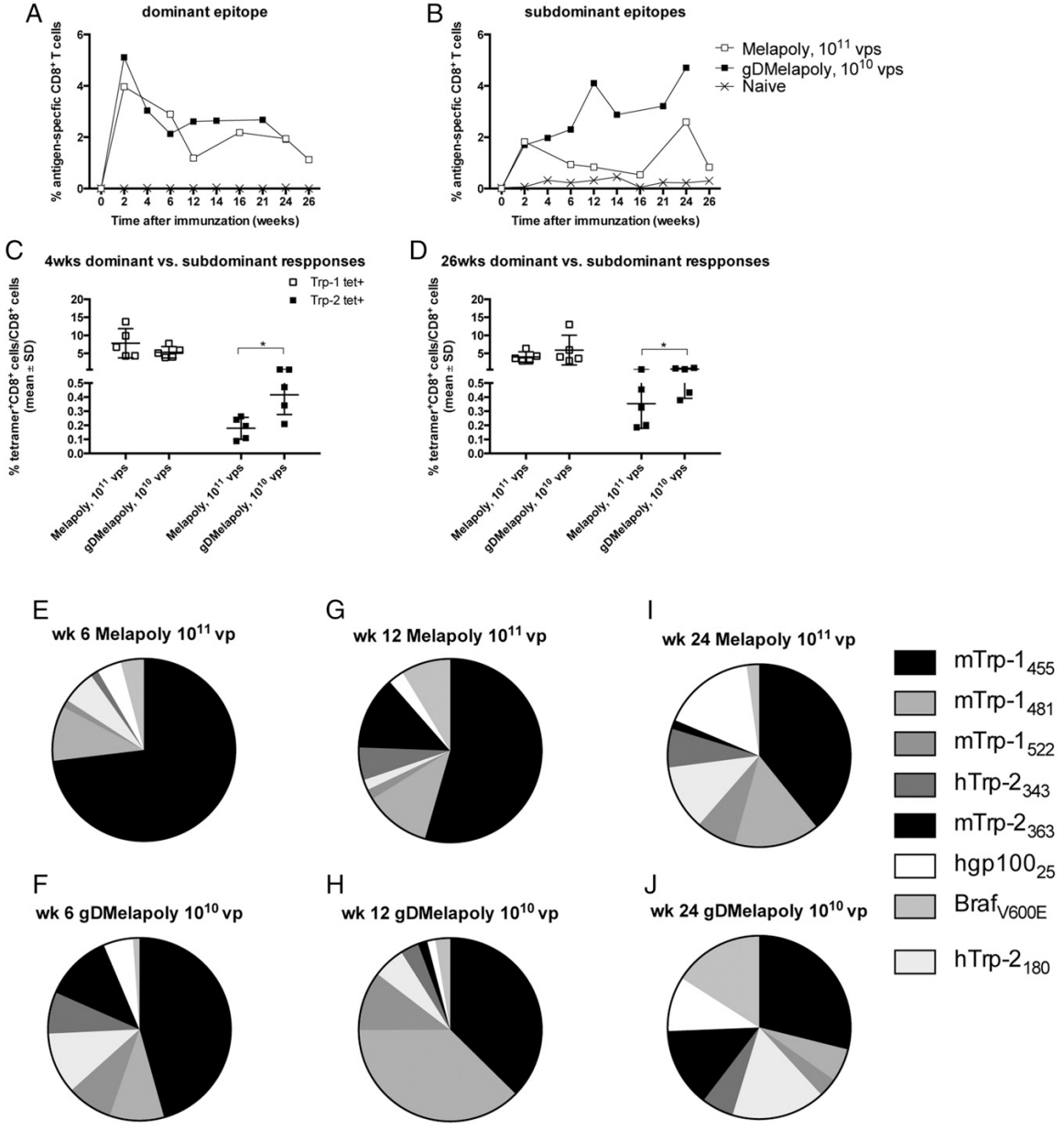

Figure 2-3: MAA-specific CD8$^+$ T cell responses to individual epitopes. Groups of C57BL/6 mice (n=7-8) were vaccinated i.m. with 10^{11}vp AdC68-Melapoly or 10^{10}vp AdC68-gDMelapoly. (**A-B**) CD8$^+$ T cell responses to individual epitopes were measured by ICS for IFN-γ, TNF-α and IL-2 upon stimulation of cells with peptides representing the T cell epitopes expressed by the vaccines over a course of 24-26 weeks. Graphs show the sum of cytokine responses. (**A**) shows responses to the dominant Trp-1$_{455}$ peptides. (**B**) shows the sum of responses over time for the other peptide; responses to individual peptides (but for Trp-1$_{455}$) were totaled. (**C-D**) shows Trp-1-teramer$^+$ and Trp-2 tetramer$^+$ CD8$^+$ T cell responses 4 weeks and 26 weeks after vaccination in tumors of vaccinated mice. Differences between the two vaccines were not significant for Trp-1-specific CD8$^+$ T cells (p = 0.12 and 0.18, respectively) but significant for Trp-2-specific CD8$^+$ T cells (p = 0.0053 and 0.035, respectively). (**E-J**) The patterns of the sum of cytokine responses to the 8 CD8$^+$ T cell epitopes at 3 time points, i.e., week 6 (**E,F**), 12 (**G,H**) and 24 (**I,J**) after vaccination.

Figure 2-4: Gating scheme for cytokine producing CD8$^+$T cells

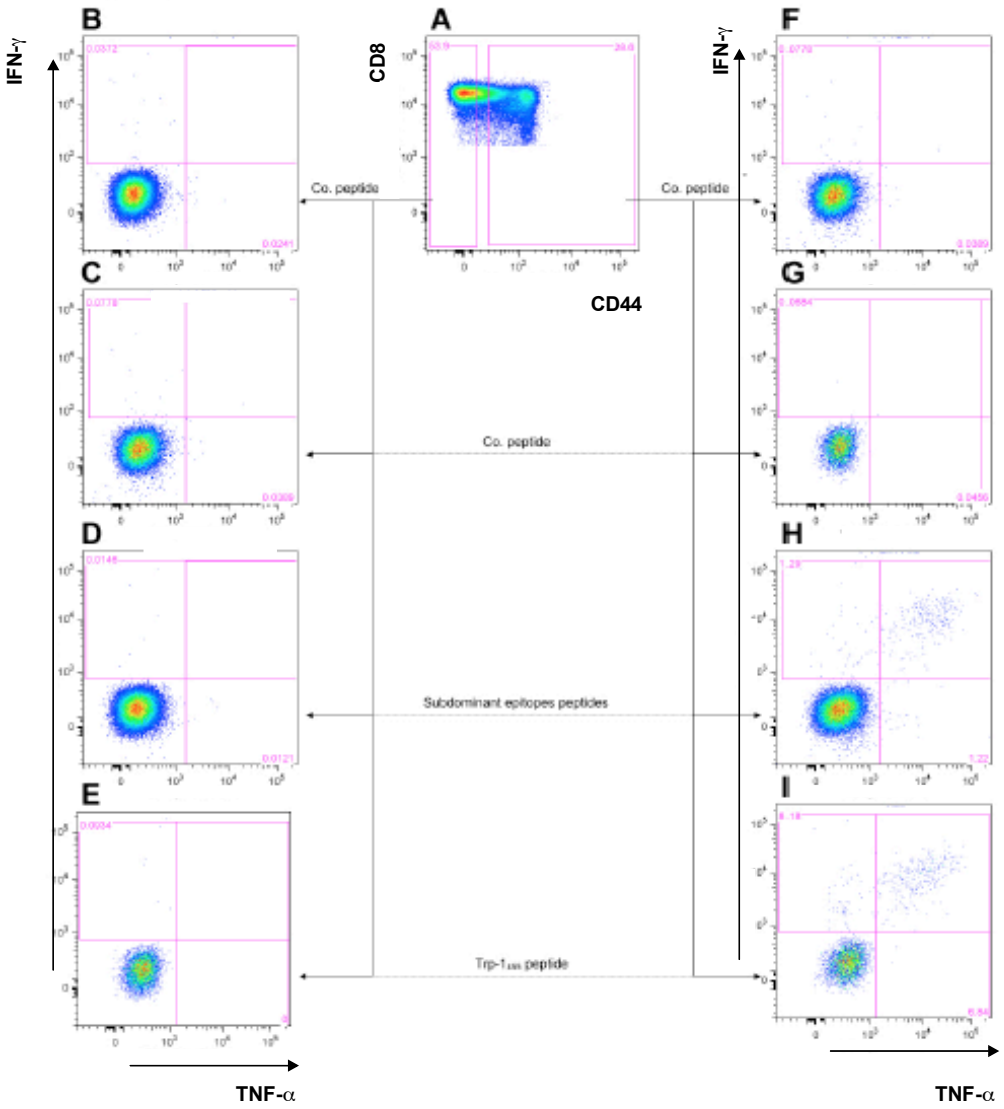

Figure 2-4: Gating scheme for cytokine producing CD8$^+$T cells. Cells were stimulated with a control peptide or the MAA peptides present in the Ad vector encoded antigen. Cells were then stained for surface expression of CD44 and CD8 and intracellular cytokines such as IGN-γ, TNF-α and IL-2. Cells were analyzed and blots were generated. Cells were gates onto lymphoid, single, live CD8$^+$ cells as described in Figure 2-1. They were then gated onto CD44^{low} and CD44^{hi}CD8$^+$ cells (**A**). Both populations were gated on cells positive for TNF-α and/or IFN-γ (**B-I**) and TNF-α over IL-2 (not shown). To better illustrate the gates blots cells stimulated with the peptides carrying the subdominant epitopes (**B,C**) were concatenated. (**B,C,F,G**) show gates for cells stimulated with the control peptides, in B and F blots were concatenated, (**C**) and (**G**) show a single blot, (**B**) and (**C**) show blots for CD44low cells, (**F**) and (**G**) show blots for CD44^{hi} cells. **D** and **H** show concatenated blots for CD44^{low} (**D**) and CD44^{hi} (**H**) cells stimulated with peptides carrying subdominant epitopes. (**E**) and (**I**) show blots for the same populations stimulated with the peptide carrying the immunodominant Trp-1$_{455}$ epitope. Boolean gates were set by FlowJo to determine counts and frequencies of cells producing the different combinations of cytokines. Counts were recorded and those obtained for each possible combination of cytokines with cells stimulated with the control peptide were subtracted from those obtained with peptides expressing an MAA-specific epitopes (for this results obtained with original blots rather than concatenated blots were used). Counts obtained for CD8$^+$ T cells were then used to determine frequencies of cytokine producing cells over CD8$^+$ cells. Frequencies for the 7 possible combinations of cytokines were summed to provide overall frequencies of responding cells. In Figure 2 the frequencies of CD44^{low} and CD44^{hi} cells producing cytokines over all CD8$^+$ cells in response to the Trp-1$_{455}$ epitope are shown while Figure 2B shows the sum of frequencies to the other 6 peptides carrying immunosubdominant epitopes.

In a pre-tumor challenge vaccination model, the increased efficacy of the gD adjuvanted vaccine is solely linked to magnitude of the MAA-specific CD8$^+$ T cell responses

To determine if vaccination with the AdC68-gDMelapoly vector resulted in superior protection against tumor growth than vaccination with the AdC68-Melapoly vector, I immunized groups of mice (n=5-18) with 10^{10} vp of AdC68-gDMelapoly, 10^{11} vp of AdC68-Melapoly or 10^{11} vp of AdC68-gD, the latter as a control for non-specific effects of the vector or gD. The dose for each vaccine was chosen to elicit relatively similar frequencies of MAA-specific CD8$^+$T cells with overlaps between the groups. Fourteen days later mice were challenged with B16Braf$_{V600E}$ cells given s.c. Total cytokine$^+$CD8$^+$ T cell responses to the eight CD8$^+$ T cell epitopes were measured before tumor challenge. As shown in **Figure 2-5A**, both vaccines induced significantly higher responses when compared to background stains of naïve T cells (mean frequencies 4.5% and 9.3% for Melapoly and gD-Melapoly, 0.02% for control cells). The AdC68-gDMelapoly vector induced significantly higher CD8$^+$ T cell responses compared to the AdC68-Melapoly vector ($p < 0.0001$) and this was linked to enhanced survival rates upon tumor challenge (**Figure 2-5C**, $p = 0.0018$ by Gehan-Breslow-Wilcoxon test). Specifically > 60% of AdC68gD-Melapoly vaccinated

mice as compared to < 20% of AdC68-Melapoly vaccinated mice remained tumor-free. When I compared subgroups with similar frequencies of MAA-specific $CD8^+$ T cells by removing the low responders from the Melapoly group and the high responders from the gD-Melapoly group (**Figure 2-5B**, mean frequencies of the Melapoly subcohort: 5.7% and the gD-Melapoly subcohort: 6.5% p = 0.1), survival rates of the two vaccine groups were comparable (p = 0.08, **Figure 2-5D**). This suggests that in the pre-tumor challenge model vaccine efficacy is significantly influenced by the magnitude of MAA-specific $CD8^+$ T cell responses.

Figure 2-5: Vaccine efficacy in mice vaccinated before tumor cell challenge

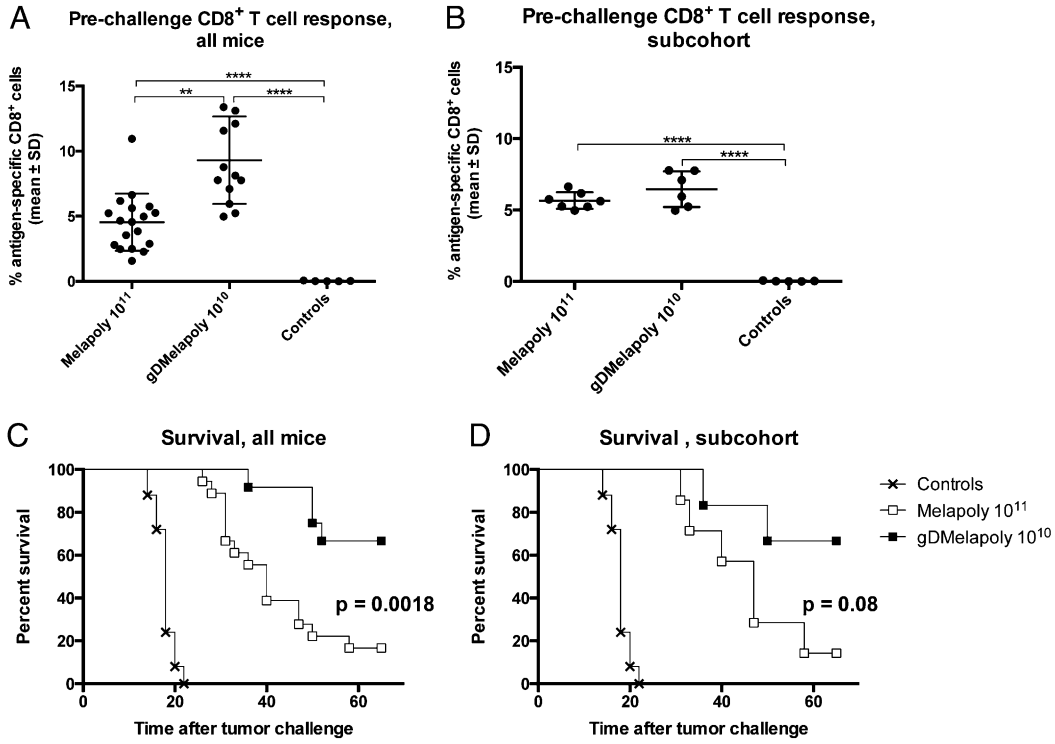

FIGURE 2-5. Vaccine efficacy in mice vaccinated before tumor cell challenge. Groups of C57BL/6 mice (n=5-18) were vaccinated with 10^{11}vp AdC68-gD, 10^{11}vp AdC68-Melapoly or 10^{10}vp AdC68-gDMelapoly vectors. Fourteen days later PBMC samples were tested for $CD8^+$ T cell responses to all of the MAA epitopes present in the vaccine. (**A**) The sum of tumor antigen-specific $CD8^+$ T cell percentages for individual mice. (*) indicates significant differences as detailed in legend to Fig. 1. Melapoly vs. gDMelapoly: p < 0.0001, Melapoly vs. naïve: p = 0.0014, gDMelapoly vs. naïve: p < 0.0001. (**B**) The sum of tumor antigen-specific $CD8^+$ T cell percentages in the two subcohorts that showed comparable $CD8^+$ T cell responses. Subcohorts were selected by excluding animals with frequencies of MAA-specific $CD8^+$ T cells below the mean of the Melapoly group or above the mean of the gDMelapoly group. Melapoly vs. gDMelapoly, p = 0.1, Melapoly vs. naïve: p < 0.0001, gDMelapoly vs. naïve: p < 0.0001. (**C**) Survival rates of the entire group, measured for 60 days. Melapoly vs. naïve: p < 0.0001, gD-Melapoly vs. naïve: p < 0.0001, Melapoly vs. gDMelapoly: p = 0.0018 (**D**) Survival rates of the of the Melapoly subcohort in comparison to the gDMelapoly and the control group. Melapoly vs. controls: p < 0.0001, gD-Melapoly vs. controls: p = 0.0003, Melapoly vs. gDMelapoly: p = 0.08. In (**C**) and (**D**) control animals are shown as X, AdC68-

Melapoly-vaccinated mice are shown as open squares, AdC68-gDMelapoly-vaccinated mice are shown as closed squares.

In a post-tumor challenge vaccination model, the efficacy of the gD adjuvanted vaccine is not solely linked to the magnitude of MAA-specific $CD8^+$ T cell responses

I further compared the efficacy of the two vectors in a post-challenge vaccination model. $B16Braf_{V600E}$ cells grow very rapidly in vivo; after tumor cell inoculation most control mice require euthanasia within 14-18 days. AdC68-induced T cell responses on the other hand do not peak till 12-14 days after vaccination. Therefore, I chose a fairly short interval of 3 days between tumor cell inoculation and vaccination for my therapeutic vaccine studies. Accordingly, groups of mice (n=5-10) were challenged with $B16Braf_{V600E}$ tumor cells on day 0 and vaccinated three days later with either 10^{11}vp of the AdC68-Melapoly vector (n=9) or $3x10^9$vp and 10^{10}vp of the AdC68-gDMelapoly vector (n=8 and 10 for $3x10^9$vp and 10^{10}vp, respectively). A control group (n=28) was vaccinated with 10^{11}vp of the AdC68-gD vector. $CD8^+$ T cell responses were measured two weeks later from blood by ICS for production of IFN-γ, TNF-α, granzyme B and perforin. In addition, I assessed $CD8^+$ T cell responses by staining with the Trp-1_{455}- and Trp-2_{180}-specific tetramers. MAA-specific $CD8^+$ T cell responses tested by ICS were significantly higher compared to background stains for both vaccine groups, and higher in gDMelapoly than Melapoly vaccinated mice (means: Melapoly: 3.6%, gD-Melapoly: 5.2%, controls :0.27%, adjusted p-values are shown in the figure legend, **Figure 2-6Aa**). The AdC68-gDMelapoly and Melapoly vectors induced significantly higher frequencies of Trp-1_{455} (means: Melapoly: 5.2%, gD-Melapoly: 6.3%, controls: 0.037%, **Figure 2-6Ba**) and Trp-2_{180} tetramer$^+CD8^+$ T cells (means: Melapoly: 0.19% and gD-Melapoly: 0.14% control cells: 0.042%, **Figure 2-6Ca**) compared to controls. Both vaccines significantly delayed tumor growth and prolonged overall survival compared to control mice ($p<0.0001$, **Figure 2-6Da**). Comparing the two vaccine groups showed that AdC68-gDMelapoly vaccinated mice survived significantly longer than AdC68-Melapoly vaccinated mice ($p = 0.0039$, **Figure 2-6Da**).

As MAA-specific $CD8^+$ T cell responses were higher in the AdC68-gDMelapoly group than in the Melapoly group, I selected 8 mice from the AdC68-Melapoly vaccine group and 14 mice from the AdC68-gDMelapoly vaccine group with comparable frequencies of total $cytokine^+CD8^+$ T cell responses (means: Melapoly: 3.9%, gDMelapoly: 4.0%, **Figure 2-6Ab**), Trp-1_{455} $tetramer^+$ $CD8^+$ T cells (means: Melapoly: 3.0% and gDMelapoly: 3.1%, **Figure 2-6Bb**) and Trp-2_{180} $tetramer^+$ $CD8^+$ T cell responses (means: Melapoly: 0.19% and gD-Melapoly 0.14%, **Figure 2-6Cb**). Again in the subcohorts both vaccines significantly delayed tumor growth and prolonged survival compared to control mice ($p<0.0001$). Although mice had been selected based on comparable frequencies of MAA-specific $CD8^+$ T cell responses, the AdC68-gDMelapoly vaccinated subcohort showed significantly prolonged survival rates compared to the AdC68-Melapoly vaccinated subcohort ($p=0.015$, **Figure 2-6Db**).

To assess if vaccine-induced T cell responses differed in tissues, I analyzed MAA-specific $CD8^+$ T cell responses to all epitopes by ICS in blood, spleens and tumors at the time of necropsy, when the size of tumor exceeded a surface area of ~ 100 mm^2. Interestingly, total $cytokine^+CD8^+$ T cell responses in the blood and tumors of AdC68-Melapoly vaccinated mice were significantly higher than those of AdC68-gDMelapoly vaccinated mice (mean frequencies: blood, spleens, tumors: Melapoly: 2.2%, 1.5%, 3.7%; gD-Melapoly: 1.2%, 1.4%, 2.1%; controls: 0.049%, 0.12%, 0.027%; **Figure 2-6Ac**, p-values are shown in the figure legend). For Trp-1_{455}-specific $CD8^+$ T cell responses, both vaccines induced significant responses in the different compartments compared to naïve cells. The AdC68-Melapoly group again showed significantly higher responses in tumors compared to mice immunized with AdC68-gDMelapoly (mean frequencies: blood, spleens, tumors: Melapoly: 2.7%, 2.0%, 7.8%; gD-Melapoly: 1.6%, 1.0%, 2.7%; controls: 0.085%, 0.043%, 0.14%; **Figure 2-6Bc**; gating strategies **Figure 2-7**). Trp-2_{180}-specific responses were insignificant in blood but reached significance for both vaccine groups for cells from spleens and tumors compared to naive samples (mean frequencies: blood, spleens, tumors: Melapoly: 0.18%, 0.25%, 0.66%; gDMelapoly: 0.14%, 0.33%, 0.89%; controls: 0.016, 0.02, 0.13%; **Figure 2-6Cc**). MAA-specific $CD4^+$ T cell responses were analyzed in parallel; they

showed no differences before challenge but after challenge were higher in spleens of Melapoly-vaccinated mice (mean frequencies in spleens 1.5% and 0.59% for Melapoly and gD-Melapoly, respectively, p = 0.012, data not shown). Overall these results indicated that in the post-challenge vaccine model better protection achieved with the gD adjuvanted vaccine could not solely be explained by induction of higher frequencies of MAA-specific $CD8^+$ T cells.

Figure 2-6: Vaccine efficacy in mice vaccinated after tumor cell challenge

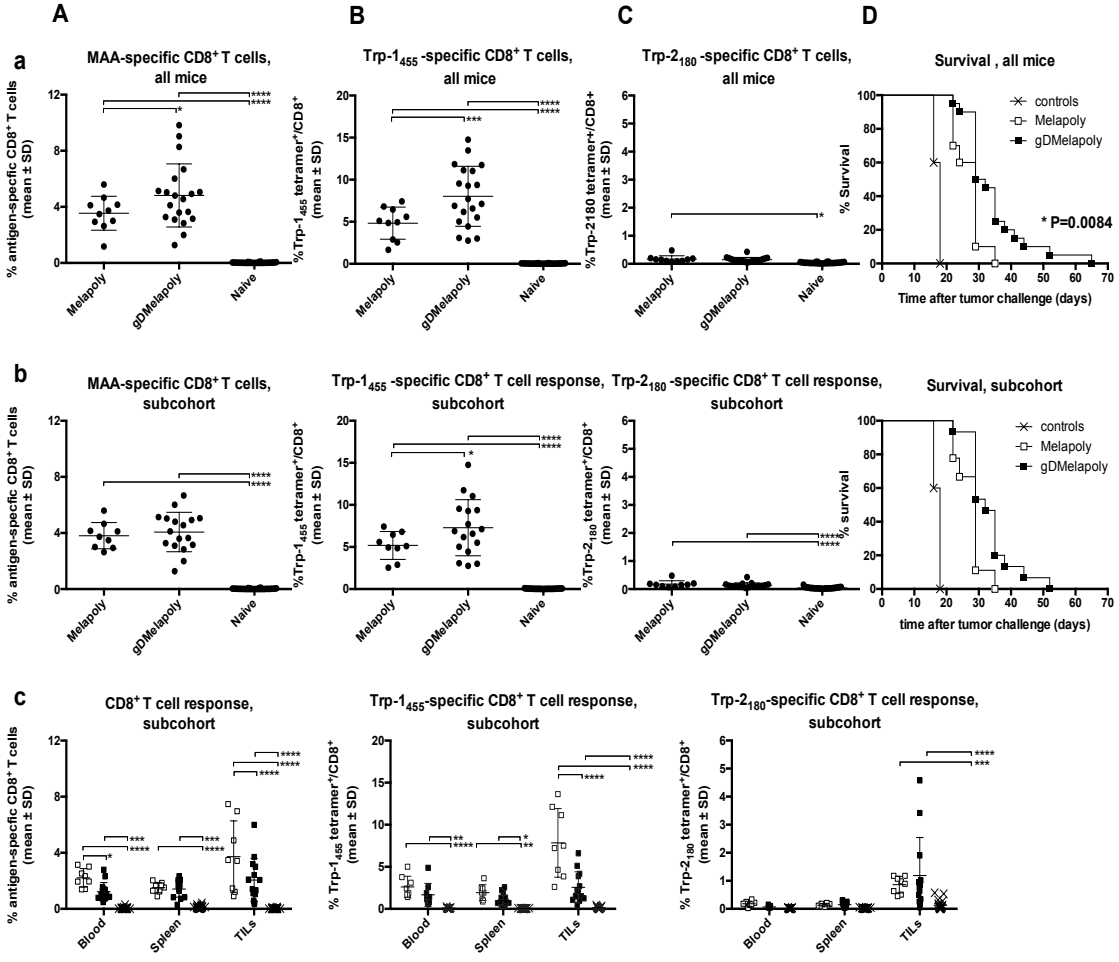

FIGURE 2-6. Vaccine efficacy in mice vaccinated after tumor cell challenge. Groups of C57BL/6 mice (n=9-30) were challenged with $B16Braf_{V600E}$ cells given s.c. 3 days before vaccination with 10^{11}vp AdC68-gD, 10^{11}vp AdC68-Melapoly or 3 x10^9 vp and 10^{10} vp AdC68-gDMelapoly vector. Subcohorts were selected by excluding animals that had frequencies of MAA-specific $CD8^+$T cells below the mean of the Melapoly group divided by the fold difference between the gD-Melapoly over Melapoly group (1.34) or above the mean of the gDMelapoly group multiplied by the fold difference. **(a, b)** PBMCs were tested 12 days after vaccination. (**c)** Cells from blood, spleens and tumors were tested at necropsy. (**aA-aD**) shows responses and survival rates of all mice, (**bA-bD) and (cA-cC**) show responses and survival rates of the subcohorts. (*) indicates significant difference between two groups as described in legend to Fig. 2-2 with the following p-values: (**Aa**) both vaccine groups vs. controls: p < 0.0001; Melapoly vs. gDMelapoly: p = 0.01. (**Ab**) both vaccine groups vs. to controls: p < 0.0001; Melapoly vs. gDMelapoly: p = 0.99. (**Ac**) Blood: Melapoly vs.

controls: p < 0.0001, gDMelapoly vs. controls: p = 0.0003, Melapoly vs. gDMelapoly: p = 0.011, Spleen: Melapoly vs. controls: p = 0.0003, gDMelapoly vs. controls: p < 0.0001, Tumors: all comparisons: p < 0.0001. (**Ba**) both vaccines vs. controls p < 0.0001, Melapoly vs. gDMelapoly p = 0.28. (**Bb**) both vaccine groups vs. controls: p < 0.0001, Melapoly vs. gDMelapoly: p = 0.07. (**Bc**) Blood: Melapoly vs. controls: p < 0.0001, gDMelapoly vs. controls: p = 0.0029, Melapoly vs. gDMelapoly p =0.047, Spleen: Melapoly vs. controls: p < 0.0001, gDMelapoly vs. controls: p = 0.04, Tumors: all comparisons: p < 0.0001. (**Ca**) both vaccines vs. controls: p < 0.0001. (**Cb**) Melapoly vs. controls: p < 0.0001, gDMelapoly vs. controls: 0.0002. (**Cc**) Spleen: Melapoly vs. controls: p = 0.02, gDMelapoly vs. controls: p < 0.0001, Tumors: both vaccine groups vs. controls: p < 0.0001, Melapoly vs. gDMelapoly p = 0.0187.

Figure 2-7: Gating Scheme for MAA-specific TILs and their production of cytokines and lytic enzymes

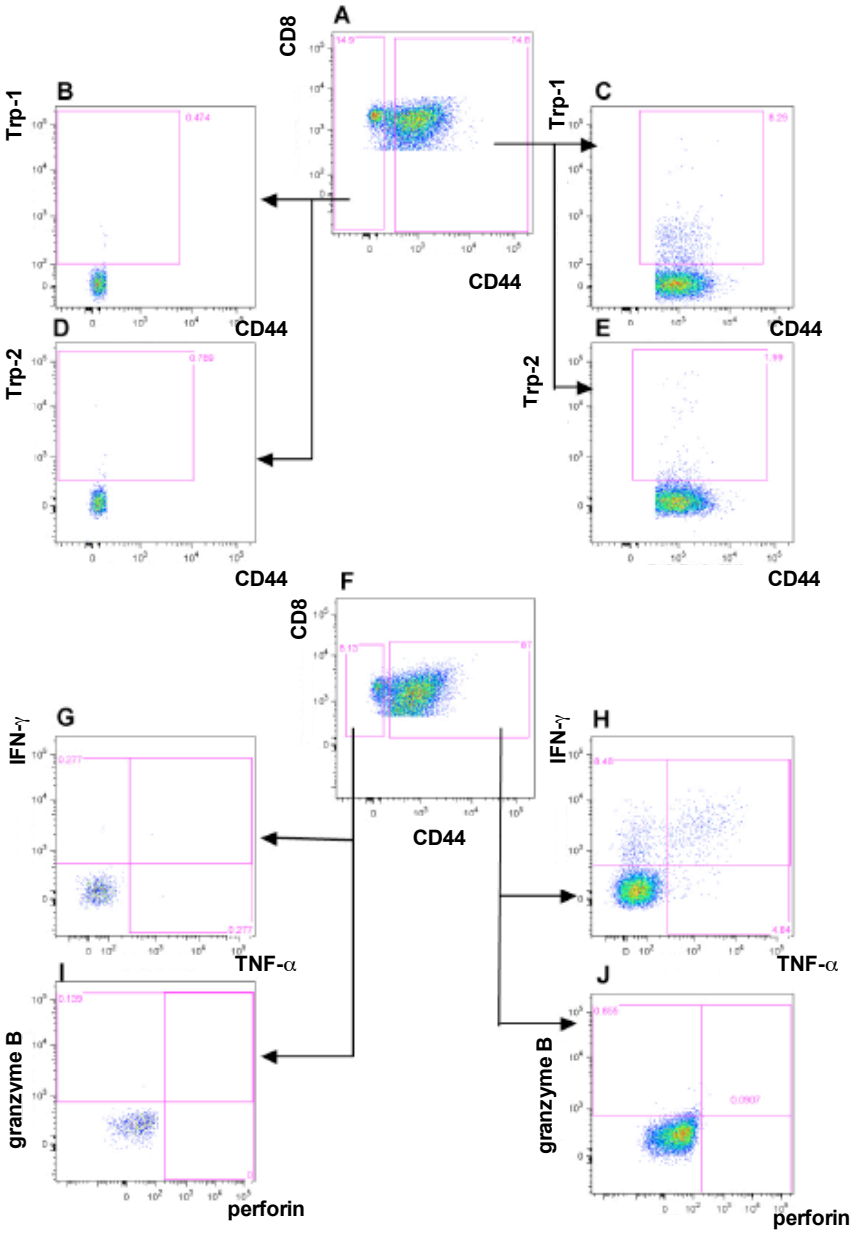

FIGURE 2-7. Gating Scheme for MAA-specific TILs and their production of cytokines and lytic enzymes. MAA-specific TILs were gated on lymphoid, live, single $CD8^+$T cells. $CD8^+$T cells were gated on $CD44^-$ and $CD44^+$ cells (**A, F**). For tetramer stains $CD44^-CD8^+$(**B,D**) and $CD44^+CD8^+$(**C,E**) cells were gated on cells positive for the Trp-1(**B,C**) and Trp-2(**D,E**) tetramer. For ICS $CD44^-CD8^+$(**G,I**) and $CD44^+CD8^+$ cells were gated on TNF-α over IFN-γ (G,H) or perforin over granzyme (**I,J**). Frequencies were calculated after subtraction of background data obtained with cells cultured with a control peptide.

MAA-specific $CD8^+$ T cell phenotypes

Chronic exposure to antigen can lead to T cell exhaustion, which is characterized by progressive loss of T cell functions and eventual cell death (43,111). To determine if gD affected the differentiation pathways of T cells, I assessed the expression of several exhaustion markers, i.e., 2B4, LAG-3 and PD-1 on Trp-1_{455}-and Trp-2_{180}-specific $CD8^+$ T cells in spleens and tumors at the time of necropsy, using the two subcohorts with comparable $CD8^+$ T cell responses. Expression of exhaustion markers was also assessed on $CD44^-CD8^+$ (naïve) T cells and $CD44^+tet^-CD8^+$ (memory) T cells. The latter population, negative for Trp-1_{455} and Trp-2_{180} tetramer-specific $CD8^+$ T cells, presumably contained $CD8^+$ T cells to other MAAs in the vaccine, to antigens of the Ad vaccine carrier and to unrelated antigens encountered previously. **Figure 2-8A** shows expression levels of the three exhaustion markers as mean fluorescence intensity (MFI) of the different dyes attached to the marker-specific antibodies. Significant differences were found between $CD44^-CD8^+$ and $CD44^+CD8^+$ T cells in spleens and tumors only for 2B4 (**Figure 2-8A**). Differences between $CD44^-CD8^+$ or $CD44^+CD8^+$ T cells and vaccine-induced tetramer-positive $CD8^+$ T cells were seen for all markers with the exceptions of 2B4 on Trp-$1_{455}{}^+CD8^+$ cells from spleens and 2B4 and PD-1 on Trp-$2_{180}{}^+CD8^+$TILs. I also observed significant differences between the two vaccine subcohorts as well as between $CD8^+$ T cells to the two epitopes. In particular, 2B4 showed higher expression on Trp-2_{180}- than Trp-1_{455}- specific $CD8^+$ T cells induced by either vaccine in spleens (mean MFI Melapoly: Trp-1_{455} vs. Trp-2_{180}: 158 vs. 269, gDMelapoly: Trp-1_{455} vs. Trp-2_{180}: 166 vs. 284, adjusted p-values are shown in the legend to **Figure 2-8A**). In both vaccine groups LAG-3 expression in spleens and in tumors was higher on Trp-1_{455}- than Trp-2_{180}-specific $CD8^+$ T cells. In tumors, Trp-1_{455}- specific $CD8^+$ T cells showed significantly lower level of LAG-3 expression in AdC68-gDMelapoly vaccinated animals compared

to those from AdC68-Melapoly vaccinated mice (mean MFI: spleen: Melapoly: Trp-1_{455} vs. Trp-2_{180}: 436 vs. 224, gDMelapoly: Trp-1_{455} vs. Trp-2_{180}: 401 vs. 313; tumors: Melapoly: Trp-1_{455} vs. Trp-2_{180}: 875 vs. 504, gDMelapoly: Trp-1_{455} vs. Trp-2_{180}: 728 vs. 609). In spleens, PD-1 was expressed at higher levels on Trp-2_{180}- than Trp-1_{455}-specific $CD8^+$ T cells and this reached significance for those induced by AdC68-gDMelapoly. Within tumors again Trp-1_{455}-specific $CD8^+$ T cells that had been elicited by the AdC68-gDMelapoly vaccine showed lower PD-1 expression compared to those elicited by the AdC68-Melapoly vaccine. In both vaccine groups, Trp-1_{455}-specific $CD8^+$ T cells expressed higher levels of PD-1 compared to those specific for Trp-2_{180} (mean MFI: spleen: Melapoly: Trp-1_{455} vs. Trp-2_{180}: 97 vs. 126, gDMelapoly: Trp-1_{455} vs. Trp-2_{180}: 89 vs. 151; tumors: Melapoly: Trp-1_{455} vs. Trp-2_{180}: 1190 vs. 400, gDMelapoly: Trp-1_{455} vs. Trp-2_{180}: 721 vs. 297).

In addition, I determined the percentages of Trp-1_{455}- and Trp-2_{180}- specific $CD8^+$TILs that were positive for either of the exhaustion markers and compared the results with those on naïve ($CD44^-$) or memory $tetramer^-$ $CD8^+$ T cells **(Figure 2-8B, a-c, Figure 2-9**). Only very low percentages of $CD44^-CD8^+$ T cells expressed any of the three exhaustion markers (< 2%). Percentages of $marker^+CD44^+tet^-CD8^+$ T cells were intermediate (2B4: 19%, 15%; LAG-3: 17%, 12%; PD-1: 23%, 41% for Melapoly and gDMelapoly vaccinated mice). Expression of individual markers was significantly higher on $CD44^+CD8^+$ cells than on naïve cells. Percentages of Trp-1_{455}-or Trp-2_{180}-specific $CD8^+$ T cells positive for any of the three exhaustion markers were again significantly higher when compared to $CD44^-CD8^+$ or $tetramer^-CD44^+CD8^+$ cells. Comparing the two vaccine subcohorts or Trp-1_{455}- and Trp-2_{180}-specific $CD8^+$ T cells within each vaccine group showed no significant differences for percentages of $2B4^+$ cells (means: Melapoly: Trp-1_{455} vs. Trp-2_{180}: 52% vs. 39%, gDMelapoly: Trp-1_{455} vs. Trp-2_{180}: 44% vs. 33%). $LAG\text{-}3^+$ cells were significantly more common within Trp-1_{455}- specific $CD8^+$ T cells in both vaccine groups (means: Melapoly: Trp-1_{455} vs. Trp-2_{180}: 87% vs. 48%, gDMelapoly: Trp-1_{455} vs. Trp-2_{180}: 81% vs. 58%) as were $PD\text{-}1^+CD8^+$ cells in Melapoly-vaccinated mice. Interestingly percentages of $PD\text{-}1^+$ Trp-1_{455}-specific $CD8^+$ cells were significantly lower in the AdC68gD-Melapoly group than in mice

immunized with AdC68-Melapoly (means: Melapoly: Trp-1_{455} vs. Trp-2_{180}: 84% vs. 67%, gDMelapoly: Trp-1_{455} vs. Trp-2_{180}: 63% vs. 57%).

Exhaustion leads to sequential expression of several markers (43). Accordingly, I further analyzed tumor-derived T cells for co-expression of PD-1, LAG-3 and 2B4 (**Figure 2-8B, d-f**). Again I found that higher percentages of Trp-1_{455}- and Trp-2_{180}-specific $CD8^+$ T cells co-expressed two or three markers compared to $CD44^-CD8^+$ or tetramer$^-CD44^+CD8^+$ cells. Trp-1_{455}-specific $CD8^+$ T cells had in general higher frequencies of $PD\text{-}1^+LAG\text{-}3^+$ and $PD\text{-}1^+LAG\text{-}3^+2B4^+$ cells compared to Trp-2_{180}-specific $CD8^+$ T cells. Trp-1_{455}-specific $CD8^+$ cells expressing two or three of the markers were present at significantly lower frequencies in gDMelapoly than Melapoly-immunized mice (means: Melapoly vs. gDMelapoly: $PD\text{-}1^+2B4^+$: Trp-1_{455}: 47% vs. 35%, Trp-2_{180}: 32% vs. 24%; $PD\text{-}1^+LAG\text{-}3^+$: Trp-$1_{455:}$ 69% vs. 53%, Trp-2_{180}: 29% vs. 24%; $PD\text{-}1^+2B4^+LAG\text{-}3^+$: Trp-$1_{455:}$ 45% vs. 34%, Trp-2_{180}: 25% vs. 20%).

Figure 2-8: MAA-specific CD8$^+$ T cell phenotype

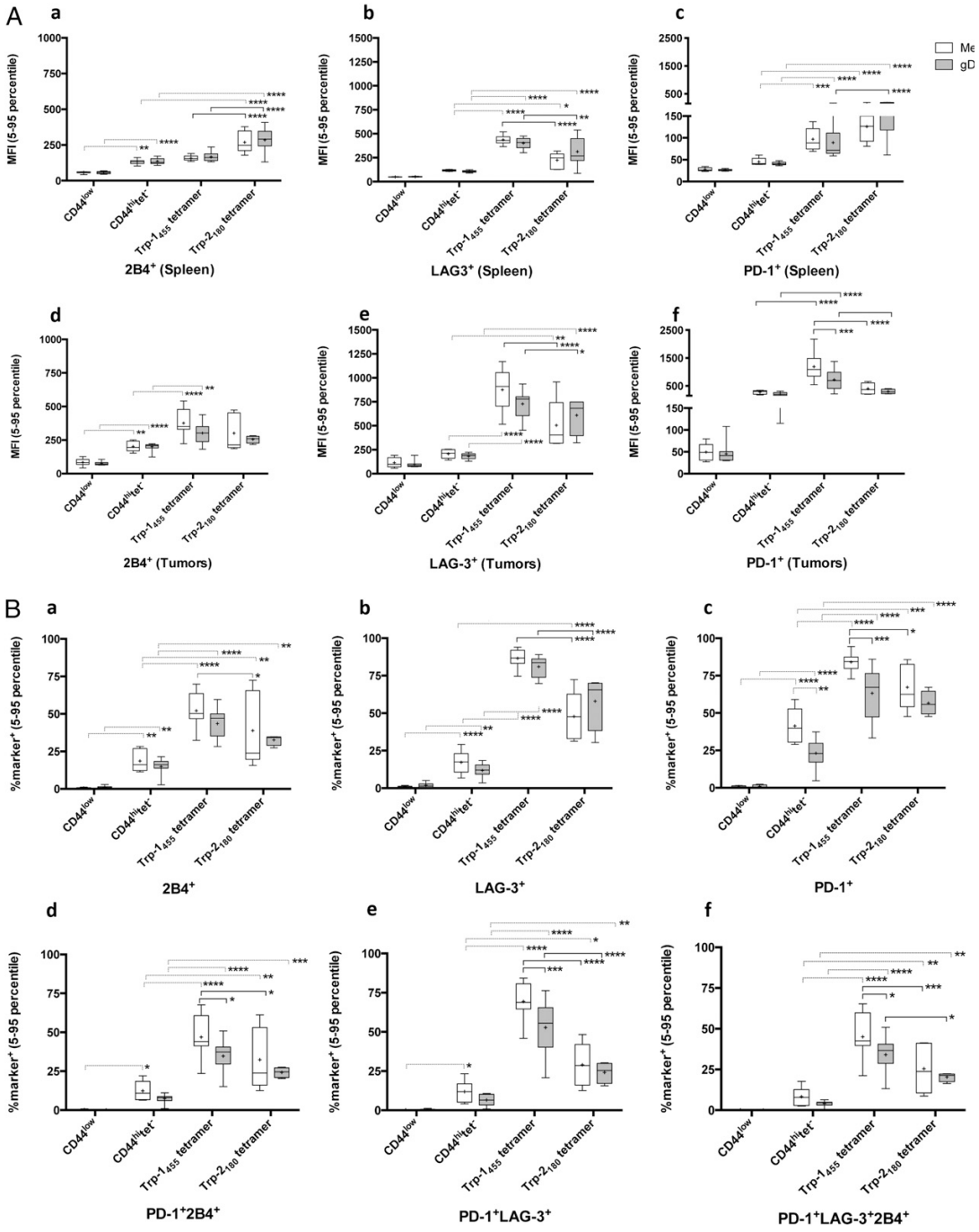

FIGURE 2-8. MAA-specific CD8$^+$ T cell phenotypes. Phenotypes of CD8$^+$ T cells isolated from spleens and tumors of the two subcohorts shown in Fig. 4 were tested for expression of 2B4, LAG-3 and PD-1. **A** Mean fluorescence intensity (MFI) of 2B4 (a, d), LAG-3 (b, e) and PD-1 (c, f) fluorochrome-labeled antibodies on CD44$^-$CD8$^+$, tetramer$^-$CD44$^+$CD8$^+$ and tetramer$^+$CD44$^+$CD8$^+$ T cells from spleens (**a-c**) and tumors (**d-f**). Open boxes show results for CD8$^+$ T cells from AdC68-Melapoly vaccinated mice, grey boxes

indicated $CD8^+$ T cells from AdC68-gDMelapoly vaccinated mice. (*) indicates significant differences as detailed in legend to Fig. 1 between groups connected by lines (dashed lines for differences between control cells or between control cells and antigen-specific $CD8^+$ T cells , solid lines for differences between specific $CD8^+$ T cells). The following p-values were obtained for Trp-1_{455} and Trp-2_{180} comparisons: (**Aa**): Trp-1_{455} vs. Trp-2_{180}: Melapoly: $p < 0.0001$, gDMelapoly: $p < 0.0001$; (**Ad**): none; (**Ab**) Trp-1_{455} vs. Trp-2_{180}: Melapoly: $p < 0.0001$, gDMelapoly: $p = 0.0056$; (**Ae**) Trp-1_{455} vs. Trp-2_{180}: Melapoly: $p < 0.0001$; (**Ac**) Trp-1_{455} vs. Trp-2_{180}: gDMelapoly: $p < 0.0001$; (**Af**) Trp-1_{455} vs. Trp-2_{180}: Melapoly: $p < 0.0001$, gDMelapoly: $p = 0.028$, Melapoly vs. gDMelapoly: Trp-1_{455}: $p = 0.0008$. **5B** Percentages of tumor-derived naïve $CD44^-CD8^+$, $tetramer^-CD44^+CD8^+$, and $tetramer^+CD44^+CD8^+$ T cells that were positive for a given marker or combinations of exhaustion markers. Cells from AdC68-Melapoly vaccinated mice are shown as open boxes, cells from AdC68-gDMelapoly vaccinated mice are shown as grey boxes. Whiskers show 5-95 percentile, lines show 50 percentile, + within boxes indicates means. (*) indicates significant differences between groups as described in legends to Fig. 1. (**Ba**) Trp-1_{455} vs. Trp-2_{180}: Melapoly: $p = 0.031$. (**Bd**) Melapoly vs. gDMelapoly: Trp-1_{455}: $p = 0.035$; Trp-1_{455} vs. Trp-2_{180}: Melapoly: 0.019. (**Bb**): Trp-1_{455} vs. Trp-2_{180}: Melapoly: $p < 0.0001$, gDMelapoly: $p < 0.0001$. (**Be**) Melapoly vs. gDMelapoly: Trp-1_{455}: $p = 0.0036$; Trp-1_{455} to Trp-2_{180}: Melapoly: $p < 0.0001$, gDMelapoly: $p < 0.0001$. (**Bc**) Melapoly vs. gDMelapoly: Trp-1_{455}: $p = 0.0006$, Trp-1_{455} vs. Trp-2_{180}: Melapoly $p = 0.016$. (**Bf**) Melapoly vs. gDMelapoly: Trp-1_{455}: $p = 0.039$; Trp-1_{455} vs. Trp-2_{180}: Melapoly: $p = 0.0004$, gDMelapoly: $p = 0.021$.

Figure 2-9: Gating scheme for expression of markers on $CD8^+$T cells

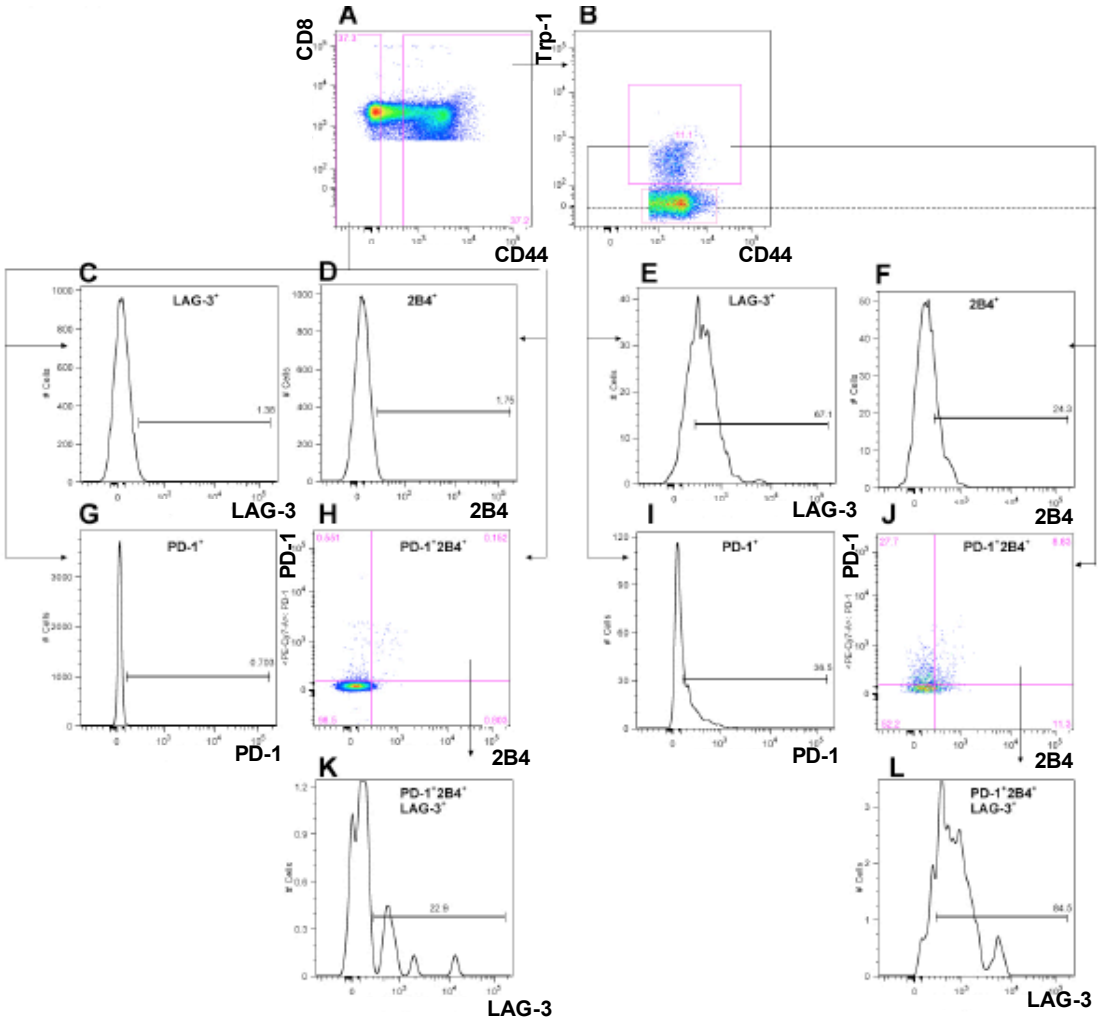

FIGURE 2-9. Gating scheme for expression of markers on CD8$^+$T cells. Cells were gated on lymphoid, single live CD8$^+$ cells as shown in Figure 1. Cells were then gated onto CD44^{low} and CD44^{hi} cells (**A**). CD44^{hi} cells were gated on cells positive for either of the two tetramers and on cells negative for either of the two tetramers (**B**). CD44$^-$ (**C,D,G,H,K**), tetramer$^+$CD44$^+$ (**E,F,I,J,L**) and tetramer-CD44+ cells were then gated onto LAG-3 (**C,E**), 2B4 (**D,F**) and PD-1 (**G,I**). The gates were adjusted so that CD44-CD8+ cells had less than 2% of marker positive cells. Cells were then gated onto 2B4 over PD-1 to identify cells positive for both markers (**H,J**). Cells double positive for PD-1 and 2B4 were then gated onto LAG-3 (**K,L**) to identify cells positive for all three markers.

Markers that are indicative for exhaustion are also upregulated upon activation. To ensure that AdC68-gDMelapoly-induced TILs showed better preservation of function as would be expected of less exhausted CD8$^+$ T cells, I compared the proportions of Trp-1 specific CD8$^+$ T cells that produced only IFN-γ or IFN-γ together with TNF-α between the two vaccine groups. For these comparisons cells were isolated from tumors at days 30-35 after vaccination. AdC68-gDMelapoly-induced Trp-1-specific CD8$^+$ T cells had significantly higher proportions of Trp-1 specific CD8$^+$ TILs that produced both cytokines compared to AdC68-Melapoly-induced TILs (mean AdC68-gDMelapoly: 0.47, AdC68-Melapoly: 0.3, p = 0.04 by two-tailed t-test). To further ensure that Trp-1-specific TILs with increased expression of PD-1 or PD-1 and LAG-3 were indeed exhausted rather than recently activated, I tested PD-1$^+$ and PD-1$^-$ TILs for production of IFN-γ and TNF-α upon stimulation with the Trp-1$_{455}$ peptide. As shown in **Figure 2-10A**, slightly higher frequencies of Trp-1 specific CD8$^+$ T cells from blood produced IFN-γ together with TNF-α than IFN-γ only. In tumors this proportion shifted and nearly 70% of Trp-1 specific TILs produced only IFN-γ suggesting loss of function (mean frequencies of Trp-1-specific CD8$^+$ T cells: blood: IFN-γ^+TNF-α^- vs. IFN-γ^+TNF-α^+: 0.32% vs. 0.57%; tumor: 1.85% vs. 0.84%). Co-stains for PD-1 showed significantly higher PD-1 expression on mono-functional Trp-1-specific CD8$^+$ TILs as compared to those that produced both cytokines (mean PD-1 MFI values: blood: IFN-γ^+TNF-α^- vs. IFN-γ^+TNF-α^+: 174 vs. 143, tumor: 1236 vs. 774, **Figure 2-10B**). An analysis for expression of T-bet, which controls transcription of effector molecules and inhibits expression of PD-1, showed that T-bet levels were low on naïve circulating CD8$^+$ T cells and markedly increased on blood-derived Trp-1-specific CD8$^+$ T cells. Tumor-infiltrating Trp-1-specific CD8$^+$ T cells showed a marked reduction in T-bet expression (**Figure 2-10C**), which corresponded to expression levels of

exhaustion/activation markers (mean T-bet MFI values: $CD44^-CD8^+$ T cells: 6.2; Trp-1 specific $CD8^+$ T cells blood vs. TILs: 464.2 vs. 204.6); Trp-1-specific $CD8^+$ TILs that expressed high levels of PD-1 or PD-1 and LAG-3 had reduced levels of T-bet as compared to those with low PD-1 or PD-1 and LAG-3 expression (**Figure 2-10D-F**) (mean T-bet MFI values: $PD\text{-}1^+$ vs. $PD\text{-}1^-$: 191.4 vs. 286.2; $PD\text{-}1^+LAG\text{-}3^+$ vs. $PD\text{-}1^-LAG\text{-}3^-$: 181.3 vs. 256). Overall these results show that increased expression of PD-1 was associated with loss of polyfunctionality and downregulation of T-bet, confirming that MAA-specific $CD8^+$ T cells induced by the vaccines were differentiation towards exhaustion within the TME.

Figure 2-10: MAA-specific T cell functions in relation to phenotypes

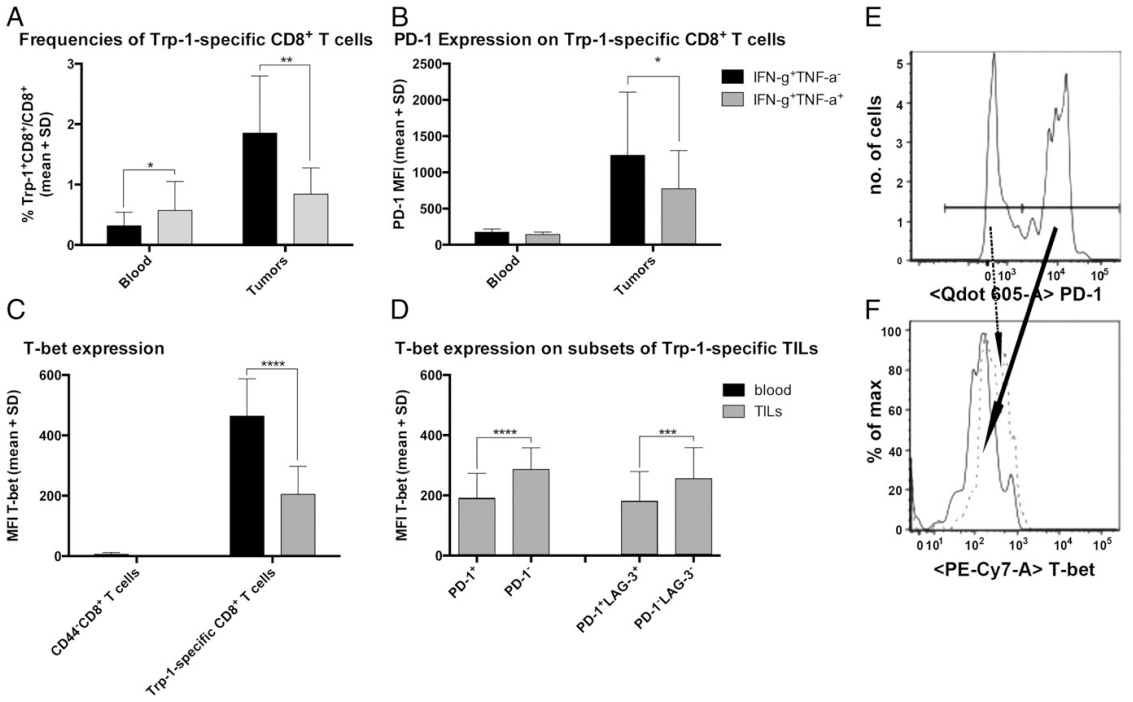

FIGURE 2-10 MAA-specific T cell functions in relation to phenotypes. Mice with 3-day old $B16Braf_{V600E}$ tumors were vaccinated with 10^{10} vp of AdC68-gDMelapoly. Lymphocytes from blood and tumors were isolated 4 weeks later. (**A**) Frequencies of $CD8^+$ T cells producing IFN-g only or IFN-g together with TNF-a were determined by ICS. By t-tests frequencies of Trp-1-specific $IFN\text{-}g^+TNF\text{-}a^+CD8^+$ T cells were higher in blood than those of $IFN\text{-}g^+TNF\text{-}a^-CD8^+$ T cells ($p = 0.036$) while in TILs frequencies of Trp-1-specific $CD8^+$ T cells producing only IFN-g were significantly higher ($p = 0.0066$). (**B**) shows levels of PD-1 expression on Trp-1-specific $CD8^+$ T cells that produced only IFN-g or IFN-g together with TNF-a. Expression levels were comparable in blood-derived cells but significantly higher on TILs that were only positive for IFN-g than on those that produced both cytokines ($p = 0.024$). (**C**) shows levels of T-bet expression on naïve $CD44^-CD8^+$ lymphocytes from blood and on Trp-1-specific $CD8^+$ T cells from blood and tumors. Trp-1-specific $CD8^+$ T cells expressed significantly higher levels of T-bet as compared to naïve $CD8^+$ T cells ($p < 0.0001$). T-bet expression was higher on blood than on tumor-derived Trp-1-specific $CD8^+$ T cells ($p < 0.0001$). (**D**) shows levels of T-bet expression on Trp-1-specific TILs separated into subgroups according to levels of PD-1 or PD-1 and LAG-3 expression. Levels of T-bet expression were significantly higher on $PD\text{-}1^-$ as compared to

PD-1$^+$ cells (p = 0.0001) and on PD-1$^-$LAG-3$^-$ cells than on PD-1$^+$LAG-3$^+$ cells (p = 0.0002). (**E**) Gating scheme onto PD-1$^+$ and PD-1$^-$ cells following initial gating on live lymphoid cells, CD8$^+$ cells, CD44^{hi} cells and Trp-1 tetramer$^+$ cells as shown in Suppl. Fig. 1. (**F**) Expression levels of T-bet on PD-1$^-$ (dashed line) and PD-1$^+$ Trp-1-specific CD8$^+$ T cells.

Taken together these results demonstrate complex patterns of up-regulation of exhaustion markers during tumor progression that were affected by the vaccines, the TcR specificity as well as the anatomic sites from which T cell had been isolated. Within tumors MAA-specific CD8$^+$ T cells induced by the AdC68-gDMelapoly vector were less exhausted compared to those induced by the AdC68-Melapoly vector, fewer cells expressed exhaustion markers and they were able to delay tumor progression for longer periods of time. In addition, tumor-infiltrating CD8$^+$ T cells specific to the dominant Trp-1$_{455}$ epitopes showed more evidence of exhaustion compared to those specific to the subdominant Trp-2$_{180}$ epitope.

DISCUSSION

T cell activation is finely tuned upon binding of the TcR to its cognate antigen-MHC class I molecule complex through additional interactions with co-stimulatory and co-inhibitory receptors (264,265). Co-inhibitory receptors include CTLA-4, PD-1, BTLA and others. BTLA, unlike PD-1 and CTLA-4, is expressed on both naïve and activated T cells (266) and thereby presumably regulates T cell activation at several stages. PD-1 and CTLA-4 inhibit downstream signals transmitted upon TcR ligation such as induction of the protein kinase B pathway (PKB), albeit through distinct pathways (114,267). PKB in turn regulates cell survival as well as glucose metabolism and is therefore crucial for successful activation and expansion of T cells (268). The exact signaling pathway downstream of BTLA remains unknown. Similar to PD-1 and CTLA-4, the cytoplasmic domain of BTLA contains immune-receptor tyrosine based inhibitory motifs (269) that may dampen TcR signaling.

Although modulators of HVEM signaling have not yet been tested in humans, the TNFRSF14 locus, which encodes HVEM, has been linked to increased risks for ulcerative colitis (270), systemic lupus erythomatodus (271) and rheumatoid arthritis (272), stressing the

importance of this regulatory pathway. Similarly, genetic deletions of BTLA or HVEM cause exacerbated inflammatory reactions (273) and accelerated rejection of partially mismatched transplants in mice (274).

It has been shown that HVEM is expressed on tumor cells such as B cell lymphomas (275) or metastatic melanomas. BTLA on the other hand is highly expressed on melanoma-specific $CD8^+$ T cells and it has been argued that the impaired proliferative capacity of MAA-specific T cell in melanoma patients is linked to immunoinhibitory signals from $HVEM^+$ tumor cells (276). In another study NY-ESA-1-specific $CD8^+$ T cells from end-stage melanoma patients were shown to express elevated levels of PD-1 and BTLA (277). T cells were defective in their ability to proliferate or secret factors in response to antigenic stimulation, which could in part be restored by blocking PD-1 and/or BTLA signaling. This suggests that inhibitors of BTLA should be explored as additives to active immunotherapy of melanoma.

As we showed previously, blockade of the BTLA-HVEM pathway through HSV-1 gD during antigen-driven T cell stimulation numerically augments $CD8^+$ T cell responses (244,263). This was confirmed in the current study using vaccines expressing multiple epitopes derived from MAAs. In a prophylactic melanoma model, the superior protection achieved upon gD-mediated blockade of the HVEM pathways at the time of T cell induction was correlated with the magnitude of MAA-specific $CD8^+$ T cell responses. Using different doses of the two vaccines, i.e., AdC68-Melapoly and AdC68-gDMelapoly, mice that developed approximately equal frequencies of MAA-specific T cells showed comparable levels of protection against tumor challenge. In contrast, in mice that were inoculated first with melanoma cells and then vaccinated with either of the two vectors, the magnitude of the vaccine-induced MAA-specific $CD8^+$ T cell responses was not the sole factor that determined vaccine efficacy; in mice with approximately comparable frequencies of MAA-specific $CD8^+$ T cells following vaccination with the AdC68-Melapoly or AdC68-gDMelapoly vectors, those that received the latter survived significantly longer. Cytokine profiles of antigen-specific $CD8^+$ T cells were largely comparable between the two vaccine groups before

and after challenge with responses being dominated by $CD8^+$ T cells producing IFN-γ alone or in combination with TNF-α(not shown) as is typical for T cells induced by Ad vectors.

Paradoxically, at the time of necropsy AdC68-Melapoly vaccinated animals had significantly higher frequencies of MAA-specific $CD8^+$ T cells in some tissues compared to those vaccinated with AdC68-gDMelapoly. This again confirms that protection did not solely correlate with frequencies of vaccine-induced T cells. Further analysis of MAA-specific $CD8^+$ T cells for expression of activation/exhaustion markers showed that within tumors lower frequencies of AdC68-gDMelapoly-induced $CD8^+$ T cells expressed LAG-3, PD-1, PD-1 together with LAG-3 or 2B4 or all three markers as compared to AdC68-Melapoly induced $CD8^+$ T cells. These markers are not only indicative for exhaustion but they are also increased upon recent $CD8^+$ T cells activation. Antigens derived from the tumor may have provided further activation signals to the MAA-specific $CD8^+$ T cells, which then contributed to their elevated levels on tumor-infiltrating MAA-specific $CD8^+$ T cells. Nevertheless, as these activation signals should have been provided to T cells in both vaccine cohorts, I assume that the differences in expression levels on tumor-infiltrating MAA-specific $CD8^+$ T cells in Melapoly and gDMelapoly-vaccinated mice reflected differences in their stage of exhaustion. This was further confirmed by loss of polyfunctionality and T-bet expression on cells with increased expression of immunoinhibitory markers. In turn, my finding suggests that the relative resistance to tumor-driven exhaustion of MAA-specific $CD8^+$ T cells generated in presence of gD resulted in prolonged control of tumor progression.

T cell exhaustion, a consequence of continued antigen-driven-stimulation of T cells, was initially described in chronic viral diseases such as those caused by lymphocytic choriomeningitis virus infection of mice (111) or human immunodeficiency virus (278) or hepatitis C virus infection (279) of humans. It was subsequently observed in cancer patients. Differentiation towards exhaustion is initially characterized by increased expression of PD-1 on the T cell surface, which over time is joined by other co-inhibitors (103). Expression of PD-1 is regulated by TcR ligation (280) and at the transcriptional level by NFAT1c (281). T cells with high affinity TcRs appear to be more sensitive to antigen-driven exhaustion compared to those with

lower affinity TcRs (282). This is supported by my finding that within tumors $CD8^+$ T cells specific to the subdominant Trp-2_{180} epitope appeared less exhausted; vaccine-induced Trp-2_{180}-specific $CD8^+$T cells expressed lower levels of PD-1 or LAG-3 as compared to $CD8^+$ T cells specific to the more dominant Trp-1_{455} epitope. The same pattern was seen for MAA-specific $CD8^+$ T cells that were double or triple positive for PD-1, 2B4 and/or LAG-3. Notwithstanding, it should be pointed out that the finding that higher TcR affinity promotes exhaustion remains debatable, although it is compatible with the highly reproducible finding that exhaustion is primarily driven by continued TcR ligation (283). Other pathways that prevent antigen-driven exhaustion of $CD8^+$ T cells induced by the gD-adjuvanted vaccine may have contributed the results, but cannot be explored without additional knowledge of the BTLA/CD160 signaling pathways.

Active cancer immunotherapy with traditional vaccines that boost tumor-specific T cell responses has performed poorly in patients with advanced cancer. Additional strategies that block immunoinhibitory pathways may improve the efficacy of cancer vaccines. Here I show that adjuvanting a tumor vaccine with HSV-1 gD could induce tumor antigen-specific $CD8^+$ T cells with increased resistance to exhaustion. This approach, unlike other reagents that block immunological checkpoints such as antibodies to PD-1 or CTLA-4, selectively affects tumor antigen-specific T cells and presumably will not globally perturb the exquisitely fine-tuned balance of the immune system.

MATERIALS AND METHODS

Mice

Female C57Bl/6 mice (6-8 weeks) were purchased from the National Cancer Institute (NCI) and housed at the Wistar Institute Animal Facility. All procedures were performed under the guideline of protocols approved by the IACUC of the Wistar Institute.

Cell lines

The B16Braf$_{V600E}$ cell line was derived from B16.F10 cells transduced with lentiviral vector pLU-EF1a-mCherry expressing mouse Braf$_{V600E}$ (provided by Dr. M Herlyn lab, Wistar Institute, Philadelphia, PA). The mutant cell line showed the same in vivo growth characteristics as unmodified B16.F10 cells. E1-transfected HEK 293 cells were used to propagate Ad vectors. Cells were cultured with DMEM supplemented with 10% FBS.

Construction of recombinant Ad vectors

I designed the Melapoly transgene to express a number of MAA-specific CD4$^+$ T cell and CD8$^+$ T cell epitopes. An endoplasmic reticulum (ER) targeting signal sequence was included at the N-terminal end of the sequence(284). Three human (h)Trp-2-specific CD4$^+$ T cell epitopes(285) as well as the universal T helper cell epitope PADRE(286) were incorporated into the Melapoly construct. CD8$^+$ T cell epitopes were derived from human and mouse Trp-2, human gp100, mouse Trp-1 and Braf$_{V600E}$. Epitopes from Trp-1 and Braf antigens were modified to enhance their binding to MHC class I molecules(287). A Flag-tag was added to the C-terminal end. I designed the spacer sequences according to several analysis programs, including PAPROC I (http://www.paproc.de), Netchop 3.1 (http://www.cbs.dtu.dk/services/NetChop/), and IEBD Analysis Resource (http://tools.immuneepitope.org/main/). The spacers were inserted between each CD4$^+$ and CD8$^+$ T cell epitope to reduce interference of epitope processing(288,289). The Melapoly gene was codon optimized and inserted into the pUC57 vector (Genescript, Piscataway, NJ). The Melapoly transgene was sequenced and cloned it into the pShuttle vector by EagI digestion. To construct the AdC68-gDMelapoly vector, the Melapoly transgene was fused into the N terminus of HSV-1 gD. The pShuttle gDMelapoly vector was generated by PCR using pShuttle Melapoly as the template, gDMelaFwAgeI CGACCGGTTAGCTAAGTTTGTGGCCGCTTG and gDMelaRvAvrII CGCCTAGGTGCTGCTGCTGCAATGCTC as primers. The PCR product was cleaved by AgeI and AvrII and cloned into the pShuttle gD-Flag vector. The inserts containing regulatory sequences of the pShuttle vector were subcloned into the E1-deleted AdC68 viral molecular clone using I-CeuI and PI-SceI sites. Recombinant AdC68 vectors were rescued, propagated on HEK 293 cells, purified by CsCl-gradient centrifugation and titrated as

described(290). The concentration of each virus batch was determined by measuring virus particles (vp) by spectrophotometry at 260nm.

Real-Time PCR

I infected HEK 293 cells with 10^{10}vp and 10^{11}vp doses of AdC68-Melapoly and AdC68-gDMelapoly vectors. Cells were harvested 24 hours later and total RNA was isolated from each sample using RNeasy Mini Kit (Qiagen, Venlo, Netherlands). cDNA samples were obtained by reverse transcription using 2ug RNA/sample with high capacity cDNA reverse transcription kit (Applied Biosystems, Foster City, CA). 20ng cDNA/sample was used for real-time PCR using Fast SYBR green mastermix (Applied Biosystems, Foster City, CA). To obtain standards for real-time PCR, I performed regular PCR for Melapoly and GAPDH (housekeeping gene as internal control) using the cDNA samples. I ran the PCR products on 1% agarose gel, purified the PCR products of the expected sizes (MiniElute gel extraction kit, Qiagen, Netherlands) and measured the DNA concentration using spectrometry. I diluted the purified Melapoly and GAPDH DNAs from 5ng to 0.156ng for real-time PCR standards. For real-time PCR, cDNA samples were replicated for both Melapoly and GAPDH using the 7500 Fast real-time PCR machine (Applied Biosystems, Foster City, CA). The primer sequences are as follows: regular PCR MelapolyFw ACAGGAAACTTCGCCGCTGC, MelapolyRv TGCCATATATCCGAGGTTGTCTG, real-time PCR MelapolyRv1 TGATCGGCTGCAGCCACGTC; regular PCR GAPDHFw GGTGAAGGTCGGTGTGAACGGATTT, GAPDHRv AATGCCAAAGTTGTCATGGATGACC and real-time PCR GAPDHFw1 TGCCCCCATGTTTGTGATGG. The final concentrations of Melapoly cDNA from both vector-infected samples were analyzed and compared after normalization to GAPDH.

Immunization and challenge of mice

Groups of C57BL/6 mice were vaccinated i.m. with the AdC68 vectors diluted in PBS into the tribialis anterior muscle of each hind limb, with doses ranging from 3 x 10^9 to 10^{11} vp per mouse.

In tumor challenge experiments, B16Braf$_{V600E}$ cells suspended in serum-free medium were inoculated s.c. into the right flank of mice. For pre-and post-tumor challenge experiments, 5x10^4 cells were injected and mice were vaccinated 14 days before or 3 days after tumor cell challenge. I monitored tumor growth by measuring the perpendicular diameters of tumors at least three times a week. Mice were euthanized once tumors exceeded a surface area of 100 mm^2. Mice were monitored for a period of 60 days post tumor challenge.

Isolation of lymphocytes

PBMCs and splenocytes were harvested as described before(244). To obtain tumor-infiltrating lymphocytes (TILs), tumors were cut into small fragments and treated with 2mg/ml collagenase P and 1mg/ml DNase I (Life Technologies, Carlsbad, CA) diluted in Hank's balanced salt solution (HBSS,1X) (Thermo Fisher Scientific, Pittsburgh, PA) with agitation for 1 hour. Tumor fragments were homogenized, filtrated and lymphocytes were purified by Percoll-gradient centrifugation.

Tetramer and intracellular cytokine staining

To detect tetramer-specific CD8$^+$T cells, I stained cells with a PE-labeled tyrosinase-related protein 1 (Trp-1)-specific MHC class I (H-2D^b) tetramer carrying the TAPDNLGYM peptide and an Alexa647-labeled tyrosinase-related protein 2 MHC class I (H-2K^b) tetramer carrying the SVYDFFVWL peptide (obtained from the NIAID Tetramer Facility, Atlanta, GA). The following antibodies were also used for staining: anti-CD8-PerCPCy5.5, PacBlue or Alexa700, CD4-PercpCy5.5, CD44-PacBlue or Alexa700, LAG-3 PercpCy5.5, PD-1 PE-Cy7 (all from Biolegend, San Diego, CA), 2B4 FITC (eBioscience, San Diego, CA) and Amcyan fluorescent reactive dye (Life Technologies). For intracellular cytokine staining (ICS), CD8$^+$ and CD4$^+$ T cell responses to individual epitopes were measured using ~10^6 lymphocytes per samples. Cells were cultured in 2% FBS DMEM medium with individual MHC class I or class II restricted peptides at a concentration of 5ug/ml (for peptides representing CD8$^+$ T cell epitopes): mTrp-1$_{455-463}$ TAPDNLGYA, mTrp-1$_{481-489}$ IAVVAALLL, mTrp-2$_{522-529}$ YAEDYEEL, hTp-2$_{180-188}$ SVYDFFVWL,

hTrp-$2_{343-357}$ STFSFRNAL, mTrp-$2_{363-371}$ SQVMNLHNL, hgp100_{25-33} KVPRNQDWL and mBRaf $_{594-602}$ FGLANEKSI; or 10ug/ml (for peptides representing $CD4^+$ T cell epitopes): PADRE: AKFVAAWTLKAAA, hTrp-2_{88-102}: RKFFHRTCKCTGNFA, hTrp-$2_{237-256}$: NESFALPYWNFATGRNECDV and mTrp-$2_{363-376}$: SQVMNLHNLAHSPL (Genescript, Piscataway, NJ). To determine overall MAA-specific T cell responses, a peptide pool including all $CD8^+$ and $CD4^+$ T cell epitopes expressed by the Melapoly or gDMelapoly vectors was used for lymphocytes stimulation. A rabies virus glycoprotein peptide was used as a negative control. ICS was conducted as described before(261). Produced cytokines, enzymes were stained with the following antibodies: anti-IFN-γ-APC, IL-2-Alexa700 or FITC, TNF-α-PE-Cy7 (BioLegend, San Diego CA). Transcription factor T-bet was stained using Foxp3/Transcription factor staining buffer set (ebioscience) using anti-T-bet-PE-Cy7 antibody (eBioscience, San Diego CA). Cells tested by ICS were co-stained for exhaustion marker PD-1using anti-PD-1-Brilliant Violet 605 antibody (BioLegend, San Diego CA). Cells were analyzed by an LSRII (BD Biosciences, Franklin Lakes, NJ). Data were analyzed with FlowJo (TreeStar, Ashland, OR). Experiments using ICS or tetramer stains were controlled assessing responses of $CD44^-CD8^+$ cells within the same animals after preliminary experiments confirmed that results were comparable to those obtained with $CD44^+CD8^+$ cells of naïve mice or mice vaccinated with the AdC68-gD control vector.

Statistical analysis

I compared the differences of immune responses between more than two groups using one-way ANOVA followed by Holm-Sidak's multiple comparisons. Immune responses affected by two factors (vaccine and tissue type or vaccine and cell type) were analyzed by two-way ANOVA with Holm-Sidak's multiple comparisons. I performed Holm-Bonferroni correction for multiple comparisons within the same dataset. Survival rates between different treatment groups were compared using Gehan-Breslow-Wilcoxon test. Significance was set at p-values of or below 0.05. All statistical analyses were performed using Graphpad Prism6. Throughout the manuscript p-values adjusted for type 1 errors are shown.

Chapter 3

Depletion of FAP$^+$ cells reduces immunosuppressive cells and improves metabolism and functions of CD8$^+$T cells within tumors

ABSTRACT

The tumor stroma, which is essential to support growth and metastasis of malignant cells, provides targets for active immunotherapy of cancer. Previous studies have shown that depleting fibroblast activation protein (FAP)-expressing stromal cells reduces tumor progression and concomitantly increases tumor antigen (TA)-specific T cell responses. However the underlying pathways remain ill defined. Here I identify that immunosuppressive cells (ISCs) from tumor-bearing mice impose metabolic stress on CD8$^+$T cells, which is associated with increased expression of the co-inhibitor PD-1. In two mouse melanoma models, depleting FAP$^+$ stroma cells from the tumor microenvironment (TME) upon vaccination with an adenoviral-vector reduces frequencies and functions of ISCs. This is associated with changes in the cytokine/chemokine milieu in the TME and decreased activity of STAT6 signaling within ISCs. Decreases in ISCs

upon FAP^+ stromal cell depletion is associated with reduced metabolic stress of vaccine-induced tumor infiltrating $CD8^+$T cells and their delayed progression towards functional exhaustion, resulting in prolonged survival of tumor-bearing mice.

Portions of this chapter were adapted from:

Zhang Y, Ertl HC. Depletion of FAP+ cells reduces immunosuppressive cells and improves metabolism and functions of $CD8^+$T cells within tumors. **Oncotarget** 2016; doi:10.18632/oncotarget.7818.

INTRODUCTION

Solid tumors are composed of neoplastic cells and tumor stroma. The stroma, which includes connective tissue, cancer-associated fibroblasts (CAFs), blood vessels and infiltrating inflammatory cells, is essential for progression of solid tumors (291-294). Tumor stroma also protects malignant tumor cells from an onslaught by the immune system by subverting protective immune responses, while supporting those that are immunosuppressive (295-297). Targeting tumor stroma is thus being explored for treatment of cancer patients (298-300).

The supporting stroma of melanoma contains an abundance of CAFs, which are functionally distinct from fibroblasts in normal tissues (301-303). One key distinguishing feature is their selective expression of FAP, which is not present at high levels on cells of a healthy adult organism (304-306). FAP^+ stromal fibroblasts are essential to maintain the TME and promote cancer progression. They inhibit TA-specific immune responses by producing cytokines and chemokines, which attract immunosuppressive cells (ISCs) including regulatory T cells (Tregs), myeloid-derived suppressor cells (MDSCs) and tumor-associated macrophages (TAMs) (128,129). Factors secreted by FAP^+ stromal cells may also interfere with T cell-tumor cell interactions and hinder tumor cell lysis (130). Genetic depletion of FAP, vaccines targeting FAP or T cells with a FAP-specific chimeric antigen receptor (CAR) inhibit tumor growth in part by enhancing tumor-specific immune responses (124,131-133); however the underlying mechanisms remain poorly understood.

T cell responses within tumors are impaired by numerous mechanisms such as increases of co-inhibitors upon chronic antigen stimulation and accumulation of tumor-infiltrating ISCs. Recently it has been reported that lack of glucose within the TME poses metabolic stress on tumor-infiltrating T lymphocytes (TILs), which contributes to their functional exhaustion and impairs their antitumor performances (192,197). I hypothesized that depletion of FAP^+ stromal cells may reduce the metabolic stress of TA-specific TILs and thereby improve their effector

functions and the overall efficacy of active immunotherapy. To test this hypothesis, I used a replication-defective adenovirus (Ad)-based vaccine expressing FAP given together with an Ad vaccine expressing multiple epitopes from melanoma-associated antigens (MAAs) in two mouse melanoma models. My data show that vaccination against FAP significantly improves the therapeutic efficacy of the traditional cancer vaccine by destroying FAP^+ stroma cells. In addition it reduces numbers and functions of tumor-infiltrating ISCs by changing the cytokine/chemokine milieu within the TME and inhibiting the activity of the STAT6 signaling pathway within ISCs. I show *in vitro* that ISCs enhance the mitochondrial metabolic stress of activated $CD8^+$T cells and increases expression of the co-inhibitor PD-1. In the same token, the decreased levels of ISCs within the TME upon FAP vaccination is associated with reduced metabolic stress of vaccine-induced MAA-specific $CD8^+$T cells, improved frequencies and effector functions of these cells and their delayed progression towards exhaustion.

My data support further exploring the tumor-stroma-targeting vaccines for active immunotherapy of cancer.

RESULTS

The AdC68-mFAP vaccine elicits robust antibody and T cell responses in different mouse melanoma models

To achieve immune-mediated destruction of the tumor stroma, I developed a vaccine based on a replication-defective Ad vector of chimpanzee serotype 68 (AdC68), which expresses full-length murine FAP from a CMV promoter-driven transgene incorporated into the vector's deleted E1 domain. The vaccine expressed FAP in transduced HEK 293 cells in a dose-dependent fashion (**Figure 3-1A**). The vaccine, termed AdC68-mFAP, elicited robust FAP-specific antibody responses in mice as tested by a FAP- specific ELISA with sera from individual vaccinated mice (**Figure 3-1B**). I further tested AdC68-mFAP for induction of FAP-specific $CD8^+$T cells by measuring vaccine-induced responses to 16 potential $CD8^+$T cell epitopes of

mouse FAP (**Figure 3-1C**). The epitopes were selected based on their predicted high affinity to MHC class I antigens H-2D^{b} and H-2K^{b}. The vaccine was tested in wild-type C57BL/6 mice and transgenic Tyr::CreER, Braf$^{CA/+}$ Pten $^{lox+/lox}$ mice. The transgenic mice were genetically engineered to develop melanoma upon Cre-mediated disruption of Pten expression (307). This model, which recapitulates the genetic mutations of human melanoma, is a highly clinically relevant model for pre-clinical evaluation of therapies for melanoma. In both mouse strains AdC68-mFAP induced CD8^{+}T cells that produced mainly interferon (IFN)-γ or tumor necrosis factor (TNF)-α in response to *in vitro* stimulation with FAP-derived peptides representing each of the 16 epitopes expressed by the vaccine (**Figure 3-1D-E**). Frequencies of FAP-specific CD8^{+}T cell responses were significantly higher in transgenic mice. FAP-specific CD8^{+}T cells elicited in C57BL/6 mice mainly recognized epitopes 1 and 5-9, while those in Braf$^{CA/+}$ Pten $^{lox+/lox}$ mice mainly responded to epitopes 5, 9, 10, 12 and 15. To confirm that the FAP-specific CD8^{+}T cells were able to kill their target cells, I performed *in vivo* cytotoxicity assay in C57BL/6 mice immunized with AdC68-mFAP or a control Ad vector. Syngeneic splenocytes were pulsed either with FAP peptides (i.e., peptides 1, 5, 7, 8 and 9) or a control peptide. They were then labeled with high or low concentrations of CFSE, respectively. The two cell populations were mixed in a 1:1 ratio and transferred to recipient mice that had been immunized 2 weeks earlier with either AdC68-mFAP or a control Ad vector. Compared to control mice, the transferred cells showed significant loss of the CFSE ^{hi} FAP peptide-pulsed cell population in relation to the CFSE^{low} control population in AdC68-mFAP vaccinated mice (34.5% of CFSE ^{hi} cells were lysed in the AdC68-mFAP vaccine group, FAP group vs. control group p=0.0011), suggesting that FAP-specific CD8^{+}T cells elicited by AdC68-mFAP vaccine mediated specific target cell lysis (**Figure 3-1F**). Together these data show that the AdC68-mFAP vaccine is immunogenic and induces robust FAP-specific B and T cell responses in different mouse strains.

Figure 3-1: The AdC68-mFAP vaccine induces FAP-specific antibody and CD8$^+$T cell responses

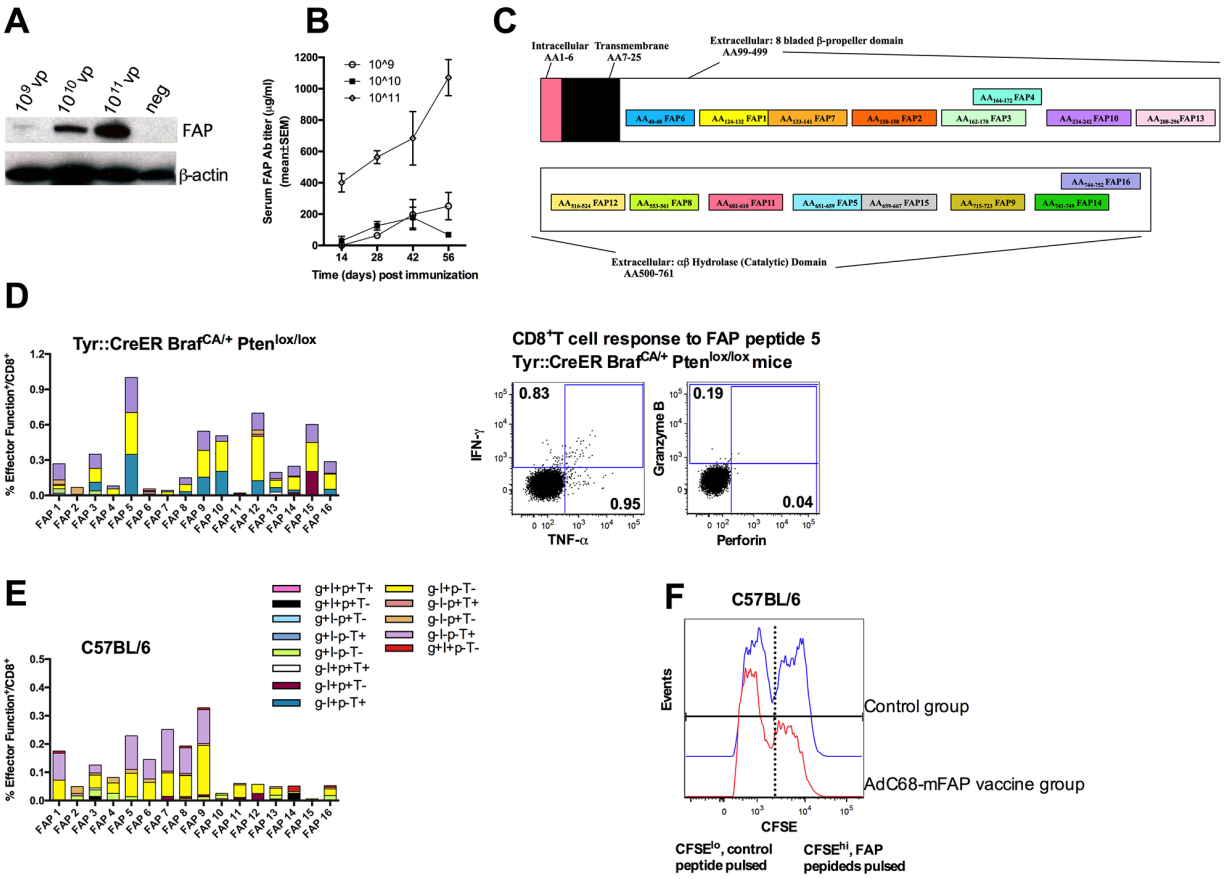

Figure 3-1: The AdC68-mFAP vaccine induces FAP-specific antibody and CD8$^+$T cell responses. (**A**) HEK 293 cells were infected with different doses of AdC68-mFAP vector and protein was harvested 48 hours later. Full-length murine FAP was visualized by Western blot using β-actin as an internal control. (**B**) FAP-specific antibody responses elicited by the AdC68-mFAP vaccine at different time points after vaccination. Results show mean values of FAP antibody titers in serum with standard error of mean (SEM) determined by indirect ELISA. (**C**) Schematic cartoon shows different components of FAP and the 16 CD8$^+$T cell epitopes within FAP that are predicted to bind H-2K^b or H-2D^{b}with high affinity. (**D**) Left: Magnitude and polyfunctions of CD8$^+$T cells directed to individual FAP epitopes in transgenic mice. Right: Representative flow plots illustrate vaccine-induced CD8$^+$T cell response to FAP peptide 5. The production of IFN-γ, TNF-α, granzyme B and perforin were measured. (**E**) Magnitude and polyfunctions of CD8$^+$T cell responses to individual FAP epitopes in C57BL/6 mice. (**D-E**) Color scheme illustrates different combinations of factors that were produced. (**F**) Representative histograms show *in vivo* cell lysis by AdC68-mFAP vaccine-induced CD8$^+$T cells of CFSE^{hi}cells pulsed with FAP peptides. Blue histograms: CFSE$^+$ splenocytes from mice vaccinated with control vector 2 weeks earlier. Red histogram: CFSE$^+$ splenocytes from mice vaccinated with AdC68-mFAP vector 2 weeks earlier.

AdC68-mFAP delays tumor growth and improves survival of melanoma-bearing mice

To assess if the FAP vaccine was likely to influence tumor progression, I analyzed FAP^+ tumor stroma cells from $Braf^{CA/+}Pten^{lox+/lox+}$mice that upon treatment with 4-hydroxyltamoxifen (4-HT) developed tumors. C57Bl/6 mice challenged with a B16F10 cell line modified to express $Braf_{V600E}$ ($B16Braf_{V600E}$, referred to as B16) were tested as well. The $Braf_{V600E}$ epitope, which is highly prevalent in human melanoma, was included to better assess the potential of the vaccine in treating melanoma patients. Expression of FAP within the stroma of ~ 4 week- old $Braf^{CA/+}Pten^{lox+/lox+}$ and B16 tumors was confirmed at the mRNA (not shown) and protein level (**Figure 3-2A, 2C**). A high percentage (~40-50%) of $CD3^-CD14^-CD4^{low}$ cells from tumors of the transgenic mice stained positive for FAP. In contrast, the proportion of FAP^+ cells was lower in B16 tumors. The expression of mutated Braf within the B16 tumor cells may have affected levels of FAP^+ cells, as a different B16.F10 tumor with wild-type Braf but modified to express GFP had markedly higher percentages of FAP^+ cells (~ 25%, data not shown). Most of the FAP^+ cells within either tumor only expressed low to intermediate levels of CD45. Compared to FAP^- cells, FAP^+ cells from either tumors expressed significantly higher levels of mesenchymal stromal cell markers CD90 and Sca-1, confirming the stromal cell lineage of FAP^+ cells [14] (**Figure 3-2B, 2D**).

Figure 3-2: Vaccination with the AdC68-mFAP vector improves survival of tumor-bearing mice

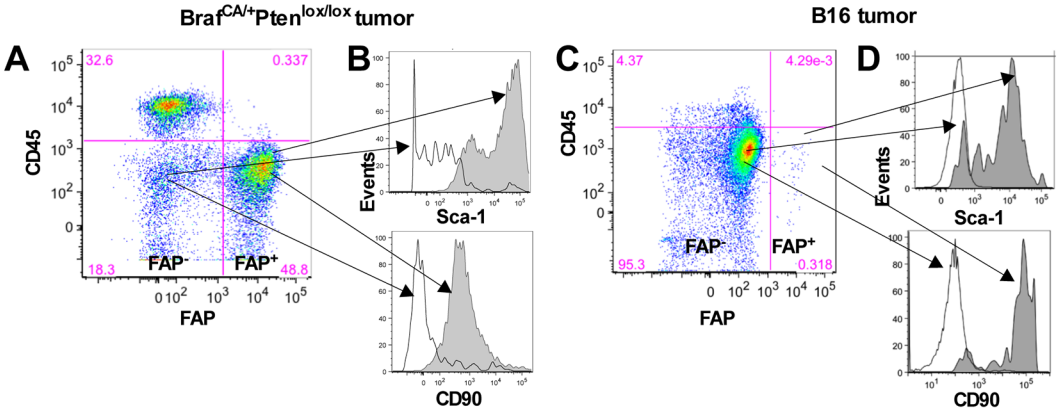

Figure 3-2: Vaccination with the AdC68-mFAP vector improves survival of tumor-bearing mice. (**A, C**) Representative flow plot shows the presence of $CD45^-FAP^+$ cells within tumors from $Braf^{CA/+}Pten^{lox/lox}$

transgenic mice (**A**) or within B16 tumors (**C**). (**B, D**) Histograms indicate the expression of mesenchymal stroma cell markers CD90 and Sca-1 on $CD45^{-}FAP^{+}$ (dark grey) and $CD45^{-}FAP^{-}$ cells (white) in tumors from transgenic mice (**B**) or in B16 tumors (**D**).

To measure the effect of AdC68-mFAP vaccination on tumor progression, I first used $Braf^{CA/+}Pten^{lox+/lox+}$ mice, in which tumors had been initiated 3 weeks earlier (**Figure 3-2E**). I vaccinated mice bearing similar sized tumors with either a control AdC68 vector or AdC68-mFAP. Additional groups received AdC68-mFAP together with a tumor-cell targeting melanoma vaccine termed AdC68-gDMelapoly. AdC68-gDMelapoly vaccine expresses a series of melanoma-associated antigen (MAA) epitopes within herpes simplex virus glycoprotein D (gD) and can elicit robust $CD8^{+}$T cell responses to multiple MAAs as described before (308). Other mice received AdC68-gDMelapoly mixed with a control AdC68 vector, the latter to ensure that mice received equal doses of vaccine. AdC68-mFAP or AdC68- gDMelapoly vector given alone each achieved significant delay in tumor progression compared to the control vaccine. Tumor growth was comparable in the two groups that received single vectors (p=0.31) (**Figure 3-2F**), but was further retarded when the vaccines were combined (gDMelapoly+Co vs. gDMelapoly+FAP: p=0.0096).

I further assessed vaccine efficacy in the transplantable B16 tumor model. C57Bl/6 mice were vaccinated with the different vectors three days after tumor challenge (**Figure 3-2G**). I chose an early time point after tumor challenge to assess the vaccines, as my previous studies showed that the AdC68-gDMelapoly vaccine, which completely protects mice that are vaccinated before tumor challenge can only rarely lead to cures if given three days after tumor challenge (308). Compared to the control group, mice immunized only with AdC68-mFAP showed delayed tumor progression and significantly prolonged survival (p=0.0089, **Figure 3-2H**). Vaccine efficacy was further improved when mice were immunized with a mixture of AdC68-mFAP and AdC68-gDMelapoly; while ~16% of AdC68-gDMelapoly-vaccinated mice were completed protected from tumor challenge, immunization with the vaccine mixture early after tumor challenge more than doubled the numbers of mice (~35%) that remained tumor-free for at least 90 days after tumor induction. In mice that developed tumors, those that received the AdC68-mFAP or AdC68-gDMelapoly vaccine alone showed significantly reduced tumor weight on day 25 after tumor

challenge compared to control mice. Combining AdC68-gDMelapoly with AdC68-mFAP further decreased tumor weight (**Figure 3-2I**).

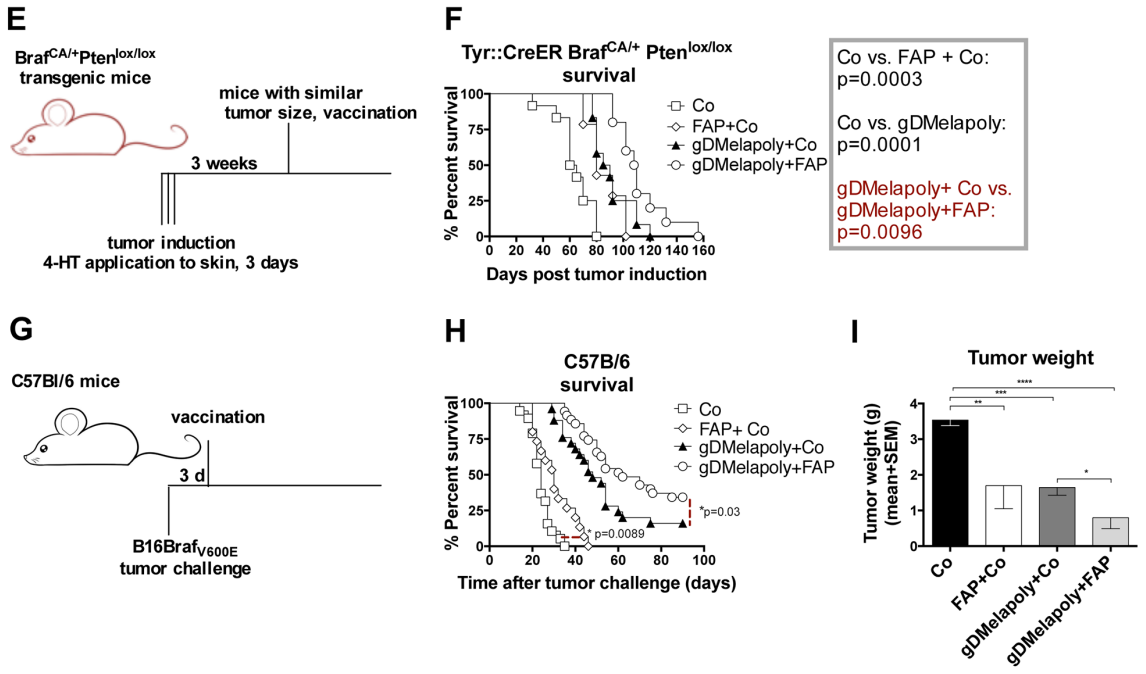

Figure 3-2. (E) Schematic representation of experimental set up to test vaccine efficacy in transgenic mice. Tumors were induced in transgenic mice by 4-HT treatment for 3 consecutive days. Mice were vaccinated with different vectors 3 weeks after tumor induction. (**F**) Graph shows Kaplan-Meier survival curves of mice that received the different vaccine regimens (n=10-14/group). Open square: control group (AdC68-gD vector); Diamond: control+AdC68-mFAP vaccine group; Black triangle: AdC68-gDMelapoly+ AdC68-gD vaccine group; Circle: AdC68-gDMelapoly+ AdC68-mFAP vaccine group. AdC68-gD vs. FAP+ AdC68-gD: p=0.0003; AdC68-gD vs. gDMelapoly + control: p=0.0001; gDMelapoly + AdC68-gD vs. gDMelapoly + FAP: p=0.0096. (**G**) Schematic representation of experimental set up to test vaccine efficacy in mice bearing transplantable B16 tumors. C57BL/6 mice were challenged with B16 tumor cells and vaccinated three days later with different vectors. (**H**) Graph shows Kaplan-Meier survival curves of mice that received the different vaccine regimens (n=15-35/group). Symbols representing each vaccine group are the same as those used in 2F. Control vs. FAP + control: p=0.0089; gDMelapoly+ AdC68-gD vs. gDMelapoly + FAP: p=0.03. (**I**) Tumor weight comparisons among different vaccine groups on day 25 after B16 tumor challenge. Data are presented as mean with SEM. AdC68-gD vs. FAP + AdC68-gD: p=0.014; AdC68-gD vs. gDMelapoly + AdC68-gD: p=0.0001; AdC68-gD vs. gDMelapoly + FAP: p<0.0001; gDMelapoly + AdC68-gD vs. gDMelapoly + FAP: p=0.03.

Both sets of data confirm that targeting FAP^+ tumor stroma cells results in significantly prolonged survival of melanoma-bearing mice. Combining a conventional tumor cell-targeting vaccine with a vaccine directed against the tumor stroma offers further therapeutic benefits in mouse melanoma models.

AdC68-mFAP-induced $CD8^+$T cell responses reduce FAP^+ stromal cells within the TME.

To determine the mechanism by which the AdC68-mFAP vaccine delayed tumor progression, I first analyzed whether AdC68-mFAP vaccine-induced immune responses could destroy FAP^+ stroma cells. Tyr::CreER, $Braf^{CA/+}Pten^{lox+/lox+}$ transgenic mice bearing 3 week-old tumors and C57Bl/6 mice with 3 day-old B16$Braf_{V600E}$ tumors were vaccinated with the control vector only, AdC68-mFAP with the control vector or AdC68-gDMelapoly mixed with either the control vector or the AdC68-mFAP vector. Numbers and percentages of $CD45^-FAP^+$ stroma cells within tumors were measured 3 month later from transgenic mice and ~ 4 weeks later from B16 tumor-bearing mice. AdC68-mFAP given alone or with AdC68-gDMelapoly significantly reduced FAP^+ stroma cells within tumors in both models, reflected by decreases in percentages (**Figure 3-3A**) and numbers (**Figure 3-3B, 3C**). Within transgenic tumors the FAP vaccine caused a significant reduction in FAP^+ cells and this was slightly more pronounced if the AdC68-gDMelapoly vaccine was given simultaneously (**Figure 3-3B**). Mice immunized only with AdC68-gDMelapoly also had lower levels of FAP^+ cells. I assume that this may reflect that FAP^+ cells become more frequent during tumor growth so that a vaccine that delays tumor progression also reduces accumulation of FAP^+ cells. Results differed for B16 tumors. In this model the FAP vaccine reduced FAP^+ cells as in the transgenic tumors. In contrast, the AdC68-gDMelapoly vaccine given together with a control vector did not affect levels of the tumors' FAP^+ stroma cells (**Figure 3-3C**). Nevertheless, when AdC68-gDMelapoly and AdC68-mFAP vectors were combined FAP depletion was more pronounced than upon vaccination with AdC68-mFAP only.

Reduction of FAP^+ cells upon vaccination with AdC68-mFAP suggests their depletion by vaccine-induced T cells. This was confirmed indirectly by testing whether T cells are required for AdC68-mFAP-mediated delay in tumor progression. I depleted $CD4^+$ or $CD8^+$ or both T cell subsets from mice challenged with B16 tumors and then vaccinated them 3 days later with AdC68-mFAP. Depletion of $CD8^+$T cells completely abrogated the effect of the AdC68-mFAP vaccine on tumor progression. Depletion of $CD4^+$T cells had no effect (**Figure 3-3D**).

Figure 3-3: Immunization with AdC68-mFAP reduces numbers of FAP$^+$ cells within both transgenic Braf$^{CA/+}$Pten$^{lox/lox}$ and transplantable B16 tumors in a CD8$^+$T cell dependent manner

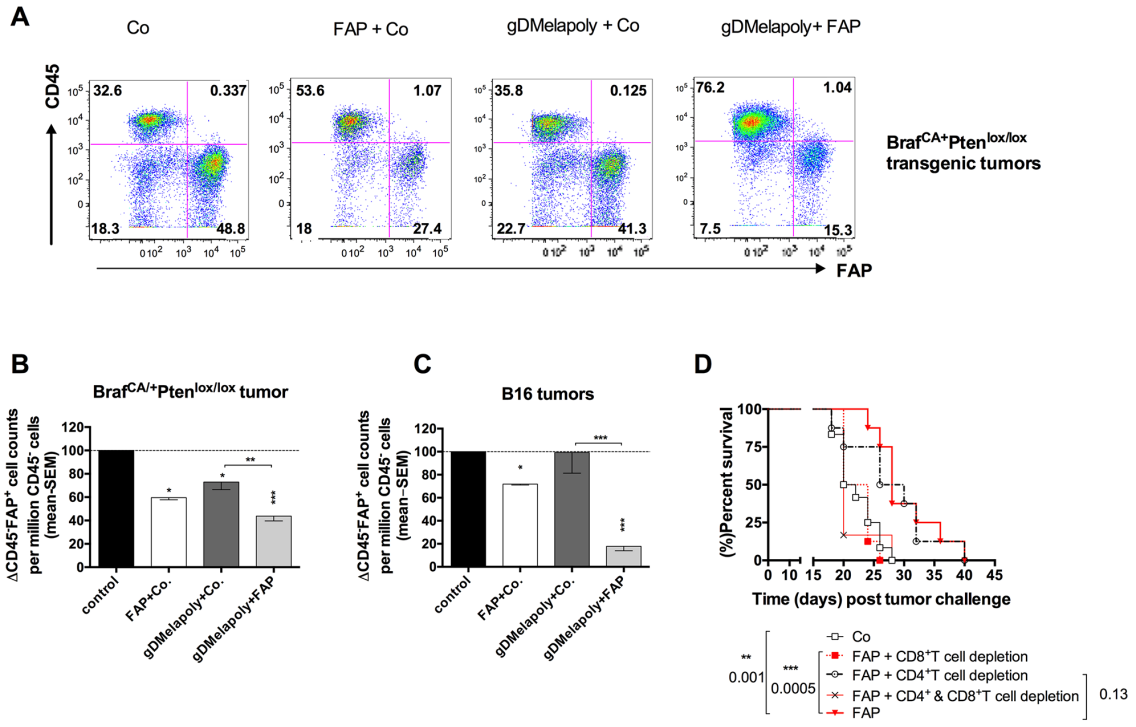

Figure 3-3: Immunization with AdC68-mFAP reduces numbers of FAP$^+$ cells within both transgenic Braf$^{CA/+}$Pten$^{lox+/lox+}$ and transplantable B16 tumors in a CD8$^+$T cell dependent manner. (**A**) Representative flow plots show percentages of CD45$^-$FAP$^+$ cells from 3 month-old tumors of transgenic mice that received AdC68-gD (control), AdC68-mFAP + AdC68-gD, AdC68-gDMelapoly + AdC68- gD or AdC68-gDMelapoly + AdC68-mFAP 3 weeks after initial tumor-induction with 4-HT. (**B**) Relative numbers of CD45-FAP$^+$ cells per million CD45$^-$CD3$^-$CD14$^-$CD19$^-$ cells from 3 month-old tumors isolated from transgenic mice that received the control vector (AdC68-gD, black bar), the AdC68-mFAP + AdC68-gD (open bar), the AdC68-gDMelapoly+ AdC68-gD (dark grey bar), or the AdC68- gDMelapoly + AdC68-FAP (light grey bar) (n=4-5/group). Data were normalized to results from control group. AdC68-gD vs. FAP+ control: p=0.015; AdC68-gD vs. gDMelapoly + FAP: p=0.0006; AdC68-gD vs. gDMelapoly + AdC68-gD: p=0.049; gDMelapoly + AdC68- gD vs. gDMelapoly + FAP: p=0.0083. (**C**) Relative numbers of CD45-FAP$^+$ cells per million CD45$^-$ CD3$^-$CD14$^-$CD19$^-$ cells from 1-month B16 tumors isolated from C57BL/6 mice that received different combinations of vectors 3 days after tumor challenge (n=5-10/group). Data were normalized to results from the control group. AdC68-gD vs. FAP + AdC68-gD: p<0.0001; AdC68-gD vs. gDMelapoly + FAP: p<0.00001; AdC68-gD vs. gDMelapol + AdC68-gD: p=0.9625; gDMelapoly + AdC68-gD vs. gDMelapoly +

FAP: p=0.0001. FAP + AdC68- gD vs. gDMelapoly + FAP: p=0.0001. (**D**) Kaplan-Meier survival curves of mice challenged with tumor cells and vaccinated with control or AdC68-mFAP vector. Mice were depleted of $CD8^+$, $CD4^+$ T cells or both (n=8-12/group). Statistical significant differences in terms of survival length and corresponding p-values are marked on the graph.

ISCs that intensify metabolic stress if in vitro activated $CD8^+$T cells are reduced upon FAP^+ stroma cell depletion

Cytokines and chemokines produced within tumors are known to recruit ISCs, such as MDSCs and $FoxP3^+CD4^+$ regulatory T cells (Treg) (309). I hypothesized these ISCs may enhance the metabolic stress of MAA-specific TILs within TME and contributes to their functional exhaustion. I measured two subsets of MDSCs, i.e., monocytic (MO) MDSCs, which are phenotypically Gr-1^{int} $CD11b^+$, and granulocytic (polymorphonuclear, PMN) MDSCs, which are Gr-1^{hi} $CD11b^+$ and TAMs (**Figure 3-4A**). Most of TAMs within TME were skewed towards a M2 phenotype with high expression of mannose receptor CD206 (310). I confirmed *in vitro* that the ISCs affected T cell proliferation by activating splenic naïve $CD8^+$ T cells *in vitro* with antibodies to CD3 and CD28. Proliferation tested for at 5 days after activation significantly decreased upon co-culture with PMN-MDSCs and TAMs. Some inhibition was seen upon co-culture with Gr-$1^{hi}CD11b^+$ MDSCs although this failed to reach significance (**Figure 3-4B**).

Figure 3-4: ISCs that enhance the metabolic stress and PD-1 expression of activated $CD8^+$T cells were reduced by FAP^+ tumor stromal cell depletion

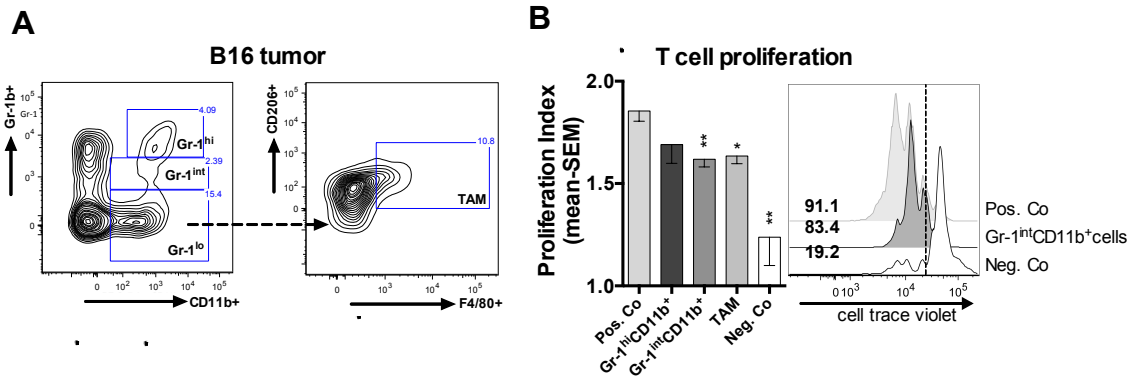

Figure 3-4. ISCs that enhance the metabolic stress and PD-1 expression of activated $CD8^+$T cells were reduced by FAP^+ tumor stromal cell depletion. (**A**) Gating strategy for Gr-1^{hi} and Gr-1^{int} MDSCs and $CD206^+F4/80^+$ M2 type TAMs. (**B**) Gr-$1^{int}CD11b^+$ MDSCs and TAMs inhibit proliferation of $CD8^+$T cells *in vitro*. Enriched $CD8^+$T cells were labeled with celltrace violet and stimulated with anti-CD3 and anti-CD28

for 4 days, Gr-1^{int}CD11b^{+} MDSCs were added to T cells at a ratio of 1:5 from day 0. Activated CD8^{+}T cells without ISCs were used as positive control while CD8^{+}T cells cultured without antibody stimulation were used as a negative control. Left: Proliferation index of CD8^{+}T cells with or without stimulation or cocultured with MDSCs or TAM (n=4/group). Positive control vs. Gr-1^{int}CD11b^{+}co-culture: p=0.0023; positive control vs. TAM co-culture: p=0.023; positive control vs. negative control: p=0.009. Right: Histograms show cell proliferation of representative samples. Numbers on the left of the histograms show percentages of cells with reduced celltrace violet levels.

To determine whether ISCs affect T cell metabolism, I stimulated CD8^{+}T cells from spleens of naïve mice *in vitro* in presence of different populations of ISCs isolated from B16 tumor-bearing mice. Levels of mitochondrial reactive oxygen species (MROS) within activated CD8^{+}T cells were measured on day 5 of culture. T cells upon activation increasingly use glycolysis for production of energy while resting T cells primarily use the more efficient tricarboxylic acid (TCA) cycle and oxidative phosphorylation (OXPHOS) (311). MROS, which is mainly produced by OXPHOS, is highly toxic and can induce cell damage and death through activating intracellular signaling pathways (184). In healthy cells MROS is rapidly converted to water and oxygen. Its accumulation within cells is a hallmark of metabolic stress indicative of mitochondrial dysfunctions. Activated CD8^{+}T cells co-cultured with MDSCs and TAMs showed significantly higher MROS levels compared to those stimulated without ISCs (**Figure 3-4C**), suggesting that ISCs impose metabolic stress on activated CD8^{+}T cells. I next assessed whether increased metabolic stress contributes to inhibitory signaling in activated CD8^{+}T cells by measuring expression of the co-inhibitor PD-1. PD-1 initially increases on activated CD8^{+}T cells upon T cell receptor and CD28 ligation (114). Its constitutive high expression is viewed as a hallmark of exhaustion that limits the effectiveness of CD8^{+}TILs (43). PD-1 dampens T cell responses in part by inhibiting the Akt/mTOR pathway and thereby energy production through glycolysis (267). In my CD8^{+}T cells-ISCs co-culture system, addition of ISCs significantly increased PD-1 expression on CD8^{+}T cells (**Figure 3-4D**).

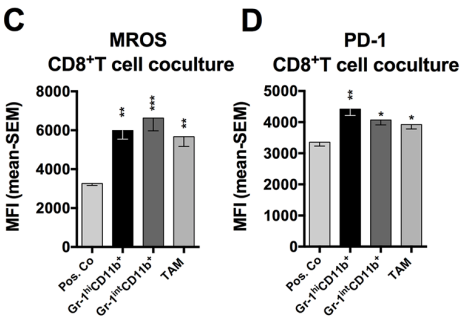

Figure 3-4. (**C**) Enriched CD8^{+}T cells from spleens of naive mice were stimulated *in vitro* with or without different subsets of ICSs from tumor-bearing mice. MROS levels in CD8^{+}T cells stimulated for 5 days under different culture conditions are shown as mean MFI values with SEM. Positive Co. vs. Gr-1^{hi}: p=0.0018; vs. Gr-1^{int}: p=0.0003; vs. TAM: p=0.0047. (**D**) PD-1 expression on CD8^{+}T cell on day 5 after co-culture

with different ISC subsets are shown as MFI with SEM. Positive Co. vs. Gr-1^{hi}: p=0.0022; vs. Gr-1^{int}: p=0.028; vs. TAM: p=0.029.

I next analyzed whether depleting FAP^{+} stroma cells can reduce ISCs within the TME. Transgenic mice bearing 3 months old tumors of similar sizes were analyzed first. Tumors from mice that received AdC68-mFAP alone compared to those from the control group showed significantly reduced percentages of both MDSC subsets; this was not achieved with mice that received AdC68-gDMelapoly with a control vector (**Figure 3-4E**). Combining AdC68-mFAP with AdC68-gDMelapoly caused a reduction in the more suppressive Gr-1^{int}CD11b^{+}MDSC subset while percentages of Gr-1^{hi} CD11b^{+}MDCSs reverted back to levels seen in control mice. Numbers of Tregs declined upon immunization with either vaccine regimen (**Figure 3-4F**), indicating that this was unrelated to FAP but more likely reflected the effect of enhanced immune response within the tumor upon vaccination with Ad vectors.

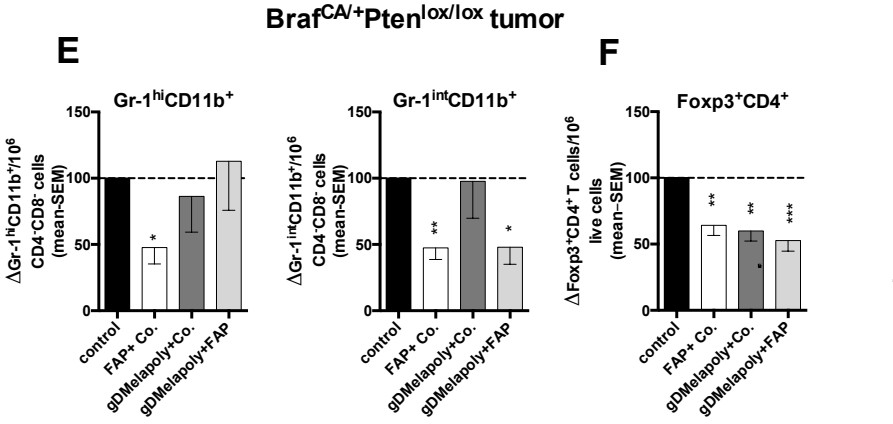

Figure 3-4. (**E–F**) Transgenic mice bearing 3-week tumors were vaccinated with control vector (AdC68-gD, black bar), FAP+AdC68-gD (empty bar), gDMelapoly+AdC68-gD (dark grey bar) or gDMelapoly+FAP (light grey bar) (n=5/group). Data show normalized cell counts of Gr-1^{hi} and Gr-1^{int}MDSCs over CD4^{-}CD8^{-} live cells (**E**) or normalized CD4^{+}Foxp3^{+} cells (**F**) over live cells in 3 month-old tumors of mice from the different vaccine groups.

In B16 tumors I excluded the group of mice immunized with AdC68-mFAP only, as in this model reduction of FAP^{+} cells was significantly more pronounced by a vaccine regimen that combines AdC68-mFAP with the AdC68-gDMelapoly vector (**Figure 3-3C**). AdC68-gDMelapoly vaccinated-mice had slightly enhanced levels of Gr-1^{hi}CD11b^{+} MDSCs; addition of the FAP vaccine reduced this population (**Figure 3-4G**). Relative percentages of Gr-1^{int}CD11b^{+} MDSCs

were reduced upon vaccination with AdC68-gDMelapoly. This reduction became more pronounced in tumors of mice that also received the FAP vaccine, suggesting that depleting FAP^+ stromal cells contributed to the lower MDSC levels. The vaccines did not reduce Tregs (**Figure 3-4H**). In both tumor models frequencies of TAMs were not affected by the FAP vaccine. The vaccines thus had distinct effects on ISC numbers in the two tumor models.

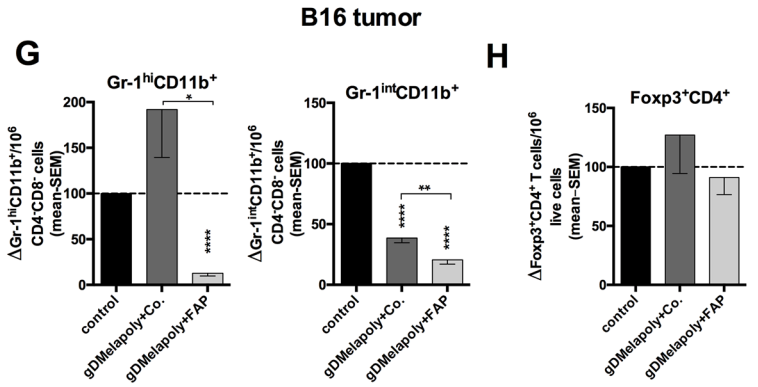

Figure 3-4. (**G–H**) Mice bearing 3 day-old B16 tumors were vaccinated with control vector (AdC68-gD, black bar), gDMelapoly+AdC68-gD (dark grey bar) or gDMelapoly+FAP (light grey bar) (n=14-15/group). Data show normalized cell counts of Gr-$1^{hi}$and Gr-1^{int} MDSCs over $CD4^-CD8^-$ live cells (**G**) or normalized $CD4^+Foxp3^+$ cells (**H**) over live cells in 1 month-old tumors of mice from the different vaccine groups. *: p<=0.05; **: p<0.01; ***: p<0.001; ****: p<0.0001.

Overall these data indicate that in either melanoma model targeting FAP^+ tumor stroma cells reduces the content of MDSCs within tumors, which may create a more supportive niche for antigen-specific TILs by reducing their metabolic stress.

Reduced suppressive functions of ISCs upon FAP^+ stromal cell depletion is linked to changes in JAK-STAT pathway activation

MDSCs and TAMs suppress $CD8^+$T cell functions through different mechanisms (309). It is well established that they produce high levels of inducible nitric oxide synthase (iNOS) and arginase 1(Arg1), which catabolize and deplete L-arginine, an important amino acid that is required to support T cell proliferation. In addition, iNOS generates nitric oxide (NO), which further inhibits function of T cells. MDSCs produce reactive oxygen species (ROS), which upon reaction with NO form superoxide anion, a metabolite that through nitration of T cell receptors induces T cell unresponsiveness (312). CAFs secrete chemokine (C-C motif) ligand 2 (CCL2), which recruits MDSCs. Other factors such as granulocytes macrophage colony-stimulating factor (GM-

CSF), interleukin (IL)-4, IL-10, IL-13, transforming growth factor (TGF)-β promote differentiation and immunosuppressive functions of MDSCs (309,313). I therefore assessed if depleting FAP^+ CAFs upon vaccination with AdC68-mFAP can change the functional profiles of ISCs. For these experiment I used the B16 model and combined the AdC68-gDMelapoly and AdC68-mFAP vaccines as this regimen as shown in Figure 3-3C achieved the highest reduction in FAP^+ cells. Mice bearing 3-day old B16 tumors were vaccinated with AdC68-gDMelapoly together with control or AdC68-mFAP vectors. MO-MDSCs, PMN-MDSCs and TAMs were isolated from similar-sized tumors of the two groups of mice ~4 weeks after vaccination and levels of iNOS, Arg1 and ROS were measured by antibodies staining and flow analysis. Both iNOS and Arg1 expression was significantly decreased within ISCs from tumors of mice that received both MAA- and FAP-targeting vaccines compared to those received only AdC68-gDMelapoly (**Figure 3-5A**). ROS levels were comparable between the two vaccine groups for all ICS populations. Collectively, these data suggest that depletion of FAP^+ cells reduces the immunosuppressive capacities of ISCs by decreasing their ability to produce iNOS and Arg1.

Figure 3-5: Depleting FAP^+ stromal cells reduces suppressive functions of ISCs in tumors and decreases their STAT6 activity.

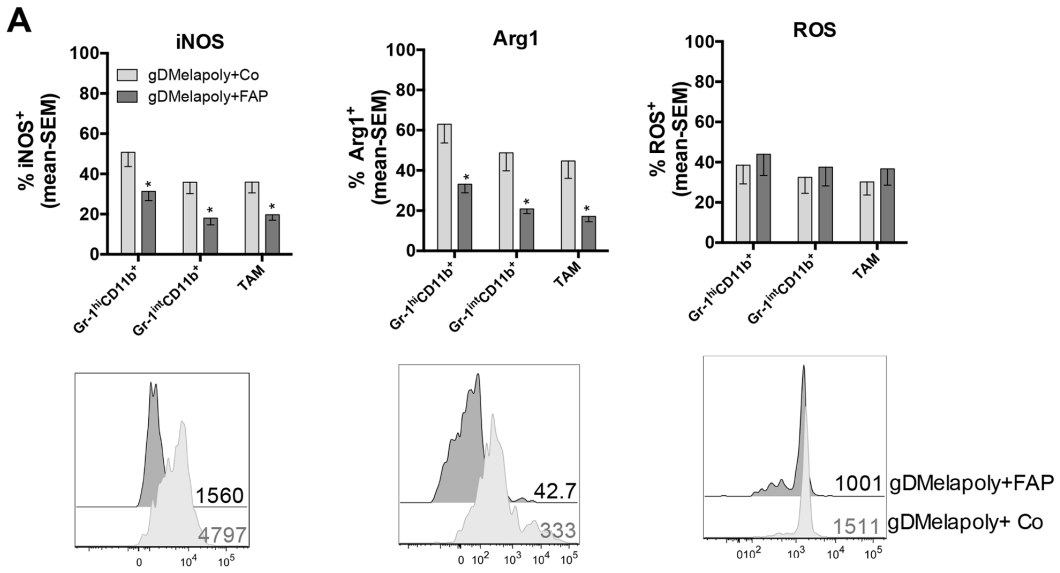

Figure 3-5. Depleting FAP^+ stromal cells reduces suppressive functions of ISCs in tumors and

decreases their STAT6 activity. (**A**) Production of iNOS, Arg1 and ROS by MDSCs and TAMs from similar-sized 1 month-old B16 tumors were compared between mice that received AdC68-gDMelapoly+AdC68-gD (light grey bar) or AdC68-gDMelapoly+ AdC68-mFAP (dark grey bar) (n=15/ group). Data are presented as percentages of cells positive for iNOS, Arg1 or ROS expression. Lower panel: representative histograms of iNOS, Arg1 and ROS expression in Gr-1$^+$PMN-MDSCs in the two different vaccine groups. Numbers next to histograms indicate MFI values for the factors in the selected samples.

Previous studies showed that factors produced by tumor and tumor stromal cells activate Janus kinase (JAK)-signal transducer and activator of transcription (STAT) pathways in ISCs, which contributes to their expansion and activation (309,313). STAT3 is induced by a number of factors including IL-5, IL-6 and IL-10. It is the main transcriptional factor regulating MDSC expansion. STAT1 activated by IFN-γ and STAT6 activated by IL-4 or IL-13 upregulate the expression of iNOS and Arg1 in MDSCs (313). As vaccination with AdC68-mFAP given together with AdC68-gDMelapoly reduced iNOS and Arg1 expression in MDSCs and TAMs of tumor-bearing mice, I analyzed whether the functional reductions of ISCs were linked to changes in STAT activation. I compared phosphorylated (p)STAT1, STAT3 and STAT6 levels in the three ISCs populations from B16 tumors of mice vaccinated with AdC68-gDMelapoly with either control or AdC68-mFAP vector. Mice received tumors cells and were vaccinated 3 days later; similar-sized tumors from each group were analyzed 4 weeks after vaccination. Addition of the FAP vaccine to AdC68-gDMelapoly had no effect on pSTAT1 or pSTAT3 levels, but significantly decreased pSTAT6 levels in all three ISC subsets (**Figure 3-5B**). These data indicate that vaccine-mediated depletion of FAP$^+$ cells reduces the suppressive functions of ISCs, which is associated with their decreased activation of the STAT6 pathway.

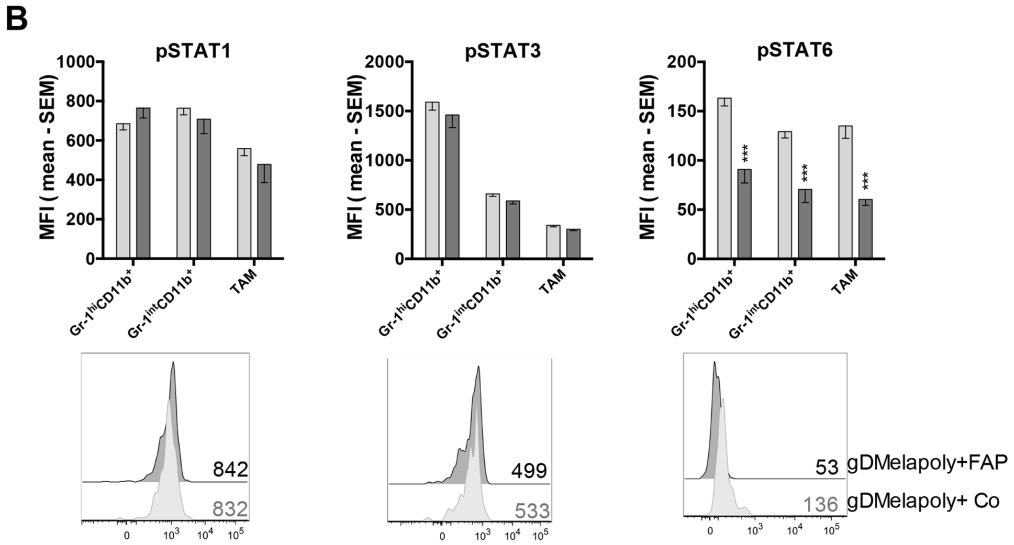

Figure 3-5. (**B**) The phosphorylation of transcription factors STAT1, STAT3 and STAT6 were measured in MDSCs and TAMs using the same tumor samples as described in 5A (n=8-10/group). Data are shown as mean MFI values with SEM. Lower panel: histograms show representative pSTAT1/pSTAT3/pSTAT6 expression in Gr-1^{int}CD11b^{+}MDSC samples from the two vaccine groups. MFI values of pSTAT expression in the selected samples are shown next to the histograms. Statistics shown as * were same as described in Figure 3-4.

Targeting FAP^{+} cells changes cytokine/chemokine production within tumors

Reduced activity of STAT6 in tumor-infiltrating ISCs of mice that received AdC68-mFAP together with AdC68-gDMelapoly most likely reflects vaccine-induced changes in cytokines or chemokines within the TME, which in turn recruit and activate ISCs.

I initially assessed whole tumors from mice that had been challenged 4-5 weeks before with B16 cells and received either AdC68-gDMelapoly with the control or the AdC68-mFAP vector three days later for a number of transcripts of cytokines and chemokine that may affect STAT signaling, ISCs recruitments or functions, or the balance of immune responses within the TME (312). Upon including AdC68-mFAP into the vaccine regimen transcripts for CCL5, CCL22, IL-4, IL-10 and TGF-β significantly decreased (**Figure 3-6A**). Th2 related chemokines CCL5 and CCL22 preferentially recruit T cells that lack the capacity to eliminate tumor cells by direct lysis, i.e., regulatory T cells and Th2 cells; the latter bias immune responses away from Th1 (314). Several cell subsets within tumors secrete IL-10 and TGF-β, which can contribute to immune suppression within the TME either through direct inhibition of cytolytic T cells or indirectly through

the recruitment and activation of ISCs. TGF-β can further activate fibroblasts, which in turn promotes their immunosuppressive activities (127,309). IL-4 activates the STAT6 pathway in ISCs, which directly supports their suppressive functions. The reduction of these factors following AdC68-mFAP vaccination indicates a less immunosuppressive TME that reduces ISC recruitment and functions and supports $CD8^+$T cell effector functions. Other factors, including C-X-C motif chemokine (CXCL) 10 and CXCL12, CCL2, IL-16 and IL-13, GM-CSF and stem cell factor (SCF) remained relatively stable upon addition of the AdC68-mFAP vaccine to AdC68-gDMelapoly.

Figure 3-6: Depleting FAP+ stromal cells changes the TME's cytokine and chemokine profile

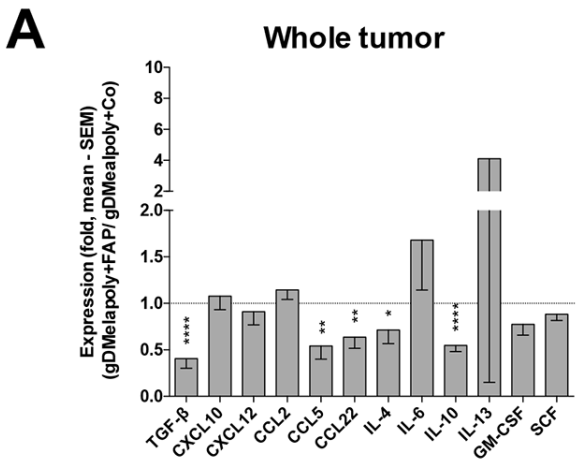

Figure 3-6: Depleting FAP+ stromal cells changes the TME's cytokine and chemokine profile. Mice (n=7-8/group) were challenged with B16 tumors and vaccinated with AdC68-gDMelapoly mixed with control or AdC68-gDMelapoly mixed with AdC68- mFAP 3 days later. Tumors grown to about 1-1.5 cm in diameter were collected at necropsy (~4-5 weeks after tumor challenge). (**A**)
Relative mRNA expression levels of selected cytokines and chemokines in tumors from the AdC68-gDMelapoly+AdC68-mFAP group were compared to those from the AdC68-gDMelapoly+AdC69-gD control group. Data are shown as mean fold changes with SEM (TGF-β: $p<0.0001$; CCL5: $p=0.0014$; CCL22: $p=0.0023$; IL-4: $p=0.030$; IL-10: $p<0.0001$).

To assess the origin of different factors, I sorted cells into tumors cells, FAP^+ stroma cells, MDSCs, TAMs, and infiltrating leukocytes (T cells [$CD3^+$], B cells [$CD19^+$], macrophages and neutrophils [$CD14^+$]) following the gating strategy shown in **Figure 3-6B**. Most factors originated from an array of different cell types (**Figure 3-6C**). FAP reduction decreased transcripts for IL-10, TGF-β, CCL5 and CCL22 from $CD14^+$ cells (**Figure 3-6D**), of which 20-40% were $F4/80^+$ TAMs; CCL5 transcripts were also reduced in tumor cells. Reductions in IL-4 and IL-10 transcripts were seen in numerous cell type including FAP^+ stromal cells and inflammatory cells. The decreased transcripts of these cytokines/chemokines in different cell compartments within the TME suggests that reduction of FAP^+ stroma cells has global effects that directly or

indirectly affect other cell subsets. FAP-reduction did not affect cytokine or chemokine production by MDSCs and TAMs, indicating that their decreased pSTAT6 activation was caused by exogenous changes in cytokine levels. Collectively my data suggest that AdC68-mFAP vaccine changes the cytokine/chemokine milieu within the TME by reducing production of inflammatory factors. This may through down-regulation of STAT6 signaling pathways decreases the recruitment and immunosuppressive functions of ISCs.

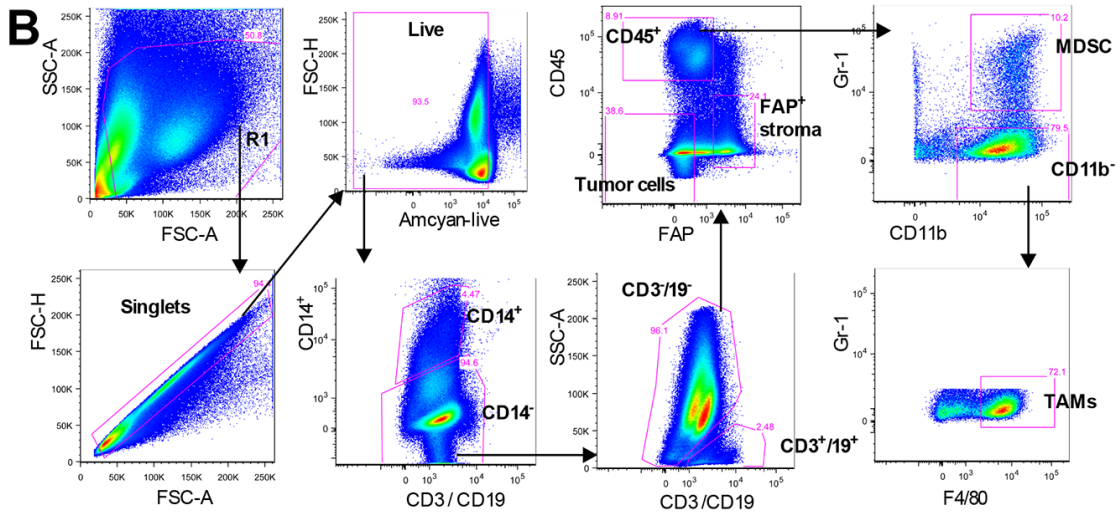

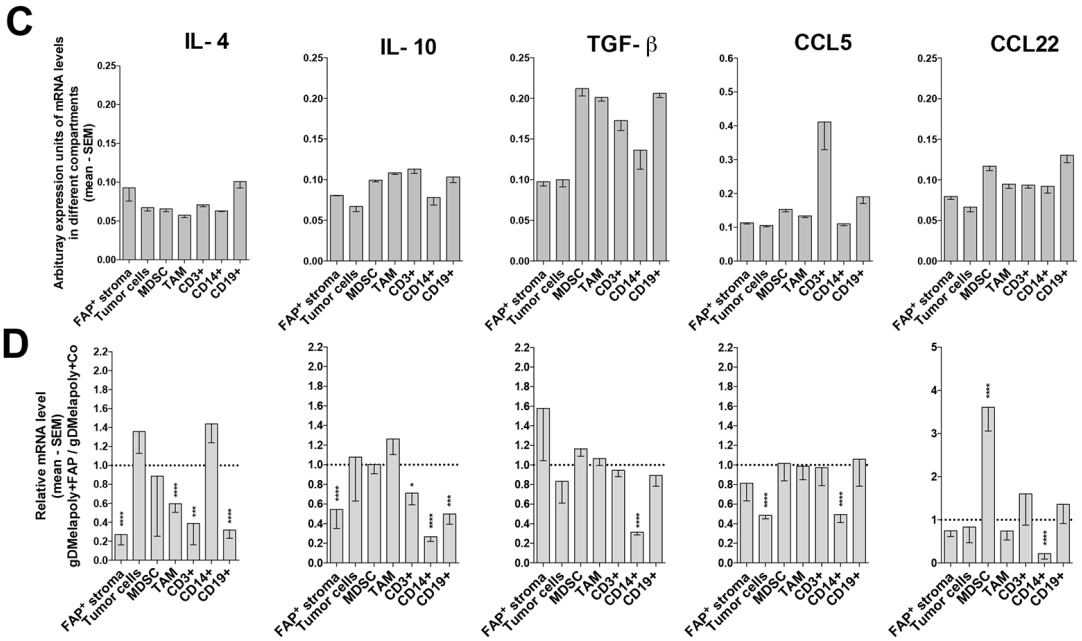

Figure 3-6. (**B**) Gating strategy used to sort different cell populations including FAP^+ stromal cells, tumor cells, MDSCs, TAMs, $CD3^+$T cells, $CD14^+$cells and $CD19^+$B cells from B16 tumors. (**C**) Abundance of selected cytokines and chemokines that show significantly reduced expression upon FAP^+ stromal cell depletion in different cell populations of the TME. Tumor samples were from mice that received AdC68-gDMelapoly+control vector. Data of mRNA levels are shown as mean values of arbitrary expression units (1/(target gene Ct - GAPDH Ct)) with SEM. (**D**) Relative mRNA levels of the indicated cytokines and chemokines in different cell populations from tumors of mice that received AdC68-gDMelapoly+AdC68-mFAP over those of mice that received AdC68-gDMelapoly+control vector (n=6/group). (IL-4: FAP^+ stroma: $p<0.0001$, TAM: $p<0.0001$, CD3: $p=0.000065$, CD14: $p=0.033$, CD19: $p<0.0001$; IL-10: FAP^+ stroma: $p<0.0001$, CD3: $p=0.016$, CD14: $p<0.0001$, CD19: $p<0.0001$; TGF-β: CD14: $p<0.0001$; CCL5: tumor cells: $p<0.0001$, CD14: $p<0.0001$; CCL22: MDSC: $p<0.0001$, CD14: $p<0.0001$).

Reducing FAP^+ stromal cells reduces metabolic stress, decreases co-inhibitor expression and improves functions of vaccine-induced $CD8^+$T cells

It has been shown previously that FAP^+ stromal cells suppress tumor-specific immune responses (133) and FAP^+ cell depletion enhances tumor infiltration by T lymphocytes (131,315). I hypothesized that depleting FAP^+ cells, which reduced the frequencies and functions of ISCs within the TME, may lessen metabolic stress and delay exhaustion of MAA-specific $CD8^+$TILs as suggested by my *in vitro* co-culture assay. Indeed, increased metabolic stress indicated by high MROS levels is associated with enhanced expression of the co-inhibitor PD-1 on MAA-specific $CD8^+$TILs from either transgenic or C57BL/6 mice (**Figure 3-7A**). In either transgenic or C57BL/6 mice with similar sized tumors, reducing FAP^+ stromal cells significantly decreased percentages of $MROS^{hi}$ Trp-1-specific $CD8^+$TILs, especially those with lower mitochondrial membrane potential (MMP) (**Figure 3-7B**). Furthermore, co-inhibitor PD-1 levels were also significantly lower on MAA-specific $CD8^+$TILs upon FAP^+ cell depletion in both tumor models, suggesting that these cells were partially protected from exhaustion (**Figure 3-7C**).

Figure 3-7: Depleting FAP$^+$ stromal cells with AdC68-mFAP vaccine reduces metabolic stress and improves effector functions of AdC68-gDMelapoly-induced CD8$^+$T cells.

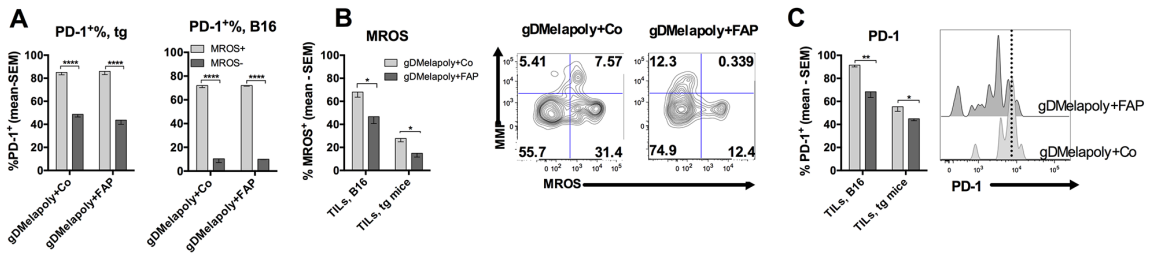

Figure 3-7: Depleting FAP$^+$ stromal cells through AdC68-mFAP vaccine reduces metabolic stress and improves effector functions of AdC68-gDMelapoly-induced CD8$^+$T cells. (**A**) Percentages of PD-1^{hi} cells within MROS^{hi} or MROS^{lo} Trp-1-specific CD8$^+$TILs populations from tumors of mice that received either the control or the FAP vaccine. Both TILs from transgenic mouse tumors (left, n=5 mice/group) or C57/Bl6 tumors (right, n=5 mice/group) were analyzed. (**B**) Percentages of Trp-1-specific CD8$^+$T cells with high levels of MROS from similar sized transgenic tumors (collected 3 month after tumor challenge, n=4-5/group) or B16 tumors (collected 1 month after tumor challenge, n=9-14/group) of mice that received either AdC68-gDMelapoly+control (light grey) or AdC68- gDMelapoly+AdC68-mFAP (dark grey). TILs B16: p=0.018; TILs transgenic (tg): p=0.04. Flow plots show representative MMP and MROS expression in Trp-1$^+$CD8$^+$T cells from transgenic tumors of mice that received either AdC68-gDMelapoly+AdC68-gD or AdC68- gDMelapoly+AdC68-FAP. (**C**) PD-1 expression on Trp-1-specific CD8$^+$TILs from transgenic or B16 tumor-bearing mice that received either AdC68-gDMelapoly+AdC68-gDMelapoly (light grey) or AdC68-gDMelapoly+AdC68-mFAP (dark grey). Data are presented as percentages of Trp-1-specific CD8$^+$T cells that show high expression of PD-1. TILs B16: p=0.0029; TILs transgenic (tg): p=0.045. Histograms: PD-1 expression on representative Trp-1-specific CD8$^+$TILs samples from the transgenic tumors of mice that received either combination of vaccines.

To further determine whether destroying FAP$^+$ cells by AdC68-mFAP vaccination affects the functions of MAA-specific CD8$^+$TILs, mice bearing 3 day-old B16 tumors were vaccinated with AdC68-gDMelapoly together with either the control or the AC68-mFAP vector. CD8$^+$T cell responses to Trp-1$_{455\text{-}463}$, the immunodominant epitope expressed by the AdC68-gDMelapoly vector, were monitored by tetramer staining of peripheral blood mononuclear cells (PBMCs) from the two vaccine groups over the course of 50 days. Depleting FAP$^+$ tumor stromal cells significantly increased the overall Trp-1-specific CD8$^+$T cell response in blood (p=0.038, area under the curve); differences were more pronounced at later time points, i.e. on days 35 and 50 after vaccination (**Figure 3-7D**). Mice were euthanized once tumors exceeded 1-1.5 cm in diameter and splenocytes and TILs were isolated. The mice that received the FAP vaccine exhibited significantly higher Trp-1-specific CD8$^+$T cell responses in tumors (**Figure 3-7E**). The experiment was repeated with tumor-bearing Tyr::CreER, Braf$^{CA/+}$Pten$^{lox+/lox+}$ transgenic mice and

results were comparable (**Figure 3-7F**). To assess whether the enhanced Trp-1-specific $CD8^+$T cell frequencies were accompanied by an improvement of MAA-specific $CD8^+$T cell effector functions, I tested PBMCs from B16 tumor-challenged mice for production of cytokines upon their *in vitro* stimulation with the MAA peptide pool, which included peptides representing the eight $CD8^+$T cell epitopes expressed by the AdC68-gDMelapoly vaccine. Cells were then analyzed by intracellular cytokine staining (ICS) for production of IFN-γ and TNF-α. Overall frequencies of $cytokine^+CD8^+$T cells, i.e., the sum of percentages of T cells producing the two cytokines alone or in combination, were markedly higher in blood of mice that received the FAP vaccine together with the gDMelapoly vaccine (p=0.031, area under the curve) (**Figure 3-7G**). This effect was mainly observed at the later time point, i.e. on day 35 after vaccination. On day 10 after vaccination MAA-specific $CD8^+$T cells from blood of the two vaccine groups showed comparable patterns for single or double functions; by day 35 T cells from mice that received the FAP vaccine were significantly more polyfunctional compared to those from the control group (Fig 7H). At the time of euthanasia mice that received both vaccines had higher percentages of factor-producing MAA-specific $CD8^+$ TILs compared to those received AdC68-gDMelapoly with control vector (**Figure 3-7I**) and $CD8^+$TILs were more polyfunctional (**Figure 3-7J**), i.e., a significantly higher percentage of MAA-specific $CD8^+$TILs cells produced both IFN-γ and TNF-α.

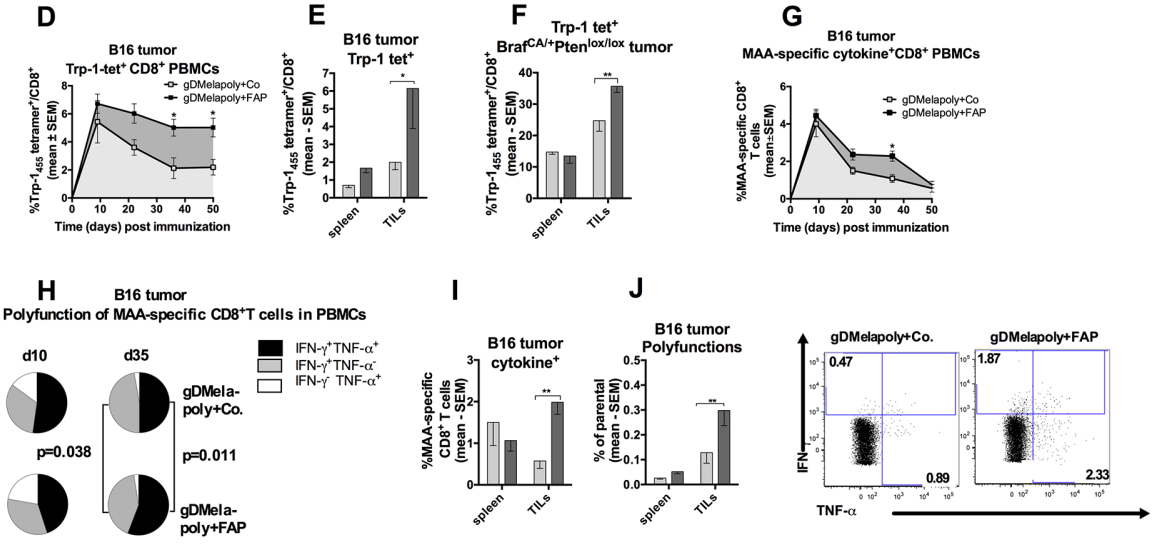

Figure 3-7. (**D**) Percentages of Trp-1 tetramer$^+$CD8$^+$T cells in blood of mice (n=15/group) challenged with B16 tumor cells and vaccinated with either AdC68-gDMelapoly+AdC68-gD (empty square) or AdC68-gDMelapoly+AdC68-mFAP (black square). Responses were monitored for 50 days after vaccination. Responses compared by area under the curve (AUC): p=0.038; responses compared at individual time points on days 35: p=0.038; 42: p=0.047. (**E)** Trp-1-specific CD8$^+$T frequencies in spleens and tumors of B16-tumor bearing mice (n=9-14/group) that received AdC68-gDMelapoly+AdC68-gD (light grey bar) or AdC68-gDMelapoly+AdC68-mFAP (dark grey bar) were compared ~1 month after tumor challenge. Spleen: p=0.66, TILs: p=0.03. (**F)** Trp-1-specific CD8$^+$T frequencies in spleens and tumors of transgenic tumor-bearing mice (n=5/group) received AdC68-gDMelapoly+AdC68-gD (light grey bar) or AdC68-gDMelapoly+AdC68- mFAP (dark grey bar) were compared ~3 months after tumor induction. Spleen: p=0.70, TILs: p=0.0054. (**G)** Mice (n=15/group) were challenged with B16 tumor cells and vaccinated with vectors three days later. Percentages of factor-producing CD8$^+$T cells upon stimulation with the MAA-specific peptide pool was monitored in blood for 50 days after vaccination. Cells producing IFN-γ and/or TNF-α were measured and data are presented as the mean value of the sum of the responses with SEM. AUC: p=0.031; responses compared on day 35: p=0.032. (**H)** MAA-specific CD8$^+$T cell polyfunctionality in PBMCs of B16 tumor challenged mice from two vaccine groups were compared on days 10 and 35 after vaccination. Pie slice colors black: IFN-γ^+TNF-α^+, grey: IFN-γ^+TNF- α^+, white: IFN-γ^+TNF- α^+. (**I)** Percentages of MAA-specific CD8$^+$T cells from spleens and tumors of B16 tumor-bearing mice in each vaccine group that produced one or two cytokines at the time of necropsy (n=5/group). Light grey bar: AdC68-gDMelapoly+AdC68-gD, dark grey bar: AdC68-gDMelapoly+AdC68-mFAP. TILs p=0.006. (**J)** Polyfunctions of MAA-specific CD8$^+$T cells in spleen and tumors of B16 tumor-bearing mice in each vaccine group at the time of necropsy (n=5/group), data are presented as percentage of MAA-specific CD8$^+$T cells that produce two cytokines. TILs p=0.0053. Flow blots show cytokines production in representative TIL samples from the different vaccine groups. Numbers on the corner indicate the percentages of CD8$^+$T cells producing either IFN-γ or TNF-α.

Overall my data suggest that depleting FAP$^+$ tumor stromal cells can decrease the metabolic stress of MAA-specific CD8$^+$ TILs, which delay their differentiation towards functional exhaustion within the TME and result in significantly improved antitumor efficacy.

DISCUSSION

Manipulating cells of the tumor stroma can achieve tumor regression. Decreases of MDSCs by factors that drive their differentiation towards mature antigen-presenting cells or macrophages has been shown to block their expansion or immune-inhibitory functions and prolong survival of tumor-bearing mice (316). Reduced tumor progression is also achieved by targeting FAP, an antigen that is selectively expressed on fibroblasts present in tumors or at sites of chronic inflammation or wound healing (131-133,317). Mice with a genetic deletion of the FAP gene show prolonged survival after tumor challenge (122). Accordingly, targeting FAP by active immunotherapy or T cells engineered to express a FAP-specific CAR decreases tumor growth and this is linked to reduced angiogenesis, changes in extracellular matrix proteins and

augmented anti-tumor immunity (317). Data presented here point to an additional mechanism in which an Ad vector designed to induce FAP^+ cell-depleting $CD8^+$T cells combined with a traditional cancer vaccine changes the immune balances within the TME by reducing levels of immunosuppression while enhancing functions of MAA-specific $CD8^+$T cells through reducing their metabolic stress.

My combination vaccine achieved complete remission of a transplantable highly aggressive B16 tumor in ~35% of mice while median survival of those that develop tumors was extended ~ 3 fold. This strategy also significantly prolonged survival of transgenic melanoma mice, although in this model the vaccine was given to mice, which already had substantial tumor burdens. It has been reported that eliminating FAP^+ cells with CAR-T cells causes significant bone marrow toxicity and cachexia in some mice (304,318), thus dampening enthusiasm for the use of FAP-targeting immunotherapy. I failed to witness significant adverse events in mice that received the FAP vaccine. These opposing results may reflect fundamental differences between vaccine-induced $CD8^+$T cells, which recognize MHC class I-associated peptides, and CAR-T cells, which are triggered by cell surface expressed protein. Accordingly CAR-T cells have resulted in serious adverse events in human recipients due to off target activity against cells that express barely detectable amounts of the T cells' antigen (319). Several other studies that tested FAP-specific CAR-T cells failed to observe significant toxicity in mice, which may reflect differences in the avidity and signaling capacity of different CARs (132,133,317,320).

Combining the FAP vaccine with a TA-expressing vaccine resulted in increased T cell recruitment to tumors (320) and improved TA-specific $CD8^+$T cell responses as has been reported previously (131,315). In my study numbers of MAA-specific $CD8^+$T cells increased within tumors upon depletion of FAP^+ cells. This was mainly due to less pronounced contraction of vaccine-induced $CD8^+$T cells. Better preservation of vaccine-induced MAA-specific $CD8^+$T cell response may also have been caused by the marked reduction of tumor-infiltrating ISCs after FAP^+ stromal cell depletion.

MDSCs are a heterogeneous population of immature myeloid cells. In most cancers

PMN-MDSCs, which are highly immune-suppressive, represent the majority of the total MDSC population. Targeted depletion of MDCSs increases survival of tumor-bearing mice (316,321). FAP^+ fibroblasts through secretion of factors recruit and activate ISCs (314) and previous reports showed that an anti-fibrotic agent, which inhibits CAF functions, reduces ISC recruitment and functions (322,323). In my study, depletion of FAP^+ cells upon vaccination reduced both MO- and PMN-MDSCs within the TME. This could reflect their reduced recruitment from the periphery, blockade of their expansion within tumors or increased differentiation into non immune-suppressive, more mature myeloid cells. Reduced expression of immune-inhibitors, such as iNOS and Arg1 by ISCs in FAP vaccine-treated mice argues for the latter mechanism.

STAT signaling plays a key role in fate decisions of ISCs. Specifically STAT3 controls their expansion, while STAT1 and STAT6 regulate activation of MDSCs and production of immune-inhibitory factors. The FAP vaccine reduced STAT6 signaling, which is the likely cause for the observed reduction of Arg1 and iNOS production by ISCs in FAP-vaccinated mice. STAT signaling in turn is driven by the surrounding cytokine and chemokine milieu that is maintained by different cells of the TME. In mice that received the FAP vaccine the profile of cytokine/chemokine transcripts present within tumors shifted with pronounced reductions in several of those known to activate STAT6 signaling. Further reductions were seen in transcripts of cytokines that promote Th2 at the expense of Th1 responses; the latter are typically associated with potent $CD8^+$T cell responses. The membrane bound form of FAP reshapes extracellular matrix components, which in turn affects leukocyte/macrophages adhesion and migration. Reduction of FAP would thus be expected to remodel the composition of the tumor infiltrates and thereby the cytokine/chemokine milieu. Furthermore, factor secreted by FAP^+ stromal cells can activate other cells of the TME, thus depleting FAP^+ cells may affect the secretion of inflammatory factors by other cell populations. Indeed my data show that most of the factor-producing transcripts that changed upon FAP vaccination originated from tumor infiltrating leukocytes and $CD14^+$ cells.

Elimination of FAP^+ cells and the resulting reductions in numbers and functions of ISCs

within tumors are associated with better preservation of MAA-specific $CD8^+$ TIL frequencies and improvement of their functions. In addition, levels of MROS decreased in MAA-specific $CD8^+$TILs accompanied by lower expression of the co-inhibitor PD-1. PD-1 signaling causes a gradual loss of $CD8^+$T cell functions and eventually cell death (324,325). This is in part mediated by blockade of the Akt/mTOR pathway, which promotes glucose uptake, glycolysis and anabolic pathways. Within a hypoxic TME access to glycolysis may be especially crucial, as the alternative pathway of energy production, i.e., OXPHOS, requires O_2. As has been described tumors commonly lack glucose due to its consumption by tumor cells [24] and presumably the tumor stroma. As remains to be investigated in more depth, it is feasible that depletion of FAP^+ cells and reductions in ISCs affects metabolic pathways used by tumor cells and other cells within the TME and thereby increases the amount of glucose that is available to $CD8^+$T cells. Access to glucose in turn would reduce T cell metabolic stress and decrease PD-1 expression (200), while promoting their proliferation and effector functions (192,197). I view decreased expression of PD-1 on vaccine-induced $CD8^+$ TILs as a major benefit of FAP-vaccination, as blockade of PD-1 signaling by anti-PD-L1 or anti-PD-1 checkpoint inhibitors are showing remarkable success in delaying progression of fatal solid tumors in human patients (326,327).

In summary, data presented here demonstrate that combining a traditional cancer vaccine with a vaccine that selectively targets FAP^+ fibroblasts reduces tumor progression and even achieves cures in mouse melanoma models. Reduction of numbers and functions of tumor-infiltrating ISCs due to changes in the tumors' cytokine milieu and decreased STAT6 signaling in ISCs was identified as one of the underlying mechanism. Depletion of FAP^+ cells and reductions in numbers and functions of ISCs lead to better preservation of vaccine-induced $CD8^+$TIL functions. This is linked to decreased MROS and PD-1 levels signaling changes in the T cells' metabolism.

MATERIALS AND METHODS

Animal experiments

Female C57BL/6 mice (6-8 weeks) were purchased from the National Cancer Institute (NCI) and housed at the Wistar Institute Animal Facility. Tyr::CreER $Braf^{CA/+}$ $Pten^{lox/lox}$ transgenic mice were a generous gift from Dr. Xiaowei (George) Xu of the University of Pennsylvania (Philadelphia, PA). Experimental procedures were conducted following approved protocols. For C57BL/6 tumor challenge experiments $B16Braf_{V600E}$ tumor cells were given subcutaneously (s.c.) into the right flank at $5x10^4$ cells/mouse. In transgenic mice, tumors were induced by applying 4-hydroxyltamoxifen (4-HT, Sigma, MO) to the shaved right flank at 4ug/mouse/day for three consecutive days. Tumor growth was monitored by measuring the perpendicular diameter of tumors every other day. Mice were euthanized once the diameter of tumor exceeded 1-1.5 cm. For combined vaccination experiments, AdC68-gDMelapoly was given at a dose of 10^{10} virus particles [vp] and AdC68-mFAP or AdC68gD vectors were given at the dose of $9x10^{10}$ vp. Vectors were diluted in phosphate buffered saline (PBS). For control groups, each mouse received 10^{11} vp of the AdC68gD vector. In single vaccination experiment, the AdC68-mFAP vector was given at 10^{11} vp per mouse. All vectors were given intramuscularly (i.m.). For T cell depletion assay, mice were challenged on day 0 with B16 tumor cells and vaccinated on day 3 with the AdC68-mFAP vector. Anti-CD8 (53-6.7) or anti-CD4 (GK1.5) or both antibodies (BioXCell, West Lebanon, NH) were given intraperitoneally at 0.3mg/mouse on day 0, 2 and 4 after tumor challenge.

Cell lines

$B16Braf_{V600E}$ cells (gift from Dr. M Herlyn, Wistar Institute), referred to as B16, were produced by transducing B16.F10 cells with lentiviral vector pLU-EF1a-mCherry expressing mouse $Braf_{V600E}$. These cells rather than wild-type B16F10 cells were use as my vaccine carries the mutated Braf

epitope. Ad vectors were grown in HEK 293 cells. Cells were grown in Dulbecco's Modified Eagles medium (DMEM) with 10% fetal bovine serum (FBS), and 1% penicillin-streptomycin.

Ad vector production

The molecular clone of pAdC68-mFAP vector was constructed by digesting the pcDNA:mFAP vector (gift from Dr. E Puré, University of Pennsylvania) with ApaLI and ligating the mFAP insert into the pShuttle vector. The insert of mFAP from the pShuttle-mFAP vector was transferred to the molecular clone of AdC68 through I-CeuI, PI-SceI and PvuI digestion. Construction, rescue, purification, titration and quality control of AdC68 vectors have been described previously(308).

Western blotting

HEK 293 cells were grown in 6-well plates until they reached 70-80% confluency. Medium was replaced with 1ml serum-free DMEM and different doses of Ad vectors from 10^9-10^{11} vps were added to each well and incubated for two hours before 1ml of 10% FBS DMEM was added. AdC68-gD vector-transduced HEK 293 cells served as negative control. Cells were harvested 48 hours later, washed twice with cold PBS and lysed in RIPA buffer (Invitrogen, Grand Island, NY) with protease inhibitor (Roche, Indianapolis, IN). Protein samples were separated with 4-15% SDS-PAGE and transferred to a PVDF membrane. After blocking and washing, the membrane was incubated with primary sheep anti-FAP antibody (0.5ug/ml, R&D, Minneapolis, MN, AF3715) diluted with 5% milk and 0.1% Tween 20 in PBS overnight at 4°C. Secondary anti-sheep HRP antibody was used for protein detection. b-actin was probed as loading control as described before(328).

Enzyme-linked immunosorbent assay (ELISA)

To measure FAP-specific antibody titers in AdC68-mFAP vaccinated C57BL/6 mice sera were collected in two-weekly intervals after vaccination. Briefly, ELISA plates were coated at 4°C overnight with mouse FAP (200ng/well, gift from Dr. J D Cheng, Fox Chase Cancer Center,

Philadelphia, PA) diluted in coating buffer (0.1M $NaHCO_3$, pH 9.6). Plates were washed with PBS/0.05% Tween- 20 and blocked using PBS with 10% BSA overnight. Serum samples were serially diluted in triplicates and incubated in wells for 2 hours at room temperature. Sheep anti-FAP antibody (Abcam, Cambridge, MA) was serially diluted as standard. After washing bound IgG was detected with alkaline phosphatase (AP) conjugated-goat anti-mouse secondary antibody for serum samples and AP-Donkey anti-sheep secondary antibody for the antibody standard (both from Abcam). A phosphatase substrate (Sigma, St. Louis, MO) dissolved in DEA buffer was added and absorbance was read about 20 minutes later at 405nm using an absorbance reader (ELx800, BioTek, Winooski, VT). Serum antibody titers were determined based on standard curves from each plate and are expressed as mg/ml.

Tissue procession

Lymphocyte isolation from spleen and tumors has been described previously (308). To prepare single cell suspensions, tumors were cut into <2mm small pieces and digested in 1mg/ml Collagenase/Dispase (Sigma) and 1mg/ml DNAse I (Roche) dissolved in Roswell Park Memorial Institute (RPMI) for 30-60mins on a shaker. 10mM EDTA was added after digestion, and single cells were prepared by mechanical mincing with metal-mesh sieves. Cells were then passed through a 70mm cell strainer.

Antibody staining, flow cytometry and cell sorting

For intracellular cytokine staining, ~10^6 lymphocytes were stimulated with peptides or peptide pools (5mg/ml/peptide) and Golgiplug (Fisher Scientific, Waltham, MA 1.5mg/ml) dissolved in DMEM with 2%FBS for 5-6 hours at 37°C. (FAP peptides: FAP1: YSYTATYYI, FAP2: IQYLCWSPV, FAP3: LAYVYQNNI, FAP4: YVYQNNIYL, FAP5: SSWEYYASI, FAP6: RALTLKDIL, FAP7: YDLQNGEFV, FAP8: FAVNWITYL, FAP9: KALVNAQVD, FAP10: IAYSYYGDG, FAP11: TAVRKFIEM, FAP12: LTFWYKMIL, FAP13: SSDYYFSWL, FAP14: SQNHLYTHM, FAP15: IYSERFMGL, FAP16: HLYTHMTHF. MAA peptides: mTrp-$1_{455-463}$:

TAPDNLGYA, mTrp-$1_{481-489}$: IAVVAALLL, mTrp-$2_{522-529}$: YAEDYEEL, hTp-$2_{180-188}$: SVYDFFVWL, hTrp-$2_{343-357}$: STFSFRNAL, mTrp-$2_{363-371}$: SQVMNLHNL, $hgp100_{25-33}$: KVPRNQDWL, $mBraf_{594-602}$: FGLANEKSI). A rabies virus glycoprotein peptide was used as negative control. After stimulation cells were stained as described previously (243,308). Cells were stained with Amcyan fluorescent reactive dye (Life technologies, Carlsbad, CA), anti-CD8-Alexa700 or –Brilliant violet (BV) 605 and CD44-FITC or -PercpCy5.5. For intracellular cytokine staining cells were stained with antibodies to IFN-g(APC or BV421), TNF-a (PE-Cy7, Biolegend, San Diego, California), granzyme B (APC, Life Technologies) and perforin (PE, eBioscience, San Diego, CA) as described (328). For Trp-1_{455} tetramer staining, cells were stained with PE-labeled Trp-1-specific MHC class I (H-$2D^b$) tetramer with TAPDNLGYM peptide (NIAID tetramer facility, Atlanta, GA) together with other surface markers including anti-CD8, CD44, and PD-1-BV605 (all from Biolegend, San Diego, CA). For mitochondrial membrane potential (MMP) and mitochondrial reactive oxygen species (MROS) staining, cells were stained with $DioC_6$ (40nM) and Mitosox red (5mM, Life technologies) for 30mins at 37°C before surface markers staining. For staining of other cell populations from tumors, single cell suspensions were blocked with CD16/CD32 Fc receptor blocking antibody (BD Pharmingen, San Jose, CA) for 30 mins at 4°C. Cells were further stained with either sheep anti-FAP antibody (10µg/ml, R&D, AF3715) or normal sheep IgG control antibody (R&D) at 4°C for 1 hour. After washing cells were stained with donkey anti-sheep APC-conjugated secondary antibody for 30 minutes together with anti-CD3-Pacblue, CD14-PercpCy5.5, CD19-FITC, Gr-1-PE, CD11b-PE-Cy7, CD206-BV605, F4/80-Alexa700, Sca-1-PE-Cy7 and CD90.2-FITC (all from Biolegend). For staining of immunosuppressive functions tumor-derived cells were first stained with CellRox green (5mm) for 30 mins at 37°C. After washing, cells were stained with surface markers for 30 mins at 4°C. Cells were then fixed and permeabilized with fixation/permeabilization buffer (Becton Dickinson, Franklin Lanes, NJ) for 30 mins on ice, followed by staining with rabbit polyclonal antibody to iNOS (10mg/ml, Abcam) in 1x permwash buffer (Becton Dickinson) for 30mins on ice. Normal rabbit IgG (R&D) was used as isotype control. Following washing cells were further stained with Alexa647-goat anti rabbit

secondary antibody (1:2000, Life Technologies) and Arginase1 PE (R&D) for 30 min at 4°C. To measure expression of phosphorylated STAT, cells were first fixed with pre-warmed Fix Buffer I (pre-warmed to37°C, Fisher) for 10 mins at 37°C. After washing with cell staining buffer (Biolegend), cells were stained with surface markers and permeabilized with PermBuffer III (pre-chilled to -20°C, Fisher) for 30 min at 4°C. Cells were washed twice with cell staining buffer and stained with STAT1(pY701) PercpCy5.5, STAT3(pS727) Alexa647 and STAT6(pY641) antibodies (all from Fisher) diluted in cell staining buffer for 60mins at room temperature. Cells were analyzed by an LSRII (BD Bioscience). Data were analyzed with FlowJo (TreeStar, Ashland, OR).

***In vivo* cell lysis assay**

C57BL/6 mice were vaccinated with either AdC68-gD or AdC68-mFAP vectors. Two weeks later splenocytes from naïve syngeneic mice were plated at 10^7 cells/100ul and pulsed with FAP peptides 1,5,7,8,9 (these peptides represents FAP-derived $CD8^+$T cell epitopes with high immunogenicity in C57/Bl6 mice), or a control peptide from the rabies glycoprotein at 5mg/ml for each peptide at 37°C for 2 hours. Following washing cells pulsed with FAP peptides were labeled with carboxyfluorescein succinimidyl ester (CFSE, Life technologies) at 2mM, while cells pulsed with the control peptide were labeled with CFSE at 0.2mM. Two cell populations were mixed at 1:1 ratio and a total of $2x10^7$ cells were transferred into mice vaccinated with either vector through tail vein injection. 16 hours later, splenocytes were isolated from recipient mice and live single cells were analyzed by flow cytometry for expression of CFSE. Loss of $CFSE^{hi}$ cells pulsed with FAP peptides was used as a measure of specific lysis. Percentage of cell lysis was calculated using the following formula: (1-(%$CFSE^{lo}$ cells in control vaccinated mice/%$CFSE^{hi}$ cells in control vaccinated mice)/(%$CFSE^{lo}$ cells in FAP vaccinated mice/%$CFSE^{hi}$ cells in FAP vaccinated mice)) x100.

Gene expression analysis

For the analyses of transcripts from whole tumors, mice were perfused immediately after euthanasia with PBS and heparin (10units/ml). The tumors were cut into small pieces, stabilized with RNA*later* RNA stabilization reagent (Qiagen, Valencia, CA) and stored at -80°C until processed for RNA isolation. To analyze transcripts in different tumor cell subsets, single cell suspensions were prepared and stained as described above. Cells were sorted (Mono Astrios, Beckman Coulter, Jersey City, NJ) on ice into RNAprotect cell reagent (Qiagen). RNA was isolated using RNeasy plus mini kit (Qiagen) and RNA concentration was determined by Nanodrop (Thermo Scientific, Waltham, MA). Reverse transcription was performed using the high capacity cDNA reverse transcription kit (Life Technologies) and relative quantitative real-time PCR was performed using Fast SYBR Green master mix and 7500 Fast Real-time PCR system (Life Technologies). All primers (listed below) were designed by Vector NTI. GAPDH is used as the internal control. The following primers were used (forward followed by reverse): CCL2: 5'-TGCTGACCCCAAGAAGAAATG-3', 5'-TGAAGACCTTAGGGCAGATGCAG-3'; CCL5: 5'-AGCTGCCCTCACCATCCTC-3', 5'-AGCGCGAGGGAGAGGTAGG-3'; CCL22: 5'-ACTCCTGGTGGCTCTCGTCC-3', 5'-TGGCAGAGGGTGACGGATGTA-3'; CXCL10: 5'-AAGGACGGTCCGCTGCAAC-3', 5'-TGATCTCAACACGTGGGCAGG-3'; CXCL12: 5'-TCGCCAGAGCCAACGTCAAG-3', 5'-TCGGGTCAATGCACACTTGTCTG-3'; IL-4: 5'-AACCCCCAGCATGTTGTCATCC-3', 5'-TGGCGTCCCTTCTCCTGTGAC-3'; IL-6: 5'-ACAAAGCCAGAGTCCTTCAGAGAG-3', 5'TTGGAAATTGGGGTAGGAAGG-3'; IL-10: 5'-AAGGTGTCTACAAGGCCATGAATG-3', 5'-TGTCTAGGTCCTGGAGTCCAGC-3'; IL-13: 5'-TGCTTGCCTTGGTGGTCTCG-3', 5'-TGCCGTTGCACAGGGGAGTC-3'; TGF-b: 5'-TACGTCAGACATTCGGGAAGC-3', 5'-TTCAGCCACTGCCGTACAAC-3'; GM-CSF: 5'-ACCCACCCGCTCACCCATC-3', 5'-TCTTCAGGCGGGTCTGCACAC-3'; SCF: 5'-ACCAAGGAGATCTGCGGGAATC-3', 5'-ACATCCATCCCGGCGACATAG-3', GAPDH: 5'-TGCCCCCATGTTTGTGATGG-3', 5'-AATGCCAAAGTTGTCATGGATGACC-3'.

MDSC *in vitro* co-culture assay

Gr-1^{hi}CD11b^{+}MO-MDSCs, Gr-1^{int}CD11b^{+}PMN-MDSCs and CD206^{+}F4/80^{+} TAMs from spleens of mice bearing 1 month-old Braf$^{CA/+}$Pten$^{lox/lox}$ transgenic tumors or B16 tumors were sorted into RPMI medium. CD8^{+}T cells were purified from spleens of naive C57BL/6 mice by negative selection using magnetic beads (MACS, Stemcell Technologies, Vanc ouver, Canada). For inhibition assays, following isolation CD8^{+}T cells were labeled with celltrace violet dye (1mM, Life Technologies, Carlsbad, CA) at 37°C for 20 min. MDSCs or TAMs (8x10^{4} cells/well) and CD8^{+}T cells (4x10^{5} cells/well) were plated at a 1:5 ratio into wells of a 96-well plate pre-coated with anti-CD3 antibody (5mg/ml, 4°C overnight, BD Bioscience, Minneapolis, MN) in RPMI medium (Life Technologies) supplemented with 10% FBS (Life Technologies), 20mM HEPES, 2mM Glutamax, 1mM sodium pyruvate, 0.05mM 2-mercaptoethanol and 1% penicillin-streptomycin. Anti-CD28 antibody (1mg/ml, BD Bioscience) and mouse IL-2 (20U/ml, Roche) were added to each well. Stimulated CD8^{+}T cell without MDSCs/TAMs served as positive controls, while CD8^{+}T cells cultured without activators were used as negative controls. MROS and PD-1 levels on T cells as well as T cell proliferation were analyzed on day 5 of culture by antibody staining and flow cytometry. T cell proliferation data are shown as Proliferation index (PI), i.e., the average number of divisions using the formula:

$$PI = \frac{\sum_{i=2}^{N-1}\left(\frac{n_i}{2^{i-1}}\right)\times(i-1)}{\sum_{i=2}^{N-1}\frac{n_i}{2^{i-1}}}$$

n_i is the cell number of the *i*-the generation (i=1,2,3,…., N).

Statistical analyses

Significance of differences between 2 populations was calculated by Student's t test; significance of differences among multiple populations was calculated by one-way or two-way ANOVA using GraphPad Prism 6. Type I errors were corrected for multiple comparisons using the Holm-Sidak method. Overall responses over time were calculated by area under the curve (AUC) analysis for

each animal followed by student's t test comparing AUC values. Differences in survival were calculated by Log-rank Mantel-Cox test. Significance was set at p-values of or below 0.05.

Chapter 4

Enhancing CD8$^+$T cell fatty acid catabolism within a metabolically challenging tumor microenvironment increases the efficacy of melanoma immunotherapy

ABSTRACT

Metabolism plays an important role in modulating T cell effector functions. However, how tumor-infiltrating T lymphocytes (TILs) adapt to the metabolic constrains within the tumor microenvironment (TME) and how this in turn affects their ability to combat tumor progression remains poorly understood. Using a mouse melanoma model, we report that metabolic challenges due to lack of glucose (Glu) combined with hypoxia within the TME impairs CD8$^+$TILs functions. When simultaneously subjected to hypoglycemia and hypoxia, CD8$^+$TILs enhance catabolism of fatty acids (FAs) including ketone bodies, which partially preserves their effector functions. Pre-conditioning CD8$^+$TILs to increase FA catabolism further improves their ability to slow tumor progression although PD-1 expression concomitantly increases. PD-1 checkpoint blockade delays tumor progression without changing TIL metabolism or functions. It synergizes with metabolic reprogramming of T cells to achieve superior antitumor efficacy. Overall our data show that metabolic interventions may improve the efficacy of cancer immunotherapy.

Portions of this chapter were adapted from:

Zhang Y, Liu L, Kurupati R, Zhou XY, Hudaihed A, Filisio F, Giles-Davis W, Rabinowitz JD and Ertl HC. Enhancing $CD8^+$T cell fatty acid catabolism within a metabolically challenging tumor microenvironment increases the efficacy of melanoma immunotherapy. Manuscript under revision.

INTRODUCTION

Despite recent progress in cancer immunotherapy (329,330), cures remain rare even for highly immunogenic tumors such as melanomas. Adoptive transfer of *ex vivo* expanded TILs may affect regression of large melanomas (331). Nevertheless, traditional vaccines that aim to induce such T cells have largely been ineffective (332). Exhaustion of tumor antigen (TA)-specific $CD8^+$T cells (333,334), which is characterized by their enhanced expression of co-inhibitors, decreased levels of the transcription factor T-bet and loss of effector functions following chronic antigen stimulation has been implicated to cause failures of active immunotherapy for solid tumors (7,(335). Treatments with immune checkpoint inhibitors partially rescue TIL functions and have yielded promising results in cancer patients (326).

The TME poses significant metabolic challenges to TILs due to disorganized vascularization, presence of toxic products derived from tumor and stromal cells and lack of nutrients and oxygen (O_2) (245). TILs require energy to eliminate tumor cells. Upon activation T cells enhance energy production through glycolysis (246), which is less efficient than OXPHOS but provides building blocks for biomass formation and cell proliferation. Tumor cells also use glycolysis (247), which may lead to Glu depletion within the TME (192,197). T cells with limited access to Glu have to rely on OXPHOS to produce energy. Although many substances including FAs can fuel OXPHOS, it requires O_2, which can become limiting within tumors due to insufficient blood supply (248). TILs therefore face dual metabolic jeopardy, which I hypothesize drives their functional exhaustion and thereby impairs the efficacy of cancer immunotherapy.

Here I study the effects of metabolic challenges within the TME on $CD8^+$TILs functions in a mouse melanoma model. Melanoma-bearing mice were immunized with a mixture of vaccines that induce $CD8^+$T cells specific for melanoma-associated antigens (MAAs) and an unrelated tumor antigen (TA), i.e., E7 of human papilloma virus (HPV)-16. Both MAA- and bystander E7-specific $CD8^+$TILs increase co-inhibitor expression and lose functions, contesting the notion that high and sustained antigenic stimulation is solely liable for TIL exhaustion (336),

although it may contribute by increasing the energy demand of $CD8^+$T cells that encounter their cognate antigen. Both $CD8^+$TIL subsets increasingly experience metabolic stress due to restricted O_2 and Glu supply during tumor progression. As shown with vaccine-induced $CD8^+$TILs and *in vitro* activated polyclonal $CD8^+$T cells, hypoxia through hypoxia-induced factor (HIF)-1a increases co-inhibitor LAG-3 expression and impairs $CD8^+$T cell functions. Limited Glu supply enhances co-inhibitor PD-1 expression, reduces effector functions and increases FA catabolism of $CD8^+$T cells; the latter is further enhanced when cells are simultaneously subjected to hypoxia. I show that $CD8^+$TILs in late stage tumors increasingly depend on FA catabolism fueled by FA uptake and triacylglycerol (TG) turnover to meet their energy demand, which increases PD-1 expression but preserves some effector functions. PD-1 blockade fails to affect $CD8^+$TILs metabolism or effector functions; it could reduce tumor growth in a T cell independent manner. Finally, promoting the TILs' ability to utilize FAs increases their ability to delay tumor progression.

My findings show that hypoglycemia and hypoxia plays a critical role in driving the metabolic reprograming and functional exhaustion of $CD8^+$TILs. They further indicate that metabolic interventions that increase FA catabolism by $CD8^+$TILs in a Glu-deprived TME improve the efficacy of cancer immunotherapy.

RESULTS

$CD8^+$T cells become functionally impaired within the TME independent of recognition of their cognate antigen

To test if the fate of $CD8^+$TILs is linked to continued recognition of antigen within tumors, I used two vaccines in a transplantable mouse melanoma model. One, termed AdC68gD-Melapoly (308) (**Figure 4-1**), is an adenovirus (Ad)-based vaccine that elicits robust MAA-specific $CD8^+$T cell responses, most notably to the Trp-$1_{455-463}$ epitope; the other, termed AdC68-gDE7 (243), stimulates bystander $CD8^+$T cells to E7.

Figure 4-1: AdC68-gDMelapoly vaccine design.

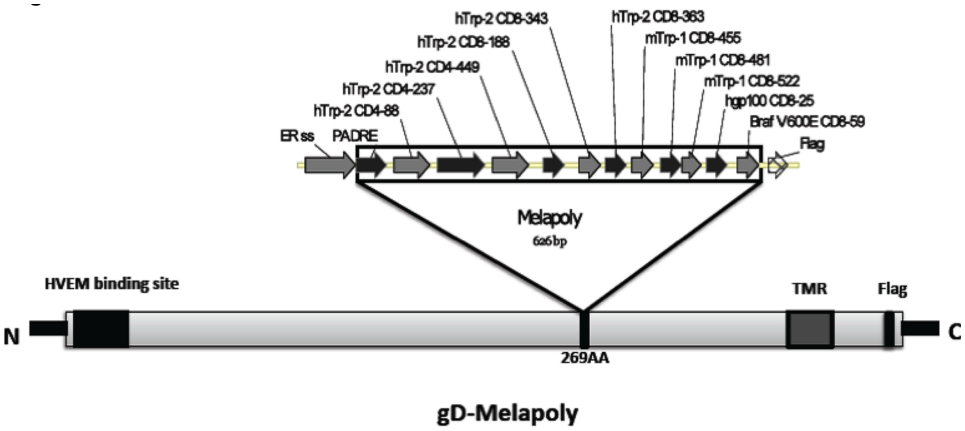

Figure 4-1: AdC68-gDMelapoly vaccine design. Illustration of the transgene construct expressed by adenoviral vector AdC68-gDMelapoly: The Melapoly sequence is composed of an ER signal sequence (ER ss) followed by a pan DR epitope (PADRE), three $CD4^+$T cell epitopes from human (h) Trp-2, and eight $CD8^+$T cell epitopes from human or mouse (m)Trp-2, mTrp-1, hgp100 and $mBraf_{V600E}$. The Melapoly gene was fused into gD following amino acid 269. TMR, transmembrane domain; HVEM, herpes simplex entry mediator.

I vaccinated mice bearing 3-day old tumors and normal mice with AdC68-gDMelapoly mixed with AdC68-gDE7. Mice received the combined vaccine treatment show significantly delayed tumor progression compared to the group vaccinated with control AdC68-gD vector only (**Figure 4-2A**). I chose to analyze vaccine-induced $CD8^+$TILs from 2-week small tumors and 1-month advanced tumors. Both vaccine-induced Trp-1- and E7-specific $CD8^+$T cells accumulate within tumors, where they contract more rapidly than in the periphery (**Figure 4-2B**). This is especially pronounced for Trp-1-specific $CD8^+$TILs although they unlike E7-specific $CD8^+$TILs proliferate within tumors. However their proliferation declines over time (**Figure 4-2C**) despite continued presence of Trp-1 antigen (not shown).

Figure 4-2: Vaccine-induced CD8+TILs independent of chronic antigen stimulation become functionally impaired within TME.

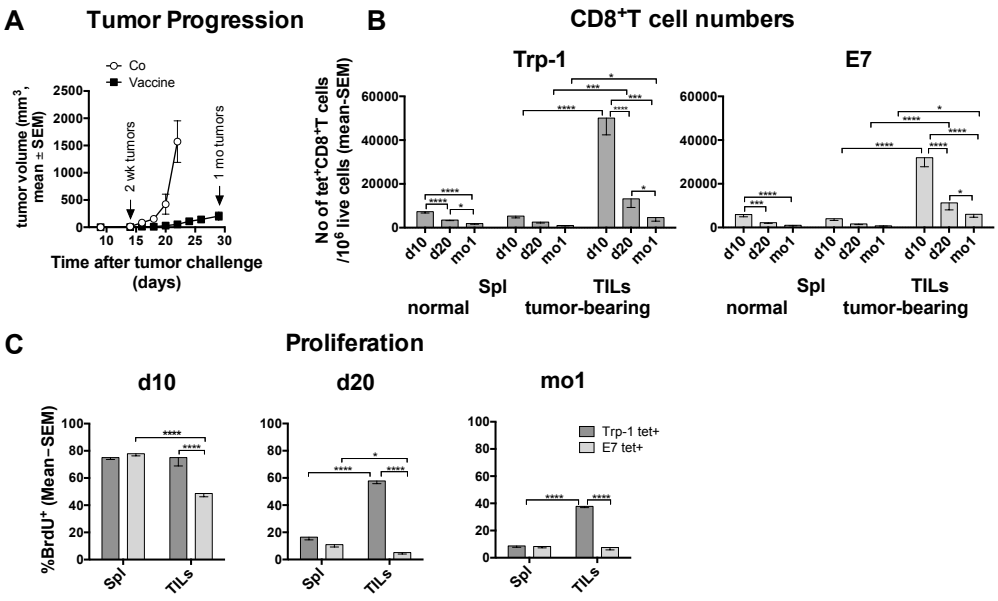

Figure 4-2: Vaccine-induced CD8$^+$TILs independent of chronic antigen stimulation become functionally impaired within TME. (**A**) B16 tumor growth curves in mice received either control vector (circle) or AdC68-gDMelapoly with AdC68-gDE7 vectors (square) three days post tumor tumor challenge (control group: n=6; vaccine group: n=14). (**B**) Trp-1-and E7-specific CD8$^+$T cell responses in spleen (Spl) and tumors of mice that had or had not been challenged 3 days before vaccination with B16Braf$_{V600E}$ cells (n=10 mice/group). Numbers of tetramer (tet)$^+$CD8$^+$ T cells per 10^6 live cells with mean and standard errors of me an (SEM) are shown. (**C**) BrdU was given one day before euthanasia for 24 hours on days 9, 19 or 29 after vaccination. Figure shows % of BrdU incorporation into Trp-1- and E7-specific CD8$^+$T cells of mice that had been challenged with B16Braf$_{V600E}$ cells 3 days before vaccination (n=5 mice/group).

Trp-1-specific CD8$^+$T cells from early and, to a more pronounced extent, late-stage tumors increase expression of PD-1 and LAG-3 (**Figure 4-2D**). Enhanced expression of both co-inhibitors on TILs from small ~ 2 week-old tumors may reflect preferential recruitment of highly activated CD8$^+$T cells. Nevertheless, additional increases of co-inhibitors over time combined with declining production of effector molecules, such as lytic enzymes and interferon (IFN)-γ as well as reduced polyfunction in 1-month tumors (**Figure 4-2E**), suggests that Trp-1-specific CD8$^+$TILs differentiate towards exhaustion. Although E7-specific CD8$^+$TILs neither encounter their cognate antigen nor proliferate within the tumors, they also augment expression of co-

inhibitors (**Figure 4-2C,D**) and lose effector functions and polyfunction in 1-month tumors (**Figure 4-2E**). Importantly, the decrease in effector functions of CD8$^+$TILs in 1-month tumors is not due to their differentiation towards memory T cells, as my analysis show that levels of differentiation markers on/in vaccine-induced CD8$^+$TILs regardless of their antigen specificity remain comparable (**Figure 4-2F**). Lack of memory formation of CD8$^+$ T cells induced by Ad vectors has been reported previously (77) and reflects that these vectors persist in a transcriptionally active form at low levels in activated CD8$^+$ T cells. This in turn provides antigen for continuous activation of the transgene product-specific T cells. Levels of antigens are very modest so that T cells do not differentiate towards exhaustion but rather remain at the effector/effector memory stage. Overall, these data demonstrate that within tumors factors other than chronic stimulation contribute to the functional impairments of CD8$^+$TILs.

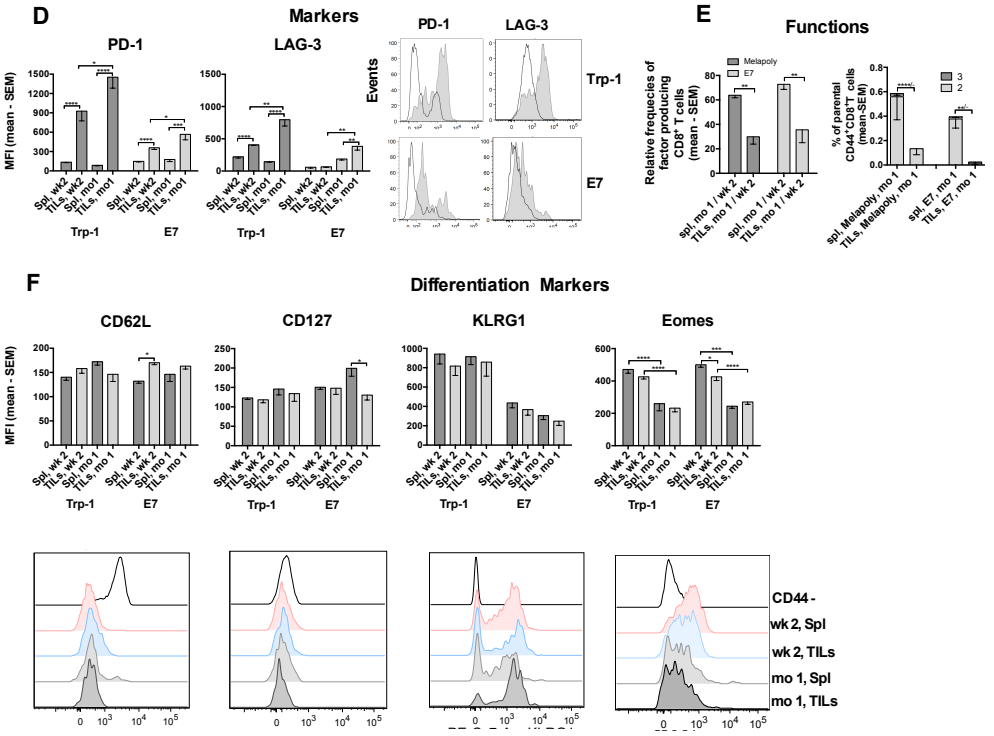

Figure 4-2. (**D**) MFI (mean-SEM) and representative histograms of PD-1 and LAG-3 expression on Trp-1- and E7-specific CD8$^+$T cells from spleens and tumors tested 2 weeks or 1 month after vaccination (n=10 mice/group). (**E**) Left: Relative frequencies of functional Trp-1- or E7- specific CD8$^+$T cells in 1-month spleen or tumors compared to those from 2-week spleen or tumors. Right: Polyfunction of Trp-1- or E7- specific CD8$^+$T cells in terms of percentage of cells producing 3 or 2 functions from 1-month spleens compared to those from 1-month tumors. The productions of granzyme B (GzmB), perforin, IFN-γ are measured by intracellular cytokine staining (ICS, n=5 mice/group). (**F**) Expression of T cell differentiation markers on/in CD8$^+$T cells from either 2-week or 1-month spleen or tumors (n=5 mice/group). *p<=0.05, **p<=0.01, *** p<=0.001, **** p<=0.0001.

Metabolic stress is known to dictate cellular fate (337-339)and could potentially affect functions and survival of vaccine-induced $CD8^+$TILs independent of their antigen specificity. My data show that both Trp-1-and E7-specific $CD8^+$TILs gradually lose mitochondrial membrane potential (MMP) (**Figure 4-3A**), which is essential for proton gradient formation that drives ATP production. They also develop increased levels of mitochondrial reactive oxygen species (MROS) during tumor progression. $MMP^{lo}MROS^{hi}$ Trp-1- and to a lesser extend E7-specific $CD8^+$TILs become prevalent in late stage tumors (**Figure 4-3B**), while corresponding $CD8^+$T cells from spleens remain largely $MMP^{hi}MROS^{lo}$. Overall these data suggest that vaccine-induced $CD8^+$TILs experience intensifying metabolic stress within growing tumors.

Figure 4-3: Vaccine-induced $CD8^+$TILs experience enhanced metabolic stress within TME.

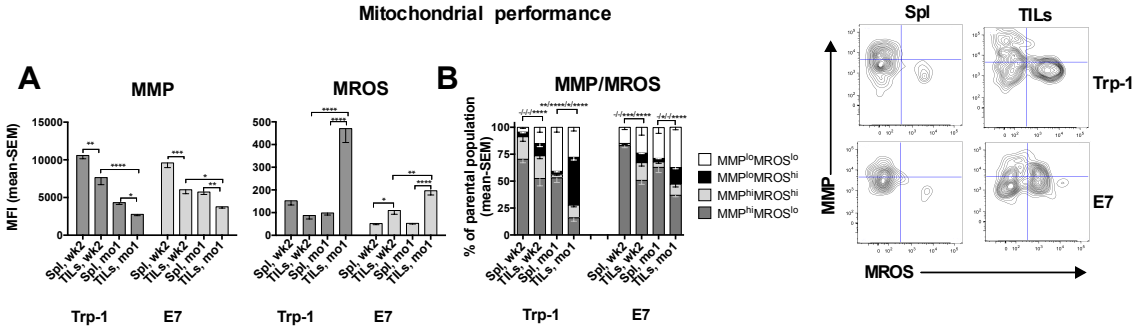

Figure 4-3: Vaccine-induced $CD8^+$TILs experience enhanced metabolic stress within TME. (**A**) MFI (mean-SEM) of MMP and MROS in Trp-1- and E7-specific $CD8^+$T cells from spleens and tumors harvested 2 weeks or 1 month after challenge (n=5 mice/group). (**B**) Quadrant gating of frequencies of Trp-1-and E7-specific $CD8^+$T cells with high or low stains for MMP and MROS (n=5 mice/group). Representative flow plots show samples from mice bearing 1 month-old tumors. For (**B**) (-) - not significant or (*) - significant are arranged so that the 1st shows differences between $MMP^{lo}MROS^{lo}$ cells, the 2nd between $MMP^{lo}MROS^{hi}$ cells, the 3rd between $MMP^{hi}MROS^{hi}$ cells and the 4th between $MMP^{hi}MROS^{lo}$ cells.

Hypoxia through HIF-1α increases LAG-3 expression and reduces T cell functions

Solid tumors commonly lack O_2. My data show that Trp-1- and E7-specific $CD8^+$TILs within the TME increasingly experience hypoxia during tumor progression as shown by enhanced expressions of HIF-1α, a transcription factor that stabilizes under hypoxia, and its downstream target Glut1, which facilitates Glu uptake, in/on vaccine-induced $CD8^+$TILs from late-stage (**Figure 4-3C**) but not small week 2 tumors (**data not shown**).

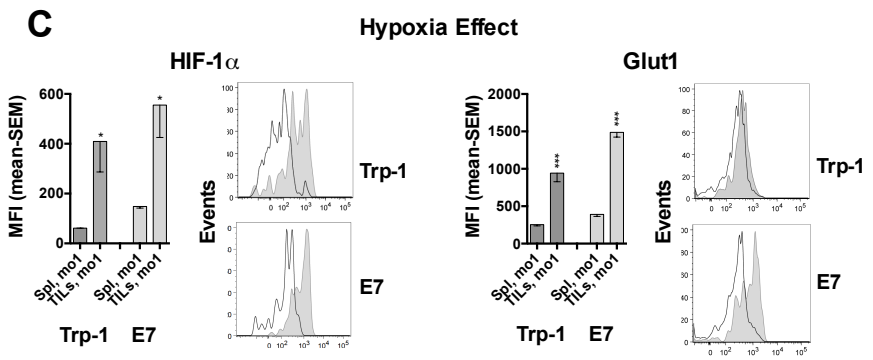

Figure 4-3. (**C**) MFI (mean-SEM) of HIF-1α and Glut1 expression in/on Trp-1-and E7-specific $CD8^+$T cells from spleens and tumors of mice bearing 1 month-old tumors (n=5 mice/group). Histograms: HIF-1α and Glut1 levels in representative samples from spleen (open) and tumor (grey). *p<=0.05, **p<=0.01, *** p<=0.001, **** p<=0.0001.

To test the effect of hypoxia, I stimulated $CD8^+$T cells *in vitro* for 4 days in regular Glu-rich medium under normoxia (21% O_2) or subjected them to hypoxia (1% O_2) for the last 16 hours of culture (**Figure 4-4A**). Hypoxia affects T cell stimulation as evidenced by reduced blast formation (**Figure 4-4B**). Activated $CD8^+$T cells under hypoxia increase expression of HIF-1α and Glut1 (**Figure 4-4C**). They become metabolically stressed as evidenced by decreases in MMP and rises in MROS, leading to an increase in the proportion of $MMP^{lo}MROS^{hi}$ $CD8^+$T cells (**Figure 4-4D**) reminiscent of the mitochondrial metabolic profile of vaccine-induced TILs in late-stage tumors.

Figure 4-4: Hypoxia affects $CD8^+$T cell metabolism, differentiation and functions.

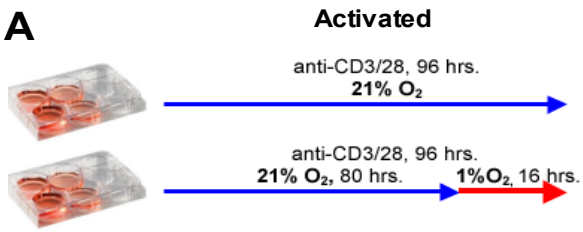

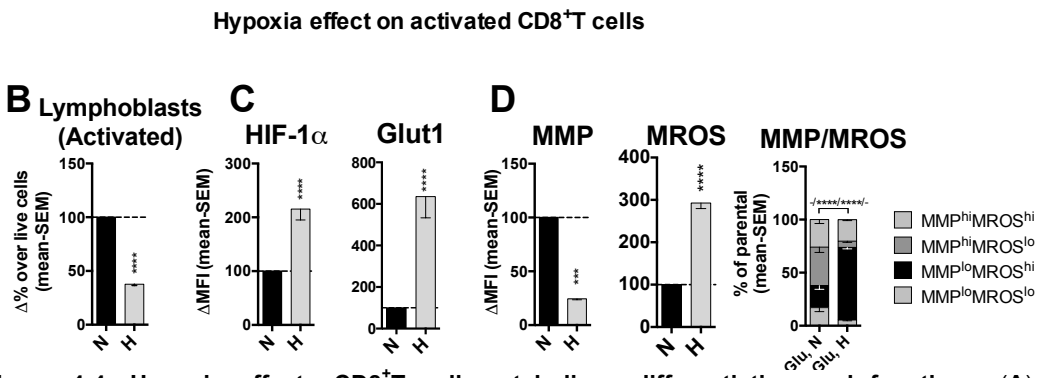

Figure 4-4: Hypoxia affects CD8$^+$T cell metabolism, differentiation and functions. (**A**) Cartoon illustrates my experimental design where cells were stimulated continuously for 96 hours. To assess the effect of hypoxia cells were moved to a 1% O_2 chamber for the last 16 hours. (**B**) Blast formation; normalized % of live CD8$^+$T cells forming blasts by day 4 of culture under hypoxia (H, light grey) compared to those cultured under normoxia (N, black) using protocol shown in **A** (n=6 samples/group, representative of more than 5 experiments). (**C**) Normalized MFI values for HIF-1α and Glut1 expression in/on CD8$^+$T cells under normoxia, N or hypoxia, H (n=5 samples/group, representative of 4 experiments). * on top of each bar indicates significant differences compared to Glu, N. (**D**) Left: Normalized MFI of MMP and MROS. Right: Quadrants gating for MMP over MROS stains (n=5 samples/group, representative of >5 experiments).

Hypoxia reduces PD-1 but augments LAG-3 expression (**Figure 4-4E**), suggesting that PD-1 declines and LAG-3 increases under conditions that promote glycolysis such as through HIF-1α signaling. CD8$^+$T cells cultured under hypoxia reduce T-bet expression (**Figure 4-4F**), decrease production of effector molecules and lose polyfunctionality (**Figure 4-4G**).

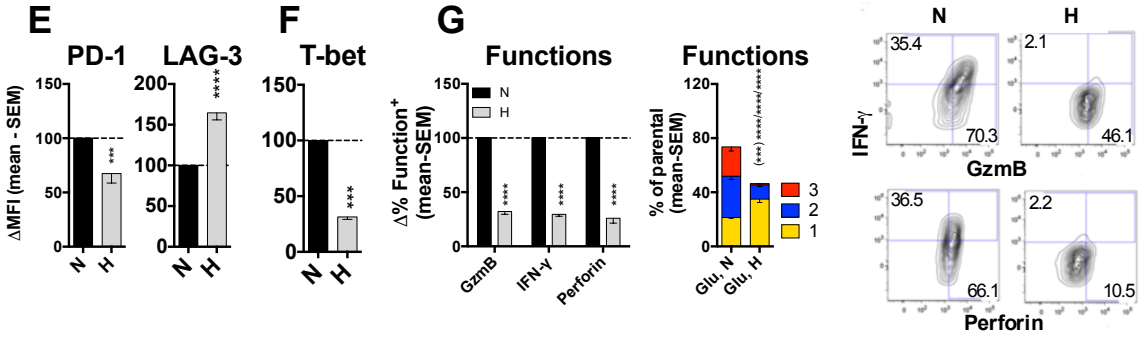

Figure 4-4. (**E**) Normalized MFI of PD-1, LAG-3 and (**F**) T-bet expression. (**G**) Left: Production of individual functions under hypoxia with data normalized to those under normoxia. Right: Functions of CD8$^+$T cells shown as % of CD8$^+$CD44$^+$T cells producing 3, 2 or 1 factors and their representative flow plots. Production of IFN-γ, granzyme B (GzmB) and perforin were measured. * within () on top of the bars indicate differences in % of total function and * outside of () indicates differences in proportions of cells producing 1-3 functions (bottom to top). Numbers on flow plots indicates % of cells positive for IFN-γ, granzyme B or perforin. (**E-G**) n=5 samples/condition, representative of more than 5 experiments.

A different previously described protocol[25] (**Figure 4-4H**), in which CD8$^+$T cells upon the initial activation are rested in IL-2 prior to hypoxia, has no effect on blast formation (**Figure 4-4I**) or PD-1 levels, although LAG-3 expression increases (**Figure 4-4J**) and T-bet levels decrease

(**Figure 4-4K**). Granzyme B (GzmB) production increases while production of other effector molecules and polyfunctionality decline (**Figure 4-4L**). As vaccine-induced $CD8^+$T cells are unlikely to rest before infiltrating tumors, I used the protocol of continuous $CD8^+$T cell activation for subsequent hypoxia experiments.

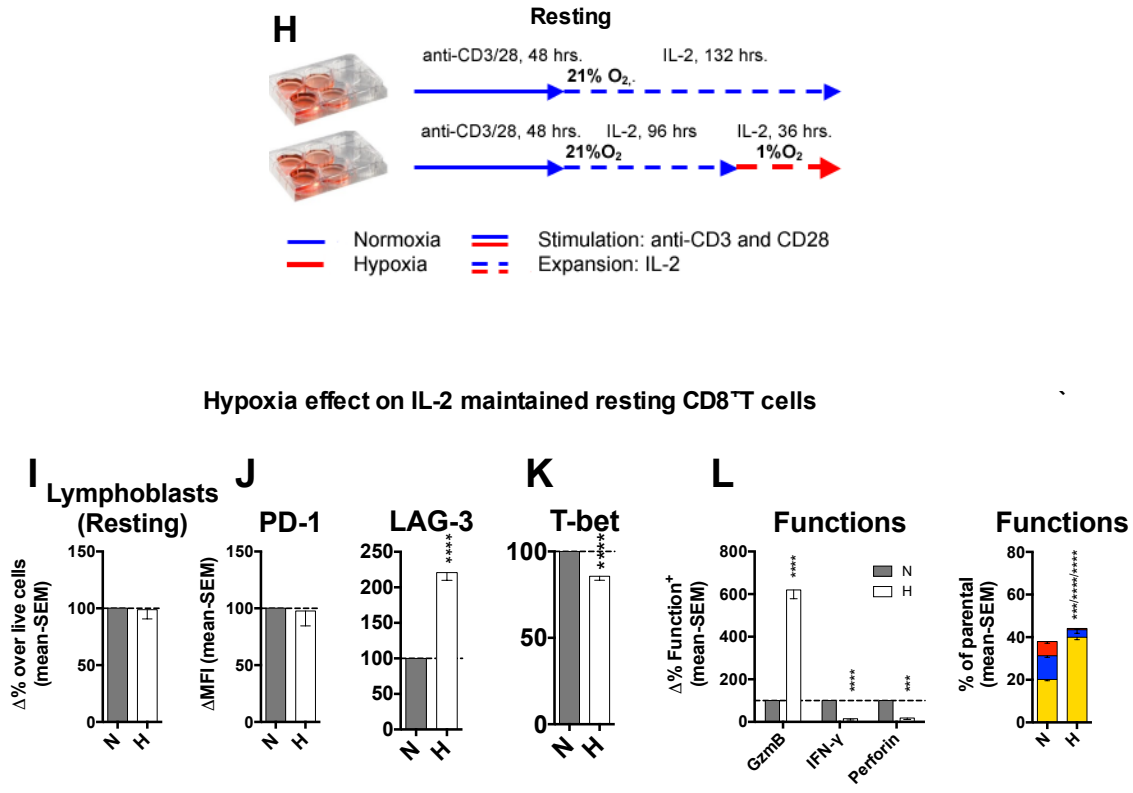

Figure 4-4. (**H**) Alternative protocol tests the effect of hypoxia on relatively resting $CD8^+$T cells. T cells were stimulated for 48 hours and then switched to IL-2 containing medium without antibodies to CD3 or CD28. The effect of hypoxia was assessed by subjecting cells cultured in IL-2 to 1% O_2 for the last 36 hours. (**I**) Blast formation; normalized % of live $CD8^+$T cells forming blasts under hypoxia compared to those cultured under normoxia using protocol shown in **H**. (**J**) Normalized expression of PD-1, LAG-3 and (**K**) T-bet on/in cells kept under hypoxia (white) compared to those cultured under normoxia (dark grey) using protocol **h**. (**I**) Left: Normalized production of individual functions by $CD8^+$T cells cultured under hypoxia compared to those cultured under normoxia, using protocol **H**. Right: % of cells over all $CD44^+CD8^+$ cells positive for 1-3 functions. * are arranged according to colors with significance for 1 function at the bottom. (**I-L**) n=6 samples/condition, representative of 2 experiments.

HIF-1α correlates with expression of LAG-3 on TILs or $CD8^+$T cells subjected to hypoxia (**Figure 4-5A**). To determine whether HIF-1α directly promotes LAG-3 expression and whether this affects $CD8^+$T cell functions, I knocked down HIF-1α transcripts by transducing $CD8^+$T cells with lentivectors that express either short-hairpin (sh)RNA to silence HIF-1α or a

control sequence, together with a Thy1.1 selection marker (**Figure 4-5B**). HIF-1α silencing reduces expression of HIF-1α in CD8$^+$T cells stimulated *in vitro* under hypoxia (**Figure 4-5C**), concomitantly decreases LAG-3 but not PD-1 (**Figure 4-5D**) and improves production of granzyme B and IFN-γ (**Figure 4-5E**).

Figure 4-5: Hypoxia-induced HIF-1α directly drives co-inhibitor LAG-3 expression and impairs effector functions of activated CD8$^+$T cells *in vitro*.

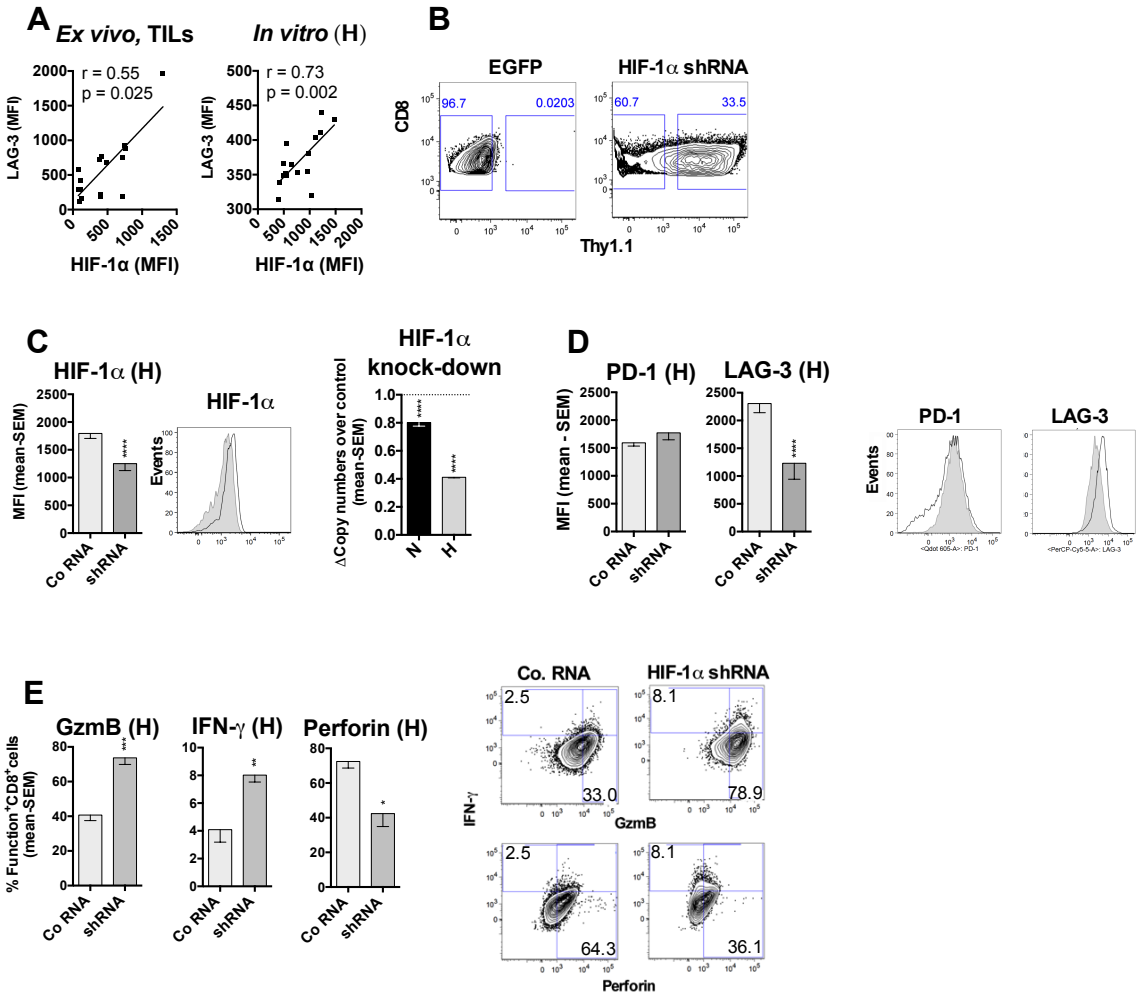

Figure 4-5: Hypoxia-induced HIF-1α directly drives co-inhibitor LAG-3 expression and impairs effector functions of activated CD8$^+$T cells *in vitro*. (**A**) Pearson correlation between MFI values of HIF-1α and LAG-3 expression in/on TILs or *in vitro* activated CD8$^+$T cells that were subjected to hypoxia. Correlation coefficient r and p values are shown on top of the graphs. Each dot represents one sample (n=17 for TILs samples, n=16 for *in vitro* samples, data were pooled from 2 independent experiments). (**B**) Flow plots illustrates the levels of Thy1.1 expression upon transduction of CD8$^+$T cells with a control lentivector expressing eGFP or the HIF-1α shRNA lentivector expressing Thy1.1 as a selection marker. (**C**)

Left: MFI values of HIF-1α expression in activated CD8$^+$T cells transduced with control vector (light grey) or HIF-1α shRNA vector (dark grey) and then cultured under hypoxia. Representative histogram is shown next to the bars (open: control group, grey: HIF-1α shRNA group). Right: Level of HIF-1α knock-down determined by testing transduced bead-enriched Thy1.1$^+$CD8$^+$T cells for HIF-1α transcripts by real-time PCR. Data shown as HIF-1α transcripts levels in cells transduced with HIF-1α shRNA normalized to those transduced with control RNA. (**D**) MFI values of PD-1 and LAG-3 expression on activated CD8$^+$T cells transduced with control or HIF-1α shRNA vector and then cultured under hypoxia. Representative histograms are shown next to the bars (open: control group, grey: HIF-1α shRNA group). (**E**) % of CD44$^+$CD8$^+$T cells transduced with control or HIF-1α shRNA vector cultured under hypoxia producing individual factors. Representative flow plots on the right show quadrant gating for IFN-γ over granzyme B or perforin. (**C-E**) n=5 samples/group, representative of 2 experiments. samples were pooled from n=30 mice for each experiment. *p<=0.05, **p<=0.01, *** p<=0.001, **** p<=0.0001.

To study whether HIF-1α contributes to the CD8$^+$TILs' co-inhibitor expression and loss of functions, I activated enriched CD8$^+$T cells *in vitro* and, after transduction with control or HIF-1α shRNA-expressing lentivectors, transferred them into tumor-bearing, AdC68-gDMelapoly-vaccinated mice (**Figure 4-6A**). I analyzed the transferred T cells ~3 weeks later (**Figure 4-6B)** using tumor samples from mice bearing similar sized tumors.

Figure 4-6: HIF-1α knock down reduces LAG-3 expression and improves MAA-specific CD8$^+$T cell functions in the TME.

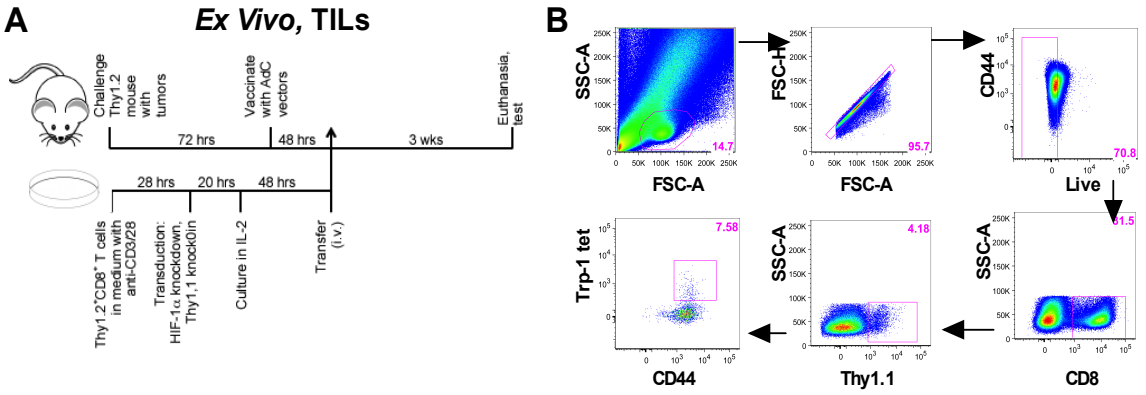

Figure 4-6: HIF-1α knock down reduces LAG-3 expression and improves MAA-specific CD8$^+$T cell functions in the TME. (**A**) Experimental set up for *in vivo* study. Enriched CD8$^+$T cells were transduced with lentivectors expressing control or HIF-1α targeting shRNA and Thy1.1 and transferred intravenously (i.v.) into Thy1.2$^+$ mice. Recipient mice at the time had been challenged with tumor cells 5 days earlier and they had been vaccinated with AdC68-gDMelapoly 2 days earlier. (**B**) Gating strategy for lentivector transduced Trp-1-specific CD8$^+$TILs. Trp-1-specific Thy1.1$^+$CD8$^+$T cells were recovered from tumors 2 weeks after transfer. Cells from tumors were first gated on mononuclear cells, singlets, live cells and CD8$^+$T cells. They were further gated on Thy1.1$^+$ cells and Trp-1-tetramer$^+$CD44$^+$ cells.

Knocking down HIF-1α (**Figure 4-6C**) reduces the Trp-1-specific CD8$^+$TILs' expression of LAG-3 without affecting PD-1 (**Figure 4-6D**) and significantly improves the MAA-specific TILs' frequencies and functions (**Figure 4-6E**). Production of perforin increases upon HIF-1α-silencing *in vivo* but not *in vitro,* which may reflect that other conditions such as differences in supply of nutrients contribute to the effect of hypoxia on activated CD8$^+$T cells. These data suggest that hypoxia through increased HIF-1α signaling directly enhances LAG-3 expression and dampens effector functions of CD8$^+$TILs. They further suggest that a HIF-1α-driven metabolic switch to glycolysis might be counterproductive for T cell functions within an O_2 and Glu-depleted TME.

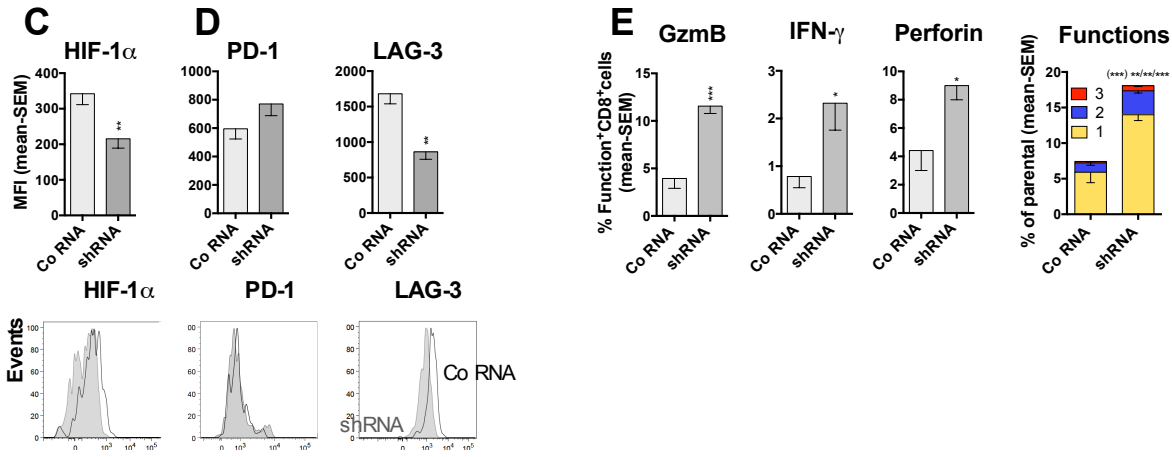

Figure 4-6. (**C-D**) Upper panel: MFI values of HIF-1α (**C**) and co-inhibitors PD-1 and LAG-3 (**D**) expression in/on Trp-1-specific CD8$^+$TILs transduced with control (Co RNA) or HIF-1α shRNA (shRNA) vector. Lower panel show representative histograms: control vector transduced samples (empty), HIF-1α shRNA vector transduced samples (grey). (**E**) Left: % of MAA-specific CD8$^+$TILs transduced with either control or HIF-1α shRNA expressing vector producing individual factors; Right: % of lentivector transduced cells in each group producing 3,2 and 1 factor. * within () indicates difference in sum of responses, * out of () left to right: difference in having 3, 2, 1 functions. (**C-E**) n=6 mice/group, data are representative of 2 experiments. *p<=0.05, **p<=0.01, *** p<=0.001, **** p<=0.0001.

Activated CD8$^+$T cells subjected to Glu and O_2 deprivation enhance FA catabolism

Not only O_2 but also the supply of Glu declines during tumor progression within the TME presumably due to its consumption by tumor cells (**Figure 4-7A**). To investigate the collective effects of Glu and O_2 restrictions, enriched CD8$^+$T cells were stimulated *in vitro* in Glu

medium with 2-deoxy-D-glucose (2-DG), a competitive inhibitor of glycolysis, or Glu was replaced with galactose (Gal). Cells were cultured under normoxia or short-term hypoxia. The extracellular acidification rate (ECAR), a measure of glycolysis, declines in T cells cultured with 2-DG or Gal. The O_2 consumption rate (OCR), a measure of OXPHOS, decreases with 2-DG but increases with Gal. $CD8^+$T cells activated under either condition show increases in the OCR/ECAR ratio, suggesting a switch towards energy production through OXPHOS (**Figure 4-7B**).

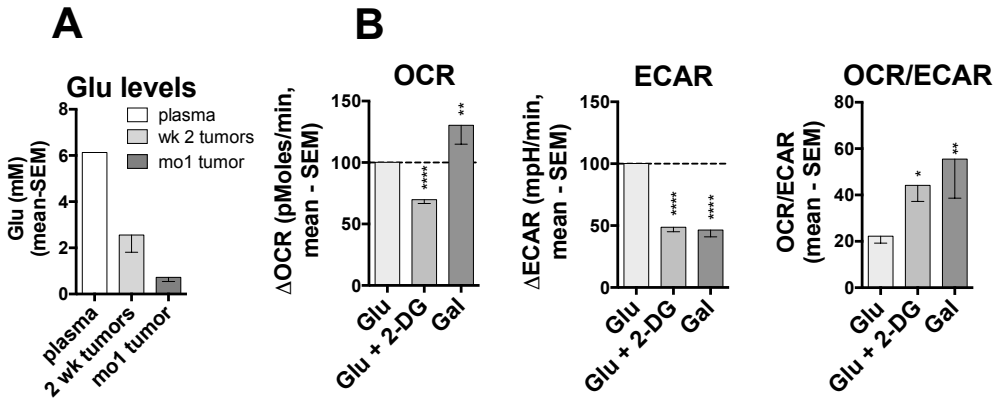

Figure 4-7: Effects of glucose limitation on metabolism, differentiation and effector functions of activated $CD8^+$T cells *in vitro* subjected to normoxia or short-term hypoxia. When indicated (D in Y-axis title) values are normalized to those obtained with Glu, N set at 100 (black dotted lines). The red dashed lines show results for cells cultured in Glu and subjected to hypoxia (H) normalized to those cultured in Glu and under normoxia. (**A**) Glu concentration in plasma or interstitial fluid of 2 week- and 1 month-old tumors (n=5 mice/group, representative of 2 experiments). (**B**) Normalized OCR, ECAR and the OCR to ECAR ratios at baseline for $CD8^+$T cells stimulated in Glu with 2-DG or medium supplumented with Gal instead of Glu for 4 days. Data are normalized to those obtained with cells kept in Glu-rich medium set at 100 (n=5 samples/group with 3 repeated measures/sample, representative of 3 experiments).

Cells cultured with 2-DG or Gal compared to those grown with Glu express more PD-1 regardless of O_2 supply, suggesting a link between use of OXPHOS and high PD-1 expression (**Figure 4-7C**). Compared to cells cultured with Glu those grown with limited access to Glu under normoxia decrease T-bet expression (**Figure 4-7D**) and lose functions including polyfunctionality (**Figure 4-7E**). Intriguingly, functions of $CD8^+$T cells without access to Glu are better preserved if cells are also subjected to hypoxia (**Figure 4-7E**).

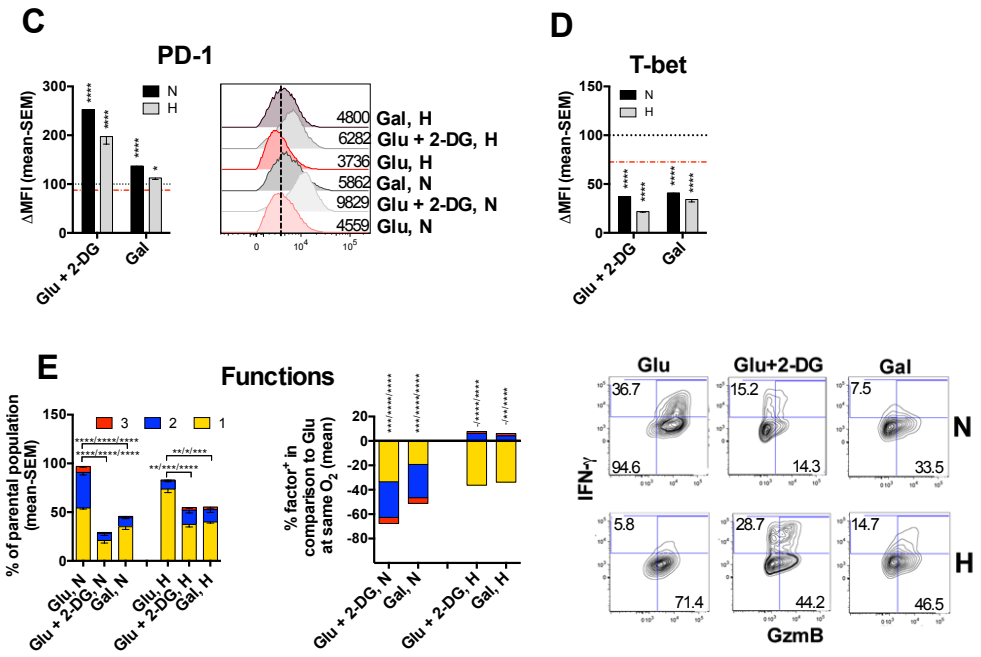

Figure 4-7. (**C**) Normalized MFI values and representative histograms for PD-1 expression on $CD8^+$T cells activated in different Glu-restricted medium under normoxia (black) or hypoxia (grey) (n=5 samples/condition, representative of more than 5 experiments). Numbers next to histograms indicate MFI values. (**D**) Normalized MFI values of T-bet (n=5 samples/group, representative of 3 experiments). (**E**) Left: % of cells producing 3, 2 and 1 factors over all $CD44^+CD8^+$ T cells cultured under different conditions. Middle: Same data as left illustrating differences in % of cells producing 3, 2 and 1 factors in Glu+2-DG or Gal medium compared to those of cells in Glu medium with the corresponding O_2 supply. Statistics on each bar indicates difference in % of cells producing 3, 2 and 1 function (bottom to top). Right: representative flow plots show IFN-γ and granzyme B production (n=5 samples/group, representative of 3 experiments).

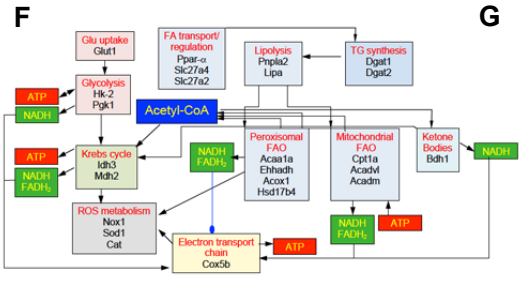

G

Function	Name	Abbreviation
Gucose uptake	glucose transporter 1	Glut1
glycolysis	hexokinase 2	Hk-2
	phosphoglycerate kinase	Pgk1
TCA cycle	isocitrate dehydrogenase subunit alpha	Idh3a
	monodehydroascorbate reductase 2	Mdh2
Regulation of FA metabolism	peroxisome proliferator-activated receptor alpha	Ppar-α
FA transport	solute carrier family 27a4	Slc27a4
	solute carrier family 27a2	Slc27a2
Triglyceride (TG) synthesis	diacylglycerol O-acyltransferase 1	Dgat1
	diacylglycerol O-acyltransferase 2	Dgat2
Triglyceride (TG) catabolism	lipase A	Lipa
	patatin-like phospholipase domain containing 2	Pnpla2
Peroxisomal FAO	acetyl-CoA acyltransferase 1	Acaa1a
	CoA dehydrogenase	Ehhadh
	acyl-CoA oxidase 1	Acox1
	hydroxysteroid (17-beta) dehydrogenase 4	Hsd17b4
Mitochondrial FAO	carnitine palmitoyltransferase 1a	Cpt-1a
	acyl-CoA dehydrogenase, very long chain	Acadvl
	acyl-CoA dehydrogenase, C-4 to C-12 straight chain	Acadm
Metabolism of ketone bodies	3-hydroxybutyrate dehydrogenase 1	Bdh1
ROS metabolism	NADPH oxidase 1	Nox1
	superoxide dismutase 1	Sod1
	catalase	Cat
Electron transport chain	cytochrome c oxidase subunit Vb	Cox5b

Figure 4-7. (**F**) Cartoon indicates roles of different factors that were analyzed at the transcriptional level. (**G**) Table summarizes functions, names and abbreviations of the analyzed factors.

These data suggest that under hypoxia cells with limited supply of Glu may more readily switch to alternative metabolic pathways to support their energy demand.

To study the metabolic pathways used by CD8$^+$T cells with limited Glu and O_2 supply *in vitro* or within the TME, I measured expression levels of transcripts for factors that participate in nutrient consumption and energy production by comparative quantitative (q)PCR (**Figure 4-8A, Figure 4-7F,G**). Upon short-term hypoxia CD8$^+$T cells stimulated with limited access to Glu compared to those stimulated in Glu-rich medium decrease transcripts for enzymes of glycolysis and the tricarboxylic acid (TCA) cycle, ROS detoxification and the electron transport chain (ETC); while transcripts for FA uptake, TG turnover, peroxisomal and mitochondrial FA oxidization (FAO) increase. This pattern is closely mirrored by Trp-1- and E7-specific CD8$^+$TILs from late-stage tumors compared to those from small 2 week-old tumors, indicating that metabolically stressed CD8$^+$T cells increasingly rely on FA catabolism to produce energy. Changes in transcripts during tumor progression are not driven by differentiation of TILs towards a more resting stage, as they are distinct from differences in vaccine-induced splenic CD8$^+$T cells tested at 3 months compared to those tested at 2 weeks after vaccination (**Figure 4-8B**).

Figure 4-8. Limited access to Glu and oxygen forces activated CD8$^+$T cells to enhance FA catabolism *in vitro*.

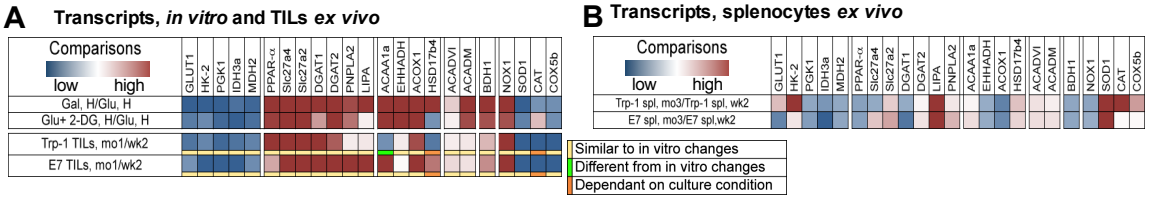

Figure 4-8: Limited access to Glu and oxygen within TME forces activated CD8$^+$T cells to enhance FA catabolism. (**A**) Relative transcripts levels: CD8$^+$T cells stimulated in Gal or Glu+2-DG vs. Glu medium under hypoxia. Or: Trp-1- and E7-specific CD8$^+$TILs from 1-month tumors vs. those from 2-week tumors. Color code compares the changes in transcripts levels between *in vivo* and *in vitro* samples. Yellow: similar; green: opposite; orange: mixed. (**B**) Relative transcripts levels of Trp-1-or E7-specific CD8$^+$T splenocytes collected 3-months vs. 2 weeks after vaccination. (**A, B**) n=5 mice/group.

Consistent with increased transcript levels of factors involved in FA metabolism, CD8$^+$T cells grown with limited access to Glu under normoxia or hypoxia significantly increase FA uptake (**Figure 4-8C**) and enhance oxidation of endogenous and exogenous FAs (**Figure 4-8D**).

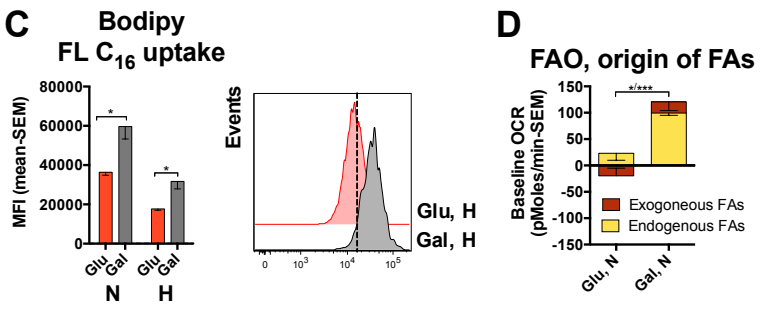

Figure 4-8. (**C**) Uptake of Bodipy FL C_{16} (fluoresent free fatty acid) by cells cultured in Glu (red) or Gal (dark grey) media under normoxia (N) or hypoxia (H). Histograms show Bodipy uptake in representative samples subjected to hypoxia (n=5 samples/condition, representative of two experiments, n=25 mice were pooled for each experiment). (**D**) Basal OCR due to consumption of exogenous (brown bars) and endogenous (yellow bars) FAs by $CD8^+$ T cells stimulated in vitro in Glu or Gal media (n=3 samples/condition with 3 repeated measures/sample, representative of two experiments, n=15 mice were pooled for each condition in every experiment).

To directly measure effects of Glu and O_2 deprivation on FA catabolism of $CD8^+$T cells, my collaborator performed liquid chromatography-mass spectrometry (LC-MS)-based metabolic analyses. Metabolites involved in FA mitochondrial transport and oxidation, i.e., acetylcarnitine, palmitoylcarnitine and the ketone body 3-hydroxybutyrate, increase in cells stimulated *in vitro* in Gal medium and this is exacerbated under hypoxia (**Figure 4-8E**). $^{13}C_6$-Glu/Gal or $^{13}C_{16}$-palmitate isotope tracing (**Figure 4-8F**) show that $CD8^+$T cells activated in Glu medium and short-term hypoxia or in medium with limited access to Glu under normoxia or hypoxia compared to those activated in Glu medium under normoxia show reduced presence of carbohydrate-derived ^{13}C in TCA cycle metabolites (**Figure 4-8G**), but significantly higher $^{13}C_{16}$-palmitate-derived carbon incorporation into acetyl-CoA and TCA cycle metabolites (**Figure 4-8H**). Cells stimulated under hypoxia show significantly higher percentages of $^{13}C_{16}$-palmitate-derived acetyl-CoA than those cultured in the same medium under normoxia, suggesting that cells further increase FAO under hypoxia.

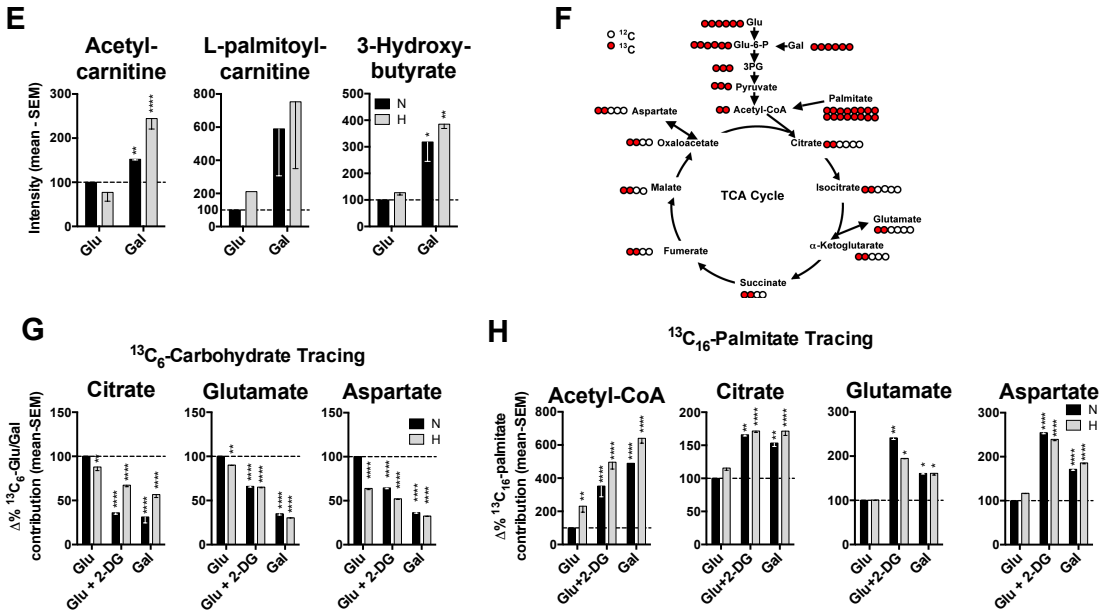

Figure 4-8. (**E**) Relative intensity of FAO-related metabolites in CD8$^+$Tcells stimulated for 4 days in vitro under different conditions normalized to those of cells cultured under Glu, Normoxia. Normoxia: black; Hypoxia: light grey. (**F**) $^{13}C_6$-Glu/Gal or $^{13}C_{16}$-palmitate-derived ^{13}C cycling into metabolites of glycolysis or TCA cycle. (**G**) Normalized contribution of $^{13}C_6$-Glu/Gal-derived ^{13}C carbon and (**H**) $^{13}C_{16}$-palmitate-derived ^{13}C-carbon to metabolites of the TCA cycle in cells cultured under different conditions compared to those cultured under Glu, Normoxia (set as 100). Data are shown as mean values of relative % of labeling with SEM. * on top of each bar indicates significant differences compared to cells cultured under Glu, N. (**E, G, H**) n=6 samples/condition, representative of 2 experiments. n=30 mice were pooled for each experiment. *p<=0.05, **p<=0.01, *** p<=0.001, **** p<=0.0001.

Next I studied the metabolism of activated CD8$^+$T cells directly *in vivo* by stable isotope tracing. Mice bearing 3-day tumors were vaccinated with mixtures of AdC68-gDMelapoly and AdC68-gDE7. Two weeks or one-month later mice were given $^{13}C_6$-Glu and levels of glycolysis metabolites and ^{13}C incorporation into TCA cycle intermediates were analyzed in CD44$^+$CD8$^+$T cells from spleen and tumors (**Figure 4-9A**). The need for sufficient cell numbers precluded an analysis of vaccine-induced CD8$^+$T cells. The intensity of glycolysis intermediates glucose-6-phosphate (G6P) and 3-phosphoglycerate (3PG) in TILs declines during tumor progression (**Figure 4-9B**), indicating reduced glycolysis. The contribution of ^{13}C-Glu-derived carbon to TCA cycle intermediates declines comparing CD44$^+$CD8$^+$T cells from late to early stage tumors or from tumors to spleens (**Figure 4-9C**), confirming that TILs decrease Glu catabolism.

Figure 4-9: Activated CD8$^+$T cells within metabolically challenging TME enhance FA catabolism.

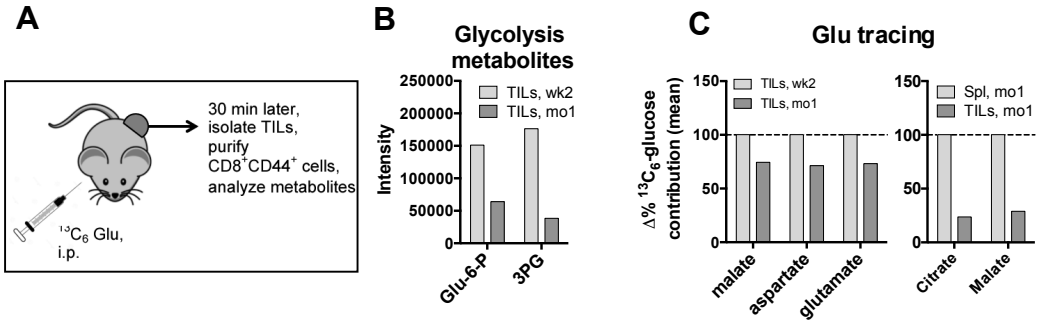

Figure 4-9: Activated CD8$^+$T cells within metabolically challenging TME enhance FA catabolism. (A) Experimental design for $^{13}C_6$-Glu *in vivo* tracing. (**B**) Relative intensity of glycolysis metabolites in CD44$^+$CD8$^+$TILs from 1-month tumors normalized to those from 2-week tumors (n=2 pooled samples/group, 30 mice/sample). (**C**) Normalized $^{13}C_6$- Glu contribution to TCA cycle metabolites in CD44$^+$CD8$^+$TILs from 1-month tumors compared to those from spleens (n=2 pooled splenocytes samples; n=1 pooled TILs sample, pooled from 60 mice).

I further performed $^{13}C_{16}$-palmitate tracing in mice bearing 2-week or 1-month tumors (**Figure 4-9D**). The intensities of acylcarnitine species, the ketone bodies 3-hydroxylbutyrate and acetoacetate increase in TILs during tumor progression (**Figure 4-9E**). Moreover, the contribution of $^{13}C_{16}$-palmitate-dervied ^{13}C to TCA metabolites becomes higher in CD44$^+$CD8$^+$T cells from 1-month tumors compared to those from 2-week tumors or 1-month spleens (**Figure 4-9F**), supporting the TILs' enhanced reliance on FA catabolism during tumor progression. In splenic CD44$^+$CD8$^+$T cells tested at different time points after vaccination, $^{13}C_{16}$-palmitate-derived carbon incorporation into TCA cycle metabolites remains stable or decreases over time.

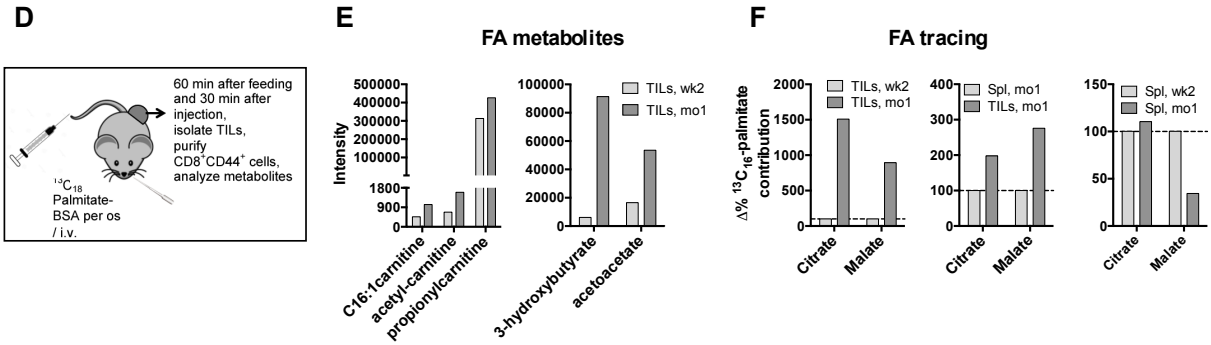

Figure 4-9. (**D**) Experimental design for $^{13}C_{16}$-palmitate *in vivo* tracing. (**E**) Relative intensity of FA metabolites in $CD44^{+}CD8^{+}$TILs from 2 wk- or 1 mo-old tumors. (**F**) Normalized $^{13}C_{16}$- palmitate contribution to TCA cycle metabolites in $CD44^{+}CD8^{+}$T cells from 1-mo vs. 2-wk tumors (left) or 1-mo tumors vs. 1-mon spleens (middle) or spleens at 1 mo vs. 2 wk after tumor challenge (right). Experiments were conducted twice with 2-3 pooled samples collected from ~ 30 mice/sample/experiment. Data are shown as mean values.

CD62L and CD127 expression are markedly lower on $CD44^{+}CD8^{+}$TILs from 1-month compared to those from 2-week tumors (**Figure 4-9G**), confirming the enhanced FA catabolism by late-stage $CD8^{+}$TILs is not reflective of their differentiation towards memory. The metabolic switch of TILs towards FA catabolism is facilitated by high abundance of different free FA species within the melanoma interstitial fluid (**Figure 4-9H**), enhanced uptake of FAs (**Figure 4-9I**) and increased expression of the FA oxidation (FAO) rate-limiting enzyme Cpt1a (**Figure 4-9J**) in vaccine-induced $CD8^{+}$T cells from late stage tumors.

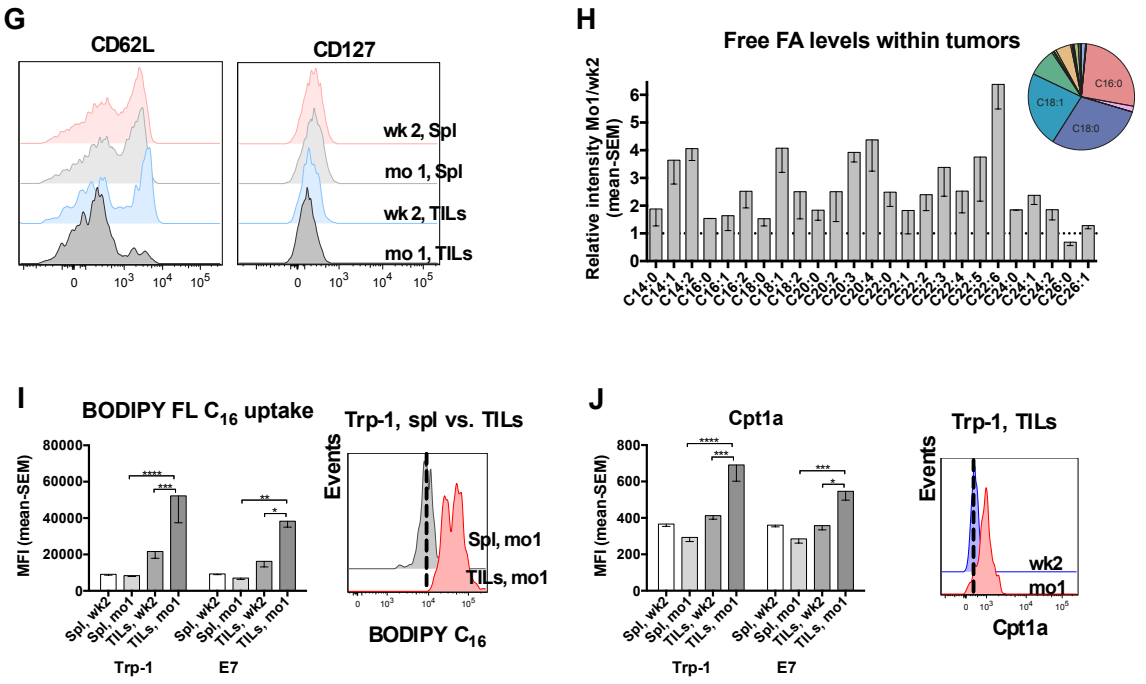

Figure 4-9. (**G**) Histograms for memory cell markers expression on $CD44^{+}CD8^{+}$T cells isolated from different tissues and at time points. (**H**) Relative intensity of free FA species in the tumor interstitial fluid shown as ratio of results obtained from 1-mo over 2-wk tumors (n=2-3 samples/group). (**I**) Uptake of BODIPY C_{16} tested directly ex vivo and representative histograms. (**J**) MFI for Cpt1a and representative histograms. (**I-J**) n=5/group.

Treatment with anti-PD-1 slows tumor progression without changing CD8$^+$ TILs' metabolism or functions

In clinical trials checkpoint inhibitors such as monoclonal antibodies (mAb) to PD-1 can delay tumor progression (54). As in my model CD8$^+$TILs increase PD-1 expression over time, I tested if treatment with anti-PD-1 mAb affects their metabolism or functions. Mice were challenged with tumor cells, vaccinated 3 days later, and starting 10 days after vaccination treated with anti-PD-1 mAb or isotype control. Within 1-month tumors, anti-PD-1 treatment reduces staining for PD-1 and enhances pAkt levels on/in vaccine-induced CD8$^+$TILs (**Figure 4-10A**) (340)without affecting their differentiation status (**Figure 4-10B**).

Figure 4-10. Metabolism and effector functions of CD8$^+$TILs are independent of PD-1.

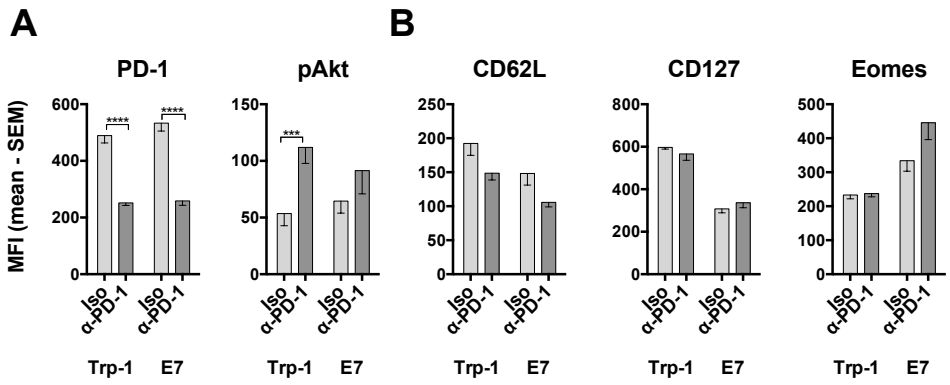

Figure 4-10. Metabolism and effector functions of CD8$^+$TILs are independent of PD-1. Vaccinated tumor-bearing mice were treated with isotype control (Iso) or anti-PD-1 antibody (α-PD-1) every 3rd day. (**A**) MFI of PD-1 and pAkt on/in specific CD8$^+$TILs at 1 mo after tumor challenge. (**B**) MFI of markers on/in specific CD8$^+$TILs from 1-mo tumors. (A,B) n=5-7 mice/group, shown as mean-SEM.

PD-1 blockade neither dramatically affects the FA or Glu catabolism of CD44$^+$CD8$^+$TILs (**Figure 4-10C-E**) nor improves effector functions of vaccine-induced CD8$^+$TILs (**Figure 4-10F**). It does effectively delay tumor progression in vaccinated as well as unvaccinated or even immune-deficient NSG mice, which lack T, B and natural killer cells (**Figure 4-10G**), suggesting that PD-1 checkpoint blockade delays tumor progression in a T cell-independent manner.

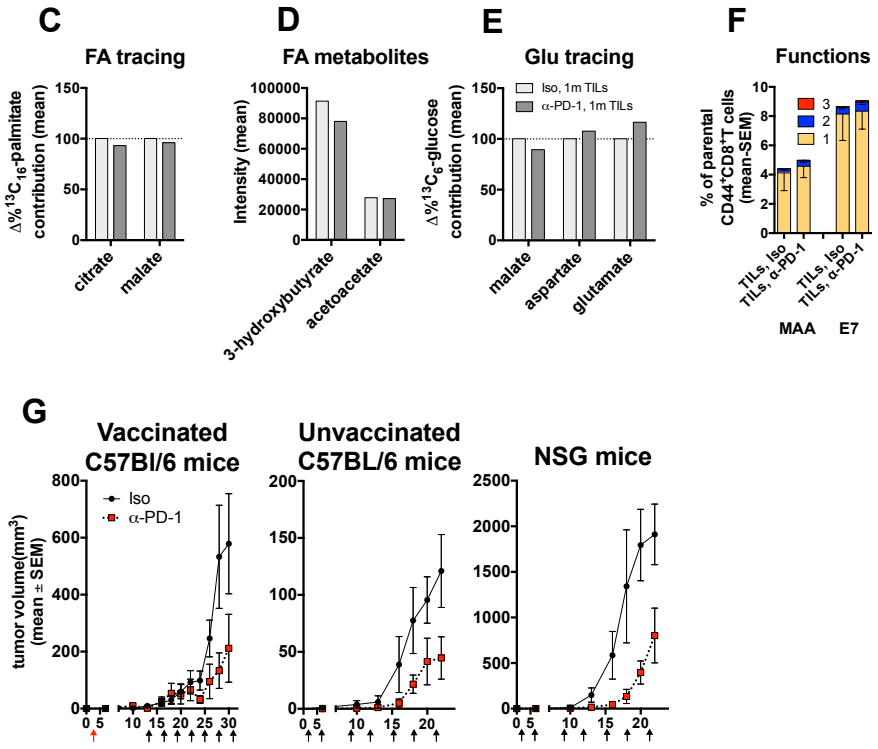

Figure 4-10. (**C**) Normalized $^{13}C_{16}$-palmitate contribution to TCA cycle metabolites in $CD44^+CD8^+$T cells from α-PD-1 treated compared to iso-treated 1-mo tumors. (**D**) Intensity of ketone bodies in $CD44^+CD8^+$T cells from 1-mo tumors. (**E**) Normalized $^{13}C_6$-Glu contribution to TCA cycle metabolites in $CD44^+CD8^+$T cells from 1-mo tumors. (**C-E**) n=2-3 samples/group, shown as mean values. Pooled from 20-30 mice/sample. (**F**) Frequencies of specific $CD8^+$TILs from 1-mo tumors of mice treated with iso or α-PD-1 producing 3, 2 or 1 factors (n=11-15 mice/group), shown as mean-SEM. (**G**) Tumor growth in mice that received iso or α-PD-1, shown as mean tumor volume +/- SEM (n=4-13mice/group). Arrows under x-axis: red (vaccine); black (antibody treatment).

Recent studies show that anti-PD-1 treatment decreases tumor progression by reducing mTOR signaling in $PD\text{-}1^+$ melanoma cells(341). As mTOR signaling increases the T cells' Glu metabolism(338), I tested whether anti-PD-1 mAbs reduce the tumor cells' Glu metabolism and thereby delay their growth. In all three models anti-PD-1 treatment increases Glu content within the tumors' interstitial fluid (**Figure 4-11A**). Cells from $B16Braf_{V600E}$ tumors of NSG mice upon anti-PD-1 treatment increase incorporation of Glu-derived carbons into metabolites of the TCA cycle or the purine synthesis pathway, indicating that PD-1 blockade actually increases their use of Glu for both catabolic and anabolic reactions (**Figure 4-11B-C**). In summary, in our

model PD-1 signaling has no major effects on metabolism or functions of $CD8^+$TILs. Anti-PD-1 treatment could reduce tumor progression in a T cell independent manner.

Figure 4-11. Anti-PD-1 treatment increases Glu concentration in the tumor interstitial fluid and the tumor cells' Glu metabolism.

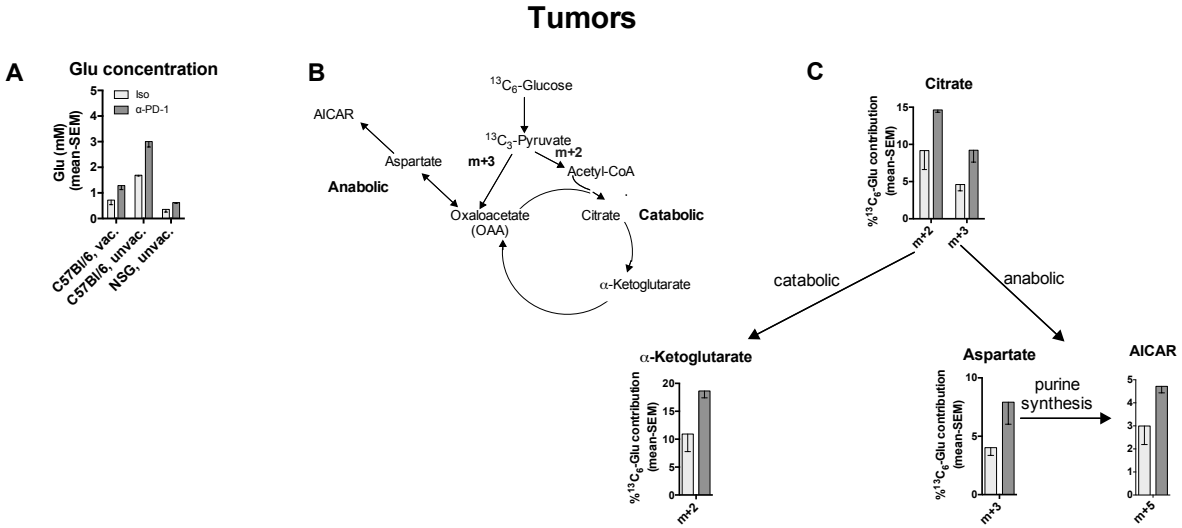

Figure 4-11. Anti-PD-1 treatment increases Glu concentration in the tumor interstitial fluid and the tumor cells' Glu metabolism. (**A**) Glu concentration in the tumor interstitial fluid from the indicated mice that had received the isotype control (Iso) or the anti-PD-1 antibody (α-PD-1). (**B**) Cartoon illustrates the $^{13}C_6$-glucose metabolism of tumor cells using catabolic pathway by contributing two ^{13}C carbons to citrate and TCA cycle intermediate a-ketoglutarate, or using anabolic pathway by contributing three ^{13}C carbons to oxaloacetate and citrate and the purine synthesis pathway intermediate AICAR. (**C**) Results for $^{13}C_6$-Glu tracing of cells isolated from day 20 tumors of NSG mice. Incorporation of 2 and 3 carbons are shown indicating the use of Glu for catabolic or anabolic downstream reactions. Data are shown as mean-SEM.

Enhanced reliance on FA catabolism is essential to maintain functions of $CD8^+$T cells

To further assess the impact of FA catabolism on $CD8^+$T cell differentiation, I stimulated $CD8^+$T cells in presence of fenofibrate (FF), an agonist of PPARα that increases FA catabolism, or etomoxir (Eto), an irreversible inhibitor of Cpt1 that decreases mitochondrial FAO (**Figure 4-12A**). *In vitro* FF-treated cells stimulated in Glu or Gal medium compared to diluent-treated cells increase FAO as shown by their enhanced transcripts of factors involved in FA catabolism (**Figure 4-12B**) and increased FA uptake (**Figure 4-12C**). $CD8^+$T cells stimulated in either Glu or Gal medium decrease OCR in presence of Eto (**Figure 4-12D**), confirming the drug's inhibitory effect on FAO. OCR declines more in cells cultured with Gal and Eto, and further

decreases when cells are also subjected to hypoxia, again confirming the cells' increased reliance on FAO when Glu and O_2 are limited.

Figure 4-12: Increased FA catabolism enhances PD-1 expression and effector functions of metabolically stressed CD8$^+$TILs *in vitro*.

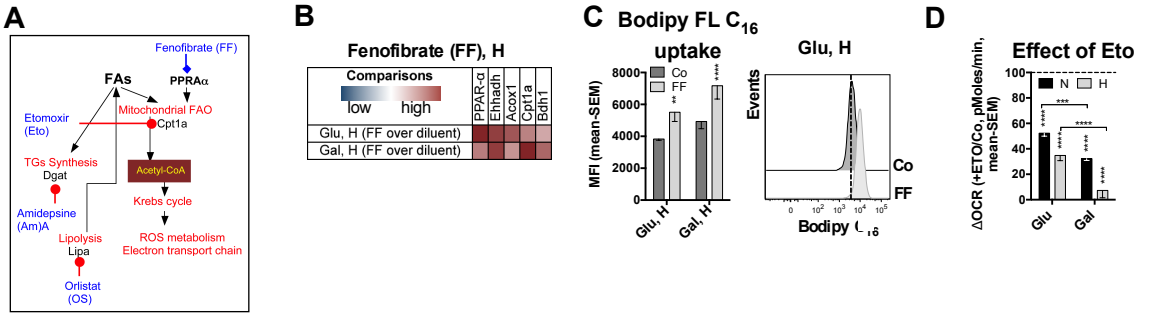

Figure 4-12: Increased FA catabolism enhances PD-1 expression and effector functions of metabolically stressed CD8$^+$TILs *in vitro*. (**A**) Drugs targeting different pathways of FA catabolism. Red lines: inhibition; blue: agonist activity. (**B**) Heatmap shows transcripts levels of enzymes involved in FA metabolism in CD8$^+$T cells stimulated in vitro in Glu or Gal medium with short-term hypoxia (H) comparing samples treated with FF to those treated with diluent (n=5 samples/condition, representative of 2 experiments, n=20 mice were pooled for each experiment). (**C**) Bodipy C_{16} uptake by CD8$^+$T cells stimulated in vitro in Glu or Gal and subjected to short-term hypoxia with the addition of FF (light grey) compared to those of cells cultured under same condition with the addition of diluent (dark grey). * above bars indicates significant differences between cells treated with FF and diluent; histograms on the right show representative samples (n=5 samples/condition, representative of 2 experiments, n=20 mice were pooled for each experiment). (**D**) Relative basal OCR of CD8$^+$T cells cultured with Eto in Glu or Gal medium under normoxia (N) or hypoxia (H) normalized to cells cultured with diluent under same condition. * above each bar indicate significant differences between Eto-and diluent-treated cells. Lines with stars above show differences between the connected samples (n=3 samples/condition with 3 repeated measures/sample, representative of 2 experiments, n=20 mice were pooled for each experiment).

Under hypoxia PD-1 increases with addition of FF but decreases in presence of Eto (**Figure 4-12E**). FF increases while Eto decreases functions and polyfunctionality of CD8$^+$T cell cultured with limited access to Glu and O_2 (**Figure 4-12F**). These results show that enhanced FA catabolism promotes effector functions of metabolically stressed CD8$^+$T cells, although it increases PD-1 expression.

As shown in **Figure 4-8A** T cells experiencing metabolic stress *in vitro* and TILs from late-stage tumors increase transcripts of enzymes participating in TG turnover. To assess if CD8$^+$T cells under metabolically challenging conditions mobilize TGs to fuel FAO and OXPHOS, I added Orlistat (OS), an inhibitor of the lipolysis enzyme lipa, or Amidepsine A (AmA), an inhibitor of the TG synthesis enzymes Dgat1 and Dgat2, to CD8$^+$T cells stimulated under different

conditions (**Figure 4-12A**). Basal OCR decreases in CD8$^+$T cells cultured with either drug in Glu (**Figure 4-12G**) or Gal medium (**data not shown**) under short-term hypoxia, suggesting that TG turnover provides fuels for OXPHOS. Under hypoxia PD-1 decreases with addition of OS regardless of other culture conditions and with addition of AmA to Gal medium (**Figure 4-12E**). AmA and to a lesser degree OS decrease functions of T cells cultured in Gal medium and subjected to hypoxia (**Figure 4-12F**). These data indicate that activated CD8$^+$T cells under hypoxia use substrates from TG turnover for OXPHOS, as OCR decreases in presence of AmA or OS. However TGs are not essential for effector functions of activated CD8$^+$T cells unless cells are concomitantly subjected to hypoglycemia.

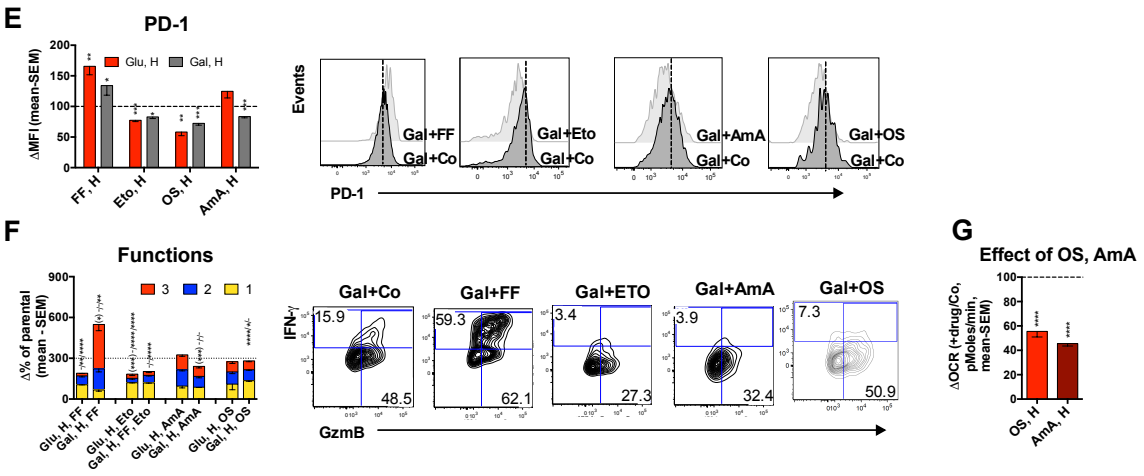

Figure 4-12. (**E**) Left: Effect of FA metabolism manipulating drugs on PD-1 expression of CD8$^+$T cells stimulated in Glu (red) or Gal (dark grey) medium and subjected to hypoxia (n=5 samples/group, representative of at least 3 experiments, n=20 mice were pooled for each experiment). Data are shown as MFI values (mean with SEM) with drug treatment normalized to those of cells treated with the vehicle control (set at 100, dashed line) * on top of bars indicates significant differences between cells treated with drug and vehicle. Right: Histograms of PD-1 expression on representative samples. (**F**) Normalized % of cells producing 3, 2 or 1 factors. Functions of cells treated with each drug are normalized to those of cells treated with diluent (set at 300, dashed line; n=5 samples/group, representative of 3 experiments, n=20 mice were pooled for each experiment). * within (): significant difference of total responses between cells treated with drug and vehicle. * outside of (): significant differences in % of 1,2 and 3 (bottom to top) factor-producing cells between samples treated with drug and those treated with diluent. Representative flow plots show levels of IFN-g and granzyme B production. (**G**) Relative basal OCR of CD8$^+$T cells cultured with OS or AmA normalized to cells cultured with diluent in Glu medium under hypoxia (n=6 samples/condition, representative of 2 experiments, n=20 mice were pooled for each experiment). * above each bar indicate significant differences between drug- and diluent-treated cells.

To assess how increased FA catabolism affects CD8$^+$TIL functions, I vaccinated CD90.2$^+$ mice congenic for CD45, and treated them for 3 weeks daily with FF (CD45.1 mice) or diluent (CD45.2 mice). Splenocytes from these mice were mixed at a 1:1 ratio of Trp-1-specific

$CD8^+$T cells from the 2 donors and transferred into $CD90.1^+$ recipient mice, which had been challenged with tumor cells and vaccinated 3 days later. Cells were transferred 2 days after vaccination (**Figure 4-13A**).

Figure 4-13. Promoting FA catabolism improves $CD8^+$TIL functions without reducing PD-1 expression.

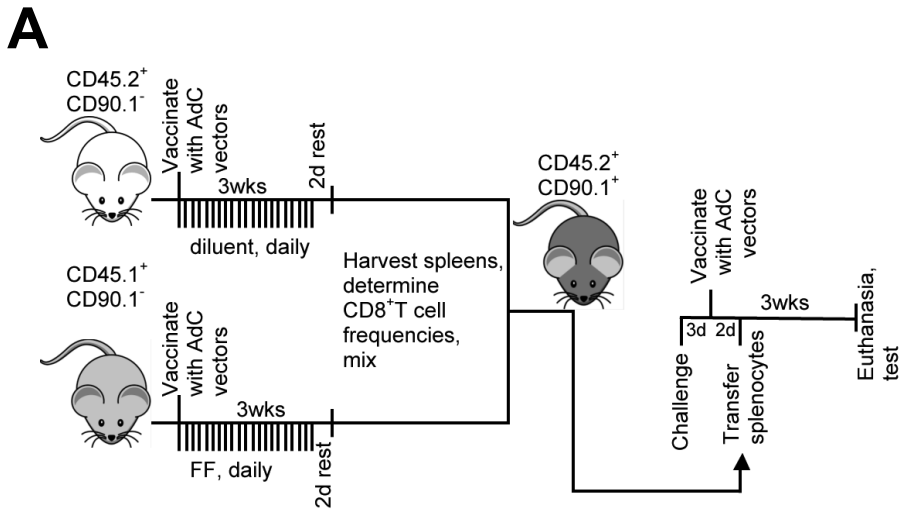

Figure 4-13. Promoting FA catabolism improves $CD8^+$TIL functions without reducing PD-1 expression. (**A**) Experimental setup of the in vivo study.

Immediately before transfer FF- and diluent- treated Trp-1- and E7-specific $CD8^+$T cells from donor mice show comparable expression of CD62L, CD127, KLRG1 and FoxO1, indicating that FF does not affect memory formation (**Figure 4-13B**). FF-treated cells show increased expression of PD-1 and T-bet, suggestive of a higher activation status. FF treatment does not significantly enhance frequencies or functions of vaccine-induced $CD8^+$T cells (**Figure 4-13C**). FF-treated splenocytes before transfer show enhanced OCR, which is blocked by Eto indicating that FF conditions vaccine-induced $CD8^+$T cells to enhance FAO (**Figure 4-13D**).

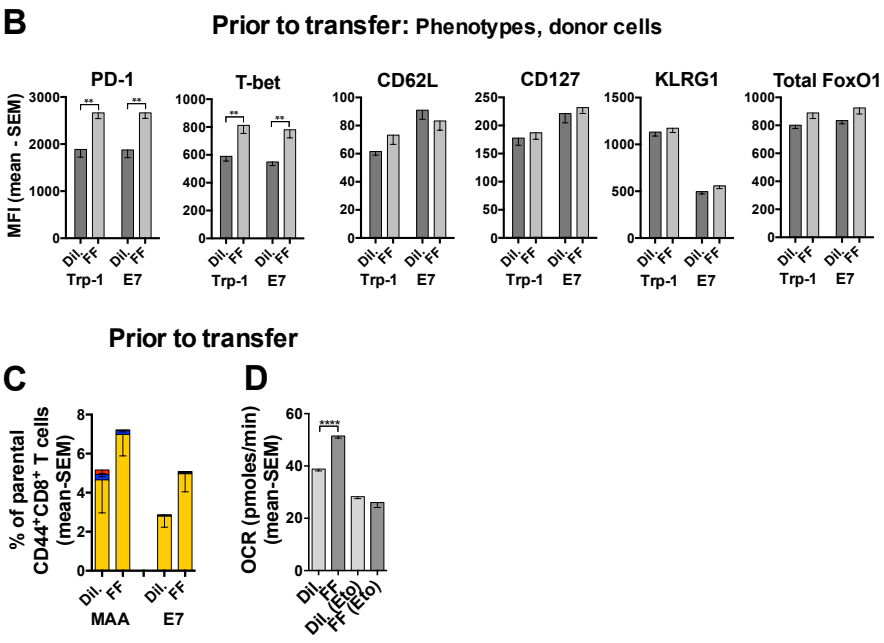

Figure 4-13. (**B**) MFI of markers on/in donor CD8$^+$T cells from mice treated with diluent (Dil.) or FF before transfer. (**C**) Functions of CD8$^+$T cells from spleens of donor mice treated with Dil. or FF before transfer as % of cells producing 3, 2 and 1 factors (B-C, n=8-10/group). (**D**) Basal OCR of CD8$^+$T cells from spleens of donor mice fed with Dil. or FF. Some samples were incubated with Eto (n=5-6 mice/group).

Donor-derived vaccine-induced CD8$^+$TILs were analyzed 3 weeks after transfer (**Figure 4-13E**). Compared to diluent-treated TILs of donor origin, FF-treated donor-derived CD44$^+$CD8$^+$TILs show enhanced levels of transcripts for factors involved in FA catabolism (**Figure 4-13F**). Both Trp-1- and E7-specific FF donor-derived CD8$^+$TILs show a trend towards increased PD-1 expression (**Figure 4-13G**). Frequencies and functions of FF-treated, vaccine-induced CD8$^+$TILs of donor origin are significantly higher compared to those of controls (**Figure 4-13H**). Upon transfer of splenocytes from FF- or diluent-treated mice into separate cohorts of tumor-bearing mice, the former significantly delays tumor growth (**Figure 4-13I**). Collectively these data confirm that enhanced FA catabolism improves antitumor functions of CD8$^+$TILs.

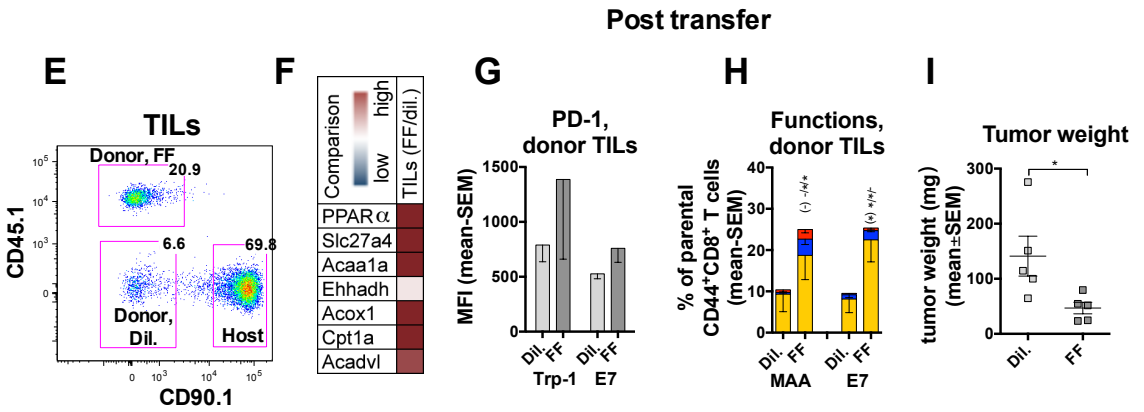

Figure 4-13. (**E**) Flow plots of donor and host CD8$^+$T cells isolated from tumors of recipient mice. (**F**) Transcript levels in CD8$^+$TILs derived from FF-treated compared to those from Dil.-treated donors (n=3-4 samples/group). (**G**) MFI of PD-1 on Dil.- or FF-treated donor CD8$^+$TILs (n=6/group). (**H**) % specific CD8$^+$TILs from Dil.- or FF-treated donors producing 3, 2, or 1 factors. (-) or (*) on top of each bar indicates significant differences in sum of the responses. * from bottom to top: differences in producing 1, 2 or 3 factors. (I) Tumor weight 2 wk after cell transfer (n=5/group).

To test if FF-induced PD-1 increases affect FF-treated CD8$^+$TIL functions, I fed vaccinated donor mice with FF or diluent daily for three weeks and then upon transfer into separate tumor-bearing mice treated the recipients with anti-PD-1 or isotype control antibodies (**Figure 4-13J**). Both FF treatment of donors and anti-PD-1 treatment of recipients strongly delay tumor progression (**Figure 4-13K**). Moreover, they act synergistically and together completely prevent tumor outgrowth in more than 30% of the vaccinated mice (**Figure 4-13K** and not shown).

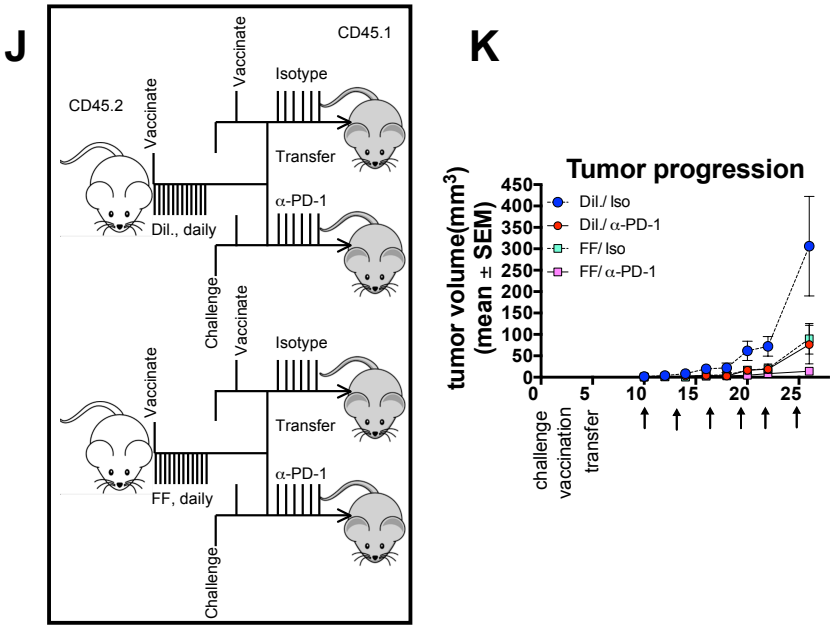

Figure 4-13. (**J**) Experimental design of PD-1 blockade combined with transfer of FF- or Dil.-treated T cells. (**K**) Tumor progression in mice that received either FF- or Dil.-treated cells and either iso or α-PD-1 treatment after cell transfer. n=6-7/group.

Anti-PD-1 treatment reduces PD-1 staining on donor cells and this is not affected by FF (**Figure 4-13L**). It only has subtle effects on frequencies and functions of MAA-specific CD8$^+$TILs derived from either set of donor mice (**Figure 4-13M**). PD-1 blockade significantly increases frequencies of monofunctional E7-specific CD8$^+$TILs derived from FF treated donors. This effect may partially reflect the smaller tumor sizes of a-PD-1 treated mice, which might rescue the bystander T cell functions more easily than those of MAA-specific CD8$^+$TILs.

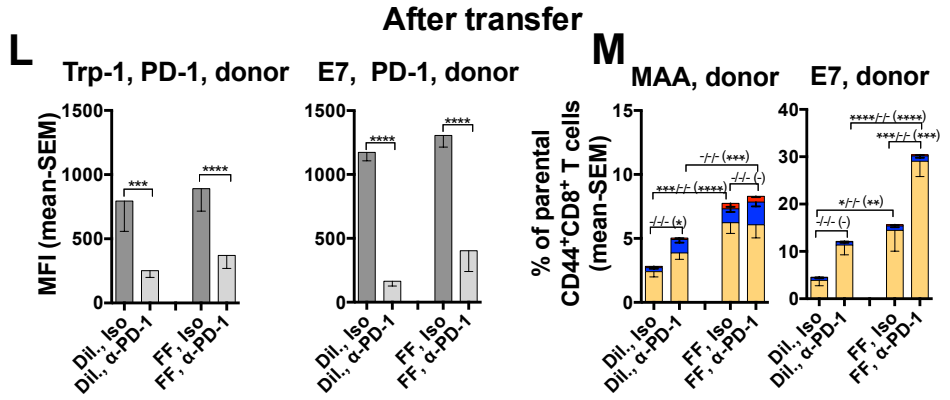

Figure 4-13. (**L**) PD-1 expression on donor-derived FF- or Dil.-treated CD8$^+$TILs recovered from recipients treated with iso or a-PD-1. (**M**) Functions of donor-derived CD8$^+$TILs from mice that received different treatments. * from left to right: differences in producing 1, 2 or 3 factors. (L-M), n=6-7/group. Data are shown as mean with SEM.

Inhibiting FA catabolism by knocking out PPAR-α decreases PD-1 expression and CD8$^+$T cell functions under metabolically stressed condition

To further study whether FA catabolism maintains functions of metabolically stressed CD8$^+$T cells, I stimulated CD8$^+$T cells from PPARα KO mice *in vitro* and compared them to those from wildtype (wt) mice. Transcripts for most factors involved in the TCA cycle and lipid catabolism are higher in PPARα KO compared to wt CD8$^+$T cells when stimulated in Glu medium and under hypoxia; this profile reverses in cells cultured in Gal medium and low O_2, suggesting that knocking out PPARα significantly decreases lipid catabolism of CD8$^+$T cells cultured without Glu (**Figure 4-14A**). PPARα KO compared to wt CD8$^+$T cells express lower levels of PD-1 when cultured with Gal-medium regardless of O_2 levels (**Figure 4-14B**). PPARα KO CD8$^+$T cell functions are lower compared to those of wt CD8$^+$T cells cultured under the same conditions

(**Figure 4-14C**), suggesting that FA catabolism is required to maintain effector functions of CD8$^+$T with limited access to Glu.

Figure 4-14. Activated PPAR-α KO CD8$^+$T cells with reduced FA catabolism decreased PD-1 expression and effector functions under metabolically challenging conditions *in vitro*.

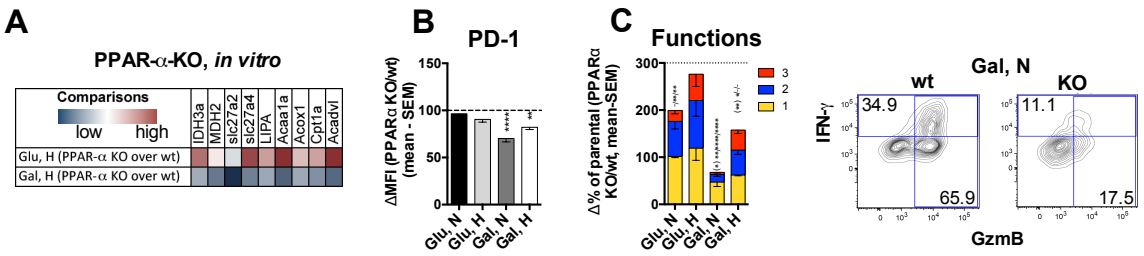

Figure 4-14: Activated PPAR-a KO CD8$^+$T cells with reduced FA catabolism decreased PD-1 expression and effector functions under metabolically challenging conditions *in vitro*. (A) Heatmap compares mRNA transcripts of enzymes involved in FA metabolism in CD8$^+$T cells from PPAR-a KO mice to those from wt mice stimulated in vitro in Glu or Gal medium and subjected to hypoxia. (**B, C**) Data are normalized to results obtained with wt cells cultured under the same conditions and set at 100 (for h) or 300 (for i) (dashed line). (**B**) Normalized MFI values of PD-1 expression on PPAR-a KO CD8$^+$T cells cultured under different conditions. * Indicates significant difference between wt and PPAR-a KO CD8$^+$T cells. (**C**) Normalized % of PPAR-a KO CD8$^+$T cells cells producing 3, 2 and 1 factors. * Indicates significant difference between wt and PPAR-a KO CD8$^+$T cells. Statistics on top of each bar follow the same rule described in Figure **4-4G**. Flow plots show factor-producing wt vs. PPAR-a KO CD8$^+$T cells cultured in Gal medium under hypoxia. (**A-C**) n=5 samples/condition, representative of 2 experiments. n=6 wt or PPARa KO mice were pooled for each experiment. *p<=0.05, **p<=0.01, *** p<=0.001, **** p<=0.0001.

To further explore the effect of FA catabolism on vaccine-induced TILs, I used an adoptive transfer system, in which splenocytes from PPARα KO and wt CD45 congenic mice were co-transferred 3 weeks after vaccination into tumor-bearing and vaccinated recipient mice (**Figure 4-15A**).

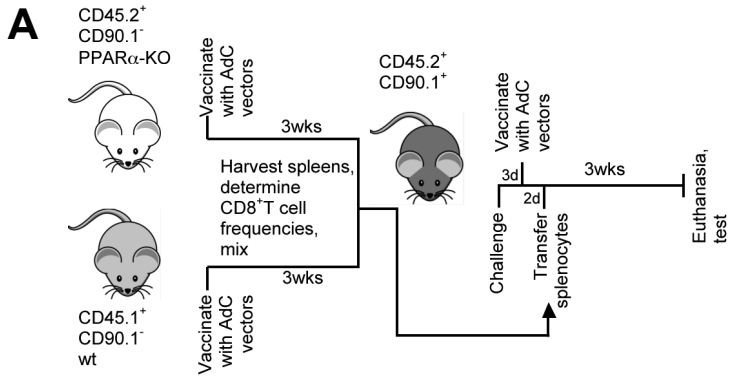

Figure 4-15: Decreasing FA catabolism reduces PD-1 expression and effector functions of metabolically stressed CD8$^+$TILs. (**A**) Cartoon show experimental setup for studying the impact of knocking out PPAR-α on the performance of vaccine-induced CD8$^+$TILs within TME.

Prior to transfer, functions and polyfunctionality of Trp-1-specific CD8$^+$T cells are similar between the two groups, while E7-specfic CD8$^+$T cells are less abundant and polyfunctional in PPARα KO mice (**Figure 4-15B**). This may reflect that strength of TcR signaling, which is lower for the E7 epitope, affects to what degree and at what time after activation cells rely on FAO. Expression of CD127 is comparable between the two T cell subsets immediately before transfer, indicating no major differences in memory formation (**Figure 4-15C**).

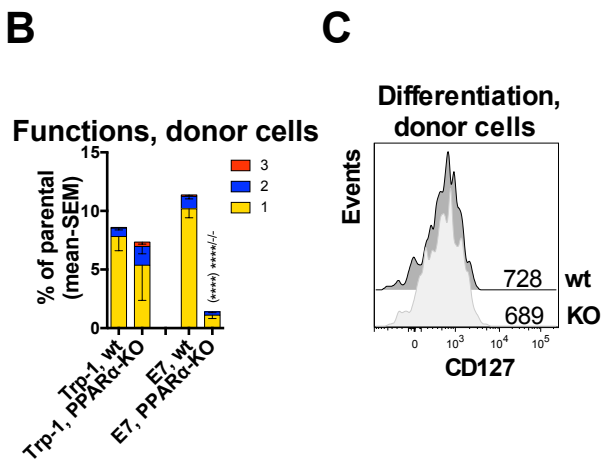

Figure 4-15. (**B**) Functions of Trp-1- and E7-specific CD8$^+$ T cells from spleens of wt and PPAR-a KO mice as % of cells producing 3, 2 and 1 factors right before transfer (n=7 mice/group). (**C**) Histogram shows CD127 expression on donor Trp-1-specific CD8$^+$T cells from spleens before transfer.

CD44$^+$CD8$^+$TILs originated from PPARα KO donors as compared to those from wt donors collected from recipient mice 3 weeks after transfer show a transcriptional profile similar to that of PPARα KO vs. wt CD8$^+$T cells cultured *in vitro* in Gal medium under hypoxia (**Figure 4-15A**), indicating reduced FA catabolism by PPARα KO CD8$^+$TILs (**Figure 4-15D**). Both Trp-1-and E7-specifc PPARα KO CD8$^+$TILs show lower levels of PD-1 expression (**Figure 4-15E**) concomitant with decreases in frequencies and functions including polyfunctionality (**Figure 4-15F**). Collectively these data confirm that FA catabolism promotes PD-1 expression but preserves CD8$^+$T cell effector functions upon metabolic stress.

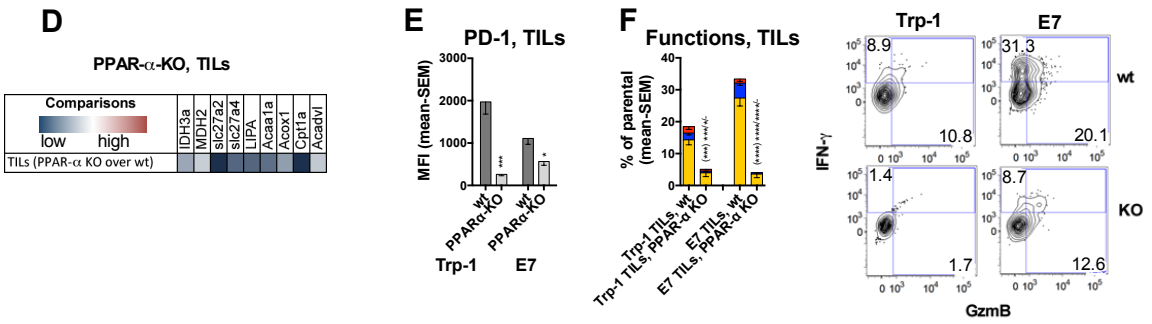

Figure 4-15. (**D**) Heatmap compares transcripts of FA catabolism enzymes in CD44^{+} CD8^{+}TILs derived from PPAR-a KO and wt donor mice (n=5 mice/group). (**E**) MFI of PD-1 expression on wt and PPAR-a KO donor Trp-1-and E7-specific CD8^{+}TILs. (**F**) % of Trp-1- and E7-specific CD8^{+}TILs from the two groups of donor mice producing 3, 2 and 1 factors. (**E, F**) n=6 mice/group. * within (): difference in sum of responses.* outside of (): differences in each proportion of cells between wt and PPAR-a KO donor derived TILs with 1-3 functions (bottom to top). Flow plots illustrate functions of donor-derived Trp-1-and E7-specific CD8^{+}TILs from each group. Data are representative of 2 experiments.

DISCUSSION

Within the TME CD8^{+}T cells experience hypoxia and have to compete for nutrients especially Glu, which tumor cells consume to fuel glycolysis. Cells can compensate for lack of Glu by switching from glycolysis to OXPHOS using alternative nutrients such as FAs. Recent studies report that hypoglycemia within the TME impairs CD8^{+}T cells functions and reduces the efficacy of active immunotherapy (192,197). My results show that metabolic challenges within the TME impair the performance of CD8^{+}TILs including bystander TILs, although TA-specific CD8^{+}TILs tend to be more affected presumably for they continue to receive stimulatory signals and may penetrate more deeply into tumors where nutrients and O_2 are especially limiting.

Solid tumors develop areas of hypoxia, which activates the HIF-1α pathway in cells of the TME. HIF-1a expression also rises upon T cell activation (342). In my study HIF-1α increases in both MAA-specific and bystander CD8^{+}TILs, pointing towards hypoxia as the underlying cause. The effect of hypoxia on CD8^{+}T cells is controversial. Some studies show that O_2 is required for T cell effector functions (343). Others using protocols in which CD8^{+} T cells were subjected to hypoxia during a resting period report that hypoxia increases functions (342,344). My data agree with the former as they show reduced HIF-1α signaling improves CD8^{+}TIL frequencies and

functions, indicating that when Glu is limiting, promoting glycolysis and inhibiting OXPHOS by HIF-1α becomes detrimental to $CD8^+$TILs. LAG-3, which according to our data is regulated by HIF-1α, inhibits T cell expansion and effector functions (345). The LAG-3 locus has several HIF-1α response elements ([A/G]CGTA) (346), which may influence LAG-3 expression under hypoxia.

Hypoxia and hypoglycemia send opposing metabolic signals. The former promotes glycolysis while the latter forces cells to use OXPHOS, which can be fueled by various nutrients but requires O_2. Cancer cells increase *de novo* lipogenesis (347) and recruit adipose progenitor cells (210). Accordingly in my model the abundance of free FA species increases during tumor progression. My data show that $CD8^+$TILs cope with lack of Glu and O_2 by augmenting FA uptake and FA catabolism to gain energy through OXPHOS. However, even with this metabolic switch $CD8^+$TILs show loss of functions, which can be improved by further promoting lipid metabolism by FF.

High expression of PD-1 is viewed to signal $CD8^+$T cell exhaustion and loss of effector functions. My results suggest that high PD-1 expression is not inevitably linked to impaired T cell functions. When activated $CD8^+$T cells are exposed to hypoxia, decreased PD-1 expression is associated with impaired functions. In contrast, FF-treated $CD8^+$T cells show a trend towards increased PD-1 expressions but their functions improve. PD-1 signaling inhibits TCR- and CD28-mediated activation of the PI3K/Akt/mTOR pathway, which in turn decreases glycolysis(267) and promotes lipolysis and FAO (348). I speculate that enhanced PD-1 signaling in $CD8^+$TILs is beneficial by facilitating their metabolic switch within a Glu-poor TME. In my model blockade of PD-1 after the initial phase of T cell activation affects neither effector functions nor metabolism of TILs although overall Glu concentrations within the tumors increase. These results differ from those of a recent study in a mouse sarcoma model, which reports improved glycolysis and IFN-γ production by $CD8^+$TILs treated with anti-PD-1 during their initial activation (192). I assume that these apparently opposing results reflect intrinsic differences in tumor models or in T cells induced by vaccination or through stimulation by tumor-derived antigens. Alternatively,

differences in timing of treatment may affect the result. PD-1 blockade during the initial stages of T cell activation may allow them to better compete for Glu within a TME; once TILs have switched to FA catabolism they remain committed to this pathway regardless of PD-1 signaling.

Anti-PD-1 treatment delays tumor progression in our model. Some of my data suggest that anti-PD-1 may promote MAA-specific $CD8^+$T cell infiltration into tumors (not shown). However, as anti-PD-1 treatment also delays tumor progression in immune-deficient mice, I assume that it acts directly on tumor cells, tumor stromal cells or immunosuppressive cells within the TME. A recent study suggests that anti-PD-1 may reduce proliferation of $PD\text{-}1^+$ tumor cells by blocking mTOR signaling (341). This mode of action of PD-1 blockade will only affect $PD\text{-}1^+$ tumor cells. As in my study the melanoma cells isolated from tumors grown *in vivo* express very low levels of PD-1 (data not shown); I view it as unlikely that they are directly affected by PD-1 blockade. Immunosuppressive cells express high levels of PD-1 (not shown) and PD-1 blockade may impair their ability to promote tumorigenesis (309). Melanoma cells express PD-L1 (not shown) and back-signaling through this ligand increases the tumor cells' resistance to Fas- or $CD8^+$T cell-mediated apoptosis (349). Anti-PD-1 treatment could thus promote tumor cell death by enhancing their susceptibility to apoptosis or, in immunocompetent mice, indirectly improve TIL functions by increasing the tumor cells' susceptibility to lytic enzymes. Either mechanism could delay tumor growth and thus enhance levels of Glu within the TME. Although the additional Glu could fuel proliferation of tumor cells this would be counterbalanced by their increased death rates.

Energy production through FAO rather than glycolysis comes at a price; more O_2 is needed to generate equivalent amounts of ATP and ROS production increases. Generating energy through FAO within a hypoxic TME may thus not be the only method by which $CD8^+$TILs maintain their functions. Ketone bodies are highly efficient fuels that require less O_2 (350) and previous studies showed that they serve as the preferred energy source for cells of the nervous system subjected to hypoxia and hypoglycemia (215). Ketone bodies could be synthesized and secreted by other cells (351), or they could be produced by TILs directly as suggested by

increased transcript levels of Bdh1, a key enzyme in ketone body metabolism. My data show that $CD8^+$TILs show pronounced increases in the intensities of ketone bodies acetoacetate and 3-hydroxybutyrate during tumor progression. I would also like to point out that levels of O_2 differ within a tumor and that TILs can randomly migrate within the TME (218). TILs could use FAO and ketone bodies alternatively depending on surrounding O_2 levels to maintain their effector functions and prolong their survival.

As suggested by my results, metabolic reprogramming of $CD8^+$T cells to increase energy production through FA catabolism prior to adoptive cell transfer might enhance the overall efficacy of cell therapy in patients with some types of cancers, especially those characterized by low Glu content like melanomas. In agreement, other studies show that memory $CD8^+$T cells, which prefer FAO and OXPHOS for energy production, are better at slowing tumor progression than effector cells (205,208). In contrast, others report that increasing the TILs' ability to use glycolysis improves their antitumor effect (192). Which metabolic manipulations are most suited to improve TIL-mediated tumor regression will likely depend on the nature of the tumor. Those with sufficient levels of Glu may benefit from $CD8^+$T cells with high glycolytic potential, while tumors with a hypoglycemic TME may best be combated by $CD8^+$T cells that favor FA catabolism.

In summary, my results show that metabolic challenges within the TME have profound impacts on $CD8^+$TILs. It forces $CD8^+$TILs to increasingly gain energy through FA catabolism, including consumption of ketone bodies, which partially preserves their functions and may improve their survival. Promoting the $CD8^+$ TILs' propensity to use FAO combined with PD-1 signaling blockade further improves treatment outcome. These results invite further investigations to assess if the outcome of cancer immunotherapy can be improved by adding metabolic manipulations to current treatment strategies.

MATERIALS AND METHODS

Mice and animal experiments

Female C57Bl/6, B6.SJL-Ptprc^{a}Pepc^{b}/BoyJ (B6 CD45.1^{+}), B6.PL-*Thy*1^{a}/CyJ (B6 CD90.1^{+}) and B6. 129S4-*Ppara*^{tm1Gonz}/J (B6 PPAR-α KO) mice (6-8 weeks) were purchased from the National Cancer Institute (NCI) or the Jackson Laboratories and housed at the Wistar Institute Animal Facility. Procedures were conducted following approved protocols by the Wistar Institutional animal care and use committee (IACUC). Groups of 5-80 C57BL/6 mice were vaccinated intramuscularly (i.m.) with AdC68 vectors (10^{10} virus particles [vp] for AdC68-gDMelapoly; 10^{11} vp for AdC68-gDE7) diluted in PBS. B16Braf$_{V600E}$ cells ($5x10^{4}$ cells/mouse) diluted in PBS were inoculated subcutaneously (s.c.) into the right flank of mice. Tumor growth was monitored by measuring the perpendicular diameters of tumors every two days. Tumor volume was calculated using the formula: tumor volume = ((tumor width)^2 x tumor length)/2. Depending on size early stage tumors were harvested 10-14 days after challenge (referred to as 2 weeks) while late stage tumors were harvested 4-5 weeks after challenge (referred to as 1 month). For PD-1 blockade antibody treatment, mice received either 0.2mg rat anti-PD-1 antibody (29F. 1A12, most kindly provided by Dr. G. Freeman, Dana Farber Cancer Center, Boston, MA) or isotype control antibody (rat IgG2a, BioXcell) via intraperitoneal injection (i.p.) every two days, starting 10 days after vaccination. Tumor growth was measured every other day. For *in vivo* treatment FF (100mg/kg/day, Sigma) was first diluted in DMSO and then further diluted in PBS and given by oral gavage daily for 3 weeks. Control mice received diluent at the same volume. For adoptive transfer experiments, $1x10^{7}$ *in vitro* activated CD8^{+}T cells transduced with lentivectors were injected intravenously (i.v.) into recipient mice. For FF/control treated splenocytes or wild type/PPAR-α KO splenocytes co-transfer experiments, splenocytes containing 10^{5} Trp-1$_{455}$ tetramer^{+}CD8^{+}T cells from each group were mixed and transferred into CD90.1^{+} recipient mice through tail vein i.v. injection.

Cell lines

The B16Braf$_{V600E}$ cell line (kindly provided by Dr. M Herlyn, Wistar Institute, Philadelphia, PA) was derived from B16.F10 cells by transduction with the lentivector pLU-EF1a-mCherry expressing mouse Braf$_{V600E}$. HEK 293 cells were used to propagate vaccine vectors. 293T cells were used to produce lentivectors. Cells were grown in Dulbecco's Modified Eagles medium (DMEM) supplemented with 10% fetal bovine serum (FBS). Both HEK293 cells and 293T cells were obtained from ADCC. All cell lines were authenticated by morphology, biological characteristics and growth kinetics *in vitro*. The B16Braf$_{V600E}$ cell line was further authenticated by its tumor-forming kinetics in C57BL/6 mice. All cell lines were tested mycoplasma-free. For each experiment cells were used within 4 weeks after resuscitation.

Construction of recombinant adenovirus and lentivectors

Molecular construction, rescue, purification and titration of AdC68-gDMelapoly and AdC68-gDE7 vectors have been described(308). Briefly, gDMelapoly or gDE7 construct was inserted into E1-deleted AdC68 viral molecular clone using I-CeuI and PI-SceI sites. The constructed plasmids were used to transfect 293 cells by calcium phosphate (Invitrogen). Cells containing adenoviral vectors were harvest 7-10 days later upon plague formation. Virus was further propagated on 293 cells by serial infection and harvested by three cycles of freeze-thawing. Cell-free supernatant from the third cycle of thawing was used for virus purification by Caesium chloride density ultracentrifugation. For production of lentivectors, five pLKO.1 lentivectors containing short hairpin RNAs (shRNAs) targeting different regions of HIF-1α or lentivector expressing control RNA were obtained from The RNAi Consortium. The selection marker Thy1.1 was cloned from the pLKO.3-Thy1.1 lentivector (Addgene plasmid#14749) into each of the shRNA lentivectors. Lentivectors were generated using the 2nd generation lentivector package system (Addgene) by transfecting 293T cells with the packaging plasmid PsPAX2, the envelope plasmid PMD2.G and each of the shRNA-Thy1.1-expressing insert plasmids at a ratio of 3:1:1. Supernatants were collected 48 and 72 hours post transfection. Lentivectors were concentrated by ultracentrifugation at 20,000rpm,

4°C for 2 hours. Vector pellets were incubated with PBS on ice for at least 2 hours before resuspension. The lentivector that showed the most pronounced reduction of HIF-1α transcripts in transduced cells was used for further studies.

***In vitro* stimulation of CD8$^+$T cells and drug treatments**

CD8$^+$T cells from pooled spleens of naive C57Bl/6 mice (20-30 mice/experiment) were enriched by negative selection using magnetic beads (MACS, STEMCELL Technologies). Enriched CD8$^+$T cells were activated for 4 days in 6-well plates pre-coated with antibodies to CD3 (5µg/ml) and CD28 (1µg/mL) (BD Bioscience). For some samples, cells were transferred for the last 16 hours to a hypoxia chamber. To study the impact of hypoxia on resting CD8$^+$T cells, enriched CD8$^+$T cells were stimulated for 48 hours under normoxia. Cells were then washed off the plates and replated in fresh medium with 100U/ml human IL-2 for 96 hours, followed by culture in normoxia or hypoxia with IL-2 for another 36 hours before analysis. Cells were cultured in Roswell Park Memorial Institute (RPMI) medium without Glu (Life Technologies) supplemented with Glu (10mM) or Gal (10mM), 10% dialyzed FBS (Life Technologies), 20mM HEPES, 2mM Glutamax, 1mM sodium pyruvate, 0.05mM 2-mercaptoethanol and 1% penicillin-streptomycin. Hypoxia experiments were performed in a Thermo Napco series 8000WJ CO_2 incubator equipped with nitrogen tank for O_2 replacement. O_2 level was kept at 1% during CD8$^+$T cells hypoxia culture for time periods indicated in each assay. Drugs and corresponding vehicle controls were added as follows: 2-deoxy-D-glucose (2-DG, 2mM, Sigma) or Fenofibrate (FF, 50µM, Sigma) for the entire culture period; Etomoxir (Eto, 200µM, Sigma), Amidepsine A (AmA, 20µM, Santa Cruz), or Orlistat (OS, 100µM, Sigma) for the last 48 hours. DMSO concentrations were kept below 0.2% for all culture conditions.

Lentivector transduction of CD8$^+$T cells

For *in vitro* experiments, 4x10^6 enriched CD8$^+$T cells were stimulated as described above for 24-28 hours. Freshly concentrated lentivectors were spin-inoculated into activated CD8$^+$T cells

supplemented with polybrene (6µg/ml, Santa Cruz) at 2000rpm, 32°C for 2 hours. Cells were washed 20 hours after transduction, transferred to new CD3 antibody pre-coated plates and stimulated for another 40 hours in medium supplemented with anti-CD28 and human IL-2 (100U/ml, Roche) under normoxia or switched to hypoxia. Lentivector-transduced $CD8^+$T cells were identified by surface staining for Thy1.1 and were analyzed with a BD LSRII. For *in vivo* experiments, cells were washed 20 hours after lentivector transduction and cultured for an additional 48 hours in Glu medium supplemented with human IL-2 (100U/ml).

Isolation of lymphocytes from mice

PBMCs and splenocytes were harvested as described (Zhang & Ertl, 2014). Briefly, blood samples were collected by retro-orbital puncture and PBMCs were isolated by Histopaque (Sigma) gradient. Spleens were harvested and single cell suspension was generated by mincing with mesh screen in Leibovitz's L15 medium and passing through 70µm filter (Fisher Scientific). For both samples red blood cells were lysed by 1x RBC lysis buffer (eBioscience). To obtain tumor-infiltrating lymphocytes, tumors were harvested, cut into small fragments and treated with 2mg/ml collagenase P, 1mg/ml DNase I (all from Roche) and 2% FBS (Tissue Culture Biologicals) in Hank's balanced salt solution (HBSS,1X, Thermo Fisher Scientific) under agitation for 1 hour. Tumor fragments were homogenized, filtrated through 70µm strainers and lymphocytes were purified by Percoll-gradient centrifugation and washed with DMEM supplemented with 10% FBS. Pre-experiments were conducted to ensure that this treatment did not affect any of the markers that were tested.

Antibodies, staining and flow cytometry

Cells were stained with a PE-labeled Trp-1-specific MHC class I ($H\text{-}2D^b$) tetramer carrying the TAPDNLGYM peptide and an Alexa647-labeled HPV-16 E7-specific MHC class I ($H\text{-}2D^b$) tetramer carrying the RAHYNIVTTF peptide (obtained from the NIAID Tetramer Facility). Lymphocytes were stained with anti-CD8-PerCPCy5.5 (Cat. #100734) or -Alexa700 (Cat.

#126618), CD4-PercpCy5.5 (Cat. #100434), CD44-PacBlue (Cat. #103020), LAG-3-APC (Cat. #125210) or -PercpCy5.5 (Cat. #125212), KLRGI-FITC (Cat. #138410), PD-1-PE/Cy7 (Cat. #329918) or -Brilliant violet (BV) 605 (Cat. #135220) (all from Biolegend), 2B4-FITC (eBio244F4, eBioscience) and Amcyan fluorescent reactive dye (Cat. #L34957, Life Technologies). For mitochondrial metabolic markers analysis, cells were stained with Mitosox Red (Cat. #M36008, 5μM, MROS) and DioC6 (Cat. #D-273, 40nM, MMP, Life Technologies) at 37°C for 30 minutes. For fatty acid uptake experiments, cells stimulated under different conditions *in vitro* or isolated from spleen and tumors of mice bearing 2 weeks or 1 month-old tumors were immediately incubated with 1μM BODIPY FL C_{16} (Cat. #D-3821, Life Technologies) for 30 mins at 37°C. Cells were washed twice with cold PBS before surface staining. For Cpt1a staining, cells were stained for surface markers followed by permeabilization with transcription factor buffer set (BD pharmingen, San Diego, CA). Cells were then stained with anti-Cpt1a antibody-Alexa488 (Cat. #ab171449) or mouse IgG2b isotype control antibody-Alexa488 (Cat. #ab171465, both from abcam) at 5μg/ml in 1x permwash for 45 mins at 4°C. For staining of T-bet, cells were first stained for surface markers, then fixed and permeabilized with Foxp3/Transcription factor staining buffer and stained with T-bet-PE/Cy7 (eBio4B10, all from eBioscience). For intracellular cytokine staining (ICS) of *ex vivo* lymphocytes, ~10^6 cells per samples were cultured in DMEM containing 2% FBS and Golgiplug (Fisher Scientific, 1.5μl/ml) for 6 hours with either a peptide pool (5ug/ml for each peptide) including all $CD8^+$T cell epitopes expressed by gDMelapoly (mTrp-$1_{455-463}$: TAPDNLGYA, mTrp-$1_{481-489}$: IAVVAALLL, mTrp-$2_{522-529}$: YAEDYEEL, hTp-$2_{180-188}$: SVYDFFVWL, hTrp-$2_{343-357}$: STFSFRNAL, mTrp-$2_{363-371}$: SQVMNLHNL, hgp100_{25-33}: KVPRNQDWL, mBraf $_{594-602}$: FGLANEKSI) or the E7 peptide: RAHYNIVTTF (all from Genescript). A rabies virus glycoprotein peptide was used as a negative control. For ICS performed with $CD8^+$T cells stimulated *in vitro*, ~10^6 cells were transferred to 96 well plates in the original medium and stimulated with PMA (500ng/ml), ionomycin (20μg/ml) and Golgiplug for 4 hours under either normoxia or hypoxia. Staining was conducted as described before[18]. Cells were stained with antibodies to IFN-γ-APC (Cat. #554413) or -BV421 (Cat. #505830, both from Biolegend),

granzyme B-APC (Cat. #MHGB05, Life Technologies) and perforin-PE (Cat. #eBioOMAK-D, eBioscience). Cells were analyzed by an LSRII (BD Biosciences) and data were analyzed with FlowJo (TreeStar).

BrdU proliferation assay

Mice were intraperitoneally injected with 1.5-2mg/mouse of BrdU solution and fed water-containing BrdU at a concentration of 0.8mg/ml for 24 hours before the assays. They were euthanized and lymphocyte samples were analyzed for BrdU incorporation. Cells were first stained for surface markers, and then for intranuclear BrdU incorporation using anti-BrdU-FTIC antibody (Cat. #51-33284X, 10μM/sample) according to the manufacture's instruction (BD Bioscience).

HIF-1α and Glut1 staining

For *ex vivo* assays mice were perfused immediately after euthanasia with PBS and heparin (10units/ml) and then with 1mM cobalt (II) chloride·$6H_2O$ ($CoCl_2$, EMD Millipore) diluted in PBS. For both *ex vivo* and *in vitro* experiments, lymphocytes isolation and staining before fixation were performed in medium containing 200μM $CoCl_2$. For staining, lymphocytes were first blocked with 10% normal goat serum (Life Technologies) for 30 minutes at room temperature and then stained with anti-Glut1 primary antibody (Cat. #ab40084) or mouse IgG2a isotype control antibody (Cat. #ab17019, abcam) at 1μg/10^6 cells for 60 minutes at room temperature. Cells were washed and stained with PacBlue labeled-goat anti-mouse secondary antibody (Cat. #P31582, 1:2000 dilution, Life Technologies) together with antibodies to other cell surface markers for 30 minutes. Cells were fixed, permeabilized, and stained for HIF-1α with anti-HIF-1α-Alexa700 antibody (Cat. #IC1935N, R&D) using the FoxP3 buffer set (eBioscience).

Extracellular Flux Analysis and FAO assay

OCR and ECAR for $CD8^+$T cells stimulated under different conditions were measured with XF24 and XF96 Extracellular Flux Analyzers (Seahorse Bioscience). Hypoxia samples were prepared in a hypoxia chamber under 1% O_2. Dead cells were removed by dead cell removal kit using MACS and live cells were pre-incubated with 100μM cobalt chloride before being removed from the hypoxia chamber and entered into the Seahorse analyzer. In experiments to determine the contribution of fatty acid oxidation (FAO) to OCR, 200mM etomoxir (Eto) was added 15 minutes before the Seahorse analysis. Briefly after repeated measures of basal respiration and lactate production, 1μM OM was added to measure ATP leakage and glycolytic capacity of the cells. 1.5μM FCCP was then added to measure maximal respiration followed by addition of 100nM Rotenone and 1μM Antimycin A to determine spare respiratory capacity and then 100mM 2-DG to determine glycolytic reserve. For measuring oxidation of exogenous and endogenous FAs, cells activated in either Glu or Gal medium for 3 days were washed and transferred to substrate-limited Glu or Gal media for overnight stimulation. Substrate limited media contained 0.5 mM Glu or Gal, 1mM GlutaMAX, 0.5mM carnitine (all form Sigma) and 1% dialyzed FBS. Samples were treated with either Eto or vehicle control 15 minutes before the assay. Palmitate: BSA or BSA was added just before the assay. The contributions of FAO to OCR was calculated as follows: Basal respiration due to exogenous FA oxidation= (Basal Palm:BSA-Eto OCR rate – basal BSA-Eto OCR rate) - OCR due to uncoupling by FFA; OCR due to uncoupling by FFA= after OM injection, Palm:BSA-Eto OCR rate - BSA-Eto rate. Basal OCR due to endogenous FAs consumption = basal BSA-Eto OCR rate - basal BSA+Eto OCR rate.

Lipid and Glucose concentration measurement in tumor interstitial fluid

Tumors interstitial fluid was collected as described(352). Free FA species concentrations were determined by LC-MS. Absolute concentration of Glu was measured by LC-MS upon adding $^{13}C_6$-Glu as the internal standard.

Isotopic labeling *in vitro* for metabolomics analysis.

For $^{13}C_6$-Glu/Gal tracing *in vitro,* cells were cultured from the onset of the assays in Glu-free RPMI medium with 10mM $^{13}C_6$-Glu/Gal (Sigma) for 4 days. For $^{13}C_{16}$-palmitate tracing *in vitro,* cells were stimulated for 3 days in Glu or Gal medium. On the night of day 3, some samples were transferred to 1% O_2 for overnight culture. $^{13}C_{16}$-palmitate (Sigma) was first dissolved in 100% ethanol at 200mM and conjugate to fatty acid-free BSA (Sigma) at a 5:1 molar ratio to a final concentration of 8mM-$^{13}C_{16}$-palmitate-BSA by vortexing at 37°C for 3-4 hours with sonication. On day 4, samples were pelleted and replated in fresh medium with 10% delipidated FBS (Cocalico Biologicals) and 400μM $^{13}C_{16}$-palmitate-BSA. Hypoxia samples were returned to 1% O_2. All samples were cultured for another 4 hour. Dead cells were removed by MACS. Samples were pelleted at 4000rpm for 5 minutes. All collection procedures were conducted at 4°C. Cell numbers in each sample were determined. Metabolism was quenched and metabolites were extracted by adding 1 ml -80°C 80:20 methanol: water per million cells. After 20 min of incubation on dry ice, samples were centrifuged at 10000 g for 5 min. Insoluble pellets were re-extracted with 1 ml -80°C 80: 20 methanol: water on dry ice. The supernatants from two rounds of extraction were combined, dried under N_2, resuspended in 1 ml water per million cells. Metabolites were normalized to cell number.

Isotope labeling *in vivo*.

Tumor-bearing mice were fasted for 16 hours. $^{13}C_6$-Glu (Cambridge) diluted in PBS was given i.p. to mice at 2g/kg. Spleens and tumors were collected 30 minutes later. $^{13}C_{16}$-potassium palmitate was conjugated to FA-free BSA (6:1 molar ratio) and given to mice at ~0.35g/kg by oral gavage. 1-hour later $^{13}C_{16}$-palmitate-BSA was given i.v. at 125mg/kg. Spleens and tumors were collected 30 mins later and cells were isolated on ice. Tumor samples were weighed and flash frozen in liquid nitrogen. $CD8^+CD44^+$T cells from pooled samples were stained and sorted at 4°C. Metabolites were extracted with -80°C 80: 20 methanol: water, dried under N_2 and resuspended in water at 100mg tissue/ml or 10^6 cells/100ml. Metabolites were normalized to cell number.

Contribution of ^{13}C to TCA cycle metabolites was calculated as [(m+1)*1+… (m+n)*n] / {[(m+0)+…+(m+n)]*n}*100%, where m+0 is the normalized signal intensity of a metabolite in ^{12}C form, m+n indicates normalized signal intensity for each form of ^{13}C labeled metabolite, n indicates the total number of ^{13}C carbon atoms in that metabolite.

LC-MS Instrumentation and method development.

Glycolytic and TCA metabolites were analyzed by reversed-phase ion-pairing chromatography coupled with negative-mode electrospray-ionization high-resolution mass spectrometer on a stand-alone orbitrap (Thermo Scientific)(353). Carnitine species were analyzed by reversed-phase ion pairing chromatography coupled with positive-mode electrospray-ionization on a Q Exactive hybrid quadrupole-orbitrap mass spectrometer (Thermo Scientific); Liquid chromatography separation was achieved on a Poroshell 120 Bonus-RP column (2.1 mm ×150 mm, 2.7 μm particle size, Agilent). The total run time is 25 min, with a flow rate of 50 μl/min from 0 min to 12 min and 200μl/min from 12 min to 25 min. Solvent A is 98: 2 water: acetonitrile with 10 mM amino acetate and 0.1% acetic acid; solvent B is acetonitrile. The gradient is 0-70 % B in 12 min. All isotope labeling patterns were corrected for natural ^{13}C-abundance.

Gene expression analysis

Lymphocytes were isolated from spleens and tumors of mice (tumor-bearing or normal) at different time points and stained with dyes and antibodies to live cells, $CD8^+$, $CD44^+$ and the Trp-1 and E7 tetramers. For co-adoptive transfer experiments, $CD8^+CD44^+$T donor cells of different origin were recovered from spleen and tumors of recipient mice three weeks later by antibodies staining and sorting. Trp-1 or E7 $tet^+CD44^+CD8^+$T cells were sorted (Mono Astrios, Beckman Coulter) on ice into RNAprotect cell reagents (QIAGEN). *In vitro* cultured $CD8^+$T cell samples were processed on ice to remove dead cells using manual cell separation columns and Mini/Midi MACS separators (Miltenyi Biotec). For lentivector transduction assays, transduced cells were further purified based on Thy1.1 expression using MACS. RNA was isolated from purified cells

using RNeasy Mini kits (Qiagen) and RNA concentrations were determined using Nanodrop (Thermo Scientific). cDNAs were obtained by reverse transcription using the high capacity cDNA reverse transcription kit (Life Technologies). Relative quantitative real-time PCR analyses were performed with Fast SYBR Green master mix using 7500 Fast Real-Time PCR system (Life Technologies). GAPDH or β-2 microglobulin were used as internal controls yielding comparable results. Primers (**Table 4-1**) for all tested transcripts were designed by Vector NTI. Differences in transcripts expression levels are visualized in heatmaps. Values were log transformed to show ratios of differences. Color scale was set as -2 (lower expression, deep blue) to 2 (higher expression, deep red).

Metabolic pathways	Gene name (Forward-F and Reverse-R)	Primer sequences
Glucose metabolism	mGLUT1-F	TGTGGGAGGAGCAGTGCTCG
	mGLUT1-R	TGGGCTCTCCGTAGCGGTG
	mHK2-F	TGATCGCCTGCTTATTCACGG
	mHK2-R	ACCGCCTAGAAATCTCCAGAAGG
	mPGK1-F	ATGTCGCTTTCCAACAAGCTG
	mPGK1-R	TGGCTCCATTGTCCAAGCAG
	mIDH3a-F	TGGGTGTCCAAGGTCTCTCG
	mIDH3a-R	TCTGGGCCAATTCCATCTCC
	mMDH2-F	TTGGGCAACCCCTTTCACTC
	mMDH2-R	TGTGACTCAGATCTGCTGCCAC
Lipid metabolism regulaion, FAs uptake, TG synthesis and lipolysis and FA synthesis	mPPARα-F	AGCCCCATCTGTCCTCTCTCC
	mPPARα-R	TCCAGAGCTCTCCTCACCGATG
	mSLC27A4-F	TGAGTTTGTGGGTCTGTGGCTAGG
	mSLC27A4-R	AAGACAGTGGCGCAGGGCATC
	mSLC27A2-F	TGCTGCTGCTGCCTCTGCTG
	mSLC27A2-R	AGGATGGTACGCACGGGTCG
	mDGAT1-F	ACCTGGCCACAATCATCTGCTTC
	mDGAT1-R	TTGGCCTTGACCCTTCGCTG
	mDGAT2-F	AGCATCCTCTCAGCCCTCCAAG
	mDGAT2-R	TAGCACCAGGAAGGATAGGACC
	mPNPLA2-F	TTCCCGAGGGAGACCAAGTG
	mPNPLA2-R	TGCCGAGGCTCCGTAGATG
	mLIPA-F	TGCTTTCTCGGGTGCCCAC
	mLIPA-R	TCCTCACCAGGATATCCCCAG
Peroxisomal FAO	mACAA1a-F	TCCGCTAGGTTCCCGCAGG
	mACAA1a-R	ACAGAAGCTCGTCGGGGGTG
	mEHHADH-F	AAAGTTCGCAAAGGGCAAGG
	mEHHADH-R	TCGCCCAGCTTCACAGAGC
	mACOX1-F	TCCCGATCTGCGCAAGGAG
	mACOX1-R	TGTTCTCCGGACTACCATCCAAG
	mHSD17B4-F	TTGTGAACGACTTAGGAGGGGAC
	mHSD17B4-R	AAATGTGTCCAGTGCCGTCTTC
Mitochondrial FAO	mACADVL-F	ACCCTCTCCTCTGATGCTTCCAC
	mACADVL-R	TGAGCACAGATGGGTATGGGAAC
	mACADM-F	AAGCAGGAGCCCGGATTAGG
	mACADM-R	TCCCCGCTTTTGTCATATTCC
Ketone body metabolism	mBDH1-F	TCGCCATACTGCATCACCAAG
	mBDH1-R	TGCCAGGTTCCACCACACTG
ROS production/detoxification and Electron transport chain (ETC)	mNOX1-F	AGAAATTCTTGGGACTGCCTTGG
	mNOX1-R	TGCCCCTCAAGAAGGACAGC
	mSOD1-F	ACAGGATTAACTGAAGGCCAGC
	mSOD1-R	TTGCCCAGGTCTCCAACATG
	mCAT-F	TGACATGGTCTGGGACTTCTGG
	mCAT-R	AGCCATTCATGTGCCGGTG
	mCOX5B-F	ACCCGCTCCATGGCTTCTG
	mCOX5B-R	AGTCCCTTCTGTGCTGCTATCATG

Table 4-1: List of primers for receptors and enzymes measured in chapter 4.

Statistical analysis

I chose sample size based on pilot experiments and literature reports in the filed. No randomization or blinding was done in the experiments and there were no inclusion/exclusion criteria. The statistics were performed based on the properties of data distribution, variation, and

biological questions asked. D'Agostino-Pearson omnibus normality test were ran for each data set. The variations were similar between the groups that were statistically compared. Significance of differences between 2 populations was calculated by two-tailed Student's t test; Multiple t-test with Holm-Sidak correction was performed for multiple 2-group comparisons within the same graph. Significance of differences among multiple populations was calculated by one-way or two-way ANOVA using GraphPad Prism 6. Data were shown as mean value with standard error of the mean (SEM). Significance was set at p-values of or below 0.05. Type I errors were corrected for multiple comparisons using the Holm-Sidak method.

Chapter 5

DISCUSSION

SIGNIFICANCE

Despite the significant breakthroughs made in recent years in the field of cancer immunotherapy, metastatic melanoma still represents one of the most life-threatening diseases that require urgent attention. Resistance or only transient responses to the current available therapeutic agents, including BRAF and MEK inhibitors, anti-PD-1/PD-L1 antibodies, anti-CTLA-4 antibody and adoptive cell transfer (ACT), is observed in the majority of melanoma patients. Continuous efforts to develop more effective treatment strategies for metastatic melanoma and other cancers are therefore essential and this is the major goal of my thesis.

Cancer immunotherapy aims to attack foreign or self-tumor antigens (TAs) through the immune system. Among various players of the immune system that may exert antitumor functions, $CD8^+$T lymphocytes are the most promising candidates with potent tumoricidal potential. The T cell receptors (TCR) have high diversity; upon stimulation T cells vigorously proliferate and acquire direct cytolytic functions. Eliciting and maintaining robust TA-specific $CD8^+$T cell responses is the major focus of numerous preclinical and clinical cancer immunotherapeutic studies, including cancer vaccine design and investigations of ACT and immunoinhibitory ligand blockade strategies.

However, as repeatedly stated throughout this thesis, there are many limitations related to the use of $CD8^+$T cells within the highly immunosuppressive tumor microenvironment (TME), which render the current therapeutic approaches largely ineffective in most patients with advanced cancers. First and foremost, tumors are a heterogeneous mass that contains a variety of cell types including fibroblasts, endothelial cells and immune inflammatory cells, i.e. myeloid-derived suppressor cells (MDSCs), tumor-associated macrophages (TAMs), regulatory T cells (Tregs) (354). Most of these cells could suppress effective $CD8^+$T cell functions through secretion of inhibitory cytokines such as IL-10 and TGF-β or enzymes such as arginase, iNOS and IDO (355-357). In addition, stromal fibroblasts, macrophages and tumor cells express ligands for co-inhibitors, such as PD-L1, HVEM and CD80/CD86, which inhibit cytotoxic $CD8^+$T cell functions through interaction with PD-1, BTLA and CTLA-4, respectively. Moreover, It is well established that effector $CD8^+$T cells gradually differentiate towards functional impairment within TME, a phenomena referred to as T cell exhaustion. Although chronic antigen stimulation is traditionally viewed as the cardinal cause of T cell functional exhaustion, our studies among other recent findings strongly suggest that the stressful metabolic conditions within the TME greatly contribute to the loss of functions of $CD8^+$ effector T cells. TA-specific tumor-filtrating $CD8^+$T cells, upon recognizing antigens within the TME, will become highly activated and energy demanding. Effector T cells enhance both glycolysis and mitochondrial OXPHOS to produce ATP, which require sufficient glucose (Glu) and oxygen supply. As the TME is poorly vascularized and tumor cells competitively consume Glu to fuel their own proliferation, $CD8^+$TILs have limited access to both Glu and oxygen. These metabolic challenges and reduced ATP production of $CD8^+$TILs have been shown to temper their antitumor functions (192,358). Overcoming any one of these metabolic obstacles could potentially improve the therapeutic efficacy of melanoma immunotherapy and benefit patients in the clinic, which is the overarching goal of my dissertation.

Numerous studies aim to block inhibitory factors within the TME and combine it with strategies to boost functions of TA-targeting effector $CD8^+$T cell. Such studies conducted in both animal models and melanoma patients have yielded some promising results. FDA-approved

immune checkpoint inhibitors, given either individually or in combination, have exhibited objective clinical responses in 30-40% of patients with metastatic melanoma (54). In addition, preliminary studies suggest that targeting T-cell immunoglobulin and mucin-domain containing (TIM)-3 achieved similar therapeutic efficacy compared to that of PD-1 pathway blockade in preclinical cancer models, while combining TIM-3 with PD-1 blockade further delayed tumor growth(359,360). Combining checkpoint inhibitors with vaccines or ACT has also been investigated. Adding gp100 vaccine to ipilimumab did not provide additional benefits for melanoma patients in a phase III clinical trial (13), while in animal models it has been demonstrated that combining anti-PD-1/PDL1 antibodies with ACT could generate optimal effects against melanoma (361). However, as checkpoint inhibitors globally target inhibitory ligands expressed in the immune system of cancer patients, their application carries the risk of inducing severe autoimmune diseases or other adverse effects. Novel approach that could locally target the upregulated inhibitory pathways in TA-specific $CD8^+$T cells may therefore result in more desirable effects. In chapter 2 this concept has been investigated in detail.

Tumor stromal fibroblasts promote tumorigenesis and suppress immune cell functions through various mechanisms (127). Depleting FAP^+ fibroblasts within the TME through genetic depletion, vaccine approaches or ACT have reduced tumor growth in a number of cancer types (122,124,131,362). It was shown that depleting FAP^+ fibroblasts could shift the polarization of T cells from a T helper 2 (Th2) to a Th1 phenotype, improve $CD8^+$T cell infiltration and functions and reduce immunosuppressive cells (ISCs) in the TME (363). However, whether combining FAP-targeting vaccine with tumor-cell targeting vaccine can further shift the immune balance within the TME and affect ISCs functions have never been studied before. More importantly, as depleting FAP^+ fibroblasts and ISCs may lift the metabolic challenges within TME, it is important to understand whether this strategy could potentially reduce the metabolic stress of TA-specific $CD8^+$TILs and thereby augment their antitumor functions. These questions are systemically addressed in chapter 3.

Last but not least, the metabolic status of immune cells and its contribution to immune cell functions in different disease settings have become the focus of intense investigations in recent years (364,365). Within the TME, it was shown that Glu deprivation due to its consumption by tumor cells dampens the glycolytic capacity of effector T cells and reduces their ability to produce IFN-γ. Moreover, restoring Glu supply or increasing the $CD8^+$T cells' ability to use glycolysis could partially restore their antitumor functions (192,197). However, the impact of other metabolic constrains on $CD8^+$TILs are still poorly understood. For example, the limited blood supply provides inadequate oxygen to $CD8^+$TILs that penetrate deeply into the TME, which could negatively affect the TILs' ability to use mitochondrial OXPHOS for energy production. How hypoxia affects effector functions of $CD8^+$TILs especially if combined with Glu deprivation is unknown. In addition, the TME contains abundant lipids of various species and lactate produced by tumor cells and stroma cells, which may modulate the nutrients uptake and metabolic pathways used by $CD8^+$TILs as well as their effector functions. Investigating these issues could facilitate the development of novel metabolic intervention strategies for $CD8^+$T cells, which may improve their antitumor performance within the TME and prolong the survival of patients with metastatic cancer. This topic is studied at length in chapter 4.

CONCLUSIONS AND FUTURE DIRECTIONS

I. Blocking the immunoinhibitory pathway:

To study whether blockade of immunoinhibitory signaling in vaccine-induced TA-specific $CD8^+$T cells during priming could enhance their antitumor functions, I focused on the BTLA/CD160-HVEM pathway and designed the cancer vaccine to express melanoma-associated antigens (MAAs) within HSV gD, which competitively blocks BTLA/CD160 interacting with HVEM. Interactions between the HVEM cysteine-rich domain (CRD)1 region on antigen presenting cells and melanoma cells with BTLA/CD160 on T cells inhibits T cell activation and might also lead to

their functional impairment within the TME. HSV gD binds its N-terminus loop to the CRD1 and CRD2 regions of HVEM that overlap with the BTLA binding site; gD has higher binding affinity, therefore blocking HVEM-BTLA interaction (261,276,366) (**Figure 5-1**).

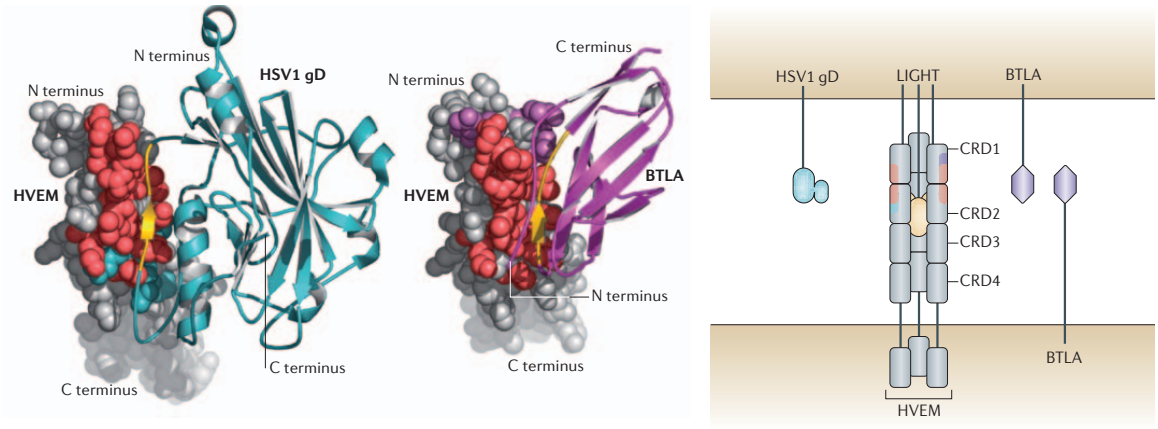

Figure 5-1. Molecular modeling of HVEM and its binding with HSV1 gD or BTLA. (**Left)** Model of HVEM is shown binding to HSV1 gD or BTLA through its cysteine-rich domain. Red indicates contacts shared beween HSV1 gD and BTLA. (**Right**) Model of HVEM interacts with its ligands on cell surface. Figure is adapted from *Murphy K.M., Nelson C.A. and Sedy JR. Nature immunology. 2006.*

Although our laboratory has shown that vaccines expressing antigens as fusion proteins within HSV gD can induce markedly enhanced antigen-specific T cell responses especially in aged mice (263) or tumor-bearing mice (244), whether adjuvanting a cancer vaccine with gD could affect T cell differentiation and functions within the TME had not been studied. In my project, I fused eight $CD8^+$T cell epitopes derived from four MAAs and four MAA-associated $CD4^+$T cell epitopes within gD to determine whether blocking the BTLA/CD160-HVEM signaling during T cell priming could improve their antitumor functions within tumors.

I chose to design a polyepitope cancer vaccine in order to reduce the chance of immune escape, as tumor cells are capable of evading the immune pressure exerted by vaccine-induced immune responses due to the advantageous growth of antigen-loss variants or non-targeted subpopulations. In designing the polyepitope vaccine, I used several strategies in order to enhance MAA-specific T cell responses. For example, among the 8 MAA-derived $CD8^+$T cell epitopes, 4 of them (mTrp-1_{455}, mTrp-$1_{481,}$ mTrp-1_{522} and murine $Braf_{V600E}$) bear amino acid

mutations at the MHC anchor positions. This allows for the induction of significantly higher frequencies of $CD8^+$T cells that could recognize the original Trp-1 or Braf epitopes presented on B16 tumor cells. In addition, one epitope of human gp100 protein is included. This also facilitates the generation of more robust T cell responses against gp100 that could recognize mouse gp100. In addition, I included the mouse Ig k signal sequence at the 5' end of the construct to facilitate processing of CTL epitopes in the endoplasmic reticulum (ER). The universal T helper cell epitope PARDE, which is highly immunogenic in C57BL/6 mouse, is incorporated to potentiate $CD8^+$T cell responses. Moreover, I designed spacer sequences (Alanine and Tyrosine) between each $CD4^+$ and $CD8^+$ T cell epitope basing on the processing results generated by several softwares, i.e. IEBD analysis, PAPROC in silico prediction, Netchop 3.1, to ensure better processing and presentation of each epitope by proteasome and enzymes (i.e. ERAP1) within the ER.

The polyepitope constructs, termed Melapoly, with or without gD induce dominant $CD8^+$T cell responses to the Trp-1_{455} epitope, the responses to other 7 epitopes are subdominant and develop with a delay. However, the gD adjuvanted vaccine only significantly enhances frequencies of functional $CD8^+$T cells specific to the subdominant epitopes compared to those induced by AdC68-Melapoly vaccine alone starting at about 4 weeks after vaccination. This difference persists and becomes more significant at later time points (up until 26 weeks after vaccination as we monitored). In contrast, frequencies of functional Trp-1-specific $CD8^+$T cells are similar between the two vaccine groups throughout the 26 weeks. It is well known that many of the immunogenic TAs are self-antigens, which means that high-avidity T cells against these antigens have undergone thymic clonal deletion and most TA-specific T cell populations available for priming in the body are of low avidity (367). Therefore the fact that gD adjuvant selectively benefit low avidity T cells make it a valuable candidate for cancer vaccines.

When estimating the efficacy of the gD adjuvanted vaccine in delaying tumor progression, I used the $B16Braf_{V600E}$ transplantable tumor model in both pre- and post-tumor challenge vaccination experiments. The gD adjuvanted vaccine yields significantly better tumor

protection compared to the non-gD vaccine in both systems, although it works more effectively if given prior to tumor challenge. Importantly, we showed that when the vaccine is given 3 days after tumor challenge, the survival advantage generated by the gD adjuvanted vaccine is not solely linked to the magnitude of MAA-specific $CD8^+$T cell responses. In mice with comparable frequencies of function$^+$ MAA-specific $CD8^+$T cells, those that received the gD adjuvanted vaccine show prolonged survival. Detailed analysis indicates that MAA-specific $CD8^+$TILs elicited by the gD vaccine show significantly reduced expression of co-inhibitors, i.e., PD-1, LAG-3 or 2B4 alone or in combinations, compared to those generated by the non-gD vector. As I showed that high expression of co-inhibitors corresponds with weaker functions, specifically reduced cytokine secretion and lower T-bet levels in MAA-specific $CD8^+$TILs, the reduced expression of co-inhibitors on gD-adjuvanted vector induced $CD8^+$TILs suggests their improved functional profile, although this was not measured directly. How blocking BTLA-HVEM interactions during T cell activation affects their differentiation and functional performance within the TME is still unknown. I assume that suppressing the immunoinhibitory BTLA-HVEM pathway during MAA-specific T cell priming by HSV gD boosts their activation status, which makes them more resistant to functional impairments within the TME. However the precise mechanism is not well studied and is an area that should be investigated further. It will also be interesting to study whether blocking other immunoinhibitory signaling during T cell priming or activation will further enhance the TILs antitumor activities.

II. Depleting immunosuppressive FAP$^+$ tumor stroma:

To explore other approaches that could further diminish the functional impairment of vaccine-induced TA-specific $CD8^+$TILs, I constructed the tumor stroma targeting AdC68-mFAP vaccine that depletes the FAP$^+$ tumor stroma cells in solid tumors and combined it with the tumor cell targeting AdC68-gDMelapoly vaccine. The combination strategy strongly delays melanoma progression as I demonstrated in two tumor models, the transplantable B16$Braf_{V600E}$ tumors and the clinically more relevant inducible tumor model with transgenic Tyr::CreER $Braf^{CA/+}Pten^{lox/lox}$

mice. The latter mice develop metastatic melanoma within 7-10 days upon applying 4-hydorxytamoxifen to the skin, and the mechanism of melanoma development in these mice closely mimicked the disease progression in patients with metastatic melanoma. FAP^+ cell staining in tumors show that most FAP^+ cells are CD45 negative with high expression of mesenchymal stromal cell markers CD90 and Sca-1. Although the inducible $Braf^{CA/+}Pten^{lox/lox}$ tumors contain significantly more FAP^+ cells compared to those in B16 $Braf_{V600E}$ tumors, the FAP^+ targeting vaccine works equally well in both tumor models in terms of delaying tumor growth compared to the groups of mice that received only the control AdC68-gD vector. This is associated with $CD8^+$T cell mediated depletion of FAP^+ stromal cells in both tumor models. Moreover, adding the FAP vaccine to the tumor cell targeting gDMelapoly vector further reduces the abundance of FAP^+ stromal cells compared to those of mice received the FAP vaccine or gDMelapoly vaccine alone, which also translates into further delay in tumor growth.

The strong correlation between reduced FAP^+ stroma cell numbers and delayed tumor growth confirms that FAP^+ tumor stromal fibroblasts support tumor growth. Indeed, my studies in both tumor models suggest that depleting FAP^+ cells reduces the number of $Gr\text{-}1^{hi}$ and $Gr\text{-}1^{int}$ MDSCs in the TME, this effect is more dramatic when the FAP vector is given together with the gDMelapoly vector. Furthermore, MDSCs and TAMs from tumors of mice that received the combination treatment show reduced immunosuppressive functions in terms of iNOS and Arg1 production compared to those from mice that received only the tumor cell targeting vaccine. Further analysis suggests that this is associated with reduced presence of immune inflammatory and inhibitory cytokines IL-4, IL-10, TGF-β, as well as certain chemokines such as CCL5 and CCL22 in the TME and diminished pSTAT6 signaling in MDSCs and TAMs. Although I did not analyze the direct cause of reduced frequencies and suppressive functions and MDSCs/TAMs in tumors upon FAP^+ stromal cell depletion, my data strongly suggest that depleting FAP^+ cells alters the cytokine/chemokine milieu within the TME. As IL-4 and IL-13 are the main upstream cytokines that activate the JAK-STA6 pathway, the decreased levels of IL-4 in the tumor may be

one of the key factors that reduce pSTAT6 signaling in ISCs and thereby blunt their suppressive functions.

My data also for the first time indicate that the presence of ISCs enhances mitochondrial metabolic stress and co-inhibitor PD-1 expression on activated $CD8^+$T cells *in vitro.* Depleting FAP^+ cell *in vivo* also reduces the metabolic stress and PD-1 expression of MAA-specific $CD8^+$TILs and enhances their frequencies and polyfunctions. It is tempting to speculate that FAP^+ cell depletion lifts the metabolic stress of $CD8^+$TILs partially through reducing the abundance of ISCs within tumors. It will be interesting to study the mechanism of how ISCs potentiate the metabolic stress of $CD8^+$T cells *in vitro* or in the TME. It is possible that ISCs compete with effector T cells for key nutrients, i.e. glucose and glutamine that are essential for their energy demand. Within tumors the presence of stromal cells, which could recruit other inflammatory cells and endothelial cells, may further increase competition for nutrients and create a more metabolically challenging environment for the tumor-infiltrating effector T cells. Moreover, my data indicate a strong correlation between enhanced MROS levels with increased PD-1 expression on activated $CD8^+$T cells *in vitro* and in the TME. As upregulation of co-inhibitor PD-1 usually signals T cell functional impairment in advanced tumors, it is important to understand whether enhanced metabolic stress could directly upregulate PD-1 expression. My studies of T cell metabolism in the TME described in chapter 4 show that lack of Glu, which enhance mitochondrial OXPHOS and reduces glycolysis for energy production by activated $CD8^+$T cells, increases MROS accumulation and co-inhibitor PD-1 expression in/on these cells. Whether FAP^+ stroma cells exert such effect on $CD8^+$TILs directly or indirectly through ISCs is still an issue that requires further investigation.

Compared to vaccines targeting tumor antigens for destruction, the FAP vaccine has broader applicability as FAP protein is universally expressed on fibroblasts in many types of cancers. In addition, the abundance of FAP^+ stromal fibroblasts differs by cancer type, i.e. pancreatic cancer and colon cancer may possess more FAP^+ stromal cells than melanoma (122,368,369). In the future it will be important to assess the efficacy of the FAP vaccine in

delaying tumor progression in other types of cancer, either by itself or in combination with tumor-cell targeting vaccines.

III. Manipulating the metabolism of CD8$^+$TILs:

To determine the factors that contribute to the functional impairment of vaccine-induced T cells within the TME, I vaccinated B16-tumor bearing mice with both AdC68-gDMelapoly and AdC68-gDE7 vectors, which induce both MAA- and E7-specific CD8$^+$T cells. T cells of the latter specificity do not recognize antigens within the TME; therefore I could ask the question whether constant antigen stimulation is required for the 'functional exhaustion' of activated CD8$^+$TILs. Interestingly my data show that even without exposure to their cognate antigens, E7 T cells enhance co-inhibitors PD-1 and LAG-3 expression and lose function within tumor during tumor progression, which is very, similar to the changes I observed with MAA-specific T cells. These data strongly factors other than chronic antigen stimulation within the TME profoundly affect the functions of activated TILs.

It is becoming increasingly clear that the metabolic status of immune cells has an important impact on their differentiation and functions. My preliminary data show that compared to small 2-week tumors, more advanced tumors contain significantly low levels of glucose and oxygen, which I hypothesize could impair the energy production of activated CD8$^+$TILs through both glycolysis and mitochondrial OXPHOS and enhance their metabolic stress. Indeed, analysis of mitochondrial metabolic markers suggests that both MAA- and E7-specific CD8$^+$TILs in 1-month tumors possess much lower mitochondrial membrane potential (MMP). In addition they show strong accumulation of mitochondrial reactive oxygen species (MROS), a toxic OXPHOS by-product, compared to those in 2-week small tumors. Together these data suggest that both vaccine-induced T cell subsets develop mitochondrial dysfunctions within metabolically challenging TME, which may affect their effector functions and antitumor activity.

Therefore I studied the impact of hypoxia and glucose limitation on activated CD8$^+$T cell metabolism and functions both *in vitro* and directly *ex vivo*. My data suggest that hypoxia

through HIF-1α signaling pathway impairs effector functions of activated $CD8^+$T cells and directly drives co-inhibitor LAG-3 upregulation both *in vitro* and in the TME. My results also imply that promoting glycolysis of $CD8^+$TILs, i.e. such as through hypoxia-induced HIF-1α signaling within a Glu-depleted TME is detrimental to their functions. However these data are in conflict with some published studies, which showed that HIF-1α increases the effector functions of $CD8^+$T cells using Von Hippel-Lindau (VHL) or Prolyl Hydroxylase Domain (PHD) Knockout (KO) cells or mice (187). VHL and PHD are O_2-sensing enzymes that target HIF for degradation under normoxia. VHL or PHD KO cells possess stabilized HIF-1α expression from the onset of $CD8^+$T cell priming and activation, which is clearly different from my system where tumor-infiltrating $CD8^+$T cells experience hypoxia and enhance HIF-1α signaling after their activation in the O_2-replete periphery lymph nodes. Therefore I suspect that the enhanced HIF-1α activity from the onset of T cell activation may affect other signaling pathways in these cells and modulate their effector functions through different mechanisms, which could explain the discrepancy between their data and my finding of the function-dampening effect of hypoxia-induced HIF1α within the TME.

To study the effect of Glu deprivation on $CD8^+$T cells, I stimulated enriched $CD8^+$T cells *in vitro* in medium supplemented with 2-DG or Galactose (Gal) instead of Glu. Both conditions force the activated $CD8^+$T cells to rely more on the mitochondrial OXPHOS pathway for energy production. This in turn leads to significantly increased co-inhibitor PD-1 expression on these T cells. Interestingly, my data show that although hypoxia by itself reduced PD-1 levels on activated $CD8^+$T cells, lack of Glu combined with hypoxia still significantly enhances PD-1 compared to cells cultured with Glu under normoxia, which may explain why in the TME $CD8^+$TILs show upregulated PD-1. Moreover, I observed that although lack of Glu impairs functions of $CD8^+$T cells under either normoxic or hypoxic condition, the reduction in functions are less significant when cells are cultured under hypoxia with limited Glu compared to those cultured under hypoxia with ample supplies of Glu. Cells actually improve their capacity to produce more

than one factor with restricted Glu and O_2 supply, suggesting that the loss of effector functions can be more easily compensated for under Glu and O_2-limited condition.

Indeed, further metabolic studies confirm that activated $CD8^+$T cells cultured with limited access to Glu show increased fatty acid (FA) uptake, triacylglyceride (TAG) turnover and FA catabolism including fatty acid oxidation (FAO) and ketone bodies metabolism. This metabolic preference is further exacerbated when cells also have limited access to oxygen. My study for the first time confirms this metabolic switch of $CD8^+$TILs using ^{13}C-labled Glu and FA stable isotope tracing directly *in vivo* followed by LC-MS based metabolomics analysis. As my data show the TME of 1-month advanced tumors contain abundant free FAs of various species. Utilizing FA catabolism for energy production could provide $CD8^+$TILs with a survival advantage and may protect them from severe and rapid functional loss.

As $CD8^+$TILs in advanced tumors increase PD-1 expression, it is important to understand whether the metabolic switch to FA catabolism requires the presence of PD-1. If so anti-PD-1 treatment would provide a disadvantage for metabolically stressed $CD8^+$TILs, which is counterintuitive as this treatment reduces tumor progression. I studied this by treating tumor-bearing mice that had received the AdC68-gDMelapoly vaccine 10 days earlier with anti-PD-1 or isotype antibody every two days until one month after tumor challenge. *In vivo* ^{13}C-glucose and ^{13}C-palmitic acid isotope-tracing studies reveal that blocking PD-1 signaling has only subtle effect on metabolism of activated $CD8^+$T cells in spleen and tumors. Furthermore, in the two groups of mice with similar sized tumors, blocking PD-1 signaling fails to affect the effector functions of $CD8^+$TILs. PD-1 blockade delays B16 tumor growth in both vaccinated and unvaccinated C57BL/6 mice, the later of which posses very few tumor-infiltrating lymphocytes. Moreover in NSG mice that lack T, B and NK cells, PD-1 blockade still strongly delays tumor progression, suggesting that this checkpoint inhibitor could exert its antitumor effect independent of T cells. These results are consistent with other studies, which show that a portion of B16 tumors express PD-1. Blocking PD-1 expressed on tumor cells from interacting with PD-L1 expressed on stromal cells or tumor cells reduces the activity of mTOR/pS6 signaling in tumor cells and inhibits

tumorigenesis (341), potentially by inhibiting the Glu metabolism in these cells. My preliminary studies show that the B16 tumor cells isolated from tumor-bearing mice express very low levels of PD-1. Anti-PD-1 treatment actually increases the rate of Glu metabolism in tumor cells, implying that it is unlikely that PD-1 blockade delays tumor growth directly through inhibiting the PD-1 signaling in these cells. In contrast, my study shows that tumor cells as well as ISCs and tumor stromal cells show high levels of PD-L1 expression. As anti-PD-1 antibody has been shown to back signal through PD-1-PD-L1 interaction to induce the apoptosis of tumor cells, I predict that in our system anti-PD-1 treatment may work through PD-L1 expressed on tumor cells or other cells in the TME to enhance their death rate, therefore increases the glucose supply within the tumor and delays tumor growth. Compared to tumor cells, ISCs and tumor stromal cells also show higher levels of PD-1 expression. It is also possible that anti-PD-1 delays tumor progression through inhibiting the tumorigenic potential of these cells within the TME. My preliminary data suggest that in vaccinated tumor-bearing mice, those treated with anti-PD-1 show increased total and MAA-specific $CD8^+$T cell infiltration into the tumor, indicating that anti-PD-1 may also delay tumor growth through increasing the number of tumor-specific T cells within the TME.

Finally, I boosted the FA catabolism capacity of activated $CD8^+$T cells in the TME using the PPARα agonist fenofibrate prior to T cell adoptive transfer. As expected, $CD8^+$TILs with enhanced FA catabolism show far better effector functions in terms of cytokine and lytic enzymes production. In addition their ability to delay tumor growth improves. Interestingly fenofibrate-treated cells show a trend towards enhanced PD-1 expression. To study the relation between PD-1 and functions in fenofibrate-treated $CD8^+$T cells upon adoptive transfer, I treated recipient mice that received either diluent- or fenofibrate-treated $CD8^+$T cells with anti-PD-1 or the isotype control starting at five days post adoptive transfer. In mice received isotype antibodies, those that received fenofibrate-treated cells show markedly slower tumor progression compared to those transferred with diluent-treated cells. In mice received either group of T cells, anti-PD-1 treatment strongly delayed tumor growth. Importantly, anti-PD-1 and fenofibrate treatment work in synergy and the mice received both treatments show markedly strong delay in tumor growth, with more

than 30% of mice completely protected. My data show that PD-1 blockade does not affect effector functions of MAA-specific $CD8^+$T cells originated from either diluent- or fenofibrate-treated donor mice, which is consistent with the result that anti-PD-1 works in a T cell independent manner. Therefore, my study suggest that PD-1 checkpoint inhibitor, which works through tumor cells or other cells within the TME, could strongly improve the efficacy of cancer immunotherapy if it is given together with metabolic manipulation that optimize the nutrient consumption capacity of tumor-specific $CD8^+$T cells.

My data show that promoting FA catabolism by $CD8^+$TILs cells improves their antitumor efficacy. This could be applied to several types of cancer immunotherapy such as adoptive transfer of ex vivo expanded TILs or CAR-T cells. It could also be used as an adjuvant for cancer vaccines or checkpoint inhibitors. Clearly additional studies are needed to confirm that increasing FA catabolism of TILs not only benefits individuals with melanomas but also other types of solid cancer, and even more importantly if my results in mouse models apply to human cancer patients.

Below, I list several research questions that are worth pursuing in the future.

1. Metabolic intervention of T cells for cancer immunotherapy

a. To determine whether different diets affect nutrients supply (glucose, FAs, glutamine etc.) and T cell metabolism within the TME. If so, whether the metabolic changes affect T cell functions. This study may provide dietary guidelines for cancer patients, which can help improve the efficacy of their cancer immunotherapy.
b. To study if metabolizing different types of lipids will affect differentiation and effector functions of T cells. If some lipid species that are abundant in tumor could promote T cell functions, one could design novel strategies to enhance the uptake/usage of this lipid by T cells and determine whether antitumor T cell efficacy can be improved.
c. Exploring novel approaches to promote T cell lipid catabolism prior to their adoptive transfer. In my study fenofibrate, a PPAR-α agonist is used. However, more efficient

methods, i.e. overexpression of lipid uptake receptor or lipid catabolism enzymes may further improve the lipid catabolism, and therefore antitumor functions of $CD8^+$TILs.

2. Combining other therapeutic approaches with metabolic intervention

a. Checkpoint inhibitors have made significant progresses in recent years. I propose to study the effect of each promising checkpoint inhibitor on the metabolism of TA-specific TILs, as pushing the metabolism of TILs towards the same direction using other methods may achieve similar or even better antitumor efficacy. In addition, I would like to determine whether combining different checkpoint inhibitors with metabolic intervention strategies could further improve the therapeutic efficacy. And if so, it will be important to understand the underlying mechanism.

b. My study has implicated that both tumor stroma and ISCs enhance the metabolic stress of active T cells. I would like to further understand how presence of tumor stroma or ICSs reprograms the metabolism of TA-specific TILs, and study the combination effect of tumor stroma/ISCs depletion with T cell metabolic intervention strategies on tumor growth.

3. Study Immunometabolism of other types of immune cells in TME

Besides T cells, metabolic challenges within the TME could potentially affect other immune cell populations. Specifically, It is important to understand how metabolism and immunosuppressive functions of ISCs are affected in solid tumors. It will be worthwhile to study if manipulating the metabolism of ICSs will affect their functions, and exploring new metabolic intervention pathways to reduce the inhibitory capacity of ISCs.

BIBLIOGRAPHY

1. Rebecca VW, Sondak VK, Smalley KSM. A brief history of melanoma: from mummies to mutations. *Melanoma Res* (2012) **22**:114–122. doi:10.1097/CMR.0b013e328351fa4d

2. Beaumont KA, Wong SS, Ainger SA, Liu YY, Patel MP, Millhauser GL, Smith JJ, Alewood PF, Leonard JH, Sturm RA. Melanocortin MC_1 receptor in human genetics and model systems. *Eur J Pharmacol* (2011) **660**:103–110. doi:10.1016/j.ejphar.2010.11.040

3. Goldstein AM, Chan M, Harland M, Gillanders EM, Hayward NK, Avril M-F, Azizi E, Bianchi-Scarra G, Bishop DT, Bressac-de Paillerets B, et al. High-risk melanoma susceptibility genes and pancreatic cancer, neural system tumors, and uveal melanoma across GenoMEL. *Cancer Res* (2006) **66**:9818–9828. doi:10.1158/0008-5472.CAN-06-0494

4. Uong A, Zon LI. Melanocytes in development and cancer. *J Cell Physiol* (2010) **222**:38–41. doi:10.1002/jcp.21935

5. Algazi AP, Soon CW, Daud AI. Treatment of cutaneous melanoma: current approaches and future prospects. *Cancer Manag Res* (2010) **2**:197–211. doi:10.2147/CMR.S6073

6. Bertolotto C. Melanoma: from melanocyte to genetic alterations and clinical options. *Scientifica (Cairo)* (2013) **2013**:635203–22. doi:10.1155/2013/635203

7. Hodis E, Watson IR, Kryukov GV, Arold ST, Imielinski M, Theurillat J-P, Nickerson E, Auclair D, Li L, Place C, et al. A landscape of driver mutations in melanoma. *Cell* (2012) **150**:251–263. doi:10.1016/j.cell.2012.06.024

8. Berger MF, Hodis E, Heffernan TP, Deribe YL, Lawrence MS, Protopopov A, Ivanova E, Watson IR, Nickerson E, Ghosh P, et al. Melanoma genome sequencing reveals frequent PREX2 mutations. *Nature* (2012) **485**:502–506. doi:10.1038/nature11071

9. Schadendorf D, Fisher DE, Garbe C, Gershenwald JE, Grob J-J, Halpern A, Herlyn M, Marchetti MA, McArthur G, Ribas A, et al. Melanoma. *Nat Rev Dis Primers* (2015)15003–20. doi:10.1038/nrdp.2015.3

10. Curtin JA, Fridlyand J, Kageshita T, Patel HN, Busam KJ, Kutzner H, Cho K-H, Aiba S, Bröcker E-B, LeBoit PE, et al. Distinct sets of genetic alterations in melanoma. *N Engl J Med* (2005) **353**:2135–2147. doi:10.1056/NEJMoa050092

11. Tsao H, Chin L, Garraway LA, Fisher DE. Melanoma: from mutations to medicine. *Genes Dev* (2012) **26**:1131–1155. doi:10.1101/gad.191999.112

12. Gray-Schopfer V, Wellbrock C, Marais R. Melanoma biology and new targeted therapy. *Nature* (2007) **445**:851–857. doi:10.1038/nature05661

13. Hodi FS, O'Day SJ, McDermott DF, Weber RW, Sosman JA, Haanen JB, Gonzalez R, Robert C, Schadendorf D, Hassel JC, et al. Improved survival with ipilimumab in patients with metastatic melanoma. *N Engl J Med* (2010) **363**:711–723.

doi:10.1056/NEJMoa1003466

14. Trinh VA. Current management of metastatic melanoma. *American Journal of Health-System Pharmacy* (2008) **65**:S3–S8. doi:10.2146/ajhp080460

15. Alexandrescu DT, Ichim TE, Riordan NH, Marincola FM, Di Nardo A, Kabigting FD, Dasanu CA. Immunotherapy for Melanoma: Current Status and Perspectives. *Journal of Immunotherapy* (2010) **33**:570–590. doi:10.1097/CJI.0b013e3181e032e8

16. Davies H, Bignell GR, Cox C, Stephens P, Edkins S, Clegg S, Teague J, Woffendin H, Garnett MJ, Bottomley W, et al. Mutations of the BRAF gene in human cancer. *Nature* (2002) **417**:949–954. doi:10.1038/nature00766

17. Daniotti M, Oggionni M, Ranzani T, Vallacchi V, Campi V, Di Stasi D, Torre GD, Perrone F, Luoni C, Suardi S, et al. BRAF alterations are associated with complex mutational profiles in malignant melanoma. *Oncogene* (2004) **23**:5968–5977. doi:10.1038/sj.onc.1207780

18. Maldonado JL, Fridlyand J, Patel H, Jain AN, Busam K, Kageshita T, Ono T, Albertson DG, Pinkel D, Bastian BC. Determinants of BRAF mutations in primary melanomas. *J Natl Cancer Inst* (2003) **95**:1878–1890.

19. YOUNG J, BARKER M, SIMMS L, WALSH M, BIDEN K, BUCHANAN D, BUTTENSHAW R, WHITEHALL V, ARNOLD S, JACKSON L. Evidence for BRAF mutation and variable levels of microsatellite instability in a syndrome of familial colorectal cancer. *Clinical Gastroenterology and Hepatology* (2005) **3**:254–263. doi:10.1016/S1542-3565(04)00673-1

20. Michaloglou C, Vredeveld LCW, Soengas MS, Denoyelle C, Kuilman T, van der Horst CMAM, Majoor DM, Shay JW, Mooi WJ, Peeper DS. BRAFE600-associated senescence-like cell cycle arrest of human naevi. *Nature* (2005) **436**:720–724. doi:10.1038/nature03890

21. Rajakulendran T, Sahmi M, Lefrançois M, Sicheri F, Therrien M. A dimerization-dependent mechanism drives RAF catalytic activation. *Nature* (2009) **461**:542–545. doi:10.1038/nature08314

22. Hoeflich KP, Gray DC, Eby MT, Tien JY, Wong L, Bower J, Gogineni A, Zha J, Cole MJ, Stern HM, et al. Oncogenic BRAF is required for tumor growth and maintenance in melanoma models. *Cancer Res* (2006) **66**:999–1006. doi:10.1158/0008-5472.CAN-05-2720

23. Joseph EW, Pratilas CA, Poulikakos PI, Tadi M, Wang W, Taylor BS, Halilovic E, Persaud Y, Xing F, Viale A, et al. The RAF inhibitor PLX4032 inhibits ERK signaling and tumor cell proliferation in a V600E BRAF-selective manner. *Proc Natl Acad Sci USA* (2010) **107**:14903–14908. doi:10.1073/pnas.1008990107

24. Bollag G, Hirth P, Tsai J, Zhang J, Ibrahim PN, Cho H, Spevak W, Zhang C, Zhang Y, Habets G, et al. Clinical efficacy of a RAF inhibitor needs broad target blockade in BRAF-mutant melanoma. *Nature* (2010) **467**:596–599. doi:10.1038/nature09454

25. Sosman JA, Kim KB, Schuchter L, Gonzalez R, Pavlick AC, Weber JS, McArthur GA, Hutson TE, Moschos SJ, Flaherty KT, et al. Survival in BRAF V600-mutant advanced

melanoma treated with vemurafenib. *N Engl J Med* (2012) **366**:707–714. doi:10.1056/NEJMoa1112302

26. Hauschild A, Grob J-J, Demidov LV, Jouary T, Gutzmer R, Millward M, Rutkowski P, Blank CU, Miller WH, Kaempgen E, et al. Dabrafenib in BRAF-mutated metastatic melanoma: a multicentre, open-label, phase 3 randomised controlled trial. *Lancet* (2012) **380**:358–365. doi:10.1016/S0140-6736(12)60868-X

27. Long GV, Stroyakovskiy D, Gogas H, Levchenko E, de Braud F, Larkin J, Garbe C, Jouary T, Hauschild A, Grob J-J, et al. Combined BRAF and MEK inhibition versus BRAF inhibition alone in melanoma. *N Engl J Med* (2014) **371**:1877–1888. doi:10.1056/NEJMoa1406037

28. Larkin J, Ascierto PA, Dréno B, Atkinson V, Liszkay G, Maio M, Mandalà M, Demidov L, Stroyakovskiy D, Thomas L, et al. Combined Vemurafenib and Cobimetinib in BRAF-Mutated Melanoma. *N Engl J Med* (2014) **371**:1867–1876. doi:10.1056/NEJMoa1408868

29. Robert C, Karaszewska B, Schachter J, Rutkowski P, Mackiewicz A, Stroiakovski D, Lichinitser M, Dummer R, Grange F, Mortier L, et al. Improved overall survival in melanoma with combined dabrafenib and trametinib. *N Engl J Med* (2015) **372**:30–39. doi:10.1056/NEJMoa1412690

30. Kalialis LV, Drzewiecki KT, Klyver H. Spontaneous regression of metastases from melanoma: review of the literature. *Melanoma Res* (2009) **19**:275–282. doi:10.1097/CMR.0b013e32832eabd5

31. Wenzel J, Bekisch B, Uerlich M, Haller O, Bieber T, Tüting T. Type I interferon-associated recruitment of cytotoxic lymphocytes: a common mechanism in regressive melanocytic lesions. *American Journal of Clinical Pathology* (2005) **124**:37–48. doi:10.1309/4EJ9KL7CGDENVVLE

32. Boon T, van der Bruggen P. Human tumor antigens recognized by T lymphocytes. *Journal of Experimental Medicine* (1996) **183**:725–729.

33. Houghton AN, Gold JS, Blachere NE. Immunity against cancer: lessons learned from melanoma. *Curr Opin Immunol* (2001) **13**:134–140.

34. Pardoll DM. The blockade of immune checkpoints in cancer immunotherapy. *Nat Rev Cancer* (2012) **12**:252–264. doi:10.1038/nrc3239

35. Linsley PS, Greene JL, Brady W, Bajorath J, Ledbetter JA, Peach R. Human B7-1 (CD80) and B7-2 (CD86) bind with similar avidities but distinct kinetics to CD28 and CTLA-4 receptors. *Immunity* (1994) **1**:793–801.

36. Rudd CE, Taylor A, Schneider H. CD28 and CTLA-4 coreceptor expression and signal transduction. *Immunol Rev* (2009) **229**:12–26. doi:10.1111/j.1600-065X.2009.00770.x

37. Qureshi OS, Zheng Y, Nakamura K, Attridge K, Manzotti C, Schmidt EM, Baker J, Jeffery LE, Kaur S, Briggs Z, et al. Trans-endocytosis of CD80 and CD86: a molecular basis for the cell-extrinsic function of CTLA-4. *Science* (2011) **332**:600–603. doi:10.1126/science.1202947

38. Wing K, Onishi Y, Prieto-Martin P, Yamaguchi T, Miyara M, Fehervari Z, Nomura T, Sakaguchi S. CTLA-4 control over Foxp3+ regulatory T cell function. *Science* (2008) **322**:271–275. doi:10.1126/science.1160062

39. Peggs KS, Quezada SA, Chambers CA, Korman AJ, Allison JP. Blockade of CTLA-4 on both effector and regulatory T cell compartments contributes to the antitumor activity of anti-CTLA-4 antibodies. *J Exp Med* (2009) **206**:1717–1725. doi:10.1084/jem.20082492

40. Robert C, Thomas L, Bondarenko I, O'Day S, Weber J, Garbe C, Lebbé C, Baurain J-F, Testori A, Grob J-J, et al. Ipilimumab plus dacarbazine for previously untreated metastatic melanoma. *N Engl J Med* (2011) **364**:2517–2526. doi:10.1056/NEJMoa1104621

41. Keir ME, Butte MJ, Freeman GJ, Sharpe AH. PD-1 and its ligands in tolerance and immunity. *Annu Rev Immunol* (2008) **26**:677–704. doi:10.1146/annurev.immunol.26.021607.090331

42. Freeman GJ, Long AJ, Iwai Y, Bourque K, Chernova T, Nishimura H, Fitz LJ, Malenkovich N, Okazaki T, Byrne MC, et al. Engagement of the PD-1 immunoinhibitory receptor by a novel B7 family member leads to negative regulation of lymphocyte activation. *Journal of Experimental Medicine* (2000) **192**:1027–1034.

43. Wherry EJ. T cell exhaustion. *Nature Publishing Group* (2011) **131**:492–499. doi:10.1038/ni.2035

44. Barber DL, Wherry EJ, Masopust D, Zhu B, Allison JP, Sharpe AH, Freeman GJ, Ahmed R. Restoring function in exhausted CD8 T cells during chronic viral infection. *Nature* (2006) **439**:682–687. doi:10.1038/nature04444

45. Terme M, Ullrich E, Aymeric L, Meinhardt K, Desbois M, Delahaye N, Viaud S, Ryffel B, Yagita H, Kaplanski G, et al. IL-18 induces PD-1-dependent immunosuppression in cancer. *Cancer Res* (2011) **71**:5393–5399. doi:10.1158/0008-5472.CAN-11-0993

46. Fanoni D, Tavecchio S, Recalcati S, Balice Y, Venegoni L, Fiorani R, Crosti C, Berti E. New monoclonal antibodies against B-cell antigens: Possible new strategies for diagnosis of primary cutaneous B-cell lymphomas. *Immunology Letters* (2011) **134**:157–160. doi:10.1016/j.imlet.2010.09.022

47. Robert C, Long GV, Brady B, Dutriaux C, Maio M, Mortier L, Hassel JC, Rutkowski P, McNeil C, Kalinka-Warzocha E, et al. Nivolumab in Previously Untreated Melanoma without BRAFMutation. *N Engl J Med* (2015) **372**:320–330. doi:10.1056/NEJMoa1412082

48. Robert C, Schachter J, Long GV, Arance A, Grob J-J, Mortier L, Daud A, Carlino MS, McNeil C, Lotem M, et al. Pembrolizumab versus Ipilimumab in Advanced Melanoma. *N Engl J Med* (2015) **372**:2521–2532. doi:10.1056/NEJMoa1503093

49. Dong H, Strome SE, Salomao DR, Tamura H, Hirano F, Flies DB, Roche PC, Lu J, Zhu G, Tamada K, et al. Tumor-associated B7-H1 promotes T-cell apoptosis: a potential mechanism of immune evasion. *Nat Med* (2002) **8**:793–800. doi:10.1038/nm730

50. Curiel TJ, Wei S, Dong H, Alvarez X, Cheng P, Mottram P, Krzysiek R, Knutson KL, Daniel B, Zimmermann MC, et al. Blockade of B7-H1 improves myeloid dendritic cell-

mediated antitumor immunity. *Nat Med* (2003) **9**:562–567. doi:10.1038/nm863

51. Parsa AT, Waldron JS, Panner A, Crane CA, Parney IF, Barry JJ, Cachola KE, Murray JC, Tihan T, Jensen MC, et al. Loss of tumor suppressor PTEN function increases B7-H1 expression and immunoresistance in glioma. *Nat Med* (2007) **13**:84–88. doi:10.1038/nm1517

52. Marzec M, Zhang Q, Goradia A, Raghunath PN, Liu X, Paessler M, Wang HY, Wysocka M, Cheng M, Ruggeri BA, et al. Oncogenic kinase NPM/ALK induces through STAT3 expression of immunosuppressive protein CD274 (PD-L1, B7-H1). *Proc Natl Acad Sci USA* (2008) **105**:20852–20857. doi:10.1073/pnas.0810958105

53. Taube JM, Anders RA, Young GD, Xu H, Sharma R, McMiller TL, Chen S, Klein AP, Pardoll DM, Topalian SL, et al. Colocalization of inflammatory response with B7-h1 expression in human melanocytic lesions supports an adaptive resistance mechanism of immune escape. *Sci Transl Med* (2012) **4**:127ra37–127ra37. doi:10.1126/scitranslmed.3003689

54. Larkin J, Chiarion-Sileni V, Gonzalez R, Grob J-J, Cowey CL, Lao CD, Schadendorf D, Dummer R, Smylie M, Rutkowski P, et al. Combined Nivolumab and Ipilimumab or Monotherapy in Untreated Melanoma. *N Engl J Med* (2015) **373**:23–34. doi:10.1056/NEJMoa1504030

55. Moreau-Aubry A, Le Guiner S, Labarrière N, Gesnel MC, Jotereau F, Breathnach R. A processed pseudogene codes for a new antigen recognized by a CD8(+) T cell clone on melanoma. *Journal of Experimental Medicine* (2000) **191**:1617–1624.

56. Van den Eynde BJ, Gaugler B, Probst-Kepper M, Michaux L, Devuyst O, Lorge F, Weynants P, Boon T. A new antigen recognized by cytolytic T lymphocytes on a human kidney tumor results from reverse strand transcription. *Journal of Experimental Medicine* (1999) **190**:1793–1800. doi:10.1084/jem.190.12.1793

57. Zarling AL, Polefrone JM, Evans AM, Mikesh LM, Shabanowitz J, Lewis ST, Engelhard VH, Hunt DF. Identification of class I MHC-associated phosphopeptides as targets for cancer immunotherapy. *Proceedings of the National Academy of Sciences* (2006) **103**:14889–14894. doi:10.1073/pnas.0604045103

58. Fratta E, Coral S, Covre A, Parisi G, Colizzi F, Danielli R, Nicolay HJM, Sigalotti L, Maio M. The biology of cancer testis antigens: putative function, regulation and therapeutic potential. *Mol Oncol* (2011) **5**:164–182. doi:10.1016/j.molonc.2011.02.001

59. Livingston PO, Wong GY, Adluri S, Tao Y, Padavan M, Parente R, Hanlon C, Calves MJ, Helling F, Ritter G. Improved survival in stage III melanoma patients with GM2 antibodies: a randomized trial of adjuvant vaccination with GM2 ganglioside. *Journal of Clinical Oncology* (1994) **12**:1036–1044.

60. Blankenstein T, Coulie PG, Gilboa E, Jaffee EM. The determinants of tumour immunogenicity. *Nat Rev Cancer* (2012) **12**:307–313. doi:10.1038/nrc3246

61. Kawakami Y, Dang N, Wang X, Tupesis J, Robbins PF, Wang R-F, Wunderlich JR, Yannelli JR, Rosenberg SA. Recognition of Shared Melanoma Antigens in Association With Major HLA-A Alleles by Tumor Infiltrating T Lymphocytes From 123 Patients With Melanoma. *Journal of Immunotherapy* (2000) **23**:17–27. doi:10.1097/00002371-

200001000-00004

62. Rosenberg SA, Yang JC, Schwartzentruber DJ, Hwu P, Marincola FM, Topalian SL, Restifo NP, Dudley ME, Schwarz SL, Spiess PJ, et al. Immunologic and therapeutic evaluation of a synthetic peptide vaccine for the treatment of patients with metastatic melanoma. *Nat Med* (1998) **4**:321–327. doi:10.1038/nm0398-321

63. Smith JW. Adjuvant Immunization of HLA-A2-Positive Melanoma Patients With a Modified gp100 Peptide Induces Peptide-Specific CD8+ T-Cell Responses. *Journal of Clinical Oncology* (2003) **21**:1562–1573. doi:10.1200/JCO.2003.09.020

64. Hargadon KM. Melanoma Immunotherapy: Overcoming Obstacles to Augment Anti-Tumor Immune Responses. *Journal of Cosmetics, Dermatological Sciences and Applications* (2013) **03**:7–27. doi:10.4236/jcdsa.2013.32A002

65. Slingluff CL, Petroni GR, Yamshchikov GV, Hibbitts S, Grosh WW, Chianese-Bullock KA, Bissonette EA, Barnd DL, Deacon DH, Patterson JW, et al. Immunologic and clinical outcomes of vaccination with a multiepitope melanoma peptide vaccine plus low-dose interleukin-2 administered either concurrently or on a delayed schedule. *Journal of Clinical Oncology* (2004) **22**:4474–4485. doi:10.1200/JCO.2004.10.212

66. Tagawa ST, Lee P, Snively J, Boswell W, Ounpraseuth S, Lee S, Hickingbottom B, Smith J, Johnson D, Weber JS. Phase I study of intranodal delivery of a plasmid DNA vaccine for patients with Stage IV melanoma. *Cancer* (2003) **98**:144–154. doi:10.1002/cncr.11462

67. Weber J, Boswell W, Smith J, Hersh E, Snively J, Diaz M, Miles S, Liu X, Obrocea M, Qiu Z, et al. Phase 1 Trial of Intranodal Injection of a Melan-A/MART-1 DNA Plasmid Vaccine in Patients With Stage IV Melanoma. *Journal of Immunotherapy* (2008) **31**:215–223. doi:10.1097/CJI.0b013e3181611420

68. Leitner WW, Hwang LN, deVeer MJ, Zhou A, Silverman RH, Williams BRG, Dubensky TW, Ying H, Restifo NP. Alphavirus-based DNA vaccine breaks immunological tolerance by activating innate antiviral pathways. *Nat Med* (2002) **9**:33–39. doi:10.1038/nm813

69. Hangalapura BN, Oosterhoff D, Gupta T, de Groot J, Wijnands PGJTB, van Beusechem VW, Haan den J, Tüting T, van den Eertwegh AJM, Curiel DT, et al. Delivery route, MyD88 signaling and cross-priming events determine the anti-tumor efficacy of an adenovirus based melanoma vaccine. *Vaccine* (2011) **29**:2313–2321. doi:10.1016/j.vaccine.2011.01.022

70. Oertli D, Marti WR, Zajac P, Noppen C, Kocher T, Padovan E, Adamina M, Schumacher R, Harder F, Heberer M, et al. Rapid Induction of Specific Cytotoxic T Lymphocytes Against Melanoma-Associated Antigens by a Recombinant Vaccinia Virus Vector Expressing Multiple Immunodominant Epitopes and Costimulatory Molecules In Vivo. *Human Gene Therapy* (2002) **13**:569–575. doi:10.1089/10430340252809856

71. Zajac P, Oertli D, Marti W, Adamina M, Bolli M, Guller U, Noppen C, Padovan E, Schultz-Thater E, Heberer M, et al. Phase I/II clinical trial of a nonreplicative vaccinia virus expressing multiple HLA-A0201-restricted tumor-associated epitopes and costimulatory molecules in metastatic melanoma patients. *Human Gene Therapy* (2003) **14**:1497–1510. doi:10.1089/104303403322495016

72. Haj-Ahmad Y, Graham FL. Development of a helper-independent human adenovirus vector and its use in the transfer of the herpes simplex virus thymidine kinase gene. *Journal of Virology* (1986) **57**:267–274.

73. Wilson JM. Adenoviruses as Gene-Delivery Vehicles. *N Engl J Med* (1996) **334**:1185–1187. doi:10.1056/NEJM199605023341809

74. Tatsis N, Ertl HCJ. Adenoviruses as vaccine vectors. *Mol Ther* (2004) **10**:616–629. doi:10.1016/j.ymthe.2004.07.013

75. Tatsis N, Tesema L, Robinson ER, Giles-Davis W, McCoy K, Gao GP, Wilson JM, Ertl HCJ. Chimpanzee-origin adenovirus vectors as vaccine carriers. *Gene Ther* (2006) **13**:421–429. doi:10.1038/sj.gt.3302675

76. Kootstra NA, Verma IM. Gene therapy with viral vectors. *Annu Rev Pharmacol Toxicol* (2003) **43**:413–439. doi:10.1146/annurev.pharmtox.43.100901.140257

77. Tatsis N, Fitzgerald JC, Reyes-Sandoval A, Harris-McCoy KC, Hensley SE, Zhou D, Lin S-W, Bian A, Xiang ZQ, Iparraguirre A, et al. Adenoviral vectors persist in vivo and maintain activated CD8+ T cells: implications for their use as vaccines. *Blood* (2007) **110**:1916–1923. doi:10.1182/blood-2007-02-062117

78. Chen H, Xiang ZQ, Li Y, Kurupati RK, Jia B, Bian A, Zhou DM, Hutnick N, Yuan S, Gray C, et al. Adenovirus-based vaccines: comparison of vectors from three species of adenoviridae. *Journal of Virology* (2010) **84**:10522–10532. doi:10.1128/JVI.00450-10

79. Zhang X, Munegowda MA, Yuan J, Wei Y, Xiang J. Optimal TLR9 signal converts tolerogenic CD4-8- DCs into immunogenic ones capable of stimulating antitumor immunity via activating CD4+ Th1/Th17 and NK cell responses. *J Leukoc Biol* (2010) **88**:393–403. doi:10.1189/jlb.0909633

80. Lambert LA, Gibson GR, Maloney M, Durell B, Noelle RJ, Barth RJ. Intranodal immunization with tumor lysate-pulsed dendritic cells enhances protective antitumor immunity. *Cancer Res* (2001) **61**:641–646.

81. Mullins DW, Sheasley SL, Ream RM, Bullock TNJ, Fu Y-X, Engelhard VH. Route of immunization with peptide-pulsed dendritic cells controls the distribution of memory and effector T cells in lymphoid tissues and determines the pattern of regional tumor control. *Journal of Experimental Medicine* (2003) **198**:1023–1034. doi:10.1084/jem.20021348

82. Aarntzen EHJG, De Vries IJM, Lesterhuis WJ, Schuurhuis D, Jacobs JFM, Bol K, Schreibelt G, Mus R, De Wilt JHW, Haanen JBAG, et al. Targeting CD4(+) T-helper cells improves the induction of antitumor responses in dendritic cell-based vaccination. *Cancer Res* (2013) **73**:19–29. doi:10.1158/0008-5472.CAN-12-1127

83. Engell-Noerregaard L, Hansen TH, Andersen MH, Thor Straten P, Svane IM. Review of clinical studies on dendritic cell-based vaccination of patients with malignant melanoma: assessment of correlation between clinical response and vaccine parameters. *Cancer Immunol Immunother* (2009) **58**:1–14. doi:10.1007/s00262-008-0568-4

84. Boczkowski D, Lee J, Pruitt S, Nair S. Dendritic cells engineered to secrete anti-GITR antibodies are effective adjuvants to dendritic cell-based immunotherapy. *Cancer Gene Therapy* (2009) **16**:900–911. doi:10.1038/cgt.2009.39

85. Han TH, Jin P, Ren J, Slezak S, Marincola FM, Stroncek DF. Evaluation of 3 Clinical Dendritic Cell Maturation Protocols Containing Lipopolysaccharide and Interferon-γ. *Journal of Immunotherapy* (2009) **32**:399–407. doi:10.1097/CJI.0b013e31819e1773

86. Jonuleit H, Giesecke-Tuettenberg A, T ting T, Thurner-Schuler B, Stuge TB, Paragnik L, Kandemir A, Lee PP, Schuler G, Knop JR, et al. A comparison of two types of dendritic cell as adjuvants for the induction of melanoma-specific T-cell responses in humans following intranodal injection. *International Journal of Cancer* (2001) **93**:243–251. doi:10.1002/ijc.1323

87. Lesimple T, Neidhard E-M, Vignard V, Lefeuvre C, Adamski H, Labarrière N, Carsin A, Monnier D, Collet B, Clapisson G, et al. Immunologic and clinical effects of injecting mature peptide-loaded dendritic cells by intralymphatic and intranodal routes in metastatic melanoma patients. *Clinical Cancer Research* (2006) **12**:7380–7388. doi:10.1158/1078-0432.CCR-06-1879

88. Butterfield LH, Comin-Anduix B, Vujanovic L, Lee Y, Dissette VB, Yang J-Q, Vu HT, Seja E, Oseguera DK, Potter DM, et al. Adenovirus MART-1-engineered autologous dendritic cell vaccine for metastatic melanoma. *Journal of Immunotherapy* (2008) **31**:294–309. doi:10.1097/CJI.0b013e31816a8910

89. Rosenberg SA, Restifo NP. Adoptive cell transfer as personalized immunotherapy for human cancer. *Science* (2015) **348**:62–68. doi:10.1126/science.aaa4967

90. Rosenberg SA, Packard BS, Aebersold PM, Solomon D, Topalian SL, Toy ST, Simon P, Lotze MT, Yang JC, Seipp CA. Use of tumor-infiltrating lymphocytes and interleukin-2 in the immunotherapy of patients with metastatic melanoma. A preliminary report. *N Engl J Med* (1988) **319**:1676–1680. doi:10.1056/NEJM198812223192527

91. Dudley ME, Wunderlich JR, Robbins PF, Yang JC, Hwu P, Schwartzentruber DJ, Topalian SL, Sherry R, Restifo NP, Hubicki AM, et al. Cancer regression and autoimmunity in patients after clonal repopulation with antitumor lymphocytes. *Science* (2002) **298**:850–854. doi:10.1126/science.1076514

92. Bronte V, Wang M, Overwijk WW, Surman DR, Pericle F, Rosenberg SA, Restifo NP. Apoptotic death of CD8+ T lymphocytes after immunization: induction of a suppressive population of Mac-1+/Gr-1+ cells. *J Immunol* (1998) **161**:5313–5320.

93. Dudley ME, Yang JC, Sherry R, Hughes MS, Royal R, Kammula U, Robbins PF, Huang J, Citrin DE, Leitman SF, et al. Adoptive cell therapy for patients with metastatic melanoma: evaluation of intensive myeloablative chemoradiation preparative regimens. *J Clin Oncol* (2008) **26**:5233–5239. doi:10.1200/JCO.2008.16.5449

94. Lawrence MS, Stojanov P, Polak P, Kryukov GV, Cibulskis K, Sivachenko A, Carter SL, Stewart C, Mermel CH, Roberts SA, et al. Mutational heterogeneity in cancer and the search for new cancer-associated genes. *Nature* (2013) **499**:214–218. doi:10.1038/nature12213

95. Carreno BM, Magrini V, Becker-Hapak M, Kaabinejadian S, Hundal J, Petti AA, Ly A, Lie WR, Hildebrand WH, Mardis ER, et al. A dendritic cell vaccine increases the breadth and diversity of melanoma neoantigen-specific T cells. *Science* (2015) **348**:803–808. doi:10.1126/science.aaa3828

96. Robbins PF, Lu Y-C, El-Gamil M, Li YF, Gross C, Gartner J, Lin JC, Teer JK, Cliften P, Tycksen E, et al. Mining exomic sequencing data to identify mutated antigens recognized by adoptively transferred tumor-reactive T cells. *Nat Med* (2013) **19**:747–752. doi:10.1038/nm.3161

97. Lu Y-C, Yao X, Crystal JS, Li YF, El-Gamil M, Gross C, Davis L, Dudley ME, Yang JC, Samuels Y, et al. Efficient identification of mutated cancer antigens recognized by T cells associated with durable tumor regressions. *Clinical Cancer Research* (2014) **20**:3401–3410. doi:10.1158/1078-0432.CCR-14-0433

98. Maude SL, Frey N, Shaw PA, Aplenc R, Barrett DM, Bunin NJ, Chew A, Gonzalez VE, Zheng Z, Lacey SF, et al. Chimeric antigen receptor T cells for sustained remissions in leukemia. *N Engl J Med* (2014) **371**:1507–1517. doi:10.1056/NEJMoa1407222

99. Kalos M, Levine BL, Porter DL, Katz S, Grupp SA, Bagg A, June CH. T cells with chimeric antigen receptors have potent antitumor effects and can establish memory in patients with advanced leukemia. *Sci Transl Med* (2011) **3**:95ra73–95ra73. doi:10.1126/scitranslmed.3002842

100. Buchholz VR, Flossdorf M, Hensel I, Kretschmer L, Weissbrich B, Gräf P, Verschoor A, Schiemann M, Höfer T, Busch DH. Disparate individual fates compose robust CD8+ T cell immunity. *Science* (2013) **340**:630–635. doi:10.1126/science.1235454

101. Gerlach C, Rohr JC, Perié L, van Rooij N, van Heijst JWJ, Velds A, Urbanus J, Naik SH, Jacobs H, Beltman JB, et al. Heterogeneous differentiation patterns of individual CD8+ T cells. *Science* (2013) **340**:635–639. doi:10.1126/science.1235487

102. Tran E, Turcotte S, Gros A, Robbins PF, Lu Y-C, Dudley ME, Wunderlich JR, Somerville RP, Hogan K, Hinrichs CS, et al. Cancer immunotherapy based on mutation-specific CD4+ T cells in a patient with epithelial cancer. *Science* (2014) **344**:641–645. doi:10.1126/science.1251102

103. Blackburn SD, Shin H, Haining WN, Zou T, Workman CJ, Polley A, Betts MR, Freeman GJ, Vignali DAA, Wherry EJ. Coregulation of CD8+ T cell exhaustion by multiple inhibitory receptors during chronic viral infection. *Nat Immunol* (2009) **10**:29–37. doi:10.1038/ni.1679

104. Doering TA, Crawford A, Angelosanto JM, Paley MA, Ziegler CG, Wherry EJ. Network analysis reveals centrally connected genes and pathways involved in CD8+ T cell exhaustion versus memory. *Immunity* (2012) **37**:1130–1144. doi:10.1016/j.immuni.2012.08.021

105. Crawford A, Angelosanto JM, Kao C, Doering TA, Odorizzi PM, Barnett BE, Wherry EJ. Molecular and transcriptional basis of $CD4^+$ T cell dysfunction during chronic infection. *Immunity* (2014) **40**:289–302. doi:10.1016/j.immuni.2014.01.005

106. Intlekofer AM, Takemoto N, Kao C, Banerjee A, Schambach F, Northrop JK, Shen H, Wherry EJ, Reiner SL. Requirement for T-bet in the aberrant differentiation of unhelped memory CD8+ T cells. *Journal of Experimental Medicine* (2007) **204**:2015–2021. doi:10.1084/jem.20070841

107. Banerjee A, Gordon SM, Intlekofer AM, Paley MA, Mooney EC, Lindsten T, Wherry EJ, Reiner SL. Cutting edge: The transcription factor eomesodermin enables CD8+ T cells

to compete for the memory cell niche. *J Immunol* (2010) **185**:4988–4992. doi:10.4049/jimmunol.1002042

108. Paley MA, Kroy DC, Odorizzi PM, Johnnidis JB, Dolfi DV, Barnett BE, Bikoff EK, Robertson EJ, Lauer GM, Reiner SL, et al. Progenitor and terminal subsets of CD8+ T cells cooperate to contain chronic viral infection. *Science* (2012) **338**:1220–1225. doi:10.1126/science.1229620

109. Buggert M, Tauriainen J, Yamamoto T, Frederiksen J, Ivarsson MA, Michaëlsson J, Lund O, Hejdeman B, Jansson M, Sönnerborg A, et al. T-bet and Eomes are differentially linked to the exhausted phenotype of CD8+ T cells in HIV infection. *PLoS Pathog* (2014) **10**:e1004251. doi:10.1371/journal.ppat.1004251

110. Youngblood B, Oestreich KJ, Ha S-J, Duraiswamy J, Akondy RS, West EE, Wei Z, Lu P, Austin JW, Riley JL, et al. Chronic virus infection enforces demethylation of the locus that encodes PD-1 in antigen-specific CD8(+) T cells. *Immunity* (2011) **35**:400–412. doi:10.1016/j.immuni.2011.06.015

111. Wherry EJ, Blattman JN, Murali-Krishna K, van der Most R, Ahmed R. Viral persistence alters CD8 T-cell immunodominance and tissue distribution and results in distinct stages of functional impairment. *Journal of Virology* (2003) **77**:4911–4927. doi:10.1128/JVI.77.8.4911-4927.2003

112. Streeck H, Brumme ZL, Anastario M, Cohen KW, Jolin JS, Meier A, Brumme CJ, Rosenberg ES, Alter G, Allen TM, et al. Antigen load and viral sequence diversification determine the functional profile of HIV-1-specific CD8+ T cells. *PLoS Med* (2008) **5**:e100. doi:10.1371/journal.pmed.0050100

113. Tumeh PC, Harview CL, Yearley JH, Shintaku IP, Taylor EJM, Robert L, Chmielowski B, Spasic M, Henry G, Ciobanu V, et al. PD-1 blockade induces responses by inhibiting adaptive immune resistance. *Nature* (2014) **515**:568–571. doi:10.1038/nature13954

114. Riley JL. PD-1 signaling in primary T cells. *Immunol Rev* (2009) **229**:114–125. doi:10.1111/j.1600-065X.2009.00767.x

115. Deaglio S, Dwyer KM, Gao W, Friedman D, Usheva A, Erat A, Chen J-F, Enjyoji K, Linden J, Oukka M, et al. Adenosine generation catalyzed by CD39 and CD73 expressed on regulatory T cells mediates immune suppression. *Journal of Experimental Medicine* (2007) **204**:1257–1265. doi:10.1084/jem.20062512

116. Thornton AM, Shevach EM. CD4+CD25+ immunoregulatory T cells suppress polyclonal T cell activation in vitro by inhibiting interleukin 2 production. *Journal of Experimental Medicine* (1998) **188**:287–296.

117. Annacker O, Asseman C, Read S, Powrie F. Interleukin-10 in the regulation of T cell-induced colitis. *J Autoimmun* (2003) **20**:277–279.

118. Thomas DA, Massagué J. TGF-beta directly targets cytotoxic T cell functions during tumor evasion of immune surveillance. *Cancer Cell* (2005) **8**:369–380. doi:10.1016/j.ccr.2005.10.012

119. Kim Y-J, Park S-J, Broxmeyer HE. Phagocytosis, a potential mechanism for myeloid-derived suppressor cell regulation of CD8+ T cell function mediated through

programmed cell death-1 and programmed cell death-1 ligand interaction. *J Immunol* (2011) **187**:2291–2301. doi:10.4049/jimmunol.1002650

120. Hurwitz AA, Watkins SK. Immune suppression in the tumor microenvironment: a role for dendritic cell-mediated tolerization of T cells. *Cancer Immunol Immunother* (2012) **61**:289–293. doi:10.1007/s00262-011-1181-5

121. Wherry EJ, Kurachi M. Molecular and cellular insights into T cell exhaustion. *Nature Reviews Immunology* (2015) **15**:486–499. doi:10.1038/nri3862

122. Santos AM, Jung J, Aziz N, Kissil JL, Puré E. Targeting fibroblast activation protein inhibits tumor stromagenesis and growth in mice. *J Clin Invest* (2009) **119**:3613–3625. doi:10.1172/JCI38988

123. Bhowmick NA, Neilson EG, Moses HL. Stromal fibroblasts in cancer initiation and progression. *Nature* (2004) **432**:332–337. doi:10.1038/nature03096

124. Kraman M, Bambrough PJ, Arnold JN, Roberts EW, Magiera L, Jones JO, Gopinathan A, Tuveson DA, Fearon DT. Suppression of antitumor immunity by stromal cells expressing fibroblast activation protein-alpha. *Science* (2010) **330**:827–830. doi:10.1126/science.1195300

125. Mueller MM, Fusenig NE. Friends or foes - bipolar effects of the tumour stroma in cancer. *Nat Rev Cancer* (2004) **4**:839–849. doi:10.1038/nrc1477

126. Huber MA, Kraut N, Park JE, Schubert RD, Rettig WJ, Peter RU, Garin-Chesa P. Fibroblast activation protein: differential expression and serine protease activity in reactive stromal fibroblasts of melanocytic skin tumors. *J Invest Dermatol* (2003) **120**:182–188. doi:10.1046/j.1523-1747.2003.12035.x

127. Brennen WN, Isaacs JT, Denmeade SR. Rationale behind targeting fibroblast activation protein-expressing carcinoma-associated fibroblasts as a novel chemotherapeutic strategy. *Mol Cancer Ther* (2012) **11**:257–266. doi:10.1158/1535-7163.MCT-11-0340

128. Mace TA, Ameen Z, Collins A, Wojcik S, Mair M, Young GS, Fuchs JR, Eubank TD, Frankel WL, Bekaii-Saab T, et al. Pancreatic cancer-associated stellate cells promote differentiation of myeloid-derived suppressor cells in a STAT3-dependent manner. *Cancer Res* (2013) **73**:3007–3018. doi:10.1158/0008-5472.CAN-12-4601

129. Comito G, Giannoni E, Segura CP, Barcellos-de-Souza P, Raspollini MR, Baroni G, Lanciotti M, Serni S, Chiarugi P. Cancer-associated fibroblasts and M2-polarized macrophages synergize during prostate carcinoma progression. *Oncogene* (2014) **33**:2423–2431. doi:10.1038/onc.2013.191

130. Poznansky MC, Olszak IT, Foxall R, Evans RH, Luster AD, Scadden DT. Active movement of T cells away from a chemokine. *Nat Med* (2000) **6**:543–548. doi:10.1038/75022

131. Gottschalk S, Yu F, Ji M, Kakarla S, Song X-T. A vaccine that co-targets tumor cells and cancer associated fibroblasts results in enhanced antitumor activity by inducing antigen spreading. *PLoS ONE* (2013) **8**:e82658. doi:10.1371/journal.pone.0082658

132. Kakarla S, Chow KKH, Mata M, Shaffer DR, Song X-T, Wu M-F, Liu H, Wang LL,

Rowley DR, Pfizenmaier K, et al. Antitumor effects of chimeric receptor engineered human T cells directed to tumor stroma. *Mol Ther* (2013) **21**:1611–1620. doi:10.1038/mt.2013.110

133. Wang L-CS, Lo A, Scholler J, Sun J, Majumdar RS, Kapoor V, Antzis M, Cotner CE, Johnson LA, Durham AC, et al. Targeting fibroblast activation protein in tumor stroma with chimeric antigen receptor T cells can inhibit tumor growth and augment host immunity without severe toxicity. *Cancer Immunol Res* (2014) **2**:154–166. doi:10.1158/2326-6066.CIR-13-0027

134. Qian B-Z, Pollard JW. Macrophage diversity enhances tumor progression and metastasis. *Cell* (2010) **141**:39–51. doi:10.1016/j.cell.2010.03.014

135. Mosser DM, Edwards JP. Exploring the full spectrum of macrophage activation. *Nature Reviews Immunology* (2008) **8**:958–969. doi:10.1038/nri2448

136. Biswas SK, Mantovani A. Macrophage plasticity and interaction with lymphocyte subsets: cancer as a paradigm. *Nat Immunol* (2010) **11**:889–896. doi:10.1038/ni.1937

137. Gajewski TF, Schreiber H, Fu Y-X. Innate and adaptive immune cells in the tumor microenvironment. *Nature Publishing Group* (2013) **14**:1014–1022. doi:10.1038/ni.2703

138. Lewis C, Murdoch C. Macrophage responses to hypoxia: implications for tumor progression and anti-cancer therapies. *Am J Pathol* (2005) **167**:627–635. doi:10.1016/S0002-9440(10)62038-X

139. Condeelis J, Pollard JW. Macrophages: obligate partners for tumor cell migration, invasion, and metastasis. *Cell* (2006) **124**:263–266. doi:10.1016/j.cell.2006.01.007

140. Goswami S, Sahai E, Wyckoff JB, Cammer M, Cox D, Pixley FJ, Stanley ER, Segall JE, Condeelis JS. Macrophages promote the invasion of breast carcinoma cells via a colony-stimulating factor-1/epidermal growth factor paracrine loop. *Cancer Res* (2005) **65**:5278–5283. doi:10.1158/0008-5472.CAN-04-1853

141. Curiel TJ, Coukos G, Zou L, Alvarez X, Cheng P, Mottram P, Evdemon-Hogan M, Conejo-Garcia JR, Zhang L, Burow M, et al. Specific recruitment of regulatory T cells in ovarian carcinoma fosters immune privilege and predicts reduced survival. *Nat Med* (2004) **10**:942–949. doi:10.1038/nm1093

142. Joyce JA, Baruch A, Chehade K, Meyer-Morse N, Giraudo E, Tsai F-Y, Greenbaum DC, Hager JH, Bogyo M, Hanahan D. Cathepsin cysteine proteases are effectors of invasive growth and angiogenesis during multistage tumorigenesis. *Cancer Cell* (2004) **5**:443–453. doi:10.1038/nrc1396

143. Gabrilovich DI, Nagaraj S. Myeloid-derived suppressor cells as regulators of the immune system. *Nature Reviews Immunology* (2009) **9**:162–174. doi:10.1038/nri2506

144. Damuzzo V, Pinton L, Desantis G, Solito S, Marigo I, Bronte V, Mandruzzato S. Complexity and challenges in defining myeloid-derived suppressor cells. *Cytometry B Clin Cytom* (2015) **88**:77–91. doi:10.1002/cyto.b.21206

145. Movahedi K, Guilliams M, Van den Bossche J, Van den Bergh R, Gysemans C, Beschin A, De Baetselier P, Van Ginderachter JA. Identification of discrete tumor-induced

myeloid-derived suppressor cell subpopulations with distinct T cell-suppressive activity. *Blood* (2008) **111**:4233–4244. doi:10.1182/blood-2007-07-099226

146. Huang B, Pan P-Y, Li Q, Sato AI, Levy DE, Bromberg J, Divino CM, Chen S-H. Gr-1+CD115+ immature myeloid suppressor cells mediate the development of tumor-induced T regulatory cells and T-cell anergy in tumor-bearing host. *Cancer Res* (2006) **66**:1123–1131. doi:10.1158/0008-5472.CAN-05-1299

147. Gallina G, Dolcetti L, Serafini P, De Santo C, Marigo I, Colombo MP, Basso G, Brombacher F, Borrello I, Zanovello P, et al. Tumors induce a subset of inflammatory monocytes with immunosuppressive activity on CD8+ T cells. *J Clin Invest* (2006) **116**:2777–2790. doi:10.1172/JCI28828

148. Goñi O, Alcaide P, Fresno M. Immunosuppression during acute Trypanosoma cruzi infection: involvement of Ly6G (Gr1(+))CD11b(+)immature myeloid suppressor cells. *Int Immunol* (2002) **14**:1125–1134. doi:10.1093/intimm/dxf076

149. Giordanengo L, Guiñazú N, Stempin C, Fretes R, Cerbán F, Gea S. Cruzipain, a major Trypanosoma cruzi antigen, conditions the host immune response in favor of parasite. *Eur J Immunol* (2002) **32**:1003–1011. doi:10.1002/1521-4141(200204)32:4<1003::AID-IMMU1003>3.3.CO;2-G

150. Serafini P, Carbley R, Noonan KA, Tan G, Bronte V, Borrello I. High-dose granulocyte-macrophage colony-stimulating factor-producing vaccines impair the immune response through the recruitment of myeloid suppressor cells. *Cancer Res* (2004) **64**:6337–6343. doi:10.1158/0008-5472.CAN-04-0757

151. Bunt SK, Yang L, Sinha P, Clements VK, Leips J, Ostrand-Rosenberg S. Reduced Inflammation in the Tumor Microenvironment Delays the Accumulation of Myeloid-Derived Suppressor Cells and Limits Tumor Progression. *Cancer Res* (2007) **67**:10019–10026. doi:10.1158/0008-5472.CAN-07-2354

152. Gabrilovich D, Ishida T, Oyama T, Ran S, Kravtsov V, Nadaf S, Carbone DP. Vascular endothelial growth factor inhibits the development of dendritic cells and dramatically affects the differentiation of multiple hematopoietic lineages in vivo. *Blood* (1998) **92**:4150–4166.

153. Sawanobori Y, Ueha S, Kurachi M, Shimaoka T, Talmadge JE, Abe J, Shono Y, Kitabatake M, Kakimi K, Mukaida N, et al. Chemokine-mediated rapid turnover of myeloid-derived suppressor cells in tumor-bearing mice. *Blood* (2008) **111**:5457–5466. doi:10.1182/blood-2008-01-136895

154. Bromberg J. Stat proteins and oncogenesis. *J Clin Invest* (2002) **109**:1139–1142. doi:10.1172/JCI15617

155. Bronte V, Zanovello P. Regulation of immune responses by L-arginine metabolism. *Nature Reviews Immunology* (2005) **5**:641–654. doi:10.1038/nri1668

156. Rodríguez PC, Ochoa AC. Arginine regulation by myeloid derived suppressor cells and tolerance in cancer: mechanisms and therapeutic perspectives. *Immunol Rev* (2008) **222**:180–191. doi:10.1111/j.1600-065X.2008.00608.x

157. Vickers SM. Association of Increased Immunostaining for Inducible Nitric Oxide

Synthase and Nitrotyrosine With Fibroblast Growth Factor Transformation in Pancreatic Cancer. *Archives of Surgery* (1999) **134**:245–251. doi:10.1001/archsurg.134.3.245

158. Cobbs CS, Whisenhunt TR, Wesemann DR, Harkins LE, Van Meir EG, Samanta M. Inactivation of wild-type p53 protein function by reactive oxygen and nitrogen species in malignant glioma cells. *Cancer Res* (2003) **63**:8670–8673.

159. Nagaraj S, Gupta K, Pisarev V, Kinarsky L, Sherman S, Kang L, Herber DL, Schneck J, Gabrilovich DI. Altered recognition of antigen is a mechanism of CD8+ T cell tolerance in cancer. *Nat Med* (2007) **13**:828–835. doi:10.1038/nm1609

160. Kusmartsev S, Nagaraj S, Gabrilovich DI. Tumor-Associated CD8+ T Cell Tolerance Induced by Bone Marrow-Derived Immature Myeloid Cells. *The Journal of Immunology* (2005) **175**:4583–4592. doi:10.4049/jimmunol.175.7.4583

161. Yang R, Cai Z, Zhang Y, Yutzy WH, Roby KF, Roden RBS. CD80 in immune suppression by mouse ovarian carcinoma-associated Gr-1+CD11b+ myeloid cells. *Cancer Res* (2006) **66**:6807–6815. doi:10.1158/0008-5472.CAN-05-3755

162. Boehmer von H, Daniel C. Therapeutic opportunities for manipulating TReg cells in autoimmunity and cancer. *Nat Rev Drug Discov* (2012) **12**:51–63. doi:10.1038/nrd3683

163. Ruiz-Cabello F, Nevot MAL, Garrido F. "MHC Class I and II Gene Expression on Human Tumors," in *Cancer Metastasis* Advances in Experimental Medicine and Biology. (Boston, MA: Springer US), 119–128. doi:10.1007/978-1-4899-5037-6_14

164. Fox CJ, Hammerman PS, Thompson CB. Fuel feeds function: energy metabolism and the T-cell response. *Nature Reviews Immunology* (2005) **5**:844–852. doi:10.1038/nri1710

165. Frauwirth KA, Riley JL, Harris MH, Parry RV, Rathmell JC, Plas DR, Elstrom RL, June CH, Thompson CB. The CD28 Signaling Pathway Regulates Glucose Metabolism. *Immunity* (2002) **16**:769–777. doi:10.1016/S1074-7613(02)00323-0

166. Elstrom RL, Bauer DE, Buzzai M, Karnauskas R, Harris MH, Plas DR, Zhuang H, Cinalli RM, Alavi A, Rudin CM, et al. Akt stimulates aerobic glycolysis in cancer cells. *Cancer Res* (2004) **64**:3892–3899. doi:10.1158/0008-5472.CAN-03-2904

167. Dang CV. MYC, metabolism, cell growth, and tumorigenesis. *Cold Spring Harbor Perspectives in Medicine* (2013) **3**:a014217–a014217. doi:10.1101/cshperspect.a014217

168. Antico Arciuch VG, Russo MA, Kang KS, Di Cristofano A. Inhibition of AMPK and Krebs cycle gene expression drives metabolic remodeling of Pten-deficient preneoplastic thyroid cells. *Cancer Res* (2013) **73**:5459–5472. doi:10.1158/0008-5472.CAN-13-1429

169. Wang R, Green DR. Metabolic checkpoints in activated T cells. *Nat Immunol* (2012) **13**:907–915. doi:10.1038/ni.2386

170. Vaupel P, Mayer A. Hypoxia in cancer: significance and impact on clinical outcome. *Cancer Metastasis Rev* (2007) **26**:225–239. doi:10.1007/s10555-007-9055-1

171. Firth JD, Ebert BL, Pugh CW, Ratcliffe PJ. Oxygen-regulated control elements in the

phosphoglycerate kinase 1 and lactate dehydrogenase A genes: similarities with the erythropoietin 3' enhancer. *Proc Natl Acad Sci USA* (1994) **91**:6496–6500.

172. Kim J-W, Tchernyshyov I, Semenza GL, Dang CV. HIF-1-mediated expression of pyruvate dehydrogenase kinase: a metabolic switch required for cellular adaptation to hypoxia. *Cell Metab* (2006) **3**:177–185. doi:10.1016/j.cmet.2006.02.002

173. Sitkovsky MV, Lukashev D, Apasov S, Kojima H, Koshiba M, Caldwell C, Ohta A, Thiel M. Physiological control of immune response and inflammatory tissue damage by hypoxia-inducible factors and adenosine A2A receptors. *Annu Rev Immunol* (2004) **22**:657–682. doi:10.1146/annurev.immunol.22.012703.104731

174. Atkuri KR, Herzenberg LA, Herzenberg LA. Culturing at atmospheric oxygen levels impacts lymphocyte function. *Proc Natl Acad Sci USA* (2005) **102**:3756–3759. doi:10.1073/pnas.0409910102

175. Larbi A, Zelba H, Goldeck D, Pawelec G. Induction of HIF-1alpha and the glycolytic pathway alters apoptotic and differentiation profiles of activated human T cells. *J Leukoc Biol* (2010) **87**:265–273. doi:10.1189/jlb.0509304

176. Zuckerberg AL, Goldberg LI, Lederman HM. Effects of hypoxia on interleukin-2 mRNA expression by T lymphocytes. *Crit Care Med* (1994) **22**:197–203.

177. Kim H, Peng G, Hicks JM, Weiss HL, Van Meir EG, Brenner MK, Yotnda P. Engineering human tumor-specific cytotoxic T cells to function in a hypoxic environment. *Mol Ther* (2008) **16**:599–606. doi:10.1038/sj.mt.6300391

178. Roman J, Rangasamy T, Guo J, Sugunan S, Meednu N, Packirisamy G, Shimoda LA, Golding A, Semenza G, Georas SN. T-Cell Activation under Hypoxic Conditions Enhances IFN-γ Secretion. *American Journal of Respiratory Cell and Molecular Biology* (2010) **42**:123–128. doi:10.1165/rcmb.2008-0139OC

179. Caldwell CC, Kojima H, Lukashev D, Armstrong J, Farber M, Apasov SG, Sitkovsky MV. Differential effects of physiologically relevant hypoxic conditions on T lymphocyte development and effector functions. *J Immunol* (2001) **167**:6140–6149.

180. Neumann AK, Yang J, Biju MP, Joseph SK, Johnson RS, Haase VH, Freedman BD, Turka LA. Hypoxia inducible factor 1 alpha regulates T cell receptor signal transduction. *Proc Natl Acad Sci USA* (2005) **102**:17071–17076. doi:10.1073/pnas.0506070102

181. Choukèr A, Thiel M, Lukashev D, Ward JM, Kaufmann I, Apasov S, Sitkovsky MV, Ohta A. Critical role of hypoxia and A2A adenosine receptors in liver tissue-protecting physiological anti-inflammatory pathway. *Mol Med* (2008) **14**:116–123. doi:10.2119/2007-00075.Chouker

182. Meehan R, Duncan U, Neale L, Taylor G, Muchmore H, Scott N, Ramsey K, Smith E, Rock P, Goldblum R. Operation Everest II: alterations in the immune system at high altitudes. *J Clin Immunol* (1988) **8**:397–406.

183. Bell EL, Klimova TA, Eisenbart J, Moraes CT, Murphy MP, Budinger GRS, Chandel NS. The Qo site of the mitochondrial complex III is required for the transduction of hypoxic signaling via reactive oxygen species production. *J Cell Biol* (2007) **177**:1029–1036. doi:10.1083/jcb.200609074

184. Kesarwani P, Murali AK, Al-Khami AA, Mehrotra S. Redox Regulation of T-Cell Function: From Molecular Mechanisms to Significance in Human Health and Disease. *Antioxidants & Redox Signaling* (2013) **18**:1497–1534. doi:10.1089/ars.2011.4073

185. Guo J, Lu W, Shimoda LA, Semenza GL, Georas SN. Enhanced interferon-gamma gene expression in T Cells and reduced ovalbumin-dependent lung eosinophilia in hypoxia-inducible factor-1-alpha-deficient mice. *Int Arch Allergy Immunol* (2009) **149**:98–102. doi:10.1159/000189191

186. Lukashev D, Klebanov B, Kojima H, Grinberg A, Berenfeld L, Wenger RH, Ohta A, Sitkovsky M. Cutting Edge: Hypoxia-Inducible Factor 1 and Its Activation-Inducible Short Isoform I.1 Negatively Regulate Functions of CD4+ and CD8+ T Lymphocytes. *J Immunol* (2006) **177**:4962–4965. doi:10.4049/jimmunol.177.8.4962

187. Doedens AL, Phan AT, Stradner MH, Fujimoto JK, Nguyen JV, Yang E, Johnson RS, Goldrath AW. Hypoxia-inducible factors enhance the effector responses of CD8(+) T cells to persistent antigen. *Nat Immunol* (2013) **14**:1173–1182. doi:10.1038/ni.2714

188. Finlay DK. Regulation of glucose metabolism in T cells: new insight into the role of Phosphoinositide 3-kinases. *Front Immunol* (2012) **3**: doi:10.3389/fimmu.2012.00247

189. Barsoum IB, Smallwood CA, Siemens DR, Graham CH. A Mechanism of Hypoxia-Mediated Escape from Adaptive Immunity in Cancer Cells. *Cancer Res* (2014) **74**:665–674. doi:10.1158/0008-5472.CAN-13-0992

190. Fang H-Y, Hughes R, Murdoch C, Coffelt SB, Biswas SK, Harris AL, Johnson RS, Imityaz HZ, Simon MC, Fredlund E, et al. Hypoxia-inducible factors 1 and 2 are important transcriptional effectors in primary macrophages experiencing hypoxia. *Blood* (2009) **114**:844–859. doi:10.1182/blood-2008-12-195941

191. Nizet V, Johnson RS. Interdependence of hypoxic and innate immune responses. *Nature Reviews Immunology* (2009) **9**:609–617. doi:10.1038/nri2607

192. Chang C-H, Qiu J, O'Sullivan D, Buck MD, Noguchi T, Curtis JD, Chen Q, Gindin M, Gubin MM, van der Windt GJW, et al. Metabolic Competition in the Tumor Microenvironment Is a Driver of Cancer Progression. *Cell* (2015)1–14. doi:10.1016/j.cell.2015.08.016

193. Cham CM, Gajewski TF. Glucose availability regulates IFN-gamma production and p70S6 kinase activation in CD8+ effector T cells. *J Immunol* (2005) **174**:4670–4677.

194. Cham CM, Driessens G, O'Keefe JP, Gajewski TF. Glucose deprivation inhibits multiple key gene expression events and effector functions in CD8+ T cells. *Eur J Immunol* (2008) **38**:2438–2450. doi:10.1002/eji.200838289

195. Jacobs SR, Herman CE, Maciver NJ, Wofford JA, Wieman HL, Hammen JJ, Rathmell JC. Glucose uptake is limiting in T cell activation and requires CD28-mediated Akt-dependent and independent pathways. *J Immunol* (2008) **180**:4476–4486.

196. Macintyre AN, Gerriets VA, Nichols AG, Michalek RD, Rudolph MC, Deoliveira D, Anderson SM, Abel ED, Chen BJ, Hale LP, et al. The glucose transporter Glut1 is selectively essential for CD4 T cell activation and effector function. *Cell Metab* (2014) **20**:61–72. doi:10.1016/j.cmet.2014.05.004

197. Ho P-C, Bihuniak JD, Macintyre AN, Staron M, Liu X, Amezquita R, Tsui Y-C, Cui G, Micevic G, Perales JC, et al. Phosphoenolpyruvate Is a Metabolic Checkpoint of Anti-tumor T Cell Responses. *Cell* (2015) **162**:1217–1228. doi:10.1016/j.cell.2015.08.012

198. Warburg O. On the Origin of Cancer Cells. *Science* (1956) **123**:309–314. doi:10.1126/science.123.3191.309

199. Fischer K, Hoffmann P, Voelkl S, Meidenbauer N, Ammer J, Edinger M, Gottfried E, Schwarz S, Rothe G, Hoves S, et al. Inhibitory effect of tumor cell-derived lactic acid on human T cells. *Blood* (2007) **109**:3812–3819. doi:10.1182/blood-2006-07-035972

200. Chang C-H, Curtis JD, Maggi LB, Faubert B, Villarino AV, O'Sullivan D, Huang SC-C, van der Windt GJW, Blagih J, Qiu J, et al. Posttranscriptional control of T cell effector function by aerobic glycolysis. *Cell* (2013) **153**:1239–1251. doi:10.1016/j.cell.2013.05.016

201. Buzzai M, Bauer DE, Jones RG, DeBerardinis RJ, Hatzivassiliou G, Elstrom RL, Thompson CB. The glucose dependence of Akt-transformed cells can be reversed by pharmacologic activation of fatty acid β-oxidation. *Oncogene* (2005) **24**:4165–4173. doi:10.1038/sj.onc.1208622

202. Blagih J, Coulombe F, Vincent EE, Dupuy F, Galicia-Vázquez G, Yurchenko E, Raissi TC, van der Windt GJW, Viollet B, Pearce EL, et al. The energy sensor AMPK regulates T cell metabolic adaptation and effector responses in vivo. *Immunity* (2015) **42**:41–54. doi:10.1016/j.immuni.2014.12.030

203. O'Neill LAJ, Hardie DG. Metabolism of inflammation limited by AMPK and pseudo-starvation. *Nature* (2013) **493**:346–355. doi:10.1038/nature11862

204. O'Sullivan D, Pearce EL. Targeting T cell metabolism for therapy. *Trends in Immunology* (2015) **36**:71–80. doi:10.1016/j.it.2014.12.004

205. Sukumar M, Liu J, Ji Y, Subramanian M, Crompton JG, Yu Z, Roychoudhuri R, Palmer DC, Muranski P, Karoly ED, et al. Inhibiting glycolytic metabolism enhances CD8+ T cell memory and antitumor function. *J Clin Invest* (2013) **123**:4479–4488. doi:10.1172/JCI69589

206. Manjunath N, Shankar P, Wan J, Weninger W, Crowley MA, Hieshima K, Springer TA, Fan X, Shen H, Lieberman J, et al. Effector differentiation is not prerequisite for generation of memory cytotoxic T lymphocytes. *J Clin Invest* (2001) **108**:871–878. doi:10.1172/JCI13296

207. Maciver NJ, Jacobs SR, Wieman HL, Wofford JA, Coloff JL, Rathmell JC. Glucose metabolism in lymphocytes is a regulated process with significant effects on immune cell function and survival. *J Leukoc Biol* (2008) **84**:949–957. doi:10.1189/jlb.0108024

208. Crompton JG, Sukumar M, Roychoudhuri R, Clever D, Gros A, Eil RL, Tran E, Hanada KI, Yu Z, Palmer DC, et al. Akt Inhibition Enhances Expansion of Potent Tumor-Specific Lymphocytes with Memory Cell Characteristics. *Cancer Res* (2015) **75**:296–305. doi:10.1158/0008-5472.CAN-14-2277

209. Currie E, Schulze A, Zechner R, Walther TC, Farese RV. Cellular fatty acid metabolism and cancer. *Cell Metab* (2013) **18**:153–161. doi:10.1016/j.cmet.2013.05.017

210. Zhang F. Dysregulated lipid metabolism in cancer. *World Journal of Biological Chemistry* (2012) **3**:167. doi:10.4331/wjbc.v3.i8.167

211. Zhang Y, Bellows CF, Kolonin MG. Adipose tissue-derived progenitor cells and cancer. *World J Stem Cells* (2010) **2**:103–113. doi:10.4252/wjsc.v2.i5.103

212. Byersdorfer CA, Tkachev V, Opipari AW, Goodell S, Swanson J, Sandquist S, Glick GD, Ferrara JLM. Effector T cells require fatty acid metabolism during murine graft-versus-host disease. *Blood* (2013) **122**:3230–3237. doi:10.1182/blood-2013-04-495515

213. Byersdorfer CA. The Role of Fatty Acid Oxidation in the Metabolic Reprograming of Activatedâ€‰T-Cells. *Front Immunol* (2014) **5**:161. doi:10.3389/fimmu.2014.00641

214. Newman JC, Verdin E. Ketone bodies as signaling metabolites. *Trends Endocrinol Metab* (2014) **25**:42–52. doi:10.1016/j.tem.2013.09.002

215. Takahashi S, Iizumi T, Mashima K, Abe T, Suzuki N. Roles and regulation of ketogenesis in cultured astroglia and neurons under hypoxia and hypoglycemia. *ASN Neuro* (2014) **6**:1759091414550997. doi:10.1177/1759091414550997

216. Curi R, Williams JF, Newsholme EA. Formation of ketone bodies by resting lymphocytes. *Int J Biochem* (1989) **21**:1133–1136.

217. Curi R, Williams JF, Newsholme EA. Pyruvate metabolism by lymphocytes: evidence for an additional ketogenic tissue. *Biochem Int* (1989) **19**:755–767.

218. Mrass P, Takano H, Ng LG, Daxini S, Lasaro MO, Iparraguirre A, Cavanagh LL, Andrian von UH, Ertl HCJ, Haydon PG, et al. Random migration precedes stable target cell interactions of tumor-infiltrating T cells. *Journal of Experimental Medicine* (2006) **203**:2749–2761. doi:10.1084/jem.20060710

219. Kudo N, Barr AJ, Barr RL, Desai S, Lopaschuk GD. High rates of fatty acid oxidation during reperfusion of ischemic hearts are associated with a decrease in malonyl-CoA levels due to an increase in 5'-AMP-activated protein kinase inhibition of acetyl-CoA carboxylase. *J Biol Chem* (1995) **270**:17513–17520.

220. van der Windt GJW, Pearce EL. Metabolic switching and fuel choice during T-cell differentiation and memory development. *Immunol Rev* (2012) **249**:27–42. doi:10.1111/j.1600-065X.2012.01150.x

221. Zaugg K, Yao Y, Reilly PT, Kannan K, Kiarash R, Mason J, Huang P, Sawyer SK, Fuerth B, Faubert B, et al. Carnitine palmitoyltransferase 1C promotes cell survival and tumor growth under conditions of metabolic stress. *Genes Dev* (2011) **25**:1041–1051. doi:10.1101/gad.1987211

222. Odorizzi PM, Pauken KE, Paley MA, Sharpe A, Wherry EJ. Genetic absence of PD-1 promotes accumulation of terminally differentiated exhausted CD8+ T cells. *Journal of Experimental Medicine* (2015) **212**:1125–1137. doi:10.1084/jem.20142237

223. Patsoukis N, Bardhan K, Chatterjee P, Sari D, Liu B, Bell LN, Karoly ED, Freeman GJ, Petkova V, Seth P, et al. PD-1 alters T-cell metabolic reprogramming by inhibiting glycolysis and promoting lipolysis and fatty acid oxidation. *Nature Communications* (1AD) **6**:1–13. doi:10.1038/ncomms7692

224. Hinrichs CS, Rosenberg SA. Exploiting the curative potential of adoptive T-cell therapy for cancer. *Immunol Rev* (2014) **257**:56–71. doi:10.1111/imr.12132

225. Maus MV, Powell DJ. Chimeric Antigen Receptor T-Cells: New Approaches to Improve Their Efficacy and Reduce Toxicity. *Cancer J* (2015) **21**:475–479. doi:10.1097/PPO.0000000000000155

226. Brentjens RJ, Davila ML, Riviere I, Park J, Wang X, Cowell LG, Bartido S, Stefanski J, Taylor C, Olszewska M, et al. CD19-targeted T cells rapidly induce molecular remissions in adults with chemotherapy-refractory acute lymphoblastic leukemia. *Sci Transl Med* (2013) **5**:177ra38–177ra38. doi:10.1126/scitranslmed.3005930

227. Grupp SA, Kalos M, Barrett D, Aplenc R, Porter DL, Rheingold SR, Teachey DT, Chew A, Hauck B, Wright JF, et al. Chimeric antigen receptor-modified T cells for acute lymphoid leukemia. *N Engl J Med* (2013) **368**:1509–1518. doi:10.1056/NEJMoa1215134

228. Kakarla S, Gottschalk S. CAR T Cells for Solid Tumors. *The Cancer Journal* (2014) **20**:151–155. doi:10.1097/PPO.0000000000000032

229. Park JR, Digiusto DL, Slovak M, Wright C, Naranjo A, Wagner J, Meechoovet HB, Bautista C, Chang W-C, Ostberg JR, et al. Adoptive transfer of chimeric antigen receptor re-directed cytolytic T lymphocyte clones in patients with neuroblastoma. *Mol Ther* (2007) **15**:825–833. doi:10.1038/sj.mt.6300104

230. Lamers CHJ. Treatment of Metastatic Renal Cell Carcinoma With Autologous T-Lymphocytes Genetically Retargeted Against Carbonic Anhydrase IX: First Clinical Experience. *Journal of Clinical Oncology* (2006) **24**:e20–e22. doi:10.1200/JCO.2006.05.9964

231. Curran KJ, Brentjens RJ. Chimeric antigen receptor T cells for cancer immunotherapy. *J Clin Oncol* (2015) **33**:1703–1706. doi:10.1200/JCO.2014.60.3449

232. Beatty GL, Moon EK. Chimeric antigen receptor T cells are vulnerable to immunosuppressive mechanisms present within the tumor microenvironment. *OncoImmunology* (2014) **3**:e970027. doi:10.4161/21624011.2014.970027

233. Beavis PA, Slaney CY, Kershaw MH, Gyorki D, Neeson PJ, Darcy PK. Reprogramming the tumor microenvironment to enhance adoptive cellular therapy. *Semin Immunol* (2015) doi:10.1016/j.smim.2015.11.003

234. John LB, Kershaw MH, Darcy PK. Blockade of PD-1 immunosuppression boosts CAR T-cell therapy. *OncoImmunology* (2013) **2**:e26286. doi:10.4161/onci.26286

235. Liu Y, Cao Y, Zhang W, Bergmeier S, Qian Y, Akbar H, Colvin R, Ding J, Tong L, Wu S, et al. A small-molecule inhibitor of glucose transporter 1 downregulates glycolysis, induces cell-cycle arrest, and inhibits cancer cell growth in vitro and in vivo. *Mol Cancer Ther* (2012) **11**:1672–1682. doi:10.1158/1535-7163.MCT-12-0131

236. Birsoy K, Wang T, Possemato R, Yilmaz OH, Koch CE, Chen WW, Hutchins AW, Gultekin Y, Peterson TR, Carette JE, et al. MCT1-mediated transport of a toxic molecule is an effective strategy for targeting glycolytic tumors. *Nat Genet* (2013) **45**:104–108. doi:10.1038/ng.2471

237. Gattinoni L, Klebanoff CA, Palmer DC, Wrzesinski C, Kerstann K, Yu Z, Finkelstein SE, Theoret MR, Rosenberg SA, Restifo NP. Acquisition of full effector function in vitro paradoxically impairs the in vivo antitumor efficacy of adoptively transferred CD8+ T cells. *J Clin Invest* (2005) **115**:1616–1626. doi:10.1172/JCI24480

238. Zeng R, Spolski R, Finkelstein SE, Oh S, Kovanen PE, Hinrichs CS, Pise-Masison CA, Radonovich MF, Brady JN, Restifo NP, et al. Synergy of IL-21 and IL-15 in regulating CD8+ T cell expansion and function. *Journal of Experimental Medicine* (2005) **201**:139–148. doi:10.1084/jem.20041057

239. Liu S, Lizée G, Lou Y, Liu C, Overwijk WW, Wang G, Hwu P. IL-21 synergizes with IL-7 to augment expansion and anti-tumor function of cytotoxic T cells. *Int Immunol* (2007) **19**:1213–1221. doi:10.1093/intimm/dxm093

240. Fewkes NM, Mackall CL. Novel gamma-chain cytokines as candidate immune modulators in immune therapies for cancer. *Cancer J* (2010) **16**:392–398. doi:10.1097/PPO.0b013e3181eacbc4

241. Klebanoff CA, Gattinoni L, Torabi-Parizi P, Kerstann K, Cardones AR, Finkelstein SE, Palmer DC, Antony PA, Hwang ST, Rosenberg SA, et al. Central memory self/tumor-reactive CD8+ T cells confer superior antitumor immunity compared with effector memory T cells. *Proc Natl Acad Sci USA* (2005) **102**:9571–9576. doi:10.1073/pnas.0503726102

242. Klebanoff CA, Gattinoni L, Palmer DC, Muranski P, Ji Y, Hinrichs CS, Borman ZA, Kerkar SP, Scott CD, Finkelstein SE, et al. Determinants of successful CD8+ T-cell adoptive immunotherapy for large established tumors in mice. *Clinical Cancer Research* (2011) **17**:5343–5352. doi:10.1158/1078-0432.CCR-11-0503

243. Lasaro MO, Tatsis N, Hensley SE, Whitbeck JC, Lin S-W, Rux JJ, Wherry EJ, Cohen GH, Eisenberg RJ, Ertl HC. Targeting of antigen to the herpesvirus entry mediator augments primary adaptive immune responses. *Nat Med* (2008) **14**:205–212. doi:10.1038/nm1704

244. Lasaro MO, Sazanovich M, Giles-Davis W, Mrass P, Bunte RM, Sewell DA, Hussain SF, Fu Y-X, Weninger W, Paterson Y, et al. Active immunotherapy combined with blockade of a coinhibitory pathway achieves regression of large tumor masses in cancer-prone mice. *Mol Ther* (2011) **19**:1727–1736. doi:10.1038/mt.2011.88

245. Bailey KM, Wojtkowiak JW, Hashim AI, Gillies RJ. “Targeting the Metabolic Microenvironment of Tumors,” in *Current Challenges in Personalized Cancer Medicine* Advances in Pharmacology. (Elsevier), 63–107. doi:10.1016/B978-0-12-397927-8.00004-X

246. Wang R, Green DR. Metabolic checkpoints in activated T cells. *Nat Immunol* (2012) **13**:907–915. doi:10.1038/ni.2386

247. Hamanaka RB, Chandel NS. Targeting glucose metabolism for cancer therapy. *Journal of Experimental Medicine* (2012) **209**:211–215. doi:10.1084/jem.20120162

248. Casazza A, Di Conza G, Wenes M, Finisguerra V, Deschoemaeker S, Mazzone M. Tumor stroma: a complexity dictated by the hypoxic tumor microenvironment. (2013) **33**:1743–1754. doi:10.1038/onc.2013.121

249. Mittendorf EA, Sharma P. Mechanisms of T-cell inhibition: implications for cancer immunotherapy. *Expert Rev Vaccines* (2010) **9**:89–105. doi:10.1586/erv.09.144

250. Finn OJ. Cancer vaccines: between the idea and the reality. *Nature Reviews Immunology* (2003) **3**:630–641. doi:10.1038/nri1150

251. Haile ST, Bosch JJ, Agu NI, Zeender AM, Somasundaram P, Srivastava MK, Britting S, Wolf JB, Ksander BR, Ostrand-Rosenberg S. Tumor cell programmed death ligand 1-mediated T cell suppression is overcome by coexpression of CD80. *J Immunol* (2011) **186**:6822–6829. doi:10.4049/jimmunol.1003682

252. Jacobs JFM, Nierkens S, Figdor CG, De Vries IJM, Adema GJ. Regulatory T cells in melanoma: the final hurdle towards effective immunotherapy? *Lancet Oncol* (2012) **13**:e32–42. doi:10.1016/S1470-2045(11)70155-3

253. Umansky V, Sevko A. Melanoma-induced immunosuppression and its neutralization. *Semin Cancer Biol* (2012) **22**:319–326. doi:10.1016/j.semcancer.2012.02.003

254. Izawa S, Mimura K, Watanabe M, Maruyama T, Kawaguchi Y, Fujii H, Kono K. Increased prevalence of tumor-infiltrating regulatory T cells is closely related to their lower sensitivity to H2O2-induced apoptosis in gastric and esophageal cancer. *Cancer Immunol Immunother* (2013) **62**:161–170. doi:10.1007/s00262-012-1327-0

255. Lipson EJ. Re-orienting the immune system: Durable tumor regression and successful re-induction therapy using anti-PD1 antibodies. *OncoImmunology* (2013) **2**:e23661. doi:10.4161/onci.23661

256. Callahan MK, Postow MA, Wolchok JD. Immunomodulatory therapy for melanoma: ipilimumab and beyond. *Clinics in Dermatology* (2013) **31**:191–199. doi:10.1016/j.clindermatol.2012.08.006

257. Duraiswamy J, Kaluza KM, Freeman GJ, Coukos G. Dual blockade of PD-1 and CTLA-4 combined with tumor vaccine effectively restores T-cell rejection function in tumors. *Cancer Res* (2013) **73**:3591–3603. doi:10.1158/0008-5472.CAN-12-4100

258. Intlekofer AM, Thompson CB. At the bench: preclinical rationale for CTLA-4 and PD-1 blockade as cancer immunotherapy. *J Leukoc Biol* (2013) **94**:25–39. doi:10.1189/jlb.1212621

259. Whitbeck JC, Peng C, Lou H, Xu R, Willis SH, Ponce de Leon M, Peng T, Nicola AV, Montgomery RI, Warner MS, et al. Glycoprotein D of herpes simplex virus (HSV) binds directly to HVEM, a member of the tumor necrosis factor receptor superfamily and a mediator of HSV entry. *Journal of Virology* (1997) **71**:6083–6093.

260. Steinberg MW, Cheung TC, Ware CF. The signaling networks of the herpesvirus entry mediator (TNFRSF14) in immune regulation. *Immunol Rev* (2011) **244**:169–187. doi:10.1111/j.1600-065X.2011.01064.x

261. Cai G, Freeman GJ. The CD160, BTLA, LIGHT/HVEM pathway: a bidirectional switch regulating T-cell activation. *Immunol Rev* (2009) **229**:244–258. doi:10.1111/j.1600-065X.2009.00783.x

262. Stiles KM, Whitbeck JC, Lou H, Cohen GH, Eisenberg RJ, Krummenacher C. Herpes

simplex virus glycoprotein D interferes with binding of herpesvirus entry mediator to its ligands through downregulation and direct competition. *Journal of Virology* (2010) **84**:11646–11660. doi:10.1128/JVI.01550-10

263. DiMenna L, Latimer B, Parzych E, Haut LH, Töpfer K, Abdulla S, Yu H, Manson B, Giles-Davis W, Zhou D, et al. Augmentation of primary influenza A virus-specific CD8+ T cell responses in aged mice through blockade of an immunoinhibitory pathway. *J Immunol* (2010) **184**:5475–5484. doi:10.4049/jimmunol.0903808

264. Sharpe AH. Mechanisms of costimulation. *Immunol Rev* (2009) **229**:5–11. doi:10.1111/j.1600-065X.2009.00784.x

265. Bakdash G, Sittig SP, van Dijk T, Figdor CG, De Vries IJM. The nature of activatory and tolerogenic dendritic cell-derived signal II. *Front Immunol* (2013) **4**:53. doi:10.3389/fimmu.2013.00053

266. Han P, Goularte OD, Rufner K, Wilkinson B, Kaye J. An inhibitory Ig superfamily protein expressed by lymphocytes and APCs is also an early marker of thymocyte positive selection. *The Journal of Immunology* (2004) **172**:5931–5939.

267. Parry RV, Chemnitz JM, Frauwirth KA, Lanfranco AR, Braunstein I, Kobayashi SV, Linsley PS, Thompson CB, Riley JL. CTLA-4 and PD-1 Receptors Inhibit T-Cell Activation by Distinct Mechanisms. *Mol Cell Biol* (2005) **25**:9543–9553. doi:10.1128/MCB.25.21.9543-9553.2005

268. Hemmings BA, Restuccia DF. PI3K-PKB/Akt pathway. *Cold Spring Harb Perspect Biol* (2012) **4**:a011189–a011189. doi:10.1101/cshperspect.a011189

269. Gavrieli M, Watanabe N, Loftin SK, Murphy TL, Murphy KM. Characterization of phosphotyrosine binding motifs in the cytoplasmic domain of B and T lymphocyte attenuator required for association with protein tyrosine phosphatases SHP-1 and SHP-2. *Biochem Biophys Res Commun* (2003) **312**:1236–1243.

270. Ananthakrishnan AN, Oxford EC, Nguyen DD, Sauk J, Yajnik V, Xavier RJ. Genetic risk factors for Clostridium difficileinfection in ulcerative colitis. *Alimentary Pharmacology & Therapeutics* (2013) **38**:522–530. doi:10.1111/apt.12425

271. Chadha S, Miller K, Farwell L, Sacks S, Daly MJ, Rioux JD, Vyse TJ. Haplotype analysis of tumour necrosis factor receptor genes in 1p36: no evidence for association with systemic lupus erythematosus. *Eur J Hum Genet* (2006) **14**:69–78. doi:10.1038/sj.ejhg.5201527

272. Jung HW, La SJ, Kim JY, Heo SK, Kim JY, Wang S, Kim KK, Lee KM, Cho HR, Lee HW, et al. High levels of soluble herpes virus entry mediator in sera of patients with allergic and autoimmune diseases. *Exp Mol Med* (2003) **35**:501–508. doi:10.1038/emm.2003.65

273. Steinberg MW, Turovskaya O, Shaikh RB, Kim G, McCole DF, Pfeffer K, Murphy KM, Ware CF, Kronenberg M. A crucial role for HVEM and BTLA in preventing intestinal inflammation. *J Exp Med* (2008) **205**:1463–1476. doi:10.1084/jem.20071160

274. del Rio M-L, Kurtz J, Perez-Martinez C, Ghosh A, Perez-Simon JA, Rodriguez-Barbosa J-I. B- and T-lymphocyte attenuator targeting protects against the acute phase of graft

versus host reaction by inhibiting donor anti-host cytotoxicity. *Transplantation* (2011) **92**:1085–1093. doi:10.1097/TP.0b013e3182339d4a

275. Costello RT, Mallet F, Barbarat B, Schiano De Colella J-M, Sainty D, Sweet RW, Truneh A, Olive D. Stimulation of non-Hodgkin's lymphoma via HVEM: an alternate and safe way to increase Fas-induced apoptosis and improve tumor immunogenicity. *Leukemia* (2003) **17**:2500–2507. doi:10.1038/sj.leu.2403175

276. Derré L, Rivals J-P, Jandus C, Pastor S, Rimoldi D, Romero P, Michielin O, Olive D, Speiser DE. BTLA mediates inhibition of human tumor-specific CD8+ T cells that can be partially reversed by vaccination. *J Clin Invest* (2010) **120**:157–167. doi:10.1172/JCI40070

277. Fourcade J, Sun Z, Pagliano O, Guillaume P, Luescher IF, Sander C, Kirkwood JM, Olive D, Kuchroo V, Zarour HM. CD8(+) T cells specific for tumor antigens can be rendered dysfunctional by the tumor microenvironment through upregulation of the inhibitory receptors BTLA and PD-1. *Cancer Res* (2012) **72**:887–896. doi:10.1158/0008-5472.CAN-11-2637

278. Kaufmann DE, Walker BD. Programmed death-1 as a factor in immune exhaustion and activation in HIV infection. *Curr Opin HIV AIDS* (2008) **3**:362–367. doi:10.1097/COH.0b013e3282f9ae8b

279. Dustin LB, Rice CM. Flying under the radar: the immunobiology of hepatitis C. *Annu Rev Immunol* (2007) **25**:71–99. doi:10.1146/annurev.immunol.25.022106.141602

280. Wherry EJ, Ha S-J, Kaech SM, Haining WN, Sarkar S, Kalia V, Subramaniam S, Blattman JN, Barber DL, Ahmed R. Molecular Signature of CD8+ T Cell Exhaustion during Chronic Viral Infection. *Immunity* (2007) **27**:824. doi:10.1016/j.immuni.2007.11.006

281. Oestreich KJ, Yoon H, Ahmed R, Boss JM. NFATc1 regulates PD-1 expression upon T cell activation. *J Immunol* (2008) **181**:4832–4839.

282. Hebeisen M, Baitsch L, Presotto D, Baumgaertner P, Romero P, Michielin O, Speiser DE, Rufer N. SHP-1 phosphatase activity counteracts increased T cell receptor affinity. *J Clin Invest* (2013) **123**:1044–1056. doi:10.1172/JCI65325

283. Bos R, Marquardt KL, Cheung J, Sherman LA. Functional differences between low- and high-affinity CD8(+) T cells in the tumor environment. *OncoImmunology* (2012) **1**:1239–1247. doi:10.4161/onci.21285

284. Bacik I, Cox JH, Anderson R, Yewdell JW, Bennink JR. TAP (transporter associated with antigen processing)-independent presentation of endogenously synthesized peptides is enhanced by endoplasmic reticulum insertion sequences located at the amino- but not carboxyl-terminus of the peptide. *The Journal of Immunology* (1994) **152**:381–387.

285. Kianizad K, Marshall LA, Grinshtein N, Bernard D, Margl R, Cheng S, Beermann F, Wan Y, Bramson J. Elevated frequencies of self-reactive CD8+ T cells following immunization with a xenoantigen are due to the presence of a heteroclitic CD4+ T-cell helper epitope. *Cancer Res* (2007) **67**:6459–6467. doi:10.1158/0008-5472.CAN-06-4336

286. Alexander J, Sidney J, Southwood S, Ruppert J, Oseroff C, Maewal A, Snoke K, Serra

HM, Kubo RT, Sette A. Development of high potency universal DR-restricted helper epitopes by modification of high affinity DR-blocking peptides. *Immunity* (1994) **1**:751–761.

287. Guevara-Patiño JA, Engelhorn ME, Turk MJ, Liu C, Duan F, Rizzuto G, Cohen AD, Merghoub T, Wolchok JD, Houghton AN. Optimization of a self antigen for presentation of multiple epitopes in cancer immunity. *J Clin Invest* (2006) **116**:1382–1390. doi:10.1172/JCI25591

288. Bergmann CC, Yao Q, Ho CK, Buckwold SL. Flanking residues alter antigenicity and immunogenicity of multi-unit CTL epitopes. *The Journal of Immunology* (1996) **157**:3242–3249.

289. Del Val M, Schlicht HJ, Ruppert T, Reddehase MJ, Koszinowski UH. Efficient processing of an antigenic sequence for presentation by MHC class I molecules depends on its neighboring residues in the protein. *Cell* (1991) **66**:1145–1153.

290. Zhou D, Zhou X, Bian A, Li H, Chen H, Small JC, Li Y, Giles-Davis W, Xiang Z, Ertl HCJ. An efficient method of directly cloning chimpanzee adenovirus as a vaccine vector. *Nat Protoc* (2010) **5**:1775–1785. doi:10.1038/nprot.2010.134

291. Angeli F, Koumakis G, Chen M-C, Kumar S, Delinassios JG. Role of stromal fibroblasts in cancer: promoting or impeding? *Tumour Biol* (2009) **30**:109–120. doi:10.1159/000218708

292. Cirri P, Chiarugi P. Cancer-associated-fibroblasts and tumour cells: a diabolic liaison driving cancer progression. *Cancer Metastasis Rev* (2012) **31**:195–208. doi:10.1007/s10555-011-9340-x

293. Wilson JS, Pirola RC, Apte MV. Stars and stripes in pancreatic cancer: role of stellate cells and stroma in cancer progression. *Front Physiol* (2014) **5**:52. doi:10.3389/fphys.2014.00052

294. Clark AG, Vignjevic DM. Modes of cancer cell invasion and the role of the microenvironment. *Curr Opin Cell Biol* (2015) **36**:13–22. doi:10.1016/j.ceb.2015.06.004

295. Bianchi G, Borgonovo G, Pistoia V, Raffaghello L. Immunosuppressive cells and tumour microenvironment: focus on mesenchymal stem cells and myeloid derived suppressor cells. *Histol Histopathol* (2011) **26**:941–951.

296. Filipazzi P, Huber V, Rivoltini L. Phenotype, function and clinical implications of myeloid-derived suppressor cells in cancer patients. *Cancer Immunol Immunother* (2012) **61**:255–263. doi:10.1007/s00262-011-1161-9

297. Becker JC, Andersen MH, Schrama D, Thor Straten P. Immune-suppressive properties of the tumor microenvironment. *Cancer Immunol Immunother* (2013) **62**:1137–1148. doi:10.1007/s00262-013-1434-6

298. Facciponte JG, Ugel S, De Sanctis F, Li C, Wang L, Nair G, Sehgal S, Raj A, Matthaiou E, Coukos G, et al. Tumor endothelial marker 1-specific DNA vaccination targets tumor vasculature. *J Clin Invest* (2014) **124**:1497–1511. doi:10.1172/JCI67382

299. Schnurr M, Duewell P, Bauer C, Rothenfusser S, Lauber K, Endres S, Kobold S.

Strategies to relieve immunosuppression in pancreatic cancer. *Immunotherapy* (2015) **7**:363–376. doi:10.2217/imt.15.9

300. Elkhattouti A, Hassan M, Gomez CR. Stromal Fibroblast in Age-Related Cancer: Role in Tumorigenesis and Potential as Novel Therapeutic Target. *Front Oncol* (2015) **5**:158. doi:10.3389/fonc.2015.00158

301. Kalluri R, Zeisberg M. Fibroblasts in cancer. *Nat Rev Cancer* (2006) **6**:392–401. doi:10.1038/nrc1877

302. Ishii G, Ochiai A, Neri S. Phenotypic and functional heterogeneity of cancer-associated fibroblast within the tumor microenvironment. *Adv Drug Deliv Rev* (2015) doi:10.1016/j.addr.2015.07.007

303. Karagiannis GS, Poutahidis T, Erdman SE, Kirsch R, Riddell RH, Diamandis EP. Cancer-associated fibroblasts drive the progression of metastasis through both paracrine and mechanical pressure on cancer tissue. *Mol Cancer Res* (2012) **10**:1403–1418. doi:10.1158/1541-7786.MCR-12-0307

304. Roberts EW, Deonarine A, Jones JO, Denton AE, Feig C, Lyons SK, Espeli M, Kraman M, McKenna B, Wells RJB, et al. Depletion of stromal cells expressing fibroblast activation protein-α from skeletal muscle and bone marrow results in cachexia and anemia. *J Exp Med* (2013) **210**:1137–1151. doi:10.1084/jem.20122344

305. Tillmanns J, Hoffmann D, Habbaba Y, Schmitto JD, Sedding D, Fraccarollo D, Galuppo P, Bauersachs J. Fibroblast activation protein alpha expression identifies activated fibroblasts after myocardial infarction. *J Mol Cell Cardiol* (2015) **87**:194–203. doi:10.1016/j.yjmcc.2015.08.016

306. Jacob M, Chang L, Pure E. Fibroblast Activation Protein in Remodeling Tissues. *Current Molecular Medicine* (2012) **12**:1220–1243. doi:10.2174/156652412803833607

307. Dankort D, Curley DP, Cartlidge RA, Nelson B, Karnezis AN, Damsky WE, You MJ, DePinho RA, McMahon M, Bosenberg M. Braf(V600E) cooperates with Pten loss to induce metastatic melanoma. *Nat Genet* (2009) **41**:544–552. doi:10.1038/ng.356

308. Zhang Y, Ertl HCJ. The effect of adjuvanting cancer vaccines with herpes simplex virus glycoprotein D on melanoma-driven CD8+ T cell exhaustion. *J Immunol* (2014) **193**:1836–1846. doi:10.4049/jimmunol.1302029

309. Marvel D, Gabrilovich DI. Myeloid-derived suppressor cells in the tumor microenvironment: expect the unexpected. *J Clin Invest* (2015) **125**:3356–3364. doi:10.1172/JCI80005

310. Umemura N, Saio M, Suwa T, Kitoh Y, Bai J, Nonaka K, Ouyang G-F, Okada M, Balazs M, Adany R, et al. Tumor-infiltrating myeloid-derived suppressor cells are pleiotropic-inflamed monocytes/macrophages that bear M1- and M2-type characteristics. *J Leukoc Biol* (2008) **83**:1136–1144. doi:10.1189/jlb.0907611

311. Fox CJ, Hammerman PS, Thompson CB. Fuel feeds function: energy metabolism and the T-cell response. *Nature Reviews Immunology* (2005) **5**:844–852. doi:10.1038/nri1710

312. Jiang J, Guo W, Liang X. Phenotypes, accumulation, and functions of myeloid-derived suppressor cells and associated treatment strategies in cancer patients. *Hum Immunol* (2014) **75**:1128–1137. doi:10.1016/j.humimm.2014.09.025

313. Nagaraj S, Schrum AG, Cho H-I, Celis E, Gabrilovich DI. Mechanism of T cell tolerance induced by myeloid-derived suppressor cells. *J Immunol* (2010) **184**:3106–3116. doi:10.4049/jimmunol.0902661

314. Baraniuk JN, Jamieson MJ. Rhinorrhea, cough and fatigue in patients taking sitagliptin. *Allergy Asthma Clin Immunol* (2010) **6**:8. doi:10.1186/1710-1492-6-8

315. Chen M, Xiang R, Wen Y, Xu G, Wang C, Luo S, Yin T, Wei X, Shao B, Liu N, et al. A whole-cell tumor vaccine modified to express fibroblast activation protein induces antitumor immunity against both tumor cells and cancer-associated fibroblasts. *Sci Rep* (2015) **5**:14421. doi:10.1038/srep14421

316. Wesolowski R, Markowitz J, Carson WE. Myeloid derived suppressor cells - a new therapeutic target in the treatment of cancer. *J Immunother Cancer* (2013) **1**:10. doi:10.1186/2051-1426-1-10

317. Lo A, Wang L-CS, Scholler J, Monslow J, Avery D, Newick K, O'Brien S, Evans RA, Bajor DJ, Clendenin C, et al. Tumor-Promoting Desmoplasia Is Disrupted by Depleting FAP-Expressing Stromal Cells. *Cancer Res* (2015) **75**:2800–2810. doi:10.1158/0008-5472.CAN-14-3041

318. Tran E, Chinnasamy D, Yu Z, Morgan RA, Lee C-CR, Restifo NP, Rosenberg SA. Immune targeting of fibroblast activation protein triggers recognition of multipotent bone marrow stromal cells and cachexia. *J Exp Med* (2013) **210**:1125–1135. doi:10.1084/jem.20130110

319. Morgan RA, Yang JC, Kitano M, Dudley ME, Laurencot CM, Rosenberg SA. Case report of a serious adverse event following the administration of T cells transduced with a chimeric antigen receptor recognizing ERBB2. *Mol Ther* (2010) **18**:843–851. doi:10.1038/mt.2010.24

320. Schuberth PC, Hagedorn C, Jensen SM, Gulati P, van den Broek M, Mischo A, Soltermann A, Jüngel A, Marroquin Belaunzaran O, Stahel R, et al. Treatment of malignant pleural mesothelioma by fibroblast activation protein-specific re-directed T cells. *J Transl Med* (2013) **11**:187. doi:10.1186/1479-5876-11-187

321. Karakhanova S, Link J, Heinrich M, Shevchenko I, Yang Y, Hassenpflug M, Bunge H, Ahn von K, Brecht R, Mathes A, et al. Characterization of myeloid leukocytes and soluble mediators in pancreatic cancer: importance of myeloid-derived suppressor cells. *OncoImmunology* (2015) **4**:e998519. doi:10.1080/2162402X.2014.998519

322. Ohshio Y, Teramoto K, Hanaoka J, Tezuka N, Itoh Y, Asai T, Daigo Y, Ogasawara K. Cancer-associated fibroblast-targeted strategy enhances antitumor immune responses in dendritic cell-based vaccine. *Cancer Sci* (2015) **106**:134–142. doi:10.1111/cas.12584

323. Ohshio Y, Hanaoka J, Kontani K, Teramoto K. Tranilast inhibits the function of cancer-associated fibroblasts responsible for the induction of immune suppressor cell types. *Scand J Immunol* (2014) **80**:408–416. doi:10.1111/sji.12242

324. Crespo J, Sun H, Welling TH, Tian Z, Zou W. T cell anergy, exhaustion, senescence, and stemness in the tumor microenvironment. *Curr Opin Immunol* (2013) **25**:214–221. doi:10.1016/j.coi.2012.12.003

325. Jiang Y, Li Y, Zhu B. T-cell exhaustion in the tumor microenvironment. *Cell Death Dis* (2015) **6**:e1792. doi:10.1038/cddis.2015.162

326. Brahmer JR, Tykodi SS, Chow LQM, Hwu W-J, Topalian SL, Hwu P, Drake CG, Camacho LH, Kauh J, Odunsi K, et al. Safety and activity of anti-PD-L1 antibody in patients with advanced cancer. *N Engl J Med* (2012) **366**:2455–2465. doi:10.1056/NEJMoa1200694

327. Hamid O, Robert C, Daud A, Hodi FS, Hwu W-J, Kefford R, Wolchok JD, Hersey P, Joseph RW, Weber JS, et al. Safety and tumor responses with lambrolizumab (anti-PD-1) in melanoma. *N Engl J Med* (2013) **369**:134–144. doi:10.1056/NEJMoa1305133

328. Leskowitz RM, Zhou XY, Villinger F, Fogg MH, Kaur A, Lieberman PM, Wang F, Ertl HC. CD4+ and CD8+ T-cell responses to latent antigen EBNA-1 and lytic antigen BZLF-1 during persistent lymphocryptovirus infection of rhesus macaques. *Journal of Virology* (2013) **87**:8351–8362. doi:10.1128/JVI.00852-13

329. Sharma P, Allison JP. Immune checkpoint targeting in cancer therapy: toward combination strategies with curative potential. *Cell* (2015) **161**:205–214. doi:10.1016/j.cell.2015.03.030

330. Chapman PB, D'Angelo SP, Wolchok JD. Rapid Eradication of a Bulky Melanoma Mass with One Dose of Immunotherapy. *N Engl J Med* (2015) **372**:2073–2074. doi:10.1056/NEJMc1501894

331. Yang JC. The adoptive transfer of cultured T cells for patients with metastatic melanoma. *Clinics in Dermatology* (2013) **31**:209–219. doi:10.1016/j.clindermatol.2012.08.019

332. Dalgleish AG. Therapeutic cancer vaccines: Why so few randomised phase III studies reflect the initial optimism of phase II studies. *Vaccine* (2011) **29**:8501–8505. doi:10.1016/j.vaccine.2011.09.012

333. Ahmadzadeh M, Johnson LA, Heemskerk B, Wunderlich JR, Dudley ME, White DE, Rosenberg SA. Tumor antigen-specific CD8 T cells infiltrating the tumor express high levels of PD-1 and are functionally impaired. *Blood* (2009) **114**:1537–1544. doi:10.1182/blood-2008-12-195792

334. Baitsch L, Baumgaertner P, Devêvre E, Raghav SK, Legat A, Barba L, Wieckowski S, Bouzourene H, Deplancke B, Romero P, et al. Exhaustion of tumor-specific CD8+ T cells in metastases from melanoma patients. *J Clin Invest* (2011) **121**:2350–2360. doi:10.1172/JCI46102

335. Mueller SN, Ahmed R. High antigen levels are the cause of T cell exhaustion during chronic viral infection. *Proc Natl Acad Sci USA* (2009) **106**:8623–8628. doi:10.1073/pnas.0809818106

336. Bucks CM, Norton JA, Boesteanu AC, Mueller YM, Katsikis PD. Chronic antigen stimulation alone is sufficient to drive CD8+ T cell exhaustion. *J Immunol* (2009)

182:6697–6708. doi:10.4049/jimmunol.0800997

337. Pearce EL, Poffenberger MC, Chang C-H, Jones RG. Fueling immunity: insights into metabolism and lymphocyte function. *Science* (2013) **342**:1242454–1242454. doi:10.1126/science.1242454

338. Palmer CS, Ostrowski M, Balderson B, Christian N, Crowe SM. Glucose metabolism regulates T cell activation, differentiation, and functions. *Front Immunol* (2015) **6**:1. doi:10.3389/fimmu.2015.00001

339. Lochner M, Berod L, Sparwasser T. Fatty acid metabolism in the regulation of T cell function. *Trends in Immunology* (2015) **36**:81–91. doi:10.1016/j.it.2014.12.005

340. Patsoukis N, Li L, Sari D, Petkova V, Boussiotis VA. PD-1 increases PTEN phosphatase activity while decreasing PTEN protein stability by inhibiting casein kinase 2. *Mol Cell Biol* (2013) **33**:3091–3098. doi:10.1128/MCB.00319-13

341. Kleffel S, Posch C, Barthel SR, Mueller H, Schlapbach C, Guenova E, Elco CP, Lee N, Juneja VR, Zhan Q, et al. Melanoma Cell-Intrinsic PD-1 Receptor Functions Promote Tumor Growth. *Cell* (2015) **162**:1242–1256. doi:10.1016/j.cell.2015.08.052

342. Doedens AL, Phan AT, Stradner MH, Fujimoto JK, Nguyen JV, Yang E, Johnson RS, Goldrath AW. Hypoxia-inducible factors enhance the effector responses of CD8+ T cells to persistent antigen. *Nat Immunol* (2013) **14**:1173–1182. doi:10.1038/ni.2714

343. Ohta A, Diwanji R, Kini R, Subramanian M, Ohta A, Sitkovsky M. In vivo T cell activation in lymphoid tissues is inhibited in the oxygen-poor microenvironment. *Front Immunol* (2011) **2**:27. doi:10.3389/fimmu.2011.00027

344. Finlay DK, Rosenzweig E, Sinclair LV, Feijoo-Carnero C, Hukelmann JL, Rolf J, Panteleyev AA, Okkenhaug K, Cantrell DA. PDK1 regulation of mTOR and hypoxia-inducible factor 1 integrate metabolism and migration of CD8+ T cells. *J Cell Biol* (2012) **199**:i8–i8. doi:10.1083/JCB1996OIA8

345. Grosso JF, Kelleher CC, Harris TJ, Maris CH, Hipkiss EL, De Marzo A, Anders R, Netto G, Getnet D, Bruno TC, et al. LAG-3 regulates CD8+ T cell accumulation and effector function in murine self- and tumor-tolerance systems. *J Clin Invest* (2007) **117**:3383–3392. doi:10.1172/JCI31184

346. Pescador N, Cuevas Y, Naranjo S, Alcaide M, Villar D, Landázuri MO, del Peso L. Identification of a functional hypoxia-responsive element that regulates the expression of the egl ninehomologue 3 (egln3/phd3) gene. *Biochem J* (2005) **390**:189–197. doi:10.1042/BJ20042121

347. Menendez JA, Lupu R. Fatty acid synthase and the lipogenic phenotype in cancer pathogenesis. *Nat Rev Cancer* (2007) **7**:763–777. doi:10.1038/nrc2222

348. Patsoukis N, Bardhan K, Chatterjee P, Sari D, Liu B, Bell LN, Karoly ED, Freeman GJ, Petkova V, Seth P, et al. PD-1 alters T-cell metabolic reprogramming by inhibiting glycolysis and promoting lipolysis and fatty acid oxidation. *Nature Communications* (2015) **6**:6692. doi:10.1038/ncomms7692

349. Azuma T, Yao S, Zhu G, Flies AS, Flies SJ, Chen L. B7-H1 is a ubiquitous antiapoptotic

receptor on cancer cells. *Blood* (2008) **111**:3635–3643. doi:10.1182/blood-2007-11-123141

350. Veech RL. The therapeutic implications of ketone bodies: the effects of ketone bodies in pathological conditions: ketosis, ketogenic diet, redox states, insulin resistance, and mitochondrial metabolism. *Prostaglandins Leukot Essent Fatty Acids* (2004) **70**:309–319. doi:10.1016/j.plefa.2003.09.007

351. Martinez-Outschoorn UE, Lin Z, Whitaker-Menezes D, Howell A, Sotgia F, Lisanti MP. Ketone body utilization drives tumor growth and metastasis. *Cell Cycle* (2012) **11**:3964–3971. doi:10.4161/cc.22137

352. Wiig H, Aukland K, Tenstad O. Isolation of interstitial fluid from rat mammary tumors by a centrifugation method. *Am J Physiol Heart Circ Physiol* (2003) **284**:H416–24. doi:10.1152/ajpheart.00327.2002

353. Lu W, Clasquin MF, Melamud E, Amador-Noguez D, Caudy AA, Rabinowitz JD. Metabolomic analysis via reversed-phase ion-pairing liquid chromatography coupled to a stand alone orbitrap mass spectrometer. *Anal Chem* (2010) **82**:3212–3221. doi:10.1021/ac902837x

354. Devaud C, John LB, Westwood JA, Darcy PK, Kershaw MH. Immune modulation of the tumor microenvironment for enhancing cancer immunotherapy. *OncoImmunology* (2013) **2**:e25961. doi:10.4161/onci.25961

355. Marigo I, Dolcetti L, Serafini P, Zanovello P, Bronte V. Tumor-induced tolerance and immune suppression by myeloid derived suppressor cells. *Immunol Rev* (2008) **222**:162–179. doi:10.1111/j.1600-065X.2008.00602.x

356. Shevach EM. Mechanisms of foxp3+ T regulatory cell-mediated suppression. *Immunity* (2009) **30**:636–645. doi:10.1016/j.immuni.2009.04.010

357. Sica A, Larghi P, Mancino A, Rubino L, Porta C, Totaro MG, Rimoldi M, Biswas SK, Allavena P, Mantovani A. Macrophage polarization in tumour progression. *Semin Cancer Biol* (2008) **18**:349–355. doi:10.1016/j.semcancer.2008.03.004

358. Buck MD, O'Sullivan D, Pearce EL. T cell metabolism drives immunity. *Journal of Experimental Medicine* (2015) **212**:1345–1360. doi:10.1084/jem.20151159

359. Ngiow SF, Scheidt von B, Akiba H, Yagita H, Teng MWL, Smyth MJ. Anti-TIM3 antibody promotes T cell IFN-γ-mediated antitumor immunity and suppresses established tumors. *Cancer Res* (2011) **71**:3540–3551. doi:10.1158/0008-5472.CAN-11-0096

360. Anderson AC. Tim-3: an emerging target in the cancer immunotherapy landscape. *Cancer Immunol Res* (2014) **2**:393–398. doi:10.1158/2326-6066.CIR-14-0039

361. Pilon-Thomas S, Mackay A, Vohra N, Mulé JJ. Blockade of programmed death ligand 1 enhances the therapeutic efficacy of combination immunotherapy against melanoma. *J Immunol* (2010) **184**:3442–3449. doi:10.4049/jimmunol.0904114

362. Loeffler M, Krüger JA, Niethammer AG, Reisfeld RA. Targeting tumor-associated fibroblasts improves cancer chemotherapy by increasing intratumoral drug uptake. *J Clin Invest* (2006) **116**:1955–1962. doi:10.1172/JCI26532

363. Liao D, Luo Y, Markowitz D, Xiang R, Reisfeld RA. Cancer Associated Fibroblasts Promote Tumor Growth and Metastasis by Modulating the Tumor Immune Microenvironment in a 4T1 Murine Breast Cancer Model. *PLoS ONE* (2009) **4**:e7965–10. doi:10.1371/journal.pone.0007965

364. Norata GD, Caligiuri G, Chavakis T, Matarese G, Netea MG, Nicoletti A, O'Neill LAJ, Marelli-Berg FM. The Cellular and Molecular Basis of Translational Immunometabolism. *Immunity* (2015) **43**:421–434. doi:10.1016/j.immuni.2015.08.023

365. Chang C-H, Pearce EL. Emerging concepts of T cell metabolism as a target of immunotherapy. *Nat Immunol* (2016) **17**:364–368. doi:10.1038/ni.3415

366. Murphy KM, Nelson CA, Sedý JR. Balancing co-stimulation and inhibition with BTLA and HVEM. *Nature Reviews Immunology* (2006) **6**:671–681. doi:10.1038/nri1917

367. Hebeisen M, Allard M, Gannon PO, Schmidt J, Speiser DE, Rufer N. Identifying Individual T Cell Receptors of Optimal Avidity for Tumor Antigens. *Front Immunol* (2015) **6**:582. doi:10.3389/fimmu.2015.00582

368. Wikberg ML, Edin S, Lundberg IV, Van Guelpen B, Dahlin AM, Rutegård J, Stenling R, Oberg A, Palmqvist R. High intratumoral expression of fibroblast activation protein (FAP) in colon cancer is associated with poorer patient prognosis. *Tumour Biol* (2013) **34**:1013–1020. doi:10.1007/s13277-012-0638-2

369. Feig C, Jones JO, Kraman M, Wells RJB, Deonarine A, Chan DS, Connell CM, Roberts EW, Zhao Q, Caballero OL, et al. Targeting CXCL12 from FAP-expressing carcinoma-associated fibroblasts synergizes with anti-PD-L1 immunotherapy in pancreatic cancer. *Proc Natl Acad Sci USA* (2013) **110**:20212–20217. doi:10.1073/pnas.1320318110